ACCELERATING DEVELOPMENT OF METAL ORGANIC FRAMEWORK MEMBRANES USING ATOMICALLY DETAILED SIMULATIONS

A Dissertation
Presented to
The Academic Faculty

by

Seda Keskin

In Partial Fulfillment
of the Requirements for the Degree
Doctor of Philosophy in the
School of Chemical and Biomolecular Engineering

Georgia Institute of Technology
December 2009

ACCELERATING DEVELOPMENT OF METAL ORGANIC FRAMEWORK MEMBRANES USING ATOMICALLY DETAILED SIMULATIONS

Approved by:

Dr. David S. Sholl, Advisor
School of Chemical and Biomolecular Engineering
Georgia Institute of Technology

Dr. William J. Koros
School of Chemical and Biomolecular Engineering
Georgia Institute of Technology

Dr. Ronald R. Chance
School of Chemical and Biomolecular Engineering
Georgia Institute of Technology

Dr. Sankar Nair
Chemical and Biomolecular Engineering
Georgia Institute of Technology

Dr. Seung Soon Jang
School of Material Science and Engineering
Georgia Institute of Technology

Date Approved: [October 8, 2009]

To my beloved parents, Yıldız and Nurullah, for always believing in me…

ACKNOWLEDGEMENTS

It is customary for acknowledgment of dissertations to be a kind prose to express gratitude to many individuals. Given my sentimental personality and excellence of the individuals who deserve much more than one sentence of appreciation, I would like to present my sincere gratitude to those beautiful people in an unusual way, unedited, deep from my heart...

Dr. David S. Sholl has been the greatest chance happened to me through my graduate school career. He has been a great mentor, a supportive advisor, a gifted teacher, an outstanding collaborator and a perfect role-model to me. He has generously invested his time (which is scarce) and his patience (which is abundant) in educating me. Being a faculty has been the dream of my life and the only reason for me to pursue a PhD degree. I will forever be indebted to Dr. Sholl for helping me to make my dream come true. I hope I can inspire my students as he has inspired me.

I have been especially fortunate to have Dr. Ronald R. Chance, Dr. Seung Soon Jang, Dr. William J. Koros and Dr. Sankar Nair as my committee members. I am thankful to them for their concrete assistance and energy to engage ideas for improving my studies. I am grateful to Dr. J. Karl Johnson who is a wonderful source of advice and encouragement. It has been a great opportunity to work with him and to learn from his insightful thoughts.

This study has brought a lot more than a doctoral degree by integrating me with amazing friends all over the world. The moments I shared with Lymarie Semidey Flecha, Emmanuel Haldoupis, Jeong Woo Han, Sang Eun Jee, Sung Gu Kang, Ki Chul Kim,

Chen Ling, Dr. Shiqiang Hao, Dr. Tom Manz, Dr. Taku Watanabe and Dr. Ji Zang have left a huge smile on my face and celebrating life with those friends has been an unforgettable experience.

I am grateful to Margaret and Rıza Kaya, who opened their warm home but most importantly their lovely hearts to me from the very first day of my life in US. They have been my second family, it would be impossible to write these lines without their support.

I owe special thanks to my dear friends, Dr. Kerem Uğuz, Dr. Berk Usta, Dr. Faik Başkaya, Nevce Gürkan and Ali Nejat İpekçi for their great friendships and for the amazing times we shared in Pittsburgh and Atlanta. A special thanks goes to Ali Nejat who has been a great neighbor but most importantly a true brother to me.

My beloved parents and my sister, Yıldız-Nurullah-Başak Keskin, have always amazed me with their incredible love and endless support, taught me to follow my dreams, believed in me unconditionally. I am extremely fortunate to have such a wonderful family, they mean everything to me.

I am indebted to a single person beyond what words can say, to my fiancé, Dr. Ahmet Kerim Avcı, who has redefined ‘patience’ and ‘love’, from 9289 kilometers away and 7 hours of time difference for the last three years.

My doctoral study has been an exceptional journey with beautiful memories that I have never dreamed of. With all these, I am coming back to home…

Seda Keskin

09.09.09, Atlanta

TABLE OF CONTENTS

LIST OF TABLES

LIST OF FIGURES

SUMMARY

A new group of nanoporous materials, metal organic frameworks (MOFs), have emerged as a fascinating alternative to more traditional nanoporous materials for membrane based gas separations. Although hundreds of different MOF structures have been synthesized in powder forms, very little is currently known about the potential performance of MOFs as membranes since fabrication and testing of membranes from new materials require a large amount of time and resources. The purpose of this thesis is to predict the macroscopic flux of multi-component gas mixtures through MOF-based membranes with information obtained from detailed atomistic simulations. First, atomically detailed simulations of gas adsorption and diffusion in MOFs combined with a continuum description of a membrane are introduced to predict the performance of MOF membranes. These results are compared with the only available experimental data for a MOF membrane. An efficient approximate method based on limited information from molecular simulations to accelerate the modeling of MOF membranes is then introduced. The accuracy and computational efficiency of different modeling approaches are discussed. A robust screening strategy is proposed to screen numerous MOF materials to identify the ones with the high membrane selectivity and to direct experimental efforts to the most promising of many possible MOF materials. This study provides the first predictions of any kind about the potential of MOFs as membranes and demonstrates that using molecular modeling for this purpose can be a useful means of identifying the phenomena that control the performance of MOFs as membranes.

CHAPTER 1

INTRODUCTION

In chemical engineering, a separation process is used to transform a mixture of substances into two or more distinct products that differ from each other in composition.[1] The traditional chemical engineering methods of separation and purification include distillation, crystallization, adsorption, absorption, stripping, solvent extraction, cryogenics, and membranes.[2] Membrane science and technology started in the mid-nineteenth century with naturally occurring membranes. In the early to middle twentieth century, it evolved from a narrow scientific discipline with limited practical applications to a broader field with applications that include food processing, water treatment, biotechnology and pharmaceutical applications, petrochemical processing, and many other process applications.[3,4] Higher energy costs in recent decades have made the membrane processes even more economically competitive with conventional separation techniques such as distillation and extraction. Energy consumption with membranes is often less than with distillation and there is no need for an organic solvent as in the extraction. Therefore, membrane based separation has become an attractive candidate for energy efficient and environmentally friendly separation processes.

1.1 Membrane Classification

Membrane materials can be categorized into three groups: polymeric membranes, inorganic membranes, and the combination of the first two categories, composite membranes.[2] Polymeric membranes are widely available and several polymeric membranes have been already commercialized for gas separation applications.[5]

Unfortunately, polymeric membranes possess a fundamental trade-off between selectivity and throughput. Furthermore, polymeric membranes are sensitive to high temperatures and harsh chemical environments. The thermal and chemical stability of polymers are not only a technical but an economic issue. For example, in gas separation applications, if the membrane can withstand high process temperatures, the need to ramp down the temperature to maintain the physical integrity of a polymeric membrane and to ramp up the temperature again after separation can be eliminated.

Thin films of crystalline nanoporous materials have great potential for avoiding the trade-off between the selectivity and throughput.[6] Moreover, inorganic membranes can often work in a wide range of pH and temperature and withstand organic solvents such as chlorine and other chemicals.[2] For example, the thermal stabilities of organic polymers, inorganic polymers (the polymers which have chemical elements except carbon in their structural units) and inorganic structures as membrane materials can be conveniently classified as, 100-150°C, 100-350°C and >350°C, respectively. The preceding discussion indicates that at high temperatures and harsh chemical conditions, inorganic membranes could become the only resource for many challenging separation applications.

Inorganic membranes can also be classified into two broad groups: dense and porous membranes.[3] The difference between these two groups is the distinction of the generally accepted transport mechanism for the permeating species, rather than the distinction of absolute size of the pores in the membrane structures. For dense membranes, a solution-diffusion type mechanism is responsible for the transport and separation of species. On the other hand, transport of gases through a porous membrane

can be described by one or combinations of three mechanisms: Knudsen diffusion, convective flow or surface diffusion.[7-9] Knudsen diffusion occurs when the mean free path of the gas molecules is larger than the pore radius of the membrane. In this case, there are more collisions with the pore walls than between the gas molecules. Knudsen diffusion is expected to be dominant for pores that range in diameter between 2 and 50 nm. When the ratio of the pore radius to the mean free path is much larger than 1, as would be the case for gas transport in pinholes or other structural defects, convective flow dominates the gas transport mechanism.[8] High quality membranes are typically characterized by the absence of convective flow. For most of nanoporous materials, such as zeolites and carbon nanotubes, the relevant transport mechanism is surface diffusion. Due to the pore diameters of at the nanoscale, the ratio of the pore radius to the mean free path is a lot less than 1 in these materials. Unlike Knudsen diffusion, gas transport in this regime does not occur via a series of distinct collisions with the pore wall since the diffusing gas molecules are essentially always in contact with the pore wall.

In this study, we focus on gas separation through nanoporous membranes in which the transport mechanism is dominated by surface diffusion. Mass transport, especially for the multi-component gas mixtures through a nanoporous membrane is complex. The work presented in this thesis is in part an effort to use calculations based on atomistic simulations to describe the complicated transport mechanism of gas mixtures through nanoporous membranes.

1.2 Gas Separations with Nanoporous Membranes

Separation processes involving membranes require two bulk phases that are physically separated by a third phase, the membrane. In a membrane based gas separation

process, the feed gas is separated into permeate and retentate phases. The permeate is the material that goes through the membrane whereas the retentate is the portion of the feed retained by the membrane. Transport of the materials between the retentate and the permeate phases is controlled by the membrane and the operation conditions. If one or more of the species in the feed gas mixture are allowed to pass through the membrane in preference to others, then the membrane is said to be selective for these species. Selectivity is one of the most important parameters which describes the separation performance of a membrane. The selectivity of a membrane for a binary gas mixture can be defined as:[10]

$$S_{1/2} = \frac{y_1^{permeate} \cdot y_2^{feed}}{y_2^{permeate} \cdot y_1^{feed}}. \qquad 1.1$$

Here, y_i is the mole fraction of species i in the feed/permeate stream. With this definition a selectivity greater (less) than one corresponds to a membrane selective for the first (second) species. It is worthwhile to note that this selectivity differs from the ideal selectivity, which is the ratio of single component fluxes for a membrane. The single component permeability is defined as:[11]

$$P = \frac{J}{\Delta P / l}, \qquad 1.2$$

where J is the flux across the membrane, ΔP is the pressure drop, and l is the membrane thickness. Together with selectivity, permeability is the other critical factor that is typically used to provide an indication of the performance of a membrane. A high selectivity is useless if the permeability is low since a membrane with low throughput may require a large surface area that makes the separation process economically unattractive. Because permeability is inversely proportional to membrane thickness, most

of the commercial membranes are consisted of thin, selective and active layers on porous supports that provide mechanical strength.[3,12]

Application of gas separation through nanoporous membranes include several industrially important processes such as purification of natural gas, separation of hydrogen from mixed gas streams and separation of flue gas. Carbon dioxide separation from methane, for example, is an important issue since CO_2 reduces the energy content of the natural gas. Moreover, CO_2 is corrosive in the presence of water within the transportation and/or storage systems. An existing technology to separate CO_2 from CH_4 is amine absorption. Unfortunately, the amine plants are complex and very costly. In the early 1980s, plants using CO_2-selective cellulose acetate membranes were installed.[3,13,14] Zeolites, inorganic crystalline structures of aluminosilicates, have become an alternative to polymeric membranes due to their high thermal, mechanical and chemical stability and have been widely studied as potential membrane candidates for CO_2/CH_4 separation.[15-17]

Zeolites and activated carbons have long played a prominent role in many large scale applications of chemical separations. A crucial feature of these materials is that they contain large numbers of pores with widths on the order of 1 nm, that is, of similar size to individual molecules. The strong confinement experienced by gas molecules inside these pores leads to physical and chemical properties that are extremely different from bulk properties. These properties often depend sensitively on the structure of the pore. Examples are known in zeolite adsorption and catalysis, for example, where small changes in pore structure lead to enormous changes in reaction selectivity or molecular diffusion rates.[18,19]

Over approximately the last decade, a new group of nanoporous materials, metal organic frameworks, have emerged as a fascinating alternative to more traditional nanoporous materials such as zeolites. Metal organic frameworks have attracted a great deal of attention as a new addition to the classes of nanoporous materials due to their extraordinary physical and chemical properties. In this thesis, we explore this new group of potential membrane materials for multi-component gas separation applications using atomically detailed computational techniques.

1.3 A New Nanoporous Material Family: Metal Organic Frameworks

Metal organic frameworks (MOFs) are comprised of metal ligand complexes forming vertices of a framework that is connected with organic linkers that form porous structures with pores of molecular dimensions. MOFs, also called porous coordination polymers (PCPs)[20] or porous coordination networks (PCNs), are hybrid materials comprised of single metal ions or polynuclear metal clusters linked by organic ligands through strong coordination bonds (see Figure 1.1). Due to the strong coordination bonds, MOFs are crystallographically well defined structures that can keep their permanent porosity and crystal structure after the removal of the guest species used during synthesis.[21] MOFs typically have low densities (0.2-1 g/cm^3), high surface areas (500-4500 m^2/g), high porosity and reasonable thermal and mechanical stability. This combination of properties has made MOFs interesting for a range of potential applications, including gas storage,[22-28] separation,[15,29-36] and catalysis.[37,38]

Much of the excitement associated with MOFs stems from the fact that their synthesis can be readily adapted to control pore connectivity, structure, and dimension by varying the linkers, ligands, and metal in the material. This type of "rational design" of

pore structures has been elusive in the development of more traditional microporous materials. Therefore, the major advantage of MOFs over materials such as zeolites, whose pores are confined by rigid tetrahedral oxide skeletons that are usually difficult to alter, is the greater scope for tailoring these materials for specific applications. If the appropriate building blocks, the metal corners and organic ligands, are chosen MOFs with pre-defined shapes and functionalities can be created.[39]

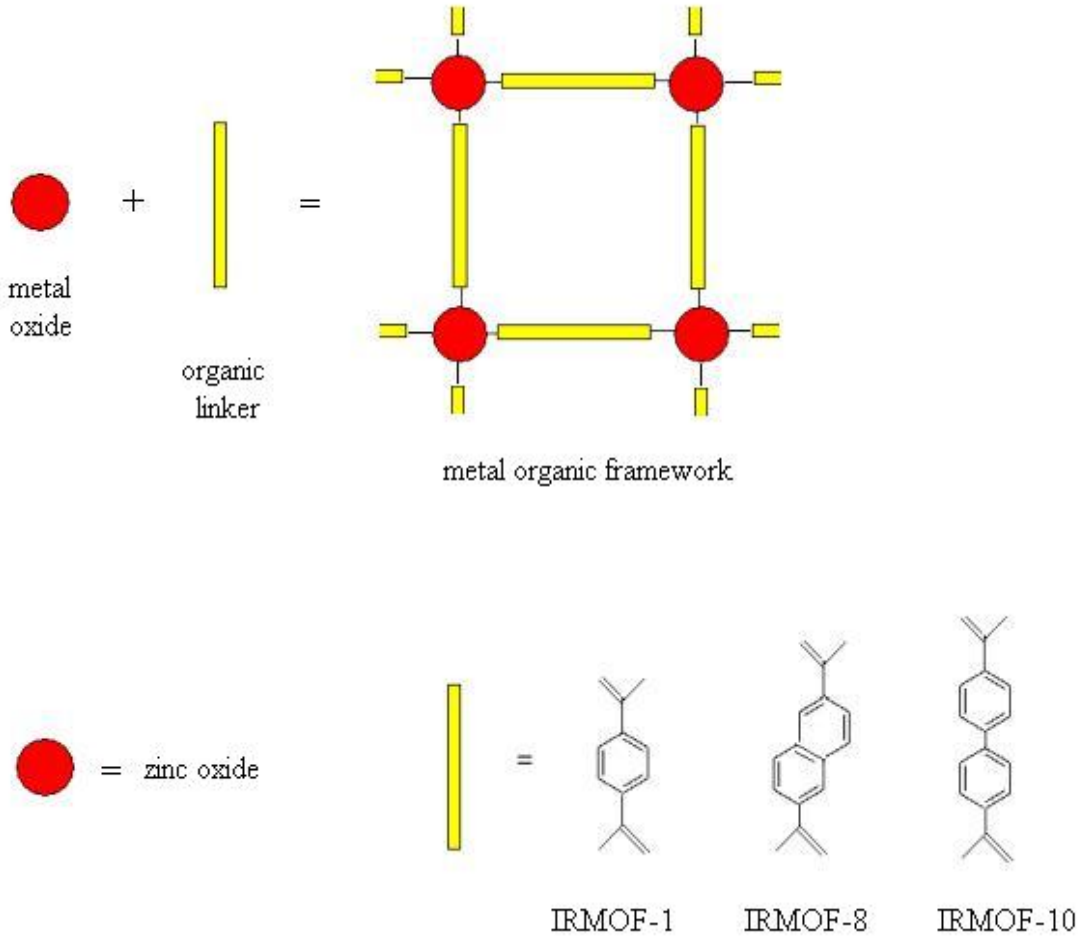

Figure 1.1 Building blocks of metal organic frameworks.

There has been a rapid growth in the number of publications relating to MOFs over the past decade.[39-41] Most of these publications are experimental in nature. Thousands of different MOFs have been synthesized and categorized in the Cambridge Structural Database (CSD) to date.[37,42-52] Of course, this number is representing only a small fraction of imaginable materials due to the large variety of possible linker and corner unit combinations. A number of reviews are available describing experimental synthesis and characterization of MOFs.[20,27,38,53-56] Although the initial focus in research on MOFs was the synthesis and structural characterization, experiments have recently started to explore MOFs for their various interesting properties such as optic, magnetic, and electronic properties.[21]

There have been numerous studies reporting various modeling efforts relating to MOFs and we recently reviewed atomically detailed modeling and quantum modeling of MOFs.[57] Most of these atomically detailed simulations and quantum modeling have focused on adsorption of single gas molecules or binary gas mixtures in MOFs. Although a good deal is known about adsorption in MOFs,[15,16,22,25,58-69] very little information is available about molecular transport in the same materials and information of multi-component diffusivity is very rare.[70-78] Since characterizing membrane performance requires information on mixture adsorption and mixture diffusion, no previous study prior to the work described in this thesis had examined the ability of MOFs to act as a gas separation membrane.

The enormous number of distinct MOFs that are known presents both a challenge and an opportunity for development of MOF-based membranes. The wide range of available pore sizes, topologies, and functionalities strongly suggests that existing MOFs

will have useful properties as membranes for separations of practical interest. The considerable resources that are necessary to fabricate membranes from new crystalline materials, however, mean that it is impractical to consider screening large numbers of potential materials experimentally. This situation suggests that quantitative computational modeling can play a useful role in selecting materials that deserve experimental development.[79] Recently, the first experimental demonstration that dense MOF membranes can be fabricated was reported.[80] In these experiments, Liu et al. prepared well-intergrown IRMOF-1 (isoreticular metal organic framework) membranes on porous α-alumina substrates by in situ solvothermal synthesis and measured single component gas permeation through these membranes. Two mixed matrix membranes that combine Cu-based MOF crystals within a polymeric membrane and IRMOF-1 crystals within a polymeric membrane have also been reported.[81,82]

Since very little is currently known about the potential performance of MOFs as membranes, efforts to predict the performance of MOF membranes using molecular modeling can potentially play an important role in selecting materials for specific applications and provide a means to complement experimental methods for screening MOFs.[33] The purpose of this thesis is to predict the macroscopic flux of multi-component gas mixtures through MOF-based membranes with the information obtained from detailed atomistic simulations. The modeling framework presented here will provide the ability to study a wide variety of MOF structures to screen various candidate materials for gas separation applications.

In this thesis, we have studied various different types of MOF structures. Most of our preliminary calculations focused on two MOF structures, IRMOF-1 and CuBTC.

These are the most widely studied MOFs in the literature (see Figure 1.2 and 1.3). IRMOF-1 ($[Zn_4O(BDC)_3$, BDC=benzenedicarboxylate]) is the prototype of IRMOF series, also referred as MOF-5.[83] IRMOF-1 has zinc oxide clusters as the metal corners and it is a three dimensional cubic network connecting the large cages (d≅14 Å) at the center of each unit cell.[72] CuBTC ($[Cu_3(BTC)_2$, BTC=benzenetricarboxylate]), also known as HKUST-1, has main channels approximately 9 Å in diameter, surrounded by tetrahedral pockets of 5 Å in diameter. The tetrahedral pockets and the main channels are connected via triangular windows of diameter of ~3.5 Å. The structural details of other MOFs that we have studied in this thesis are presented in the following chapters.

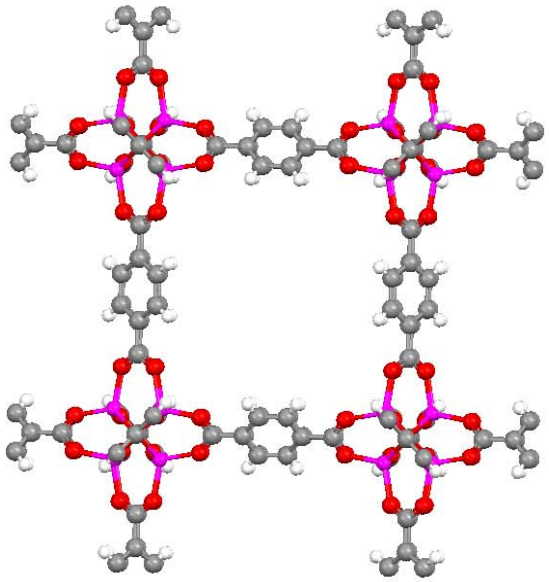

Figure 1.2 Unit cell crystal structure of IRMOF-1 viewed along the [100] direction. Zn: violet, O: red, C: gray and H: white.

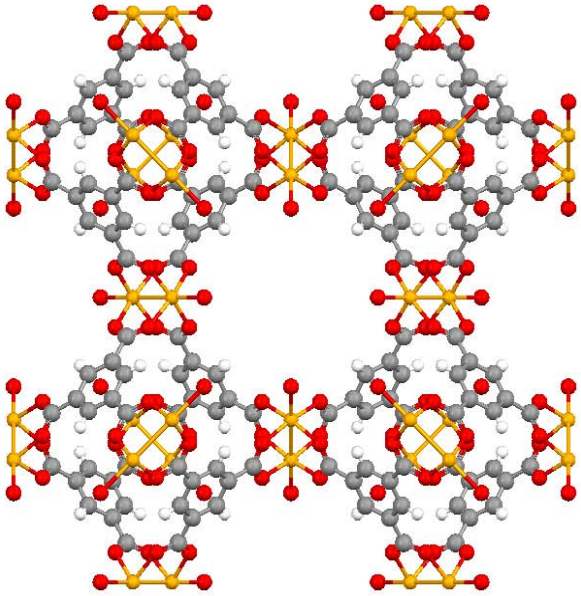

Figure 1.3 Unit cell crystal structure of Cu-BTC viewed along the [100] direction. Cu: orange, O: red, C: gray and H: white.

1.4 Thesis Summary

In Chapter 2, we describe macroscopic models for single component and multi-component gas transport through a nanoporous membrane. These models are based on an extended Fick's law of diffusion where diffusivities are a function of concentration of the adsorbed species. The atomistic models of both adsorbent (MOF structures) and adsorbate molecules (gas species) are specified and the details of molecular simulations to perform adsorption and diffusion calculations are described.

In Chapter 3, these methods described in Chapter 2 are applied to examine the permeance of binary mixtures of CO_2/CH_4, CO_2/N_2, CO_2/H_2, CH_4/H_2, CH_4/N_2 and N_2/H_2 through an IRMOF-1 membrane at room temperature. The most important observation from these calculations is that the ideal and mixture selectivities are very different from

each other. This result indicates that characterizing the properties of these membranes using mixed gas feeds rather than single component gases is crucial. We also compare the experimental measurements of single component gas permeation through IRMOF-1 membrane with our theoretical predictions of this quantity.

We describe atomically detailed simulations of gas adsorption and diffusion in CuBTC that have been used to predict the performance of CuBTC membranes for separations of H_2/CH_4, CO_2/CH_4 and CO_2/H_2 mixtures in Chapter 4. CuBTC membranes are predicted to have higher selectivities for all three mixtures than IRMOF-1 membranes and the reasons behind this outcome is discussed. The results of this chapter give insight into the physical properties that will be desirable in tuning the pore structure of MOFs for specific membrane-based separations.

We move on to study of testing the accuracy of mixing theories for adsorption and diffusion in MOFs in Chapter 5. We present the first test of three mixing theories for molecules adsorbed in a MOF structure. More specifically, we test theories to predict macroscopic transport diffusivities, self diffusivities and adsorption equilibrium of CH_4/H_2 mixture in CuBTC by comparing predictions of these theories with direct molecular simulations. These calculations provide the first direct information on mixture transport of any species in a MOF and suggest that using mixing theories may be a powerful approach for examining multi-component diffusion in MOFs.

In Chapter 6, we introduce an efficient approximate method based on limited information from molecular simulations for screening MOFs to accelerate the modeling of membrane applications. The validity of this approximate method is examined by comparison with detailed calculations for CH_4/H_2, CO_2/CH_4 and CO_2/H_2 mixtures at

room temperature permeating through IRMOF-1 and CuBTC membranes. These results allow us to hypothesize a connection between two computationally efficient correlations predicting mixture adsorption and mixture self diffusion properties and the validity of our approximate screening method. We then apply our model to six additional MOFs, IRMOF-8, -9, -10 and -14, $Zn(bdc)(ted)_{0.5}$, and COF-102, to examine the effect of chemical diversity and interpenetration on the performance of MOF membranes for light gas separations.

We compare the efficiency and the accuracy of three different modeling approaches to predict the selectivity of MOF membranes in Chapter 7. Different approaches are categorized based on their computational efficiency to perform calculations and the accuracy to approximate the selectivity of the membrane. Motivated from these comparisons, a general strategy for screening of MOF membranes for separation of binary gas mixtures is described.

Finally, we outline and discuss the main challenges and opportunities of using molecular simulations to contribute to the development of practical applications of MOFs for future chemical engineering processes in Chapter 8.

1.5 References

(1) King, C. J. *Separation Processes*, 2nd ed.; McGraw-Hill: New York, 1980.

(2) Heish, H. P. *Inorganic Membranes for Separation and Reaction*; Elsevier: Amsterdam, 1996.

(3) Baker, R. W. *Membrane Technology and Applications*; McGraw-Hill: New York, 2000.

(4) National Research Council *Separation Technology for the Industries of the Future*, 1st ed.; National Academy Press: Washington D.C., 1998.

(5) Robeson, L. M. *J. Membr. Sci.* **1991**, *62*, 165.

(6) Lai, Z.; Bonilla, G.; Diaz, I.; Nery, J. G.; Sujaoti, K.; Amat, M. A.; Kokkoli, E.; Terasaki, O.; Thompson, R. W.; Tsapatsis, M.; Vlachos, D. G. *Science* **2003**, *300*, 456.

(7) Uhlhorn, R. J. R.; Keizer, K.; Burggraaf, A. J. *J. Membrane Sci.* **1989**, *46*, 225.

(8) Bird, R. B.; Stewart, W. E.; Lightfoot, E. N. *Transport Phenomena*, 2nd ed.; John Wiley & Sons: New York, 2001.

(9) Bhatia, S. K.; Chen, H.; Sholl, D. S. *Mol. Simul.* **2005**, *31*, 643.

(10) Matsukata, M.; Kikuchi, E. *Bull. Chem. Soc. Japan* **1997**, *70*, 2341.

(11) Kapteijn, F.; Bakker, W. J. W.; Zheng, G.; Poppe, J.; Moulijn, J. *Chem. Eng. J.* **1995**, *57*, 145.

(12) Baker, R. W. *Ind. Eng. Chem. Res.* **2002**, *41*, 1393.

(13) Li, S.; Martinek, J. G.; Falconer, J. L.; Noble, R. D.; Gardner, T. Q. *Ind. Eng. Chem. Res.* **2005**, *44*, 3220.

(14) Koros, W. J.; Mahajan, R. *J. Membrane Sci.* **2000**, *175*, 181.

(15) Babarao, R.; Hu, Z.; Jiang, J.; Chempath, S.; Sandler, S. I. *Langmuir* **2007**, *23*, 659.

(16) Babarao, R.; Jiang, J. *Langmuir* **2008**, *24*, 5474.

(17) Krishna, R.; van Baten, J. M. *Chem. Eng. J.* **2007**, *133*, 121.

(18) Kärger, J.; Ruthven, D. *Diffusion in Zeolites and Other Microporous Materials*; John Wiley & Sons: New York, 1992.

(19) Chen, N. Y.; Degnan, T. F.; Smith, C. M. *Molecular Transport and Reaction in Zeolites: Design and Application of Shape Selective Catalysis*; John Wiley & Sons: New York, 1994.

(20) Kitagawa, S.; Kitaura, R.; Noro, S. *Angew. Chem. Int. Ed.* **2004**, *43*, 2334.

(21) Li, J.-R.; Kuppler, R. J.; Zhou, H.-C. *Chem. Soc. Rev.* **2009**, *38*, 1477.

(22) Düren, T.; Sarkisov, L.; Yaghi, O. M.; Snurr, R. Q. *Langmuir* **2004**, *20*, 2683.

(23) Millward, A. R.; Yaghi, O. M. *J. Am. Chem. Soc.* **2005**, *127*, 17998.

(24) Eddaoudi, M.; Li, H.; Yaghi, O. M. *J. Am. Chem. Soc.* **2000**, *122*, 1391.

(25) Wong-Foy, A. G.; Matzger, A. J.; Yaghi, O. M. *J. Am. Chem. Soc.* **2006**, *128*, 3494.

(26) Rowsell, J. L. C.; Spencer, E. C.; Eckert, J.; Howard, J. A. K.; Yaghi, O. M. *Science* **2005**, *309*, 1350.

(27) Rowsell, J. L. C.; Yaghi, O. M. *Angew. Chem. Int. Ed.* **2005**, *44*, 4670

(28) Wang, S.; Yang, Q.; Zhong, C. *Sep. Purif. Technol.* **2008**, *60*, 30.

(29) Düren, T.; Snurr, R. Q. *J. Phys. Chem. B* **2004**, *108*, 15703.

(30) Keskin, S.; Sholl, D. S. *J. Phys. Chem. C* **2007**, *111*, 14055.

(31) Pan, L.; Olson, D. H.; Ciemnolonski, L. R.; Heddy, R.; Li, J. *Angew. Chem. Int. Ed.* **2006**, *45*, 616.

(32) Wang, Q. M.; Shen, D. M.; Bulow, M.; Lau, M. L.; Deng, S. G.; Fitch, F. R.; Lemcoff, N. O.; Semanscin, J. *Micropor. Mesopor. Mater.* **2002**, *55*, 217.

(33) Snurr, R. Q.; Hupp, J. T.; Nguyen, S. T. *AIChE J.* **2004**, *50*, 1090.

(34) Yang, Q.; Chunyu, X.; Zhong, C.; Chen, J.-F. *AIChE J.* **2007**, *53*, 2832.

(35) Yang, Q.-Y.; Zhong, C.-L. *Chem. Phys. Chem.* **2006**, *7*, 1417.

(36) Yang, Q.; Zhong, C. *J. Phys. Chem. B* **2006**, *110*, 17776.

(37) Schlichte, K.; Kratzke, T.; Kaskel, S. *Micropor. Mesopor. Mater.* **2004**, *73*, 81.

(38) Mueller, U.; Schubert, M.; Teich, F.; Puetter, H.; Schierle-Arndt, K.; Pastré, J. *J. Mater. Chem.* **2006**, *16*, 626.

(39) Düren, T.; Bae, Y. S.; Snurr, R. Q. *Chem. Soc. Rev.* **2009**, *38*, 1237.

(40) Czaja, A. U.; Trukhan, N.; Müller, U. *Chem. Soc. Rev.* **2009**, *38*, 1284.

(41) Han, S. S.; Mendoza-Cortes, J. L.; Goddard III, W. A. *Chem. Soc. Rev.* **2009**, *38*, 1460.

(42) Szeto, K. C.; Kongshaug, K. O.; Jakobsen, S.; Tilset, M.; Lillerud, K. P. *Dalton Trans.* **2008**, 2054.

(43) Yang, E. C.; Li, J.; Ding, B.; Liang, Q. Q.; Wang, X. G.; Zhao, X. J. *Cryst. Eng. Comm.* **2008**, *10*, 158.

(44) Bataille, T.; Costantino, F.; Lorenzo-Luis, P.; Midollini, S.; Orlandin, A. *Inorganica Chimica Acta* **2008**, *361*, 9.

(45) Zhang, D. J.; Song, T. Y.; Shi, J.; Ma, K. R.; Wang, Y.; Wang, L.; Zhang, P.; Fan, Y.; Xu, J. N. *Inorg. Chem. Comm.* **2008**, *11*, 192.

(46) Jin, Z.; Zhu, G. S.; Zou, Y. C.; Fang, Q. R.; Xue, M.; Li, Z. Y.; Qiu, S. L. *J. Mol. Struct.* **2008**, *871*, 80.

(47) Pichon, A.; Lazuen-Garay, A.; James, S. L. *Cryst. Eng. Comm.* **2006**, *8*, 211.

(48) Yaghi, O. M.; O'Keeffe, M.; Ockwig, N. W.; K.Chae, H.; Eddaoudi, M.; Kim, J. *Nature* **2003**, *423*, 705.

(49) Li, H.; Eddaoudi, M.; O'Keeffe, M.; Yaghi, O. M. *Nature* **1999**, *402*, 276.

(50) Surble, S.; Millange, F.; Serre, C.; Düren, T.; Latroche, M.; Bourelly, S.; Liewellyn, P.; Ferey, G. *J. Am. Chem. Soc.* **2006**, *128*, 14889.

(51) Rood, J. A.; Noll, B. C.; Henderson, K. W. *Inorg. Chem.* **2006**, *45*, 5521.

(52) Yaghi, O. M.; Li, H. L. *J. Am. Chem. Soc.* **1995**, *117*, 10401.

(53) Davis, M. E. *Nature* **2002**, *417*, 813.

(54) James, S. J. *Chem. Soc. Rev.* **2003**, *32*, 276.

(55) Rosseinsky, M. J. *Micropor. Mesopor. Mater.* **2004**, *73*, 15.

(56) Rowsell, J. L. C.; Yaghi, O. M. *Micropor. Mesopor. Mater.* **2004**, *73*, 3.

(57) Keskin, S.; Liu, J.; Rankin, R. B.; Johnson, J. K.; Sholl, D. S. *Ind. Eng. Chem. Res.* **2009**, *48*, 2355.

(58) Babarao, R.; Jiang, J. *Langmuir* **2008**, *24*, 6270.

(59) Ramsahye, N.; Maurin, G.; Bourrelly, S.; Llewellyn, P.; Devic, T.; Serre, C.; Loiseau, T.; Ferey, G. *Adsorption* **2007**, *13*, 461.

(60) Ramsahye, N. A.; Maurin, G.; Bourrelly, S.; Llewellyn, P. L.; Serre, C.; Loiseau, T.; Devic, T.; Ferey, G. *J. Phys. Chem. C* **2008**, *112*, 514.

(61) Yang, Q.; C. Zhong; Chen, J.-F. *J. Phys. Chem. C* **2008**, *112*, 1562.

(62) Han, S. S.; Goddard, W. A. I. *J. Am. Chem. Soc.* **2007**, *129*, 8422.

(63) Jhon, Y. H.; Cho, M.; Jeon, H. R.; Park, I.; Chang, R.; Rowsell, J. L. C.; Kim, J. *J. Phys. Chem. C* **2007**, *111*, 16618.

(64) Wang, S. *Energy & Fuels* **2007**, *21*, 953.

(65) Zhou, W.; Wu, H.; Hartman, M. R.; Yildirim, T. *J. Phys. Chem. C* **2007**, *111* 16131.

(66) Han, S. S.; Goddard III, A. W. *J. Phys. Chem. C* **2008**, *112*, 13431.

(67) Liu, B.; Yang, Q.; Xue, C.; C. Zhong; Chen, B.; Smit, B. *J. Phys. Chem. C* **2008**, *112*, 9854.

(68) Bae, Y.-S.; Mulfort, K. L.; Frost, H.; Ryan, P.; Punnathanam, S.; Broadbelt, L. J.; Hupp, J. T.; Snurr, R. Q. *Langmuir* **2008**, *24*, 8592.

(69) Babarao, R.; Jiang, J.; Sandler, S. I. *Langmuir* **2009**, *25*, 5239.

(70) Stallmach, F.; Groger, S.; Kunzel, V.; Kärger, J.; Yaghi, O. M.; Hesse, M.; Muller, U. *Angew. Chem. Int. Ed.* **2006**, *45*, 2123.

(71) Salles, F.; Jobic, H.; Maurin, G.; Koza, M. M.; Llewellyn, P. L.; Devic, T.; Serre, C.; Ferey, G. *Phys. Rev. Lett.* **2008**, *100*, 245901.

(72) Skoulidas, A. I.; Sholl, D. S. *J. Phys. Chem. B* **2005**, *109*, 15760.

(73) Amirjalayer, S.; Tafipolsky, M.; Schmid, R. *Angew. Chem. Int. Ed.* **2007**, *46*, 463.

(74) Liu, J.; Lee, J. Y.; Pan, L.; Obermyer, R. T.; Simizu, S.; Zande, B.; Li, J.; Sankar, S. G.; Johnson, J. K. *J. Phys. Chem. C* **2008**, *112*, 2911.

(75) Liu, B.; Yang, Q.; Xue, C.; Zhong, C.; Smit, B. *Phys. Chem. Chem. Phys.* **2008**, *10*, 3244.

(76) Rosenbach, N.; Jobic, H.; Ghoufi, A.; Salles, F.; Maurin, G.; Bourrrelly, S.; Llewellyn, P. L.; Devic, T.; Serre, C.; Ferey, G. *Angew. Chem. Int. Ed.* **2008**, *47*, 6611.

(77) Greathouse, J. A.; Allendorf, M. D. *J. Phys. Chem. C* **2008**, *112*, 5795.

(78) Chmelik, C.; Kärger, J.; Wiebcke, M.; Caro, J.; van Baten, J. M.; Krishna, R. *Micropor. Mesopor. Mater.* **2009**, *117*, 22.

(79) Hao, S.; Sholl, D. S. *Energy and Environ. Sci.* **2008**, *1*, 175.

(80) Liu, Y.; Ng, Z.; Khan, E. A.; Jeong, H.-K.; Ching, C.-B.; Lai, Z. *Micropor. Mesopor. Mater.* **2009**, *118*, 296.

(81) Zhang, Y.; Musselman, I. H.; Ferraris, J. P.; Balkus, K. J. *J. Membr. Sci.* **2008**, *313*, 170.

(82) Perez, E. V.; Balkus, K. J.; Ferraris, J. P.; Musselman, I. H. *J. Membr. Sci.* **2009**, *328*, 165.

(83) Yaghi, O. M.; O'Keeffe, M.; Ockwig, N. W.; Chae, H. K.; Eddaoudi, M.; Kim, J. *Nature* **2003**, *423*, 705.

CHAPTER 2

COMPUTATIONAL METHODS

In this chapter, we describe our modeling approach to predict macroscopic mass transfer of multi-component gas mixtures through metal organic framework (MOF) membranes. We first review previous theoretical approaches of modeling transport through nanoporous membranes and then present the macroscopic models used in this study to predict single component and mixture permeations of gases through MOF membranes. Finally, the details of the molecular simulation methods that are used to calculate the adsorption isotherms and diffusion coefficients of adsorbates are presented.

2.1 Macroscopic Models of Mass Transport through Membranes

Several different mathematically equivalent methods are available to describe the multi-component mass transport through nanopores. The most successful models to date for the molecular transport though nanoporous membranes have used a macroscopic approach based on Maxwell-Stefan formulation.[1-6] Practical applications of this approach requires certain assumptions: The single and multi-component adsorption isotherms are assumed to have Langmuir form, single component Maxwell-Stefan diffusivities are constant and cross species Maxwell-Stefan diffusivities are zero.[1-3,7] Based on these approximations, the unknown parameters of the model can be fitted to single component permeation experiments. This approach has been successfully applied for the transport of mixtures of ethane/ethene and propane/propene through silicalite membranes.[6] Although this theoretical approach has a great value for interpreting existing experimental results, it cannot be used to make predictions for membranes that are not currently fabricated or in

use. As a result, these models cannot be used for computational screening of possible membrane materials. Another disadvantage of this approach is that the range of validity of the assumptions is not clear.

An alternative approach to modeling mass transport through nanoporous membranes is to use atomistic simulation methods to represent the membrane at atomic scale and to directly simulate transport through the membrane.[8-10] The advantage of this approach compared to the previous one is that it explicitly incorporates the atomic scale description of nanoporous membrane and therefore, can be used to model the membranes in a completely predictive manner. This approach is very useful to study possible membranes before they are actually fabricated yet. Direct atomic simulation of a nanoporous membrane is very computationally demanding. As a result, simulations to date have been limited to membranes that are nanometers in thickness with extremely large pressure drops across the membrane. For example, in the simulations of Takaba et al.[9] the thickness of the zeolites membrane was 2.3 nm and the effective pressure drop across the membrane was approximately 100 atm. In contrast, realistic membranes are typically 10^2-10^4 nm thick and use pressure drops on the order of 1~10 atm.[11,12] The enormous disparity between these thicknesses and pressure drops raises questions about how accurately the simulation results can be related to practical situations. Furthermore, recent computational studies have shown that resistances at the surface of very thin membranes dominate transport.[13-16] Another disadvantage of this approach is that after all the massive simulation of the transport through the membrane, the knowledge that is gained is only for one set of conditions. Knowing the performance of a membrane at one

set of physical condition does not give any immediate insight into how the membrane would behave at other conditions.

The central purpose of this thesis is to predict the performance of various MOF membranes for separation of multi-component gas mixtures. There is currently only one MOF membrane fabricated to date.[17] Therefore, the first modeling approach described above that requires data from single component permeation experiments cannot currently be used to study MOF membranes. The second modeling approach outlined above is only able to give information for a certain set of operating conditions, which limits our screening efforts to find the most promising MOF membrane. Therefore, we use an alternative approach in this chapter to predict the macroscopic transport of multi-component gas mixtures through MOF membranes. This approach has been successfully applied for zeolite membranes and carbon nanotubes membrane in the past.[18-20] The idea of this approach is to use equilibrium atomic-scale simulations to directly parameterize a macroscopic description of membrane transport. The only input to this approach is the atomistic models of gas molecules (adsorbates) and the nanoporous membrane (adsorbent). Once these atomistic models are defined, equilibrium adsorption of gas molecules and their diffusion coefficients through the nanoporous material can be calculated using grand canonical Monte Carlo (GCMC) and Molecular dynamic (MD) simulations, respectively. Once adsorption and diffusion information is available, predictions for the performance of nanoporous material as a membrane can be made based on any combinations of feed pressure, pressure drop, membrane thickness and feed gas composition.

2.1.1 Single Component Gas Permeation

As we describe in Chapter 1, the primary focus of this work is on MOFs, which are ordered nanoporous materials. In our macroscopic membrane model, we assume an unsupported membrane comprised of a single MOF crystal of thickness *l*. The membrane is assumed to lie in the *x*-*y* plane so that the transmembrane flow occurs only in the *z* direction. We consider the case of a membrane in contact with bulk single component gas phase at upstream (downstream) pressure P_f (P_p). The flux of the adsorbed species is given by Fick's law,[21,22]

$$J = D_t(c) \cdot \frac{dc}{dz}, \tag{2.1}$$

where *c(z)* is the concentration of the adsorbed species and $D_t(c)$ is the concentration dependent Fickian diffusion coefficient (also known as transport diffusivity). Under steady state conditions, this equation can be integrated to give the steady state flux,

$$J = \frac{1}{l} \int_{c_{permeate}}^{c_{feed}} D_t(c) dc. \tag{2.2}$$

Here, c_{feed} ($c_{permeate}$) is the adsorbate concentration in the membrane at $z = 0$ ($z = L$). Throughout this thesis, we frequently refer to the adsorbate concentrations as 'loadings' in the pores. It is sufficient to know the concentration dependent Fickian diffusion coefficient, $D_t(c)$, and the boundary loadings to determine the flux. Since we assume that the resistance to mass transfer is due to only intracrystalline diffusion, we can determine the boundary loadings from equilibrium adsorption isotherm.[23-25] Extensive non-equilibrium molecular dynamic (NEMD) simulations have shown that neglecting the

surface effects is accurate for light gas transport through membranes made from other nanoporous materials with a thickness larger than 0.1 μm.[26-28] Another potential source of mass transfer resistance in real membranes is due to the presence of macroporous support layers. We have not included these effects in our models, although the methods to do so have been described by Skoulidas and Sholl.[29]

We have performed all membrane calculations at room temperature. The temperature is assumed to be constant during steady state mass transport. Even though isosteric heat of adsorption of molecular species in nanoporous structures can be considerable, our assumption is valid for steady state membrane operations as long as heat transfer within the membrane material is efficient.

2.1.2 Mixture Permeation

Almost all application of membrane separations involve chemical mixtures permeating through a membrane. Similar to single component gas permeation, we consider a membrane oriented in the z direction in contact with the gas phase mixtures at upstream (downstream) pressure P_f (P_p). For multi-component mixtures, we introduce a mixture that is made of n different species with feed (permeate) concentrations of c^i_{feed} ($c^i_{permeate}$) with $i=1,\ldots,n$.

There are several mathematically equivalent formalisms such as the Onsager, Fickian and Maxwell-Stefan descriptions to describe multi-component gas transport through nanoporous materials.[3,4,4,30] The Onsager formulation is based on irreversible thermodynamics and expresses the flux of each species in terms of chemical potentials:

$$\vec{J} = -\mathbf{L}\nabla\vec{\mu} \qquad 2.3$$

Here, **L** is the Onsager coefficient matrix, also known as phenomenological coefficient matrix and μ is the chemical potential vector. If we were studying the flux in three dimensions then the chemical potential and the fluxes would be matrices and **L** would be a third rank tensor. For one dimensional flow, Equation 2.3 can be written for each individual species as,

$$J_i = -\sum_{i=1}^{n} L_{ij} \frac{\partial \mu_j}{\partial z} \tag{2.4}$$

Onsager[31,32] showed that for a suitable set of fluxes and their conjugate forces, like the molar fluxes and the chemical potential gradients, the matrix in Equation 2.3 is symmetric:

$$L_{ij} = L_{ji}, \; i \neq j \tag{2.5}$$

An equivalent approach to present multi-component mass transport is the Fickian formulation. The Fickian formulation relates the flux of each species with the concentration gradients,

$$\vec{J} = -\mathbf{D} \nabla \vec{c}. \tag{2.6}$$

Here, **D** is the Fickian diffusivity matrix, also known as transport diffusivity coefficient matrix. The application of Fickian formulation to one-dimensional transport of a binary gas mixture through a membrane leads to the two-component generalization of Fick's law:

$$\begin{pmatrix} J_1 \\ J_2 \end{pmatrix} = \begin{pmatrix} D_{11} & D_{12} \\ D_{21} & D_{22} \end{pmatrix} \cdot \begin{pmatrix} \nabla c_1 \\ \nabla c_2 \end{pmatrix} \qquad 2.7$$

Here, ∇c_i is the concentration gradient of species *i*. The elements of the Fickian diffusivity matrix, D_{ij}, are in general functions of adsorbate concentrations. This equation shows that the flux of each species depends on the concentration gradient of the other species through the off-diagonal coefficients D_{12} and D_{21}. In general, the off-diagonal coefficients are not equal to each other.

It is also important to note that Equation 2.7 differs from another approach that has been also referred as Fickian formulation in which the off-diagonal elements are neglected and the flux of each species is only related with the concentration gradient of that species using Equation 2.1.[2] To appreciate that Equation 2.1 cannot describe the mixture diffusion, it is useful to recall a multi-component gas diffusion experiment which was conducted by Duncan and Toor in 1962.[33] This experiment demonstrated that one of the components in the mixture diffuses against its own concentration gradient after a considerable period of mixing. This cannot happen if Equation 2.1 is valid for a mixture, indicating that any description of diffusion must account for diffusion of one species induced by inhomogeneity in other species.

Another equivalent approach to present multi-component mass transport is the Maxwell-Stefan formulation. This formulation expresses the flux of each species in terms of a correlation matrix, **B** and a thermodynamic correction matrix, **Γ**:[34,35]

$$\vec{J} = -\mathbf{B}^{-1}\boldsymbol{\Gamma}\nabla\vec{c}. \qquad 2.8$$

The elements of correlation matrix for a binary mixture are defined in terms of Maxwell-Stefan diffusivity ($Đ_i$), exchange coefficients ($Đ_{ij}^{corr}$) and fractional loadings of each species (θ_i):

$$B_{ii} = \frac{1}{Đ_i} + \sum_{j=1, j\neq i}^{n} \frac{\theta_j}{Đ_{ij}^{corr}}, \qquad B_{ij} = \frac{-\theta_i}{Đ_{ij}^{corr}}, \qquad i, j = 1, 2 \tag{2.9}$$

The elements of thermodynamic correction factor matrix can be calculated from the knowledge of adsorption isotherms and written in terms of partial pressures (p_i) and loadings of each species (Θ_i):

$$\Gamma_{ij} = \left(\frac{\Theta_{j,sat}}{\Theta_{i,sat}}\right)\frac{\Theta_i}{p_i}\frac{\partial p_i}{\partial \Theta_j} = \frac{\theta_i}{\theta_j}\frac{\partial \ln p_i}{\partial \ln \theta_j}, \quad i, j = 1, 2 \tag{2.10}$$

As we pointed out in the beginning of this section, the Onsager, Fickian and Maxwell-Stefan formulations can be related without any approximation:

$$\vec{J} = -\mathbf{L}\nabla\vec{\mu} = -\mathbf{D}\nabla\vec{c} = -\mathbf{B}^{-1}\mathbf{\Gamma}\nabla\vec{c} \tag{2.11}$$

The transformation between the Fickian and Maxwell-Stefan formulations is straightforward. The transformation between Onsager and Fickian formulations can be written without any approximation as:

$$D_{ii} = \frac{k_B T}{c_i}\sum_{j=1}^{N} L_{ij}\left(\frac{\partial \ln f_i}{\partial \ln c_i}\right), \qquad D_{ij} = \frac{k_B T}{c_j}\sum_{k=1}^{N} L_{ik}\left(\frac{\partial \ln f_k}{\partial \ln c_j}\right) \tag{2.12}$$

where c_i is the concentration of species i, f_j is the fugacity of species j. None of the methods is more correct than the others. In practice, we find it easier to solve the macroscopic multi-component flux problem using the Fickian formulation.

2.1.3 Numerical Solution of Macroscopic Transport

Numerical solutions to the transport models defined above were calculated as follows. Single component gas permeation is calculated as defined above by integrating Equation 2.1. For the binary mixtures, we aim to calculate the steady state properties of binary gas mixtures permeating through membranes (transient effects were not considered). The input of our mathematical model are the feed pressure, permeate pressure and the composition of the gas mixture at the feed site. The initial composition of the permeate side is set to be same as compositions in the feed side. We assumed that the mixture feed with a constant feed pressure permeates through a nanoporous membrane to a well-mixed permeate side vessel whose pressure is regulated by a backpressure regulator. The numerical integration scheme proceeds in discrete steps. At each time step, the permeate side pressure either increases due to the transmembrane flux if the pressure is less than the back regulator set point or a quantity of the well mixed gas is removed to maintain the set point. This scheme is continued until the composition in the permeate side reach to a steady state value.

In our steady state flux calculations, we use shell model[4] which approximates the concentration gradient using the boundary loadings (Equation 2.8) and evaluates the Fickian diffusivities at the mean adsorbate loading (Equation 2.9):

$$\nabla c \cong \frac{(c_i^{\,perm} - c_i^{\,feed})}{L} \qquad 2.13$$

$$c_{average} \cong \frac{(c_i^{perm} + c_i^{feed})}{2} \qquad 2.14$$

The above definitions are used within Equation 2.7 and a steady state solution is determined iteratively for the overall membrane. The shell model has been tested in a previous study[36] and gave very similar results to direct integration technique when the net concentration gradient across the membrane is mild and the diffusion coefficients are only weakly dependent on the adsorbate concentration. Since using a shell model is far more convenient for performing larger numbers of calculations, all of the mixture permeation results given in this thesis are computed based on shell model.

2.2 Molecular Simulation of Adsorption

The validity and accuracy of any computer simulation depends on the assumptions made, the models and the methods used. We use atomistic simulations to calculate the adsorption isotherms and diffusion coefficients of light gas molecules in MOFs. Below, we explain the details of the atomistic models used for the gas molecules (adsorbates) and MOF structures (adsorbents) and the specification of molecular simulation methods. More detailed specifications for atomistic models can be found in each following chapter.

Adsorption isotherms can be calculated from atomistic simulations using Grand Canonical Monte Carlo (GCMC). Simulations based on GCMC have been compared rather successfully with the adsorption experiments for several nanoporous materials including MOFs.[37-46] In the grand canonical ensemble, the temperature, volume and chemical potential are fixed. In an experimental set-up, the adsorbed gas is in equilibrium

with the gas in the reservoir. The equilibrium conditions are that the temperature and the chemical potential of the gas inside and outside of the adsorbent must be equal.[47] The gas that is in contact with the adsorbent can be considered as a reservoir that imposes a temperature and chemical potential on the adsorbed gas. Therefore, we have to know only the temperature and the chemical potential to determine the equilibrium concentration inside the adsorbent. This is exactly what is mimicked in a GCMC simulation: the number of particles is allowed to fluctuate during the simulation at an imposed temperature and chemical potential. In our GCMC simulations, we calculate the number of adsorbed molecules per unit cell of the MOF structure at fixed temperature and pressure. Observations of GCMC simulations are directly comparable with the output of adsorption experiments. The statistical mechanical basis of GCMC simulations and more details can be found elsewhere.[47]

2.3 Molecular Simulation of Diffusion

Diffusion is an observable consequence of the motion of molecules and atoms as a response to external forces such as temperature, pressure, or concentration change. Molecular Dynamic (MD) is a natural method to simulate the motion and dynamics of molecules and atoms. The main concept in an MD simulation is to generate successive configurations of a system by integrating Newton's law of motion. Various diffusion coefficients can be measured using MD from the trajectories showing how the position and velocities of the particles vary with time in the system. More details of MD simulations for nanoporous structures can be found elsewhere.[22,47,48]

In this thesis, we use equilibrium MD (EMD), which models the behavior of the system in equilibrium. We first apply a short GCMC simulation to generate the initial

configurations of the atoms. Initial velocities are randomly assigned to each particle based on Maxwell-Boltzmann velocity distribution. An initial NVT-MD simulation is performed to equilibrate the system. After the equilibration, Newton's equation is integrated and the positions of each particle in the system are recorded at a pre-specified rate. Nosé-Hoover thermostats are applied to keep the desired temperature and the integration of the system dynamics is based on the explicit N-V-T chain integrator by Martyna et al.[49,50] Thus, Newton's equations are integrated in a canonical ensemble (NVT) instead of a microcanonical ensemble (NVE). To describe the dynamics of rigid, linear molecules, the MD algorithm of Ciccotti et al.[51] is used. The so-called order *N* algorithm is implemented to calculate the self diffusivity, the corrected diffusivity and the Onsager coefficients from the saved trajectories.[47] We describe these diffusivity coefficients in the next section.

Although MD is a powerful technique to study diffusion of gas molecules in nanoporous structures, it is typically limited to diffusion rates higher than 10^{-8} cm^2/s.[47,48] There are other approaches such as Kinetic Monte Carlo (KMC)[52,53] and Transition State Theory (TST)[54,55] to overcome this limitation. Since the diffusion of gas molecules in MOF structures that we studied are fast enough to be captured by MD, we have used MD simulations to calculate several different types of diffusion coefficients. We introduce these diffusion coefficients below. Other specific details of MD simulations are reported in the following chapters.

2.3.1 Diffusion Coefficients

This section is a summary of well established results to describe several diffusion coefficients.[48,56] We have introduced the transport diffusivity coefficient in Equation 2.1.

The transport diffusivity, which is also known as Fickian diffusivity or chemical diffusivity, can be defined without approximation in terms of corrected diffusivity, D_o, and a thermodynamic correction factor, a partial derivative relating the adsorbate concentration, c, and bulk phase fugacity, f,

$$D_t(c) = D_o(c)\left(\frac{\partial \ln f}{\partial \ln c}\right)_T . \qquad 2.15$$

The thermodynamic correction factor is fully defined once the single component adsorption isotherm is known. Well developed approaches exist for calculating the corrected diffusion coefficient from MD simulations.[48,56-58] For systems with a single adsorbed component, the corrected diffusivity is equivalent to the Maxwell-Stefan diffusion coefficient.[22,59,60] The corrected diffusivity, D_o, includes information on the collective motion of multiple adsorbed molecules that is relevant to net mass transport and can be calculated from:[48,56]

$$D_{o,i} = \lim_{t\to\infty} \frac{1}{6Nt}\left\langle \left(\sum_{l=1}^{N_i} \left[r_{il}(t) - r_{il}(0) \right] \right)^2 \right\rangle \qquad 2.16$$

Here, N is the number of molecules, r_{il} (t) is the three-dimensional position vector of molecule l of species i at time t and the angular brackets denote that the ensemble average.

Another, more microscopic measure of diffusion is the self diffusion coefficient, which describes the motion of individual, tagged particles and in an isotropic three dimensional material it is related to the mean squared displacement of tagged particles by the Einstein relation:

$$D_{self,i} = \lim_{t\to\infty} \frac{1}{6t} \left\langle \frac{1}{N_t} \sum_{l=1}^{N_i} \left[r_{il}(t) - r_{il}(0) \right]^2 \right\rangle \qquad 2.17$$

This definition of self diffusivity is applicable to both single component and multi-component systems.[61] In general, all three diffusion coefficients described here, transport, corrected and self diffusivities are the functions of concentration and they are only equal in the limit of dilute concentrations.[22] In some extreme cases, the self and corrected diffusivities vary by orders of magnitude.[25,62]

As we described in the earlier sections, Onsager coefficients are one powerful way to define multi-component diffusion. We use the method by Theodorou et al. [63] to calculate the Onsager coefficient matrix:

$$L_{ij} = \frac{1}{6Vk_BT} \lim_{t\to\infty} \frac{1}{t} \left\langle \sum_{l=1}^{N_i} \left(r_{il}(t) - r_{il}(0) \right) \cdot \sum_{k=1}^{N_j} \left(r_{jk}(t) - r_{jk}(0) \right) \right\rangle \qquad 2.18$$

In this formulation, V is the subsystem volume, k_B is the Boltzman constant, T is temperature, $r_{il}(t)$ is the three-dimensional position vector of molecule l of species i at time t and N_i is the number of molecules of species i. The Onsager coefficients and the matrix of Fickian coefficients are mathematically equivalent and they are related to each other without approximation by expressions involving derivatives of the mixture adsorption isotherm for the adsorbed species.

2.4 References

(1) Krishna, R. *Chem. Eng. Sci.* **1990**, *45*, 1779.

(2) Krishna, R. *Chem. Eng. Sci.* **1993**, *48*, 845.

(3) Krishna, R.; van den Broeke, L. J. P. *Chem. Eng. J.* **1995**, *57*, 155.

(4) Wesselingh, J. A.; Krishna, R. *Mass Transfer in Multicomponent Mixtures*; Delft University Press: Delft, 2000.

(5) Li, S.; Falconer, J. L.; Noble, R. D.; Krishna, R. *Ind. Eng. Chem. Res.* **2007**, *46*, 3904.

(6) Kapteijn, F.; Bakker, W. J. W.; Zheng, G.; Poppe, J.; Moulijn, J. *Chem. Eng. J.* **1995**, *57*, 145.

(7) van den Broeke, L. J. P. *AIChE J.* **1995**, *41*, 2399.

(8) Pohl, P. I.; Heffelfinger, G. S.; Smith, D. M. *Mol. Phys.* **1996**, *89*, 1725.

(9) Takaba, H.; Koshita, R.; Mizukami, K.; Oumi, Y.; Ito, N.; Kubo, M.; Fahmi, A.; Miyamoto, A. *J. Membrane Sci.* **1997**, *134*, 127.

(10) Pohl, P. I.; Heffelfinger, G. S. *J. Membrane Sci.* **1999**, *155*, 1.

(11) Matsukata, M.; Kikuchi, E. *Bull. Chem. Soc. Japan* **1997**, *70*, 2341.

(12) Coronas, J.; Santamaria, J. *Sep. Purif. Meth.* **1999**, *28*, 127.

(13) Ahunbay, M. G.; Elliot, J. R.; Talu, O. *J. Phys. Chem. B* **2002**, *106*, 5163.

(14) Martin, M. G.; Thompson, A. P.; Nenoff, T. M. *J. Chem. Phys.* **2001**, *114*, 7174.

(15) Newsome, D. A.; Sholl, D. S. *J. Phys. Chem. B* **2005**, *109*, 7237.

(16) Newsome, D. A.; Sholl, D. S. *Nano Lett.* **2006**, *6*, 2150.

(17) Liu, Y.; Ng, Z.; Khan, E. A.; Jeong, H.-K.; Ching, C.-B.; Lai, Z. *Micropor. Mesopor. Mater.* **2009**, *118*, 296.

(18) Skoulidas, A. I.; D. S. Sholl; Bowen, T. C.; Doelling, C.; Falconer, J. L.; Noble, R. D. *J. Membr. Sci.* **2003**, *227*, 123.

(19) Chen, H.; Sholl, D. S. *J. Am. Chem. Soc.* **2004**, *126*, 7778.

(20) Chen, H.; Sholl, D. S. *J. Membr. Sci.* **2006**, *269*, 152.

(21) Sholl, D. S. *Ind. Eng. Chem. Res.* **2000**, *39*, 3737.

(22) Sholl, D. S. *Acc. Chem. Res.* **2006**, *39*, 403.

(23) Krishna, R. *Chem. Eng. Science* **1990**, *45*, 1779.

(24) Skoulidas, A. I.; Sholl, D. S. *J. Phys. Chem. B* **2002**, *106*, 5058.

(25) Skoulidas, A. I.; Ackerman, D. M.; Johnson, J. K.; Sholl, D. S. *Phys. Rev. Lett.* **2002**, *89*, 185901.

(26) Ahunbay, M. G.; Elliott, J. R.; Talu, O. *J. Phys. Chem. B* **2004**, *108*, 7801.

(27) Martin, M. G.; Thompson, A. P.; Nenoff, T. M. *J. Chem. Phys.* **2001**, *114*, 7174.

(28) Ahunbay, M. G.; Elliott, J. R.; Talu, O. *J. Phys. Chem. B* **2002**, *106*, 5163.

(29) Skoulidas, A. I.; Sholl, D. S. *AIChE J.* **2005**, *51*, 867.

(30) Krishna, R.; van den Broeke, L. J. P. *Chem. Eng. J.* **1995**, *57*, 155.

(31) Onsager, L. *Phys. Rev.* **1931**, *38*, 2265.

(32) Onsager, L. *Phys. Rev.* **1931**, *37*, 405.

(33) Duncan, J. B.; Toor, H. L. *AIChE J.* **1962**, *8*, 38.

(34) Krishna, R.; van Baten, J. M. *Ind. Eng. Chem. Res.* **2006**, *45*, 2084.

(35) Skoulidas, A. I.; Sholl, D. S.; Krishna, R. *Langmuir* **2003**, *19*, 7977.

(36) Chen, H.; Sholl, D. S. *J. Membrane Sci.* **2006**, *269*, 152.

(37) Heuchel, M.; Snurr, R. Q.; Buss, E. *Langmuir* **1997**, *13*, 6795.

(38) Goj, A.; Sholl, D. S.; Akten, E. D.; Kohen, D. *J. Phys. Chem. B* **2002**, *106*, 8367.

(39) Sarkisov, L.; Düren, T.; Snurr, R. Q. *Mol. Phys.* **2004**, *102*, 211.

(40) Garberoglio, G.; Skoulidas, A. I.; Johnson, J. K. *J. Phys. Chem. B* **2005**, *109*, 13094.

(41) Yang, Q.; Zhong, C. *J. Phys. Chem. B* **2005**, *109*, 11862.

(42) Jiang, J.; Sandler, S. I. *Langmuir* **2006**, *22*, 5702.

(43) Jung, D.; Kim, D.; Lee, T. B.; Choi, S. B.; Yoon, J. H.; Kim, J.; Choi, K.; Choi, S.-H. *J. Phys. Chem. B* **2006**, *110*, 22987.

(44) Yue, X. P.; Yang, X. N. *Langmuir* **2006**, *22*, 3138.

(45) Ramsahye, N.; Maurin, G.; Bourrelly, S.; Llewellyn, P.; Devic, T.; Serre, C.; Loiseau, T.; Ferey, G. *Adsorption* **2007**, *13*, 461.

(46) Keskin, S.; Liu, J.; Rankin, R. B.; Johnson, J. K.; Sholl, D. S. *Ind. Eng. Chem. Res.* **2009**, *48*, 2355.

(47) Frenkel, D.; Smit, B. *Understanding Molecular Simulation: From Algorithms to Applications*, 2nd ed.; Academic Press: San Diego, 2002.

(48) Keil, F. J.; Krishna, R.; Coppens, M. O. *Rev. Chem. Eng.* **2000**, *16*, 71.

(49) Martyna, G. J.; Klein, M. L.; Tuckerman, M. *J. Chem. Phys.* **1992**, *97*, 2635.

(50) Martyna, G. J.; Tuckerman, M. E.; Tobias, D. J.; Klein, M. L. *Mol. Phys.* **1996**, *87*, 1117.

(51) Ciccotti, G.; Ferrario, M.; Ryckaert, J.-P. *Mol. Phys.* **1982**, *47*, 1253.

(52) Fichthorn, K. A.; W.H., W. *J. Chem. Phys.* **1991**, *95*, 1090.

(53) Kamakoti, P.; Sholl, D. S. *Phys. Rev. B* **2005**, *71*, 014301.

(54) Tunca, C.; Ford, D. M. *J. Chem. Phys.* **1999**, *111*, 2751.

(55) Tunca, C.; Ford, D. M. *J. Chem. Phys.* **2004**, *120*, 10763.

(56) Kärger, J.; Ruthven, D. *Diffusion in Zeolites and Other Microporous Materials*; John Wiley & Sons: New York, 1992.

(57) Skoulidas, A. I.; Sholl, D. S. *J. Phys. Chem. A* **2003**, *107*, 10132.

(58) Skoulidas, A. I.; Sholl, D. S. *J. Phys. Chem. B* **2005**, *109*, 15760.

(59) Ruthven, D. M. *Principles of Adsorption and Adsorption Processes.*; Wiley: New York, 1984.

(60) Kapteijn, F.; Moulijn, J. A.; Krishna, R. *Chem. Eng. Sci.* **2000**, *55*, 2923.

(61) Sanborn, M. J.; Snurr, R. Q. *Sep. Purif. Technol.* **2000**, *20*, 1.

(62) Ackerman, D. M.; Skoulidas, A. I.; Sholl, D. S.; Johnson, J. K. *Molecular Simulation* **2003**, *29*, 677.

(63) Theodorou, D. N.; Snurr, R. Q.; Bell, A. T. *Molecular Dynamics and Diffusion in Microporous Materials. In Comprehensive Supramolecular Chemistry*; Pergamon Press: New York, 1996; Vol. 7.

CHAPTER 3

MODELING BINARY GAS MIXTURE SEPARATIONS USING IRMOF-1 MEMBRANES

In contrast to the growing body of adsorption data for metal organic frameworks (MOFs), very little information is available for molecular transport in the same materials. Because characterizing the performance of a membrane requires information both on adsorption and diffusion, it has not been possible to predict whether MOFs have useful properties when used as membranes for gas separations. In this chapter, we describe atomistic simulations used to examine the properties of IRMOF-1, one of the most widely known MOFs, for membrane based multi-component gas mixture separations. This study provides the first predictions of any kind about the potential of MOFs as membranes and demonstrates that using molecular modeling for this purpose can be a useful means of identifying the phenomena that control the performance of MOFs as membranes. We have used atomistic calculations to predict the performance of an IRMOF-1 membrane for separation of CO_2/CH_4, CO_2/H_2, CO_2/N_2, CH_4/H_2, N_2/H_2, and N_2/CH_4 mixtures at room temperature. Mixtures of these gases are relevant in a number of large-scale industrial applications. For example, separation of CO_2 and N_2 from CH_4 is important in natural gas purification, while CO_2/N_2 separation is a key issue in carbon capture from flue gas. CO_2/H_2, CH_4/H_2, and N_2/H_2 mixtures are all relevant for hydrogen recovery from plants and refineries.

3.1 Computational Details

All of our calculations are based on atomistic simulations of single component adsorption and diffusion properties of the gases of interest in IRMOF-1, which is also known as MOF-5. We used the results from the previous atomic simulations for CO_2, CH_4, H_2 and N_2 in IRMOF-1 at room temperature by Skoulidas and Sholl.[1] In these simulations, single component adsorption isotherms of CO_2, CH_4, H_2 and N_2 were computed using Grand Canonical Monte Carlo (GCMC) simulations. In addition, equilibrium molecular dynamics (MD) was used to compute the loading-dependent self and corrected diffusion coefficients of the same four species when adsorbed as single components. IRMOF-1 was assumed to be rigid and its structure was taken from experimental data.[2] CH_4 and H_2 were modeled as spherical Lennard-Jones potentials whereas CO_2 was modeled using the EPM2 model, an all atom model with Lennard-Jones potentials and atomic charges to approximate the quadrupole moment of CO_2.[3] A similar potential with partial charges was used for N_2.[4] Recent work has suggested that including framework flexibility may give more accurate results than holding the framework rigid,[5,6] but the extensive diffusion data needed to describe permeation of gas mixtures through membranes is not yet available from any simulations that include these effects.

The simulation data of Skoulidas and Sholl gives no direct information on the properties of adsorbed mixtures in IRMOF-1, but this situation is of course of great importance for considering practical applications of membranes. Mixture adsorption can be simulated quite efficiently using GCMC, and several groups have used this approach to examine mixture adsorption in MOFs.[7-10] Molecular simulation techniques are also

available to examine mixture diffusion in nanoporous materials.[11,12] Unfortunately, the computational effort required to determine the mixture diffusion coefficients relevant to net mass transfer in mixtures is considerable. To date, there are only a few molecular simulation studies of mixture diffusion in MOFs.[13,14] Even if atomistic simulations of binary diffusion were performed, an additional complication arises if the performance of a membrane is to be predicted. These simulations can at best provide data at a series of discrete state points. This complication also exists if GCMC simulations of binary adsorption are to be used. To describe mixture permeance through a membrane at a variety of operating conditions, however, the properties of the adsorbed mixtures must be specified at all conditions that exist at any location within the membrane.[15,16] In the remainder of this section, we describe how functions describing these properties are determined from the single component calculations of Skoulidas and Sholl.

Binary adsorption isotherms are described by applying Ideal Adsorbed Solution Theory (IAST) to the single component isotherms computed from GCMC data of Skoulidas and Sholl. Although multi-component adsorption can be assessed experimentally, performing this kind of experiments for a full range of operating conditions is time consuming. However, performing accurate experiments to characterize single component adsorption is relatively straightforward. As a result of this fact, many studies have been done to develop methods to predict multi-component adsorption from single component data.[17] The best known of these methods is IAST, a well developed technique to describe the calculation of the adsorption equilibria for components in a gaseous mixture, using only data for the pure component adsorption equilibria at the same temperature and on the same adsorbent.[18] IAST was originally derived from a

theory for a two dimensional homogenous adsorbed phase with a temperature invariant area that is equally accessible to all components. IAST treats each component in the adsorbed mixture as the components of an ideal mixture. As a result, IAST is frequently somewhat inaccurate at high densities of the adsorbed species, even for relatively ideal gas phase mixtures. Detailed discussions of the implementation and precision of IAST are available.[19,20] This theory is known to work accurately in many nanoporous materials except in materials which have strong energetic or geometric heterogeneity.[19,21] Furthermore, IAST has been tested recently for adsorption of light gases in IRMOF-1[8,10] and in CuBTC[14] by comparing the results of binary molecular simulations and the predictions of theory. The outcome of these tests shows that IAST successfully describes the adsorption of several gas mixtures in IRMOF-1 and CuBTC. The details of application of IAST in MOFs are discussed in Chapter 5 and Chapter 6.

Practical application of IAST requires that the functional form of the single component isotherms must be specified. In our calculations, single component adsorption isotherms are fitted to molecular simulation data obtained over a finite range of pressures. A dual-site Langmuir (Langmuir-Freundlich) model was used to fit the single component adsorption isotherms of CH_4, H_2 and N_2 (CO_2). These isotherms are reported in terms of ideal gas pressures, so fugacity corrections would be necessary to connect the highest pressures reported by Skoulidas and Sholl with real gas pressures. The resulting isotherms are

$$C_i = \frac{a_i P_i}{b_i + P_i} + \frac{c_i P_i}{d_i + P_i} \qquad 3.1$$

$$C_{CO_2} = \frac{eP^f}{g + P^f} \qquad 3.2$$

where C is the adsorbed amount (molecules/unit cell), P is the pressure (bar), i is CH_4, H_2 or N_2 and the remaining are parameters. The values of these parameters are listed in Table 3.1. Figure 3.1 shows the single component adsorption isotherm of each species at room temperature. Symbols represent the single component GCMC simulation results of Skoulidas and Sholl and the lines are the adsorption models described above.

Table 3.1 Values and units of single component isotherm parameters.

Parameters	Units	Values
CH_4		
a	molecules/unit cell	51.65
b	bar	4667
c	molecules/unit cell	168.4
d	bar	39.56
H_2		
a	molecules/unit cell	409.8
b	bar	4561
c	molecules/unit cell	197.6
d	bar	461.0
N_2		
a	molecules/unit cell	159.4
b	bar	94.95
c	molecules/unit cell	99.04
d	bar	8406
e	molecules/unit cell	174.8
f	-	2.151
g	bar	61.27

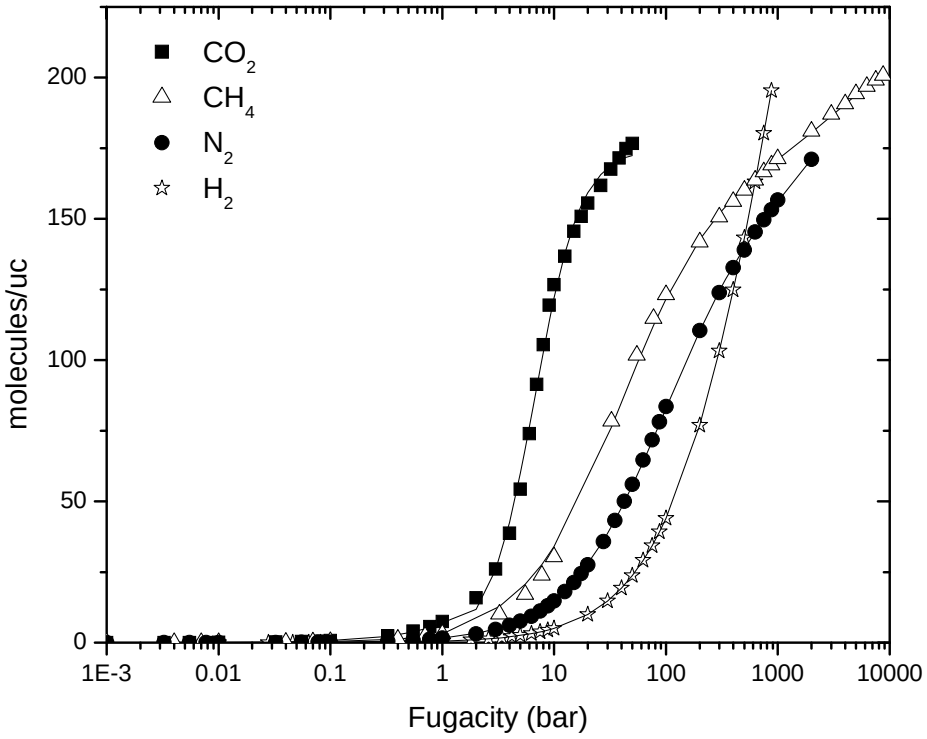

Figure 3.1 Predicted single component adsorption isotherms of CO_2, CH_4, H_2 and N_2 in IRMOF-1 at room temperature as a function of fugacity. Filled symbols (lines) show results for GCMC simulation (fitted adsorption models).

Based on the single-component adsorption isotherms defined above, binary adsorption data is generated using IAST. To use the binary isotherm efficiently within the membrane calculations, binary adsorption data from a large collection of state points calculated using IAST is fitted to a continuous functional form. For mixtures of CO_2/CH_4, CO_2/H_2, CO_2/N_2, a functional form combining the dual-site Langmuir and Freundlich isotherms is used, while a dual site Langmuir model is used for CH_4/H_2, N_2/H_2 and N_2/CH_4 mixtures. The extended dual site Langmuir and combined dual-site

Langmuir and Freundlich isotherm models are given in Equations 3.3-3.4 and Equations 3.5-3.6, respectively.

$$C_i = \frac{a_1 P_i}{a_2 P_i + a_3 P_j + a_4} + \frac{a_5 P_i}{a_6 P_i + a_7 P_j + a_8} \tag{3.3}$$

$$C_j = \frac{b_1 P_j}{b_2 P_i + b_3 P_j + b_4} + \frac{b_5 P_j}{b_6 P_i + b_7 P_j + b_8} \tag{3.4}$$

$$C_i = \frac{a_1 P_i^{a_2}}{a_3 P_i^{a_2} + a_4 P_j^{a_5} + a_6} + \frac{a_7 P_i}{a_8 P_i + a_9 P_j + a_{10}} \tag{3.5}$$

$$C_j = \frac{b_1 P_j^{b_2}}{b_3 P_j^{b_2} + b_4 P_i^{b_5} + b_6} + \frac{b_7 P_j}{b_8 P_i + b_9 P_j + b_{10}} \tag{3.6}$$

Here, C_i is the adsorbed amount (molecules/unit cell), P_i is the partial pressure of species *i* (bar) and the remaining symbols are parameters of the model. The IAST data set used in this fitting was obtained using various mixture compositions (from 0.1 to 0.9 at 9 different compositions) and a wide range of total pressures (from 0.1 bar up to 100 bar at 28 different pressures). The numerical values of the parameters in the binary adsorption isotherm are listed in Table 3.2 and 3.3. The comparisons of the fitting functions used to describe binary adsorption of mixtures in IRMOF-1 at 298 K with the IAST-based dataset are given in Figure 3.2.

Table 3.2 Values and units of extended dual site Langmuir isotherm parameters.

Species 1	Values	Species 2	Values	Units
H_2		**CH_4**		
a_1	1.3991	b_1	0.4420	molecules/unit cell
a_2	0.0064	b_2	0.8205	-
a_3	0.0497	b_3	1.0287	-
a_4	2.6906	b_4	102.4426	bar
a_5	1.9×10^{-5}	b_5	1.2218	molecules/unit cell
a_6	-0.0857	b_6	-2.2×10^{-4}	-
a_7	0.4918	b_7	0.0059	-
a_8	2.5204	b_8	0.3915	bar
H_2		**N_2**		
a_1	1.2249	b_1	0.9076	molecules/unit cell
a_2	0.0047	b_2	0.0017	-
a_3	0.0188	b_3	0.0057	-
a_4	2.3541	b_4	0.5351	bar
a_5	-0.0008	b_5	-0.2230	molecules/unit cell
a_6	-0.1828	b_6	2.0072	-
a_7	0.6686	b_7	2.8350	-
a_8	2.2751	b_8	1.7653	bar
N_2		**CH_4**		
a_1	2.37×10^{-5}	b_1	1.6156	molecules/unit cell
a_2	-1.80×10^{-7}	b_2	-0.0003	-
a_3	8.90×10^{-7}	b_3	0.0079	-
a_4	7.02×10^{-5}	b_4	0.5274	bar
a_5	6.37×10^{-5}	b_5	0.2315	molecules/unit cell
a_6	2.32×10^{-5}	b_6	-0.0022	-
a_7	1.29×10^{-5}	b_7	0.0561	-
a_8	5.17×10^{-5}	b_8	3.739	bar

Table 3.3 Values and units of combined dual site Langmuir and Freundlich isotherm parameters.

Species 1	Values	Species 2	Values	Units
CO_2		**CH_4**		
a_1	0.4223	b_1	10.02	molecules/unit cell
a_2	2.133	b_2	2.397	-
a_3	0.004091	b_3	0.862	-
a_4	0.003944	b_4	2.893×10^{-8}	-
a_5	1.157	b_5	7.957	-
a_6	0.2677	b_6	4.993	bar
a_7	3.586	b_7	31.93	molecules/unit cell
a_8	0.05039	b_8	0.188	-
a_9	0.03740	b_9	0.960	-
a_{10}	0.5128	b_{10}	10.22	bar
CO_2		**N_2**		
a_1	1.433	b_1	6.647	molecules/unit cell
a_2	2.407	b_2	4.538	-
a_3	0.0133	b_3	1.8159	-
a_4	0.2685	b_4	7×10^{-8}	-
a_5	0.4545	b_5	10.12	-
a_6	1.197	b_6	9.653	bar
a_7	10.03	b_7	14.15	molecules/unit cell
a_8	0.0880	b_8	0.0584	-
a_9	0.1189	b_9	1.076	-
a_{10}	1.434	b_{10}	9.011	bar
CO_2		**H_2**		
a_1	1.510	b_1	0.206	molecules/unit cell
a_2	3.018	b_2	2.656	-
a_3	0.110	b_3	0.116	-
a_4	14.432	b_4	1.9×10^{-6}	-
a_5	0.432	b_5	7.317	-
a_6	16.044	b_6	5.135	bar
a_7	17.925	b_7	8.981	molecules/unit cell
a_8	0.108	b_8	0.128	-
a_9	0.185	b_9	0.914	-
a_{10}	2.564	b_{10}	18.711	bar

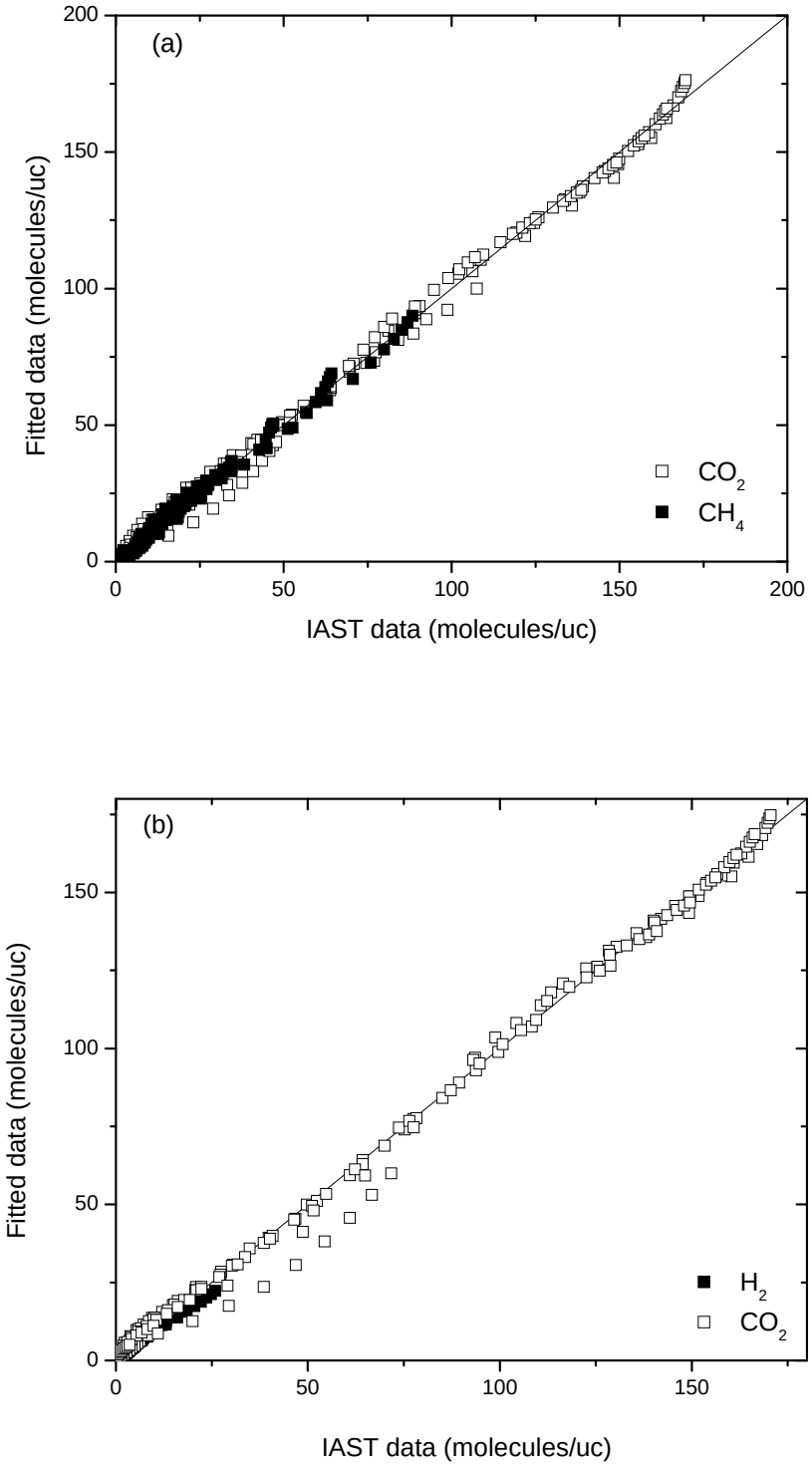

Figure 3.2 A comparison of the fitting functions used to describe binary adsorption of (a) CO_2/CH_4, (b) CO_2/H_2, (c) CO_2/N_2, (d) CH_4/H_2, (e) H_2/N_2, and (f) CH_4/N_2 in IRMOF-1 at 298 K with the IAST-based dataset used to determine these functions.

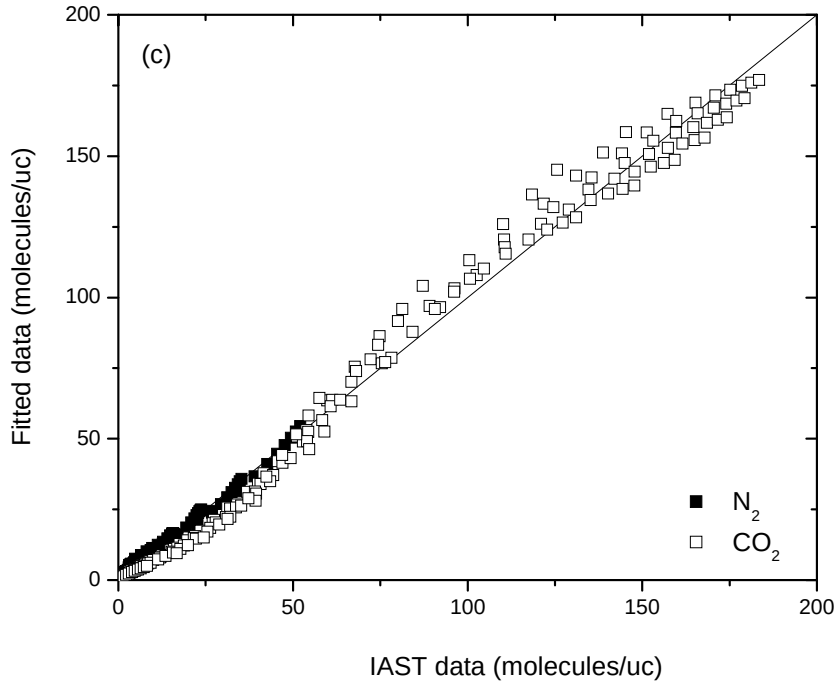

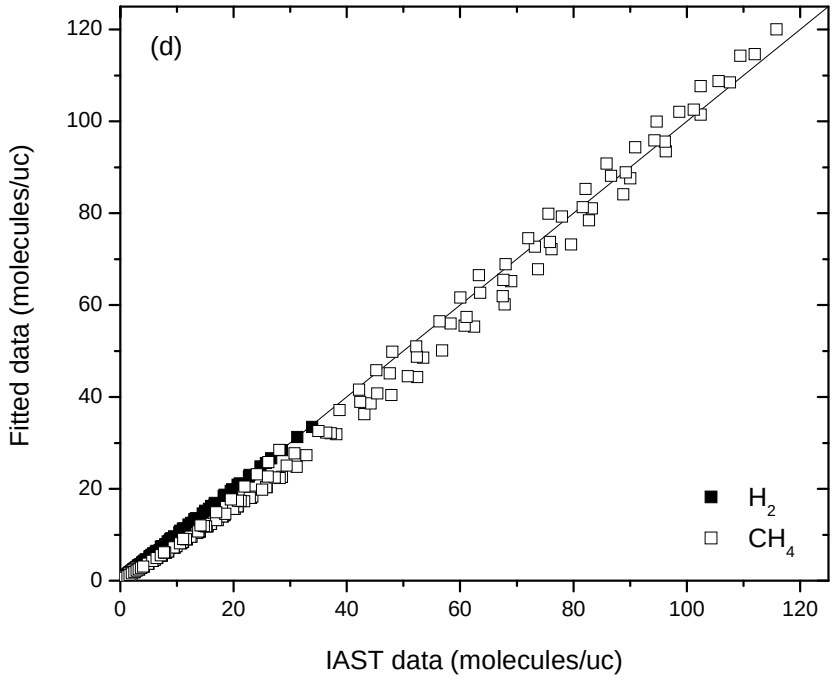

Figure 3.2 Continued

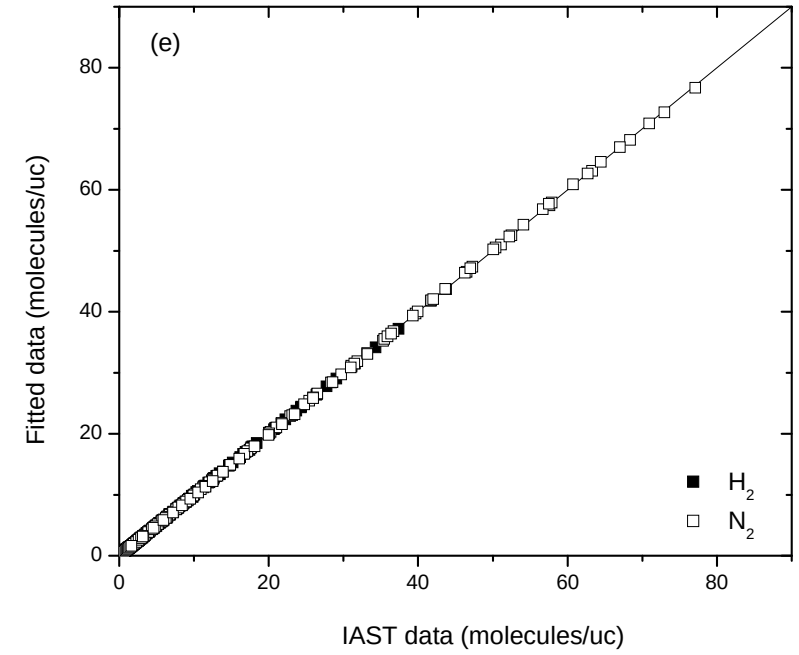

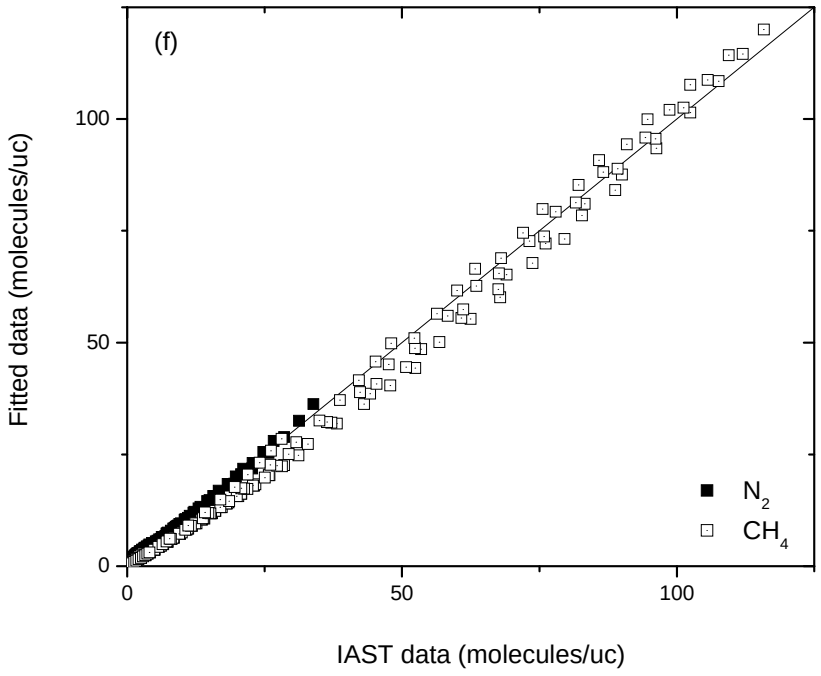

Figure 3.2 Continued

To quantify mixture diffusion in IRMOF-1, the mixing theory of Skoulidas, Sholl, and Krishna (SSK) was applied. This approach combines information from the loading-dependence of the single component self and Maxwell-Stefan diffusivities with the binary adsorption isotherm to predict the loading- and composition-dependent matrix of binary diffusion coefficients.[22] Prior tests of the SSK approach by comparison with detailed atomistic simulations of binary diffusion in silica zeolites and carbon nanotubes indicate this approach is accurate for a wide variety of adsorbed mixtures.[23-27] We test this method for CH_4/H_2 mixtures in another MOF, CuBTC, in Chapter 5 and show that the predictions of the SSK approach are in good agreement with our direct molecular simulations of binary diffusion, suggesting that this approach may be a powerful one for examining multi-component diffusion in MOFs.[14] We expect similar levels of agreement with the SSK approach and binary diffusivity simulations for IRMOF-1 since IRMOF-1 has a more energetically homogenous structure than CuBTC, which includes several energetically different adsorption sites and unsaturated metal corners.

To apply the SSK method, functions describing the single component self and corrected diffusivities of CO_2, CH_4, H_2 and N_2 as a function of their fractional loading are needed. Skoulidas and Sholl[1] computed these two distinct diffusion coefficients for the adsorbed gases of interest in IRMOF-1 using equilibrium Molecular Dynamics. They also calculated the transport diffusion coefficients of various gas species in IRMOF-1 by separately computing the adsorption isotherm and the loading-dependent corrected diffusion coefficients. Self diffusivities (D_{self}) and corrected diffusivities (D_O) of each species in IRMOF-1 obtained from MD simulation of Skoulidas and Sholl are fitted to exponential functions and polynomials:

$$D_{O,CO_2} = A_1 + A_2\theta_{CO_2} + A_3{\theta_{CO_2}}^2 + A_4{\theta_{CO_2}}^3 + A_5{\theta_{CO_2}}^4 \quad 3.7$$

$$D_{O,CH_4} = B_1 + B_2\theta_{CH_4} + B_3{\theta_{CH_4}}^2 + B_4{\theta_{CH_4}}^3 \quad 3.8$$

$$D_{O,H_2} = F_1 + F_2\theta_{H_2} + F_3{\theta_{H_2}}^2 \quad 3.9$$

$$D_{O,N_2} = G_1 + G_2\theta_{N_2} + G_3{\theta_{N_2}}^2 \quad 3.10$$

$$D_{self,CO_2} = R_2 + \frac{(R_1 - R_2)}{1 + \exp((\theta_{CO_2} - R_3)/R_4)} \quad 3.11$$

$$D_{self,CH_4} = S_2 + \frac{(S_1 - S_2)}{1 + \exp((\theta_{CH_4} - S_3)/S_4)} \quad 3.12$$

$$D_{self,H_2} = M_1 + M_3\exp(-(\theta_{H_2} - M_2)/M_4) + M_5\exp(-(\theta_{H_2} - M_2)/M_6) \quad 3.13$$

$$D_{self,N_2} = N_1 \cdot \exp(-\theta_{N_2}/N_2) + N_3 + N_4 \cdot \theta_{N_2} \quad 3.14$$

These functions are written in terms of fractional coverage ($\theta_i = C_i / C_{i,sat}$) where C_i is the loading of species (molecules/unit cell) and $C_{i,sat}$ is the saturation loading of the species as defined by the single component isotherms in Equations 3.1 and 3.2. These functions are fitted to the MD data with two constraints. First, each function is constrained to give the observed self diffusion coefficient at zero loading. The self diffusion coefficient can in general be computed more precisely than the corrected diffusivity. It is well known, however, that these two quantities must coincide exactly at zero loading.[23,28,29] Second, both diffusivities are assumed to vanish at the saturation

loading predicted by the fitted single component adsorption isotherms. The numerical values of the parameters in these fitting functions are listed in Table 3.4.

Table 3.4 Values and units of fitting functions for diffusivities as defined in Equations 3.7-3.14.

Parameters	Values	Units	Parameters	Values	Units
A_1	1.50×10^{-4}	cm^2/s	R_1	1.55×10^{-4}	cm^2/s
A_2	-1.00×10^{-5}	cm^2/s	R_2	-6.00×10^{-5}	cm^2/s
A_3	1.12×10^{-3}	cm^2/s	R_3	7.91×10^{-1}	-
A_4	-2.25×10^{-3}	cm^2/s	R_4	2.26×10^{-1}	-
A_5	9.90×10^{-4}	cm^2/s	S_1	2.90×10^{-4}	cm^2/s
B_1	2.80×10^{-4}	cm^2/s	S_2	-1.00×10^{-5}	cm^2/s
B_2	4.80×10^{-4}	cm^2/s	S_3	5.02×10^{-1}	-
B_3	-4.40×10^{-4}	cm^2/s	S_4	1.60×10^{-1}	-
B_4	-3.20×10^{-4}	cm^2/s	M_1	-9.00×10^{-5}	cm^2/s
F_1	2.19×10^{-3}	cm^2/s	M_2	-6.01×10^{-3}	-
F_2	-2.70×10^{-4}	cm^2/s	M_3	8.00×10^{-1}	cm^2/s
F_3	-1.92×10^{-3}	cm^2/s	M_4	5.90×10^{-4}	-
G_1	3.3×10^{-4}	cm^2/s	M_5	2.29×10^{-3}	cm^2/s
G_2	2.9×10^{-4}	cm^2/s	M_6	3.1×10^{-1}	-
G_3	-6.2×10^{-4}	cm^2/s	N_1	1.06×10^{-2}	cm^2/s
			N_2	6.436	-
			N_3	-1.02×10^{-2}	cm^2/s
			N_4	1.19×10^{-3}	cm^2/s

The self and corrected diffusivities of each species in IRMOF-1 at room temperature as a function of fractional loading and smooth functions describing these diffusivities are given in Figure 3.3. Symbols show the data from the MD simulations of Skoulidas and Sholl, while curves show the fitting functions defined in the text. As might be expected, H_2 has the highest self and corrected diffusivity compared to larger and more sluggish CO_2. CH_4 and N_2 have very similar diffusivities at low pressures whereas at high pressures, CH_4 diffuses faster than N_2.

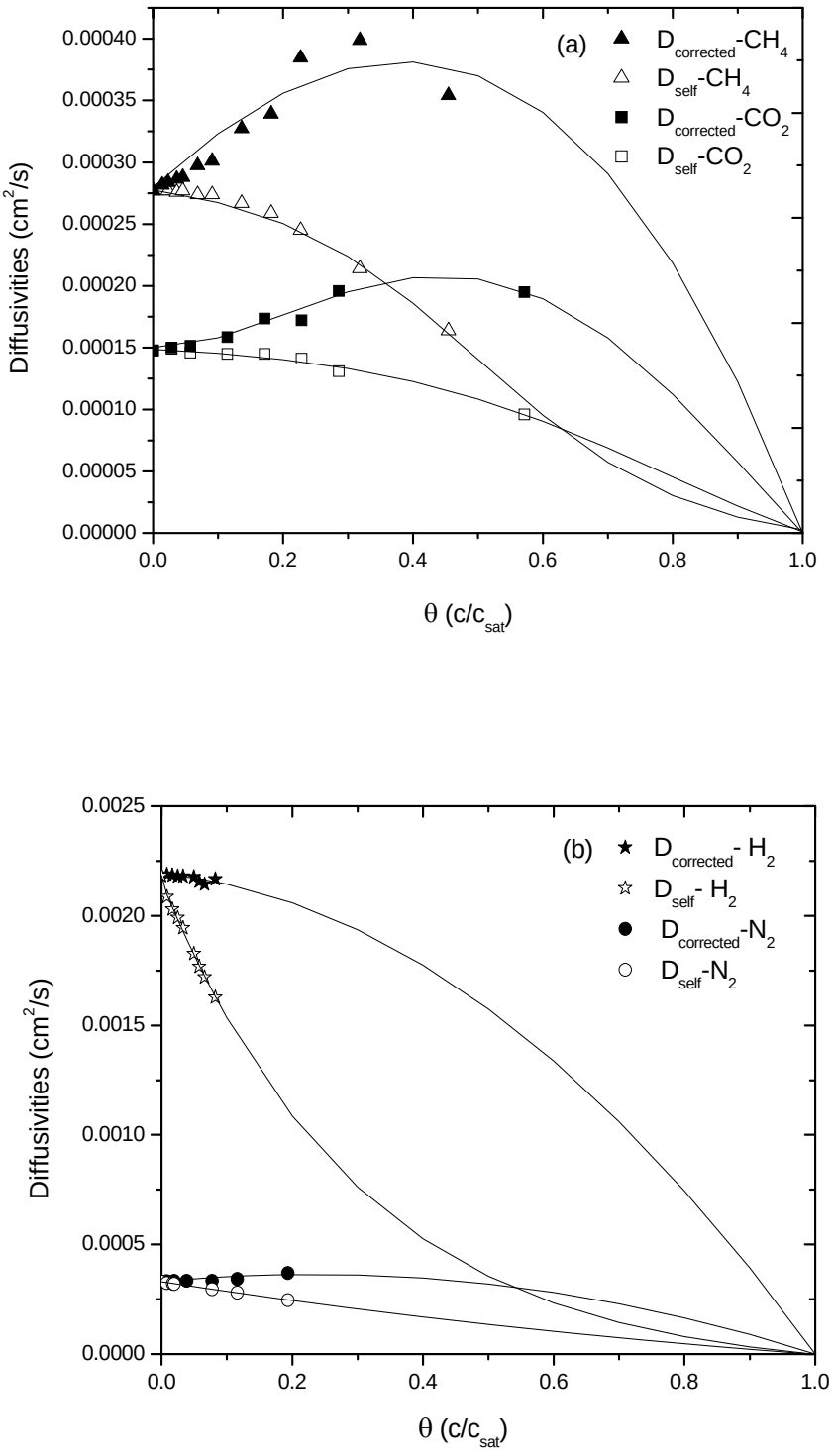

Figure 3.3 Self and corrected diffusion coefficients of single-component (a) CO_2 and CH_4 (b) H_2 and N_2 in IRMOF-1 at 298 K as a function of fractional loading.

3.2 Single Component Gas Permeation

We consider membranes where transport of gas molecules occurs by adsorption and diffusion through IRMOF-1. We assume that our membrane is composed of defect-free, single crystal IRMOF-1. In all membrane calculations, transport resistances associated with the molecules entering and leaving the pores of IRMOF-1 are neglected, thus the concentration of the adsorbates at the boundaries of the membrane is defined from the binary adsorption isotherms.[30] This assumption is known to be accurate for sufficiently thick membranes although deviations from this situation can occur for ultra-thin membranes.[31-33] The thickness of the model IRMOF-1 membrane is taken as 10 μm in all calculations.

We first examine the single component permeance of each component through our model membrane. The predicted permeances are shown as a function of fugacity for a fixed transmembrane pressure drop of 1 bar and for a pressure drop equal to 80% of the feed pressure in Figure 3.4a and 3.4b, respectively. Because of the pressure drop used for the results in Figure 3.4a, the values from this figure can also be interpreted as flux in units of mol/m^2.s. In zeolites under similar conditions, single component fluxes are typically decreasing functions of feed pressure since the molecules saturate the narrow pores at high pressures.[34] Because of the large adsorption capacity of IRMOF-1, the CH_4, N_2 and H_2 fluxes are only weakly dependent on pressure under the conditions shown in Figure 3.4.

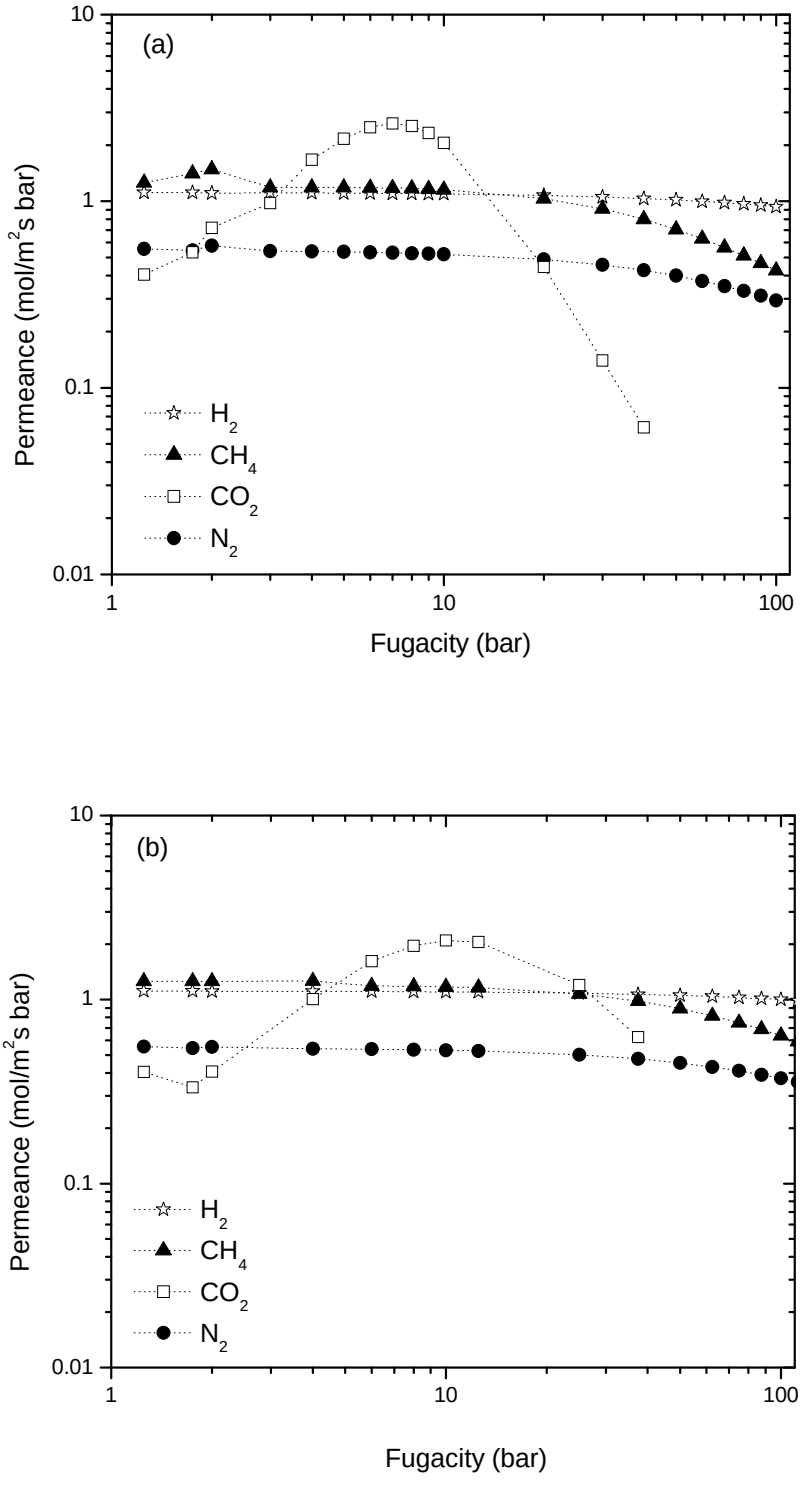

Figure 3.4 Predicted single component fluxes of CO_2, CH_4, H_2 and N_2 across a 10 μm thick IRMOF-1 membrane at room temperature as a function of fugacity. The transmembrane pressure drop is (a) 1 bar (b) equal to 80% of the feed pressure.

The CO_2 flux in Figure 3.4 has a more interesting pressure dependency. Below ~10 bar, the CO_2 flux is an increasing function of pressure whereas at higher pressures it decreases rapidly. The initial increase occurs because of the concentration dependence of the CO_2 diffusion coefficient and curvature in the adsorption isotherm. The decreasing CO_2 flux at higher pressures is dominated by the shape of the adsorption isotherm. Although increasing the pressure drop enhances the flux of species, the permeance values and trends are not significantly different, as can be seen by comparing the Figure 3.4a and 3.4b.

The first continuous and well-intergrown IRMOF-1 membrane was recently prepared on porous alpha-alumina substrate by in-situ solvothermal synthesis.[35] Liu et al. measured the single component permeation of H_2, CH_4, CO_2, N_2 and SF_6 under a constant feed pressure of 800 torr at room temperature through two IRMOF-1 membranes with thicknesses of 25 and 85 μm as well as the blank support.[35] Figure 3.5 compares the experimental measurements of single component gas permeation by Liu et al. and our theoretical predictions for the permeation of the same species under the same conditions. Sample 1 and 2 represents the membranes having thicknesses of 25 and 85 μm, respectively. The permeance of H_2, CH_4, CO_2 and N_2 is plotted as a function of the square root of the inverse of molecular weights of each species. Our theoretical predictions agree well with the experimental results for CH_4, H_2 and N_2 but overestimate the measured permeance values for CO_2 in sample 1.

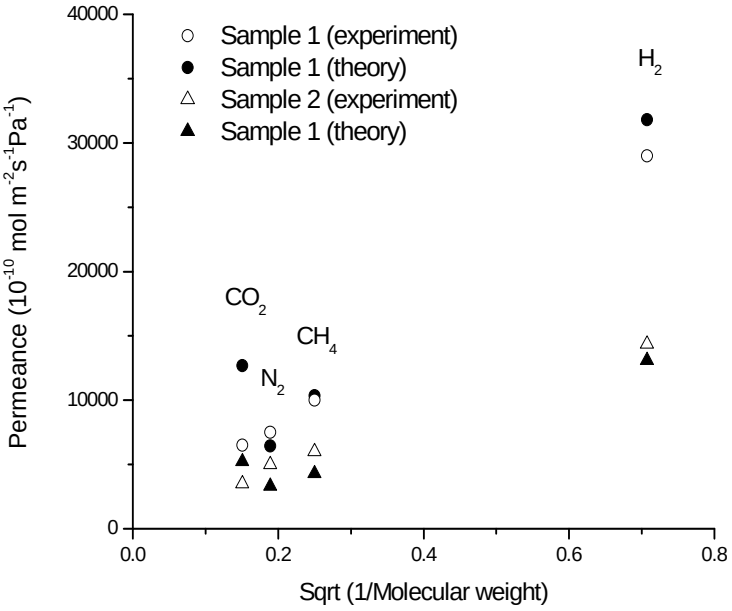

Figure 3.5 Predicted (closed symbols) and measured (open symbols) single component gas permeation results through IRMOF-1 membranes. All experimental data is from Liu et al.[35]

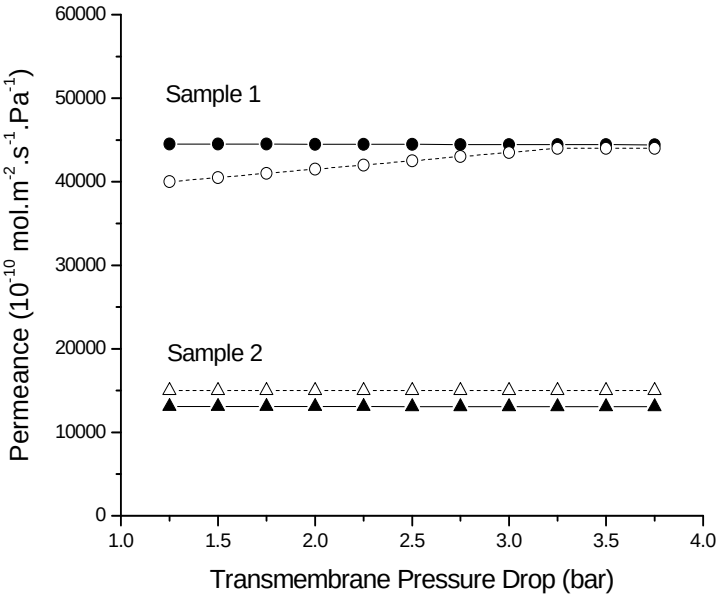

Figure 3.6 Predicted (closed symbols) and measured (open symbols) H_2 permeance results through IRMOF-1 membranes. All experimental data is from Liu et al.[35]

Figure 3.6 shows the experimental measurements and theoretical predictions for H_2 permeance through IRMOF-1 membranes as a function of transmembrane pressure drop. Our theoretical predictions for H_2 permeance under different transmembrane pressure drop agree well with the experiment measurements. Our predictions neglect the influence of microstructure and support in the polycrystalline membranes used experimentally. Bearing this in mind, Figure 3.5 and 3.6 strongly indicate that our theoretical methods make predictions that can be interpreted quantitatively, thus providing a firm bases for using these methods to screen potential membrane materials.

3.3 Binary Gas Mixture Permeations

After defining the binary adsorption isotherms and mixture diffusivities as described above, the steady state permeance of mixtures is calculated by specifying the pressure and composition on the feed side and the pressure on the permeate side of the membrane. The gases in both side of the membrane are assumed to be well mixed. The total pressure on the permeate side is assumed to be controlled by a pressure regulator to mimic a typical experiment. The pressure regulator allows the pressure to rise until the set pressure is reached and it also helps to hold the total pressure constant by allowing well mixed gases to leave. Steady state fluxes are calculated using a shell description of the membrane which assumes that the matrix of Fickian diffusivities is constant at the concentration defined by the arithmetic mean of feed and permeate concentrations.[36] Test calculations involving full integration of the transport equations for the membrane for single-component examples indicated that this shell description gave accurate results.

First, we investigate the adsorption selectivities from equimolar mixtures at room temperature. Adsorption selectivities are defined as:

$$S_{ads(A/B)} = \frac{(x_A / x_B)}{(y_A / y_B)} \qquad 3.15$$

for selectivity of component A relative to component B, where x_A (x_B) is the mole fraction of A (B) in the adsorbed phase and y_A (y_B) is the bulk phase mole fractions of A (B). Figure 3.7 illustrates the adsorption selectivities of the six mixtures studied as a function of total bulk pressure. The first species listed in the labels indicates the species that is selectively adsorbed.

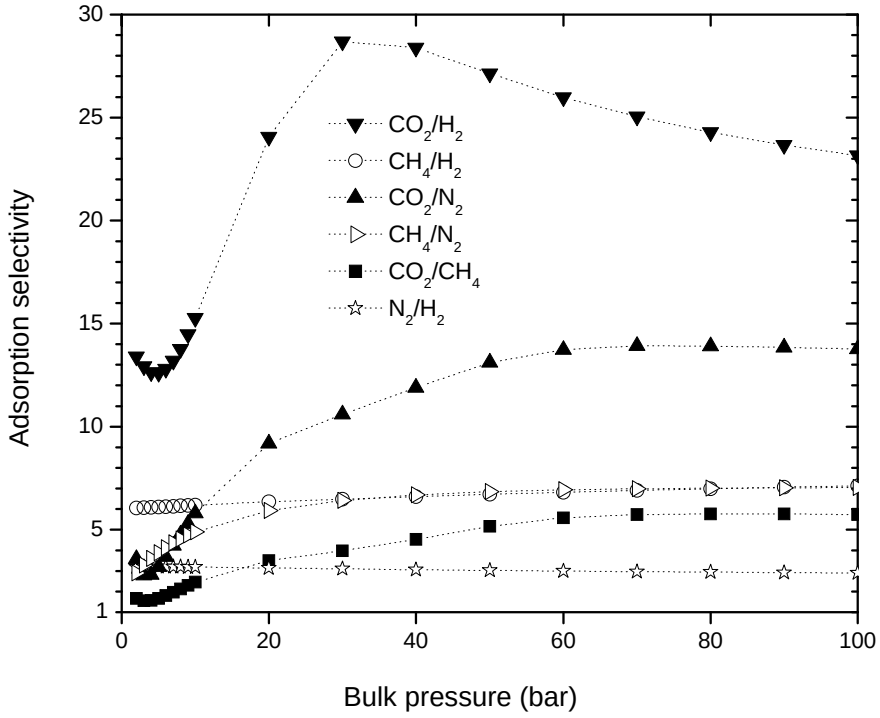

Figure 3.7 Predicted adsorption selectivities from equimolar mixtures in IRMOF-1.

In the pressure range studied, the adsorption selectivity of CO_2/H_2 is the highest among the mixtures we examined, as should be expected. The lowest adsorption selectivity values are observed for N_2/H_2 since both interactions and size effects are

competitive for these two species. The adsorption selectivities of CH_4/N_2 and CH_4/H_2 mixtures have similar trends with pressure, first an increase then a steady behavior. Since the packing effects that favor the adsorption of H_2 or N_2 are insignificant at low loadings, the energetic effects favoring CH_4 adsorption becomes predominant, leading to a slight increase of CH_4 selectivity with increasing loading.

A membrane's ideal selectivity is defined by the ratio of the single component fluxes for that membrane. Figure 3.8 shows the predicted ideal selectivities whereas Figure 3.9 shows the mixture permeation selectivities. In Figure 3.8, the ideal selectivities of mixtures including CO_2 are given up to 40 bar; at higher pressures bulk phase of CO_2 is not a gas. These calculations are performed with a transmembrane pressure drop that is 80% of the feed pressure and with equimolar feed streams for mixture transport.

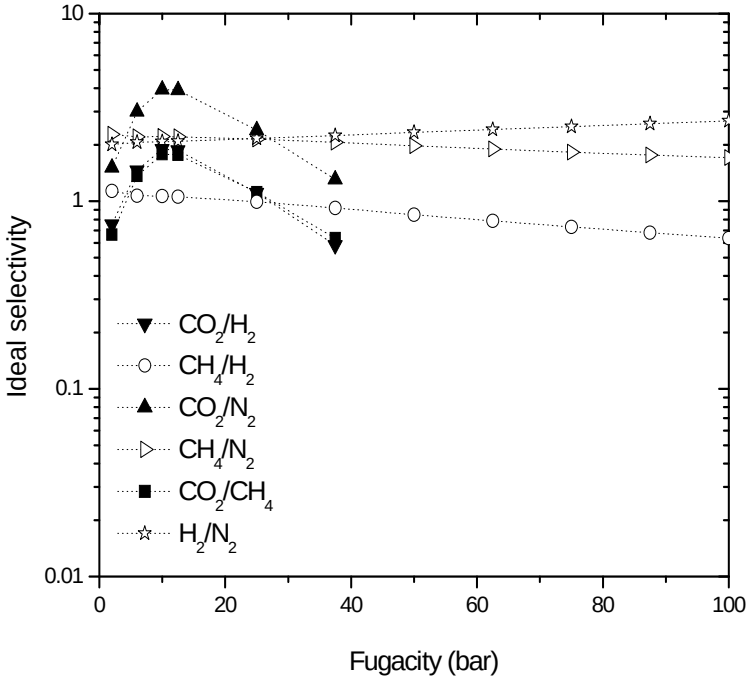

Figure 3.8 Predicted ideal selectivities for an IRMOF-1 membrane. The first species listed in the labels indicates that permeation of the species that is selected.

It is clear from Figure 3.8 and 3.9 that the ideal and mixture selectivities of mixtures including CO_2 are very different from each other at high feed pressures. At low and moderate pressures, the difference between the ideal and mixture selectivity occurs because the strongly adsorbing species reduces the concentration gradient of the other species in the mixture across the membrane and the relatively slow diffusion of the strongly adsorbing species reduces the diffusion rate of the other species. The observation that a slowly diffusing species strongly reduces the diffusivity of a faster diffusing species in an adsorbed mixture is a common one.[23] At high feed pressures, the situation is more complex and the permeation of one species is induced by the concentration gradient of the other species due to the true multi-component effects.

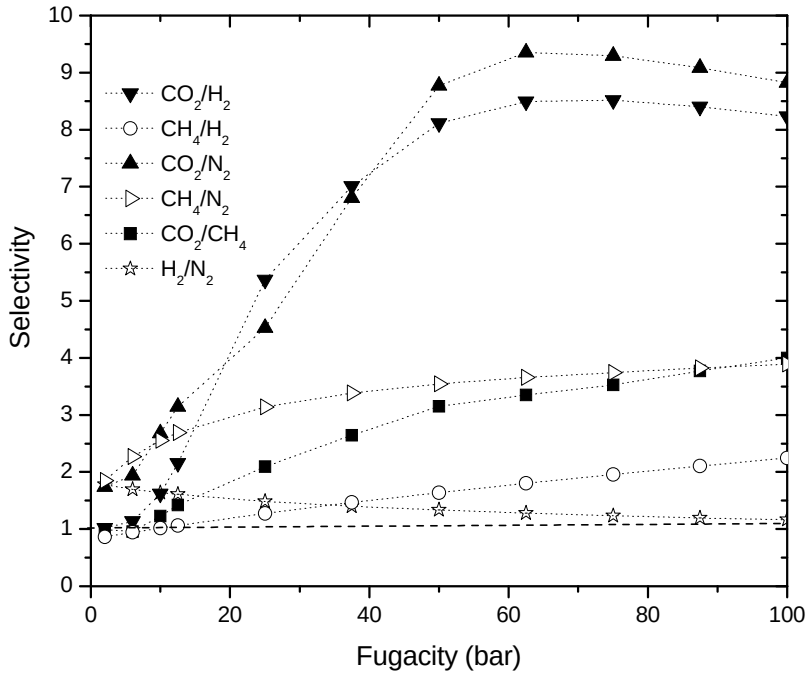

Figure 3.9 Predicted mixture permeation selectivities for an IRMOF-1 membrane. The first species listed in the labels indicates that permeation of the species that is selected.

These multi-component effects may be understood by examining the diagonal and off-diagonal Fickian diffusivity coefficients. In all of the mixtures including CO_2 that we examined, the off-diagonal diffusion coefficients associated with transport of CO_2 induced by the concentration gradient of the other species in the mixture become the dominant diffusivities for moderate feed pressures (see Figure 3.10). Additionally, the flux contribution of CO_2 due to its own concentration gradient in these mixtures becomes negative above a certain feed pressure. Because of this negative flux contribution, the CO_2 flux and selectivity of CO_2 from the feed mixture decrease as the feed pressure increases.

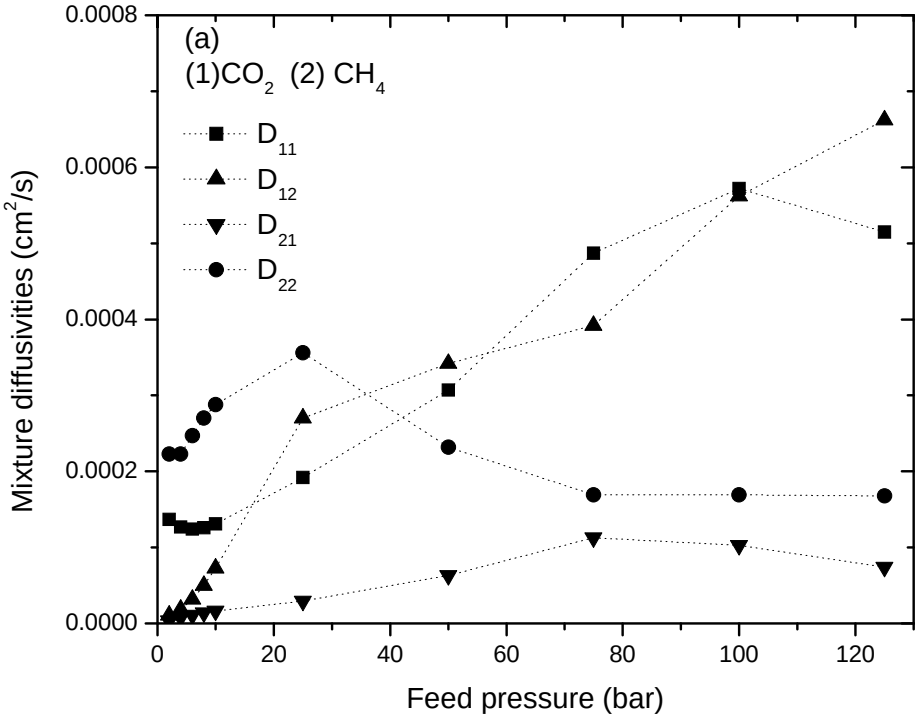

Figure 3.10 Mixture diffusivities of (a) CO_2/CH_4, (b) CO_2/H_2, (c) CO_2/N_2 mixtures at the membrane center calculated using the SSK model for an equimolar feed mixture as a function of feed pressure.

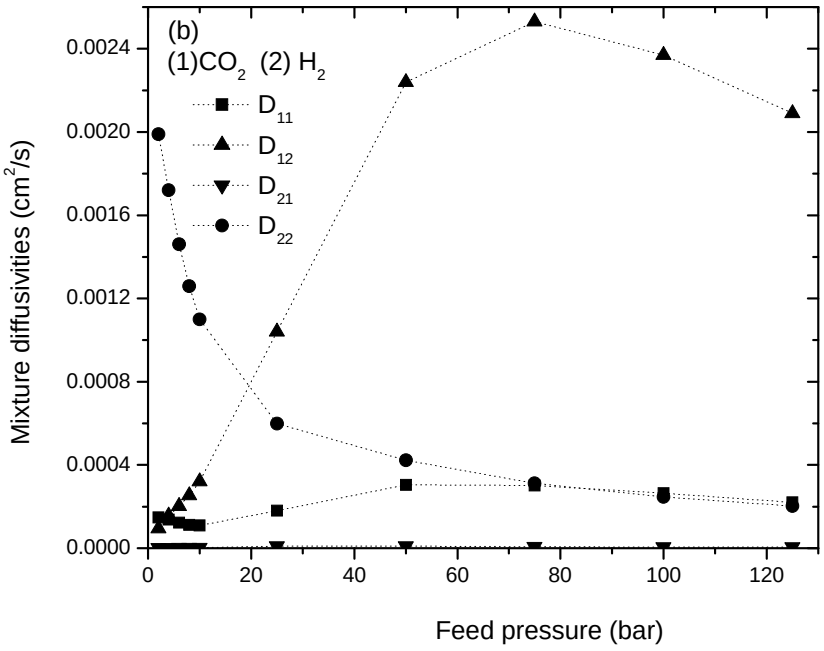

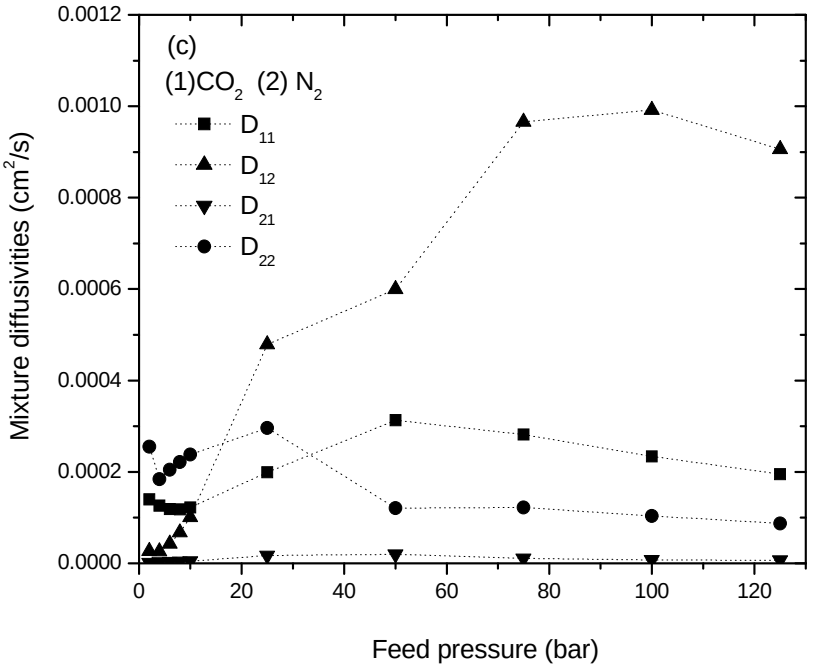

Figure 3.10 Continued

For mixtures not involving CO_2, namely CH_4/H_2, N_2/H_2 and N_2/CH_4, the multi-component effects still play a significant role. The ideal selectivities for N_2, H_2 and CH_4 are almost independent of the feed pressure. The H_2/N_2 mixture is a good example showing how considering multi-component effects can change the predictions for the performance of a membrane. For this example, the ideal selectivity of H_2 from N_2 was around ~3 at high pressures, which suggests that IRMOF-1 membrane is moderately selective for H_2 under these conditions. However the mixture selectivity of H_2 from an equimolar H_2/N_2 mixture under similar conditions is only 1.1. In this example, multi-component effects lead to the membrane being almost completely unselective. This mixture has arguably the worst properties we observed in terms of its mixture selectivity. For CH_4/N_2 and CH_4/H_2 mixtures, the mixture selectivities are not large, but they increase as the feed pressure increases. As we did for other mixtures, we examined the trends of Fickian diffusivities for CH_4/H_2, N_2/H_2 and N_2/CH_4. In these cases, the off-diagonal diffusivity coefficients are small compared to the diagonal ones in the pressure range studied (see Figure 3.11).

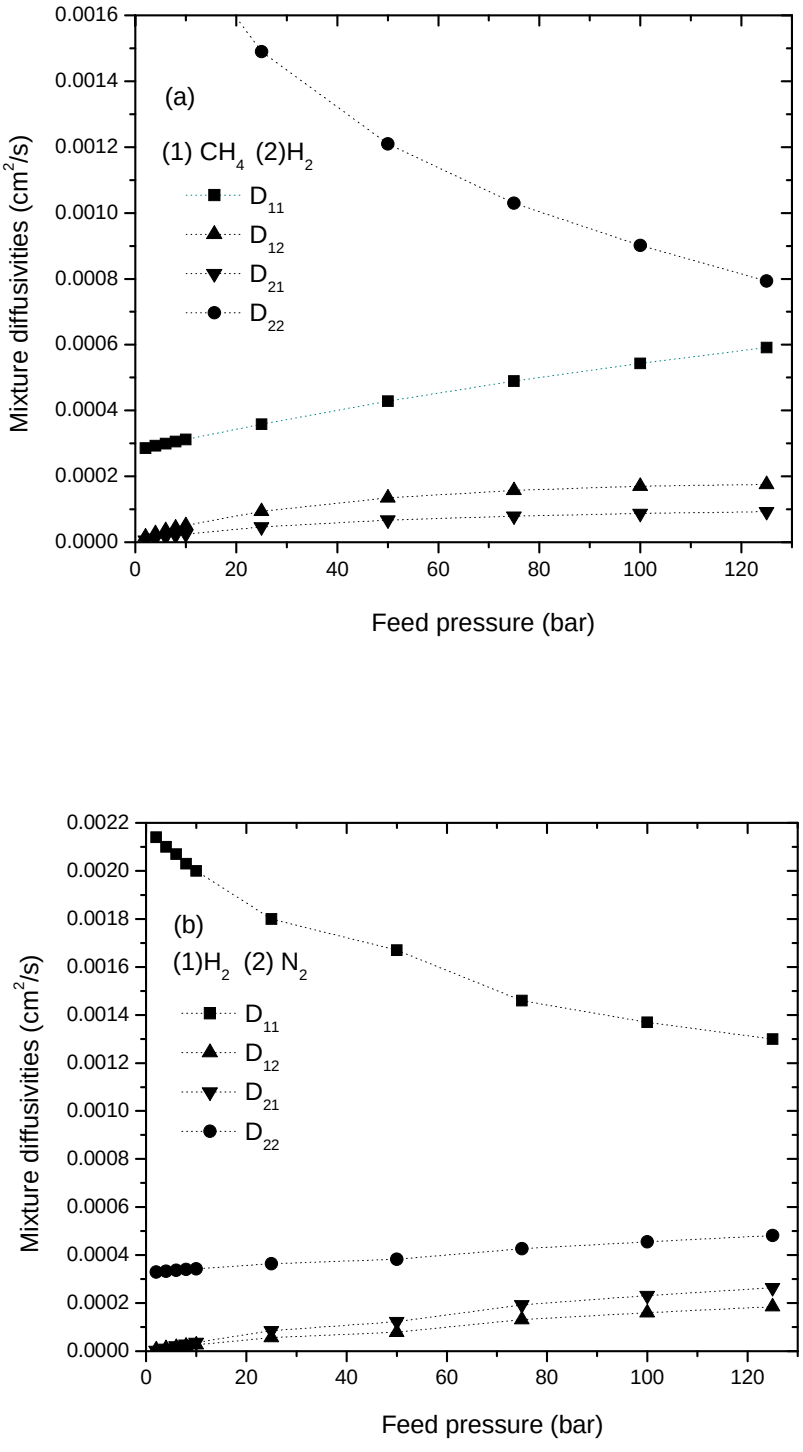

Figure 3.11 Mixture diffusivities of (a) CH_4/H_2, (b) H_2/N_2, and (c) CH_4/N_2 mixtures at the membrane center calculated using the SSK model for an equimolar feed mixture as a function of feed pressure.

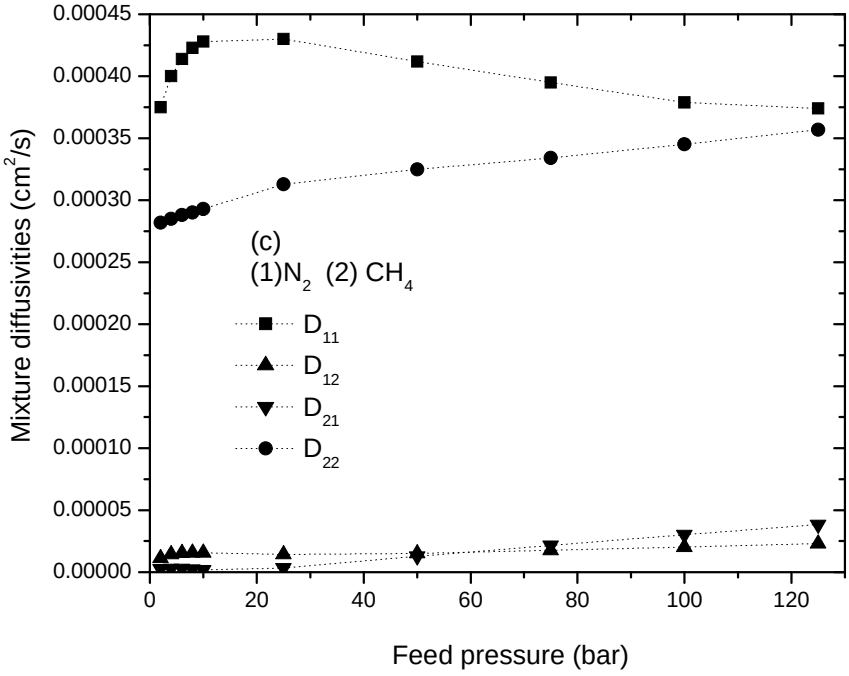

Figure 3.11 Continued

The results presented above can potentially give a misleading view of the performance of the MOF membrane we have modeled because they examined only a sample of the possible operating conditions that could be considered. In order to investigate mixture selectivities as a function of operating conditions, we varied both feed pressure and pressure drop to create a "selectivity map" for each mixture. Figure 3.12 shows the predicted mixture selectivities for CO_2/CH_4, CO_2/H_2, CO_2/N_2, CH_4/H_2, N_2/H_2 and N_2/CH_4 permeation through a IRMOF-1 membrane using an equimolar feed stream as a function of feed pressure and transmembrane pressure drop at 298 K. The first species listed in the labels indicates the species with the higher permeation rate.

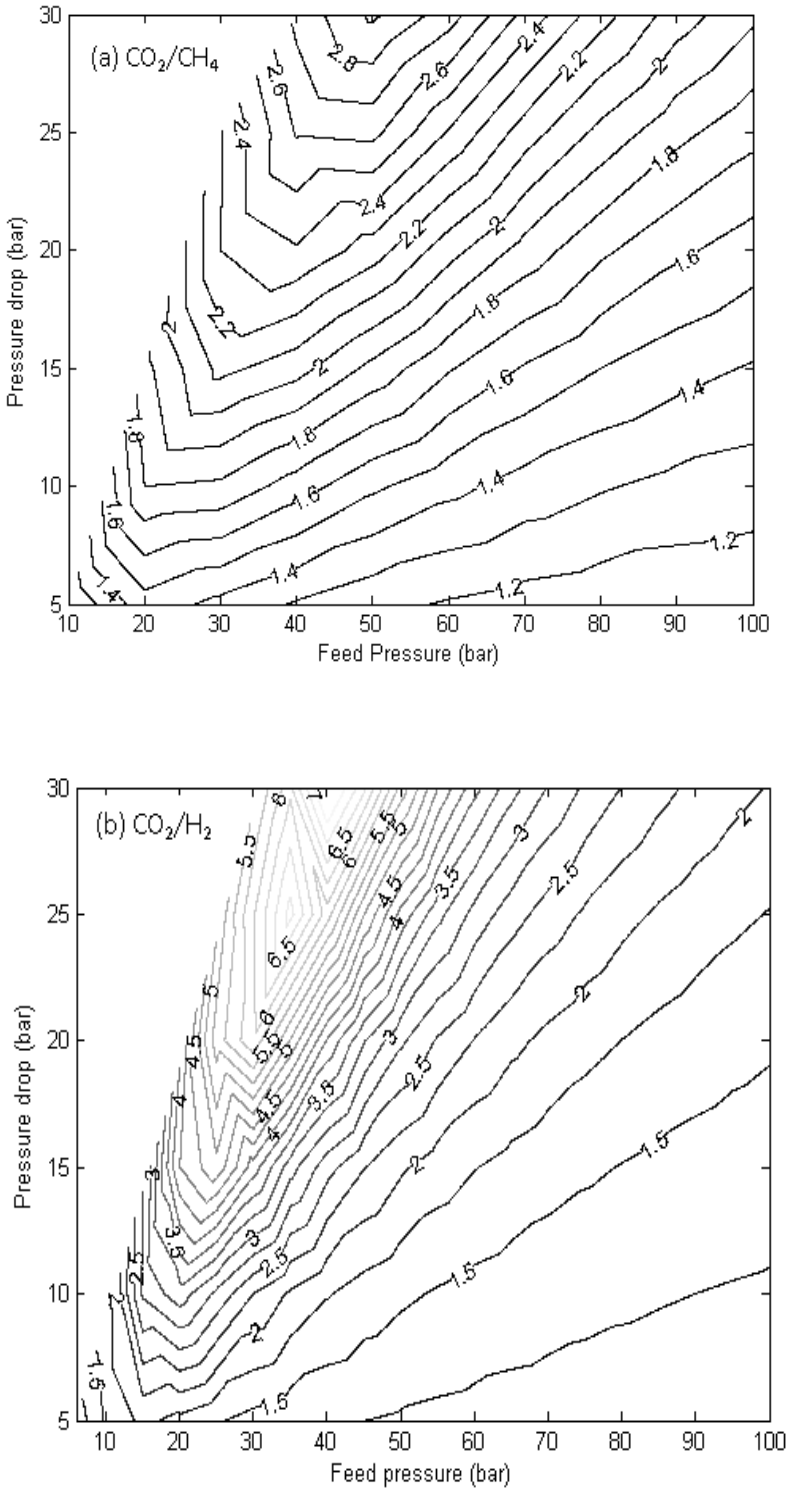

Figure 3.12 Calculated mixture selectivity for (a) CO_2/CH_4, (b) CO_2/H_2, (c) CO_2/N_2, (d) CH_4/H_2, (e) H_2/N_2, and (f) CH_4/N_2 permeation through a IRMOF-1 membrane.

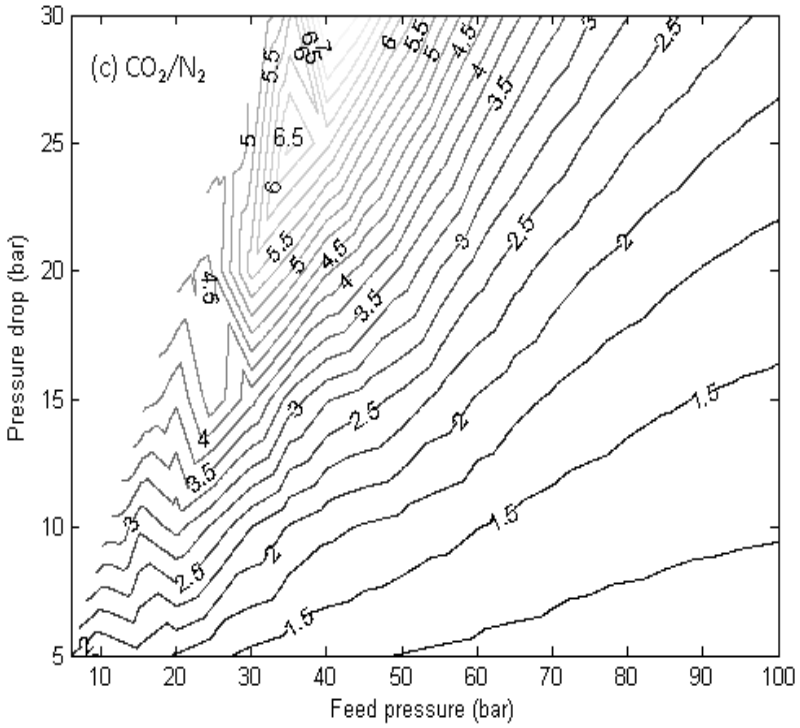

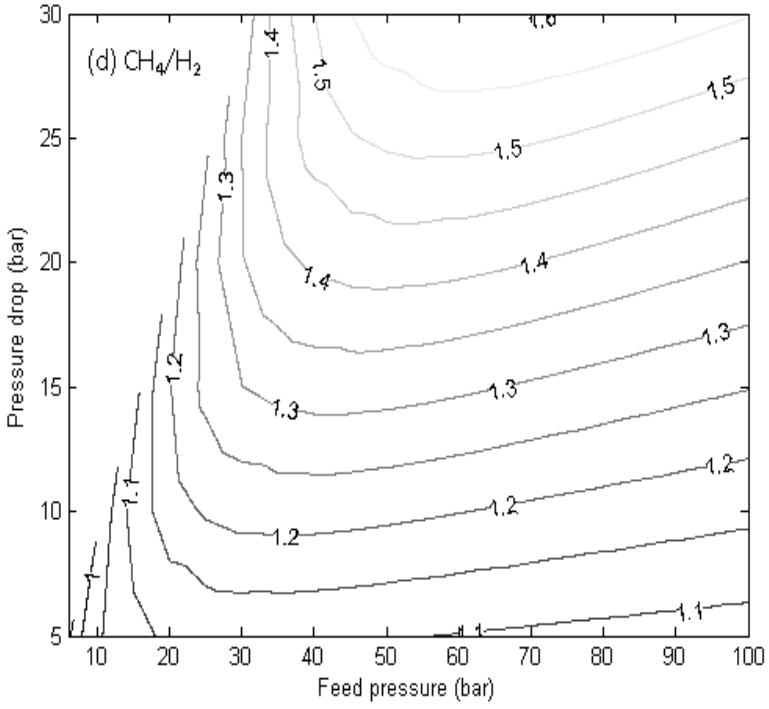

Figure 3.12 Continued

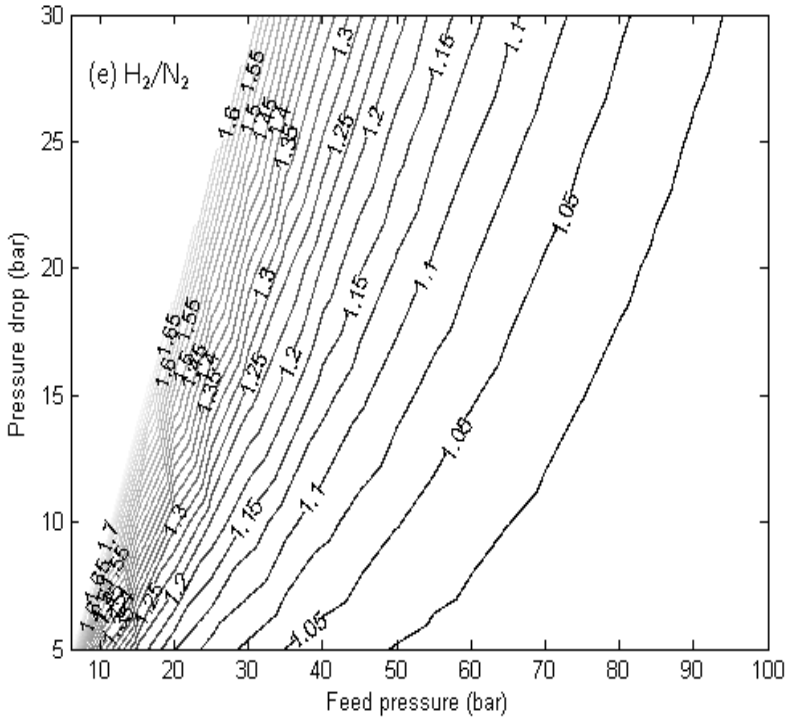

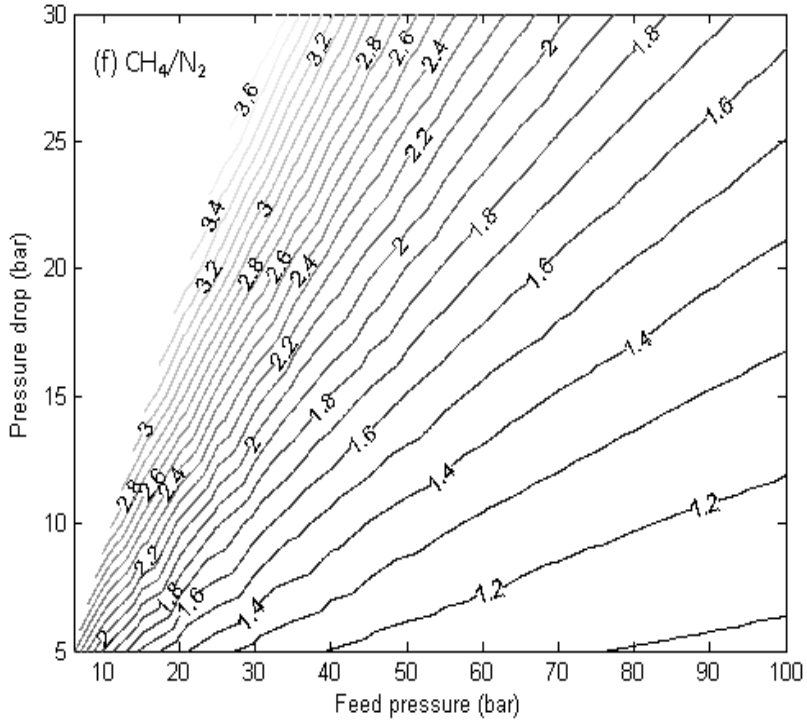

Figure 3.12 Continued

The highest mixture selectivity value observed for CO_2/H_2 mixture is ~8, whereas the highest selectivity value for CH_4/H_2 is only 1.6. Separation of an equimolar mixture of H_2 and CO_2 has been performed using other porous materials at room temperature and moderate pressure. Selectivities of 45 (3.5) have been reported using activated carbon[37] (a microporous silica membrane[38]). Separation of equimolar mixture of H_2 and CH_4 has been also performed in other porous materials at room temperature and moderate pressures. A selectivity of 8 has been reported with a SAPO-34 membrane,[39] while the selectivity reported for a microporous SSF membrane was 2.[40] Theoretical modeling of carbon nanotubes have predicted a membrane selectivity of 13 for this separation.[16] Separation of equimolar mixtures of CH_4 and CO_2 has been performed using SAPO-34 membranes at room temperature at a feed pressure of 222 kPa and a permeate pressure of 84 kPa. CO_2/CH_4 selectivities were found to be higher than 100 for all pure SAPO-34 membranes.[41] Robeson showed that various polymeric membranes achieve different CO_2 selectivities from equimolar CO_2/CH_4 mixtures between 2 and 100.[42]

For the mixtures with CO_2, the shape of the contour plots are similar to each other, having local maxima of selectivity concentrated in an area where the pressure drop is high and feed pressure is mild. These regions illustrate that IRMOF-1 has at least limited potential as membrane for the separation of CO_2 from other light gases. On the other hand, the selectivity of H_2 from CH_4 and N_2 using IRMOF-1 membrane does not seem very promising due to the low selectivities of H_2.

All of the results above used equimolar mixtures as the feed for the membrane. Figure 3.13 shows an example of varying the feed composition for each mixture with a feed pressure of 40 bar and a pressure drop of 30 bar. These calculations support the idea

that equimolar feeds are good choices for CH_4/H_2, N_2/H_2 and N_2/CH_4 to characterize the overall behavior of membrane for CH_4/H_2, N_2/H_2 and N_2/CH_4, because for these mixtures the membrane selectivity does not change strongly with the feed composition. Although we suggested above that IRMOF-1 may be a viable membrane material for the separation of CO_2, the calculations in Fig. 3.13 show that the membrane selectivity is strongly dependent on composition of the feed gas for CO_2/N_2 mixtures.

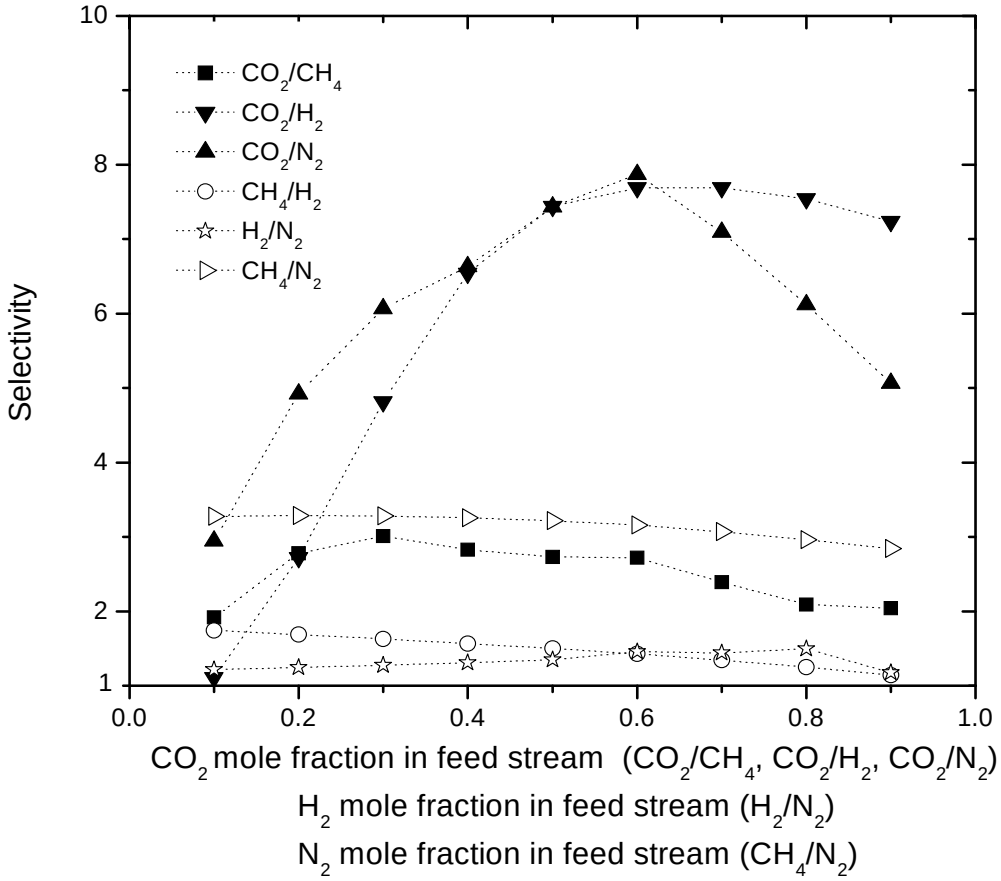

Figure 3.13 Effect of feed gas composition on mixture selectivity for IRMOF-1 membrane. The first species listed in the labels indicates the species that is favored.

To further analyze the effect of feed composition on the selectivity of CO_2 from N_2, we produced the selectivity map for a CO_2/N_2 for bulk mixtures with 10% CO_2, a situation that is relevant for flue gas applications. Figure 3.14 shows that under mild operating conditions, lower feed pressure and pressure drop, this selectivity map is very similar to that of equimolar mixture, Figure 3.12c. Although the maximum selectivity seen for feeds with 10% CO_2 is smaller than for the equimolar feeds, the qualitative features of the two selectivity maps are similar.

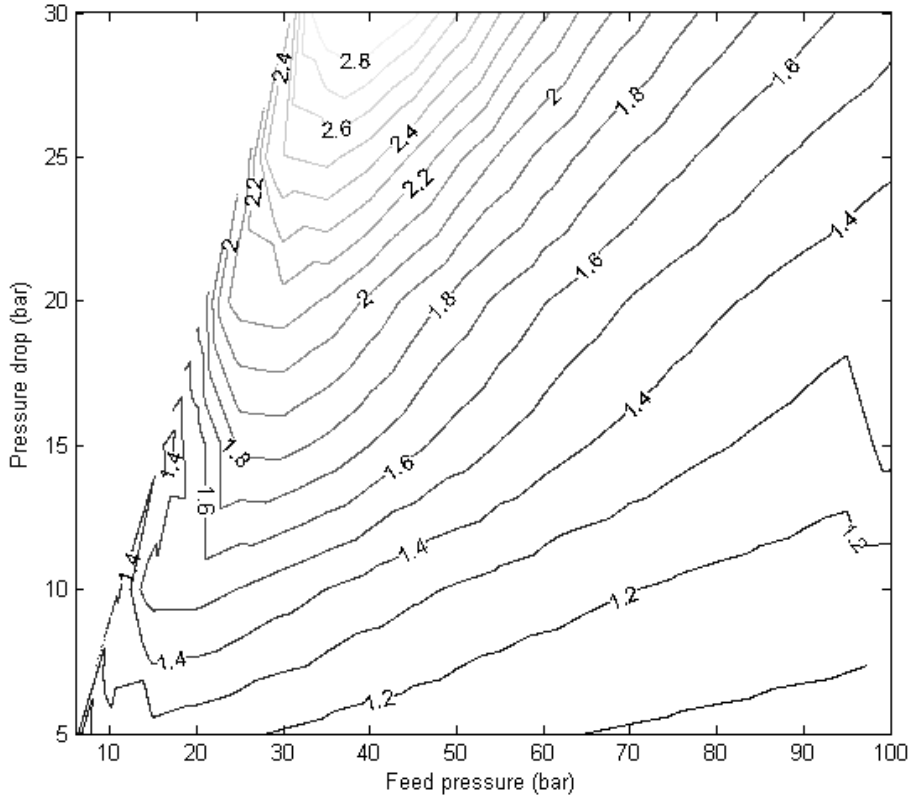

Figure 3.14 Calculated CO_2 selectivity from CO_2/N_2 mixtures permeating through an IRMOF-1 membrane using a feed stream with 10% CO_2 as a function of feed pressure and transmembrane pressure drop at 298 K.

This is a useful observation because it indicates that the equimolar selectivity map (Fig. 3.12c) can be combined with the results examining membrane selectivity as a function of feed composition at fixed operating conditions (Fig. 3.13) to give an overview of the predicted membrane performance for all possible feed compositions, feed pressures, and transmembrane pressure drops.

Selectivity is an important property to characterize the performance of a membrane; however a membrane with a high selectivity but a low flux or permeability may require such a large membrane surface area that it becomes economically unattractive. The results in Figure 3.4 showed that IRMOF-1 membrane exhibited very large fluxes for all the mixtures that we studied here. Our early calculations demonstrated that permeation of CO_2/CH_4 mixture through IRMOF-1 membrane lies above the upper bound curved established for polymeric membranes by Robeson[42] although the selectivity of IRMOF-1 membrane is low relative to many polymer membranes.[43,44] The high permeation rates of mixtures through MOF membranes may be a useful property in incorporation of MOF particles into polymers to make composite membranes.

3.4 References

(1) Skoulidas, A. I.; Sholl, D. S. *J. Phys. Chem. B* **2005**, *109*, 15760.

(2) Li, H.; Eddaoudi, M.; O'Keeffe, M.; Yaghi, O. M. *Nature* **1999**, *402*, 276.

(3) Harris, J. G.; Yung, K. H. *J. Phys. Chem. B* **1995**, *99*, 12021.

(4) Makrodimitris, K.; Papadopoulos, G. K.; Theodorou, D. N. *J. Phys. Chem. B* **2001**, *105*, 777.

(5) Amirjalayer, S.; Tafipolsky, M.; Schmid, R. *Angew. Chem. Int. Ed.* **2007**, *46*, 463.

(6) Greathouse, J. A.; Allendorf, M. D. *J. Am. Chem. Soc.* **2006**, *128*, 10678.

(7) Düren, T.; Snurr, R. Q. *J. Phys. Chem. B* **2004**, *108*, 15703.

(8) Yang, Q.; Zhong, C. *J. Phys. Chem. B* **2006**, *110*, 17776.

(9) Wang, S.; Yang, Q.; Zhong, C. *J. Phys. Chem. B* **2006**, *110*, 20526.

(10) Babarao, R.; Hu, Z.; Jiang, J.; Chempath, S.; Sandler, S. I. *Langmuir* **2007**, *23*, 659.

(11) Paschek, D.; Krishna, R. *Phys. Chem. Chem. Phys.* **2001**, *3*, 3185.

(12) Paschek, D.; Krishna, R. *Langmuir* **2001**, *17*, 247.

(13) Babarao, R.; Jiang, J. *Langmuir* **2008**, *24*, 5474.

(14) Keskin, S.; Liu, J.; Johnson, J. K.; Sholl, D. S. *Langmuir* **2008**, *24*, 8254.

(15) Skoulidas, A. I.; Sholl, D. S. *AIChE J.* **2005**, *51*, 867.

(16) Chen, H.; Sholl, D. S. *J. Membrane Sci.* **2006**, *269*, 152.

(17) Yang, R. T. *Gas separation by adsorption processes*; Butterworths: Boston, 1987.

(18) Myers, A. L.; Prausnitz, J. M. *AIChE J.* **1965**, *11*, 121.

(19) Murthi, M.; Snurr, R. Q. *Langmuir* **2004**, *20*, 2489.

(20) Krishna, R.; Paschek, D. *Phys. Chem. Chem. Phys.* **2001**, *3*, 453.

(21) Chen, H.; Sholl, D. S. *Langmuir* **2007**, *23*, 6431.

(22) Skoulidas, A. I.; Sholl, D. S.; Krishna, R. *Langmuir* **2003**, *19*, 7977.

(23) Sholl, D. S. *Acc. Chem. Res.* **2006**, *39*, 403.

(24) van Baten, J. M.; Krishna, R. *Micro. Meso. Mat.* **2005**, *84*, 179.

(25) Krishna, R.; van Baten, J. M. *Chem. Phys. Lett.* **2005**, *407*, 159.

(26) Krishna, R.; van Baten, J. M. *J. Phys. Chem. B* **2005**, *109*, 6386.

(27) Chempath, S.; Krishna, R.; Snurr, R. Q. *J. Phys. Chem. B* **2004**, *108*, 13481.

(28) Kärger, J.; Ruthven, D. *Diffusion in Zeolites and Other Microporous Materials*; John Wiley & Sons: New York, 1992.

(29) Keil, F. J.; Krishna, R.; Coppens, M. O. *Rev. Chem. Eng.* **2000**, *16*, 71.

(30) Skoulidas, A. I., D. S. Sholl, T. C. Bowen, C. Doelling, J. L. Falconer, R. D. Noble. *J. Membrane Sci.* **2003**, *227*, 123.

(31) Newsome, D. A.; Sholl, D. S. *J. Phys. Chem. B* **2005**, *109*, 7237.

(32) Martin, M. G.; Thompson, A. P.; Nenoff, T. M. *J. Chem. Phys.* **2001**, *114*, 7174.

(33) Ahunbay, M. G.; Elliott, J. R.; Talu, O. *J. Phys. Chem. B* **2002**, *106*, 5163.

(34) Skoulidas, A. I.; Ackerman, D. M.; Johnson, J. K.; Sholl, D. S. *Phys. Rev. Lett.* **2002**, *89*, 185901.

(35) Liu, Y.; Ng, Z.; Khan, E. A.; Jeong, H.-K.; Ching, C.-B.; Lai, Z. *Micropor. Mesopor. Mater.* **2009**, *118*, 296.

(36) Wesselingh, J. A.; Krishna, R. *Mass Transfer in Multicomponent Mixtures*; Delft University Press: Delft, 2000.

(37) Cao, D. P.; Wu, J. Z. *Carbon* **2005**, *43*, 1364.

(38) Richard, V.; Favre, E.; Tondur, D.; Nijmeijer, A. *Chem. Eng. J.* **2001**, *84*, 593.

(39) Poshysta, J. C.; Tuan, V. A.; Pape, E. A.; Noble, R. D.; Falconer, J. L. *AIChE J.* **2000**, *46*, 779.

(40) Vieira-Linhares, A. M.; Seaton, N. A. *Chem. Eng. Sci.* **2003**, *58*, 4129.

(41) Li, S. G.; Falconer, J. L.; Noble, R. D. *Adv. Mat.* **2006**, *18*, 2601.

(42) Robeson, L. M. *J. Membrane Sci.* **1991**, *62*, 165.

(43) Keskin, S.; Sholl, D. S. *J. Phys. Chem. C* **2007**, *111*, 14055.

(44) Keskin, S.; Sholl, D. S. *Ind. Eng. Chem. Res.* **2009**, *48*, 914.

CHAPTER 4

TRANSPORT OF BINARY GAS MIXTURES THROUGH CUBTC MEMBRANES

In this chapter, we use atomistic simulations and continuum modeling to investigate the effect of MOF structure on intrinsic properties of MOF membranes for separation of light gas mixtures. We describe atomically detailed simulations of gas adsorption and diffusion in CuBTC that have been used to predict the performance of CuBTC membranes for separation of H_2/CH_4, CO_2/CH_4 and CO_2/H_2 mixtures. CuBTC ($Cu_3(BTC)_2$, BTC = 1,3,5-benzenetricarboxylate), also known as HKUST-1, is one of the most widely studied MOFs in the literature.[1-10] Our calculations predict that CuBTC membranes have higher selectivities for separation of H_2/CH_4, CO_2/CH_4 and CO_2/H_2 mixtures than IRMOF-1 membranes, the MOF material described in the previous chapter. Our results give insight into the physical properties that will be desirable in tuning the pore structure of MOFs for specific membrane-based separations.

4.1 Computational Details

We performed adsorption and diffusion simulations using GCMC and EMD techniques, respectively. Both types of simulations were performed at room temperature using a rigid CuBTC structure with a unit cell dimension of 26.343 Å. The atomic positions of CuBTC were obtained from experimental data[11] and atoms belonging to solvents were removed. CuBTC has metal corners consisting of Cu^{2+} ions coordinated to 1,3,5-benzenetricarboxylate organic linkers.[11] It has main channels ~9 Å in diameter

surrounded by tetrahedral pockets of ~5 Å in diameter. The tetrahedral pockets and the main channels are connected by triangular windows of diameter ~3.5 Å.

The Universal Force Field (UFF)[12] was used for the framework atoms. The interaction parameters for the atoms of MOFs and for the adsorbate molecules, H_2, CH_4, and CO_2 are tabulated in Table 4.1. The partial charges of CuBTC atoms were taken from Yang and Zhong.[4] We modeled CO_2 as a rigid three-site molecule with Lennard-Jones (LJ) interactions and partial point charges located at the center of each site[13] whereas CH_4 and H_2 were modeled as spherical LJ potentials.

Table 4.1 Interaction potential parameters for adsorbent and adsorbate atoms/molecules used in this work. The partial charges for CuBTC atoms are taken from reference 4.

Atoms/Molecules	Reference	ε/k (K)	σ(Å)	q (e)
H_2-H_2	14	34.20	2.960	--
CH_4-CH_4	15	148.20	3.812	--
C-C (in CO_2)	16	27.00	2.800	+0.7
O-O (in CO_2)	16	79.00	3.050	-0.35
C1-C1 (in CuBTC)	12	52.84	3.431	+0.778
C2-C2 (in CuBTC)	12	52.84	3.431	-0.092
C3-C3 (in CuBTC)	12	52.84	3.431	-0.014
H-H (in CuBTC)	12	22.14	2.553	+0.109
O-O (in CuBTC)	12	30.19	3.118	-0.665
Cu-Cu (in CuBTC)	12	2.52	3.114	+1.098

The Lorentz-Berthelot mixing rules were employed to calculate the fluid-solid LJ cross interaction parameters. Fluid-fluid and fluid-solid intermolecular LJ potentials were truncated at 17 Å for adsorption simulations and no long-range corrections were applied. Fluid-fluid and fluid-solid intermolecular LJ potentials were truncated at 13 Å for diffusion simulations, with long-range corrections applied. We have verified that diffusivities calculated using a cut-off radius of 13 Å with long-range corrections gives results that are indistinguishable from calculations using a truncation of 17 Å without long-range corrections. Electrostatic interactions between CO_2 molecules were truncated at 25 Å. Electrostatic interactions between CO_2 molecules and the framework were calculated by summation of the charge-charge interactions between each framework atom and each charge site of the CO_2 molecule. These charge-charge interactions were pre-tabulated by direct calculation of the atomic charge-charge interactions.[17]

Our molecular simulations of CH_4/H_2, CH_4/CO_2, and CO_2/H_2 mixtures in CuBTC used similar methods to earlier simulations of single component gas adsorption and diffusion in this material.[6,17] Both adsorption and diffusion simulations were performed at 298 K. For adsorption simulations, we used a simulation volume of 2×2×2 crystallographic unit cells whereas for diffusion the size of the simulation volume was 1×1×1.

We have used a conventional GCMC technique in this work to compute adsorption isotherms,[18,19] specifying the temperature and fugacity of the adsorbing gases and calculating the number of adsorbed molecules at equilibrium. Simulations at the lowest fugacity for each system were started from an empty MOF matrix. Each subsequent simulation at higher fugacity was started from the final configuration of the

previous run. Simulations consisted of a total of 1×10^7 trial configurations, with the last half of the configurations used for data collection. The Monte Carlo moves used in these simulations included particle translation, creation, deletion, and in the case of mixtures, particle swaps. The H_2 adsorption isotherm at 298 K we obtained in this work is identical to the results of Liu et al.[6] since we used the same potential parameters and MOF structure.

We used EMD simulations to compute the self and corrected diffusivities of adsorbates. The details of using EMD simulations to obtain these diffusion coefficients once the interaction parameters for adsorbates in a nanoporous adsorbent have been described in Chapter 2 and elsewhere.[20-23] We used a Nosé-Hoover thermostat in NVT-MD simulations and performed 40 independent MD simulations, each having a simulation length of 20-30 ns, for each loading we considered. Using a large number of independent trajectories is vital in order to compute the corrected diffusivities. After creating initial states with the appropriate loading using GCMC, each system was first equilibrated with EMD for about 20 ps prior to taking data.

To use binary adsorption isotherms efficiently in our membrane calculations, we fitted binary adsorption data from GCMC for a large collection of mixture compositions using an extended Langmuir (Langmuir-Freundlich) isotherm for H_2/CH_4 (CO_2/CH_4 and CO_2/H_2) mixtures. We predicted the mixture transport diffusivities using method introduced by Skoulidas, Sholl and Krishna (SSK)[24] based on single component diffusion data taken from MD simulations. We tested the accuracy of SSK method by predicting the binary matrix of Fickian diffusivities of H_2/CH_4 mixtures in CuBTC[25] and found that the SSK predictions are in a good agreement with our direct mixture diffusion

simulations. Tests done for CO_2/CH_4 mixtures also gave good agreement with mixture simulation data. These calculations are discussed in detail in Chapter 5.

After mixture adsorption isotherms and mixture diffusivities are defined as described above, steady state permeance of mixtures through a membrane was calculated by specifying the feed pressure, the transmembrane pressure drop and the composition of the gas mixture at the entrance of the membrane. In our calculations, we assumed that the resistance to mass transfer is due to only intracrystalline diffusion. This assumption is accurate for light gas transport through membranes made from other nanoporous materials with a membrane thickness larger than 0.1 μm.[26,27] All our calculations are for membranes that are comprised of a defect-free CuBTC crystal having a thickness of 10 μm. Steady state fluxes were calculated using a shell description of the membrane.[27] We calculated the membrane selectivities for each mixture by varying the feed pressure and the pressure drop through the membrane for equimolar feed streams to examine the effect of operating conditions. An important property of these calculations is that we can routinely examine the membrane selectivity and permeability for a wide range of operating conditions.[28,29]

4.2 Mixture Selectivity of CuBTC Membranes

We first predicted the ideal selectivities and mixture selectivities for equimolar mixtures of H_2/CH_4, CO_2/CH_4 and CO_2/H_2 permeating through a CuBTC membrane at room temperature. Results from calculations using a transmembrane pressure drop that is 80% of the feed pressure are shown in Figure 4.1a and Figure 4.1b.

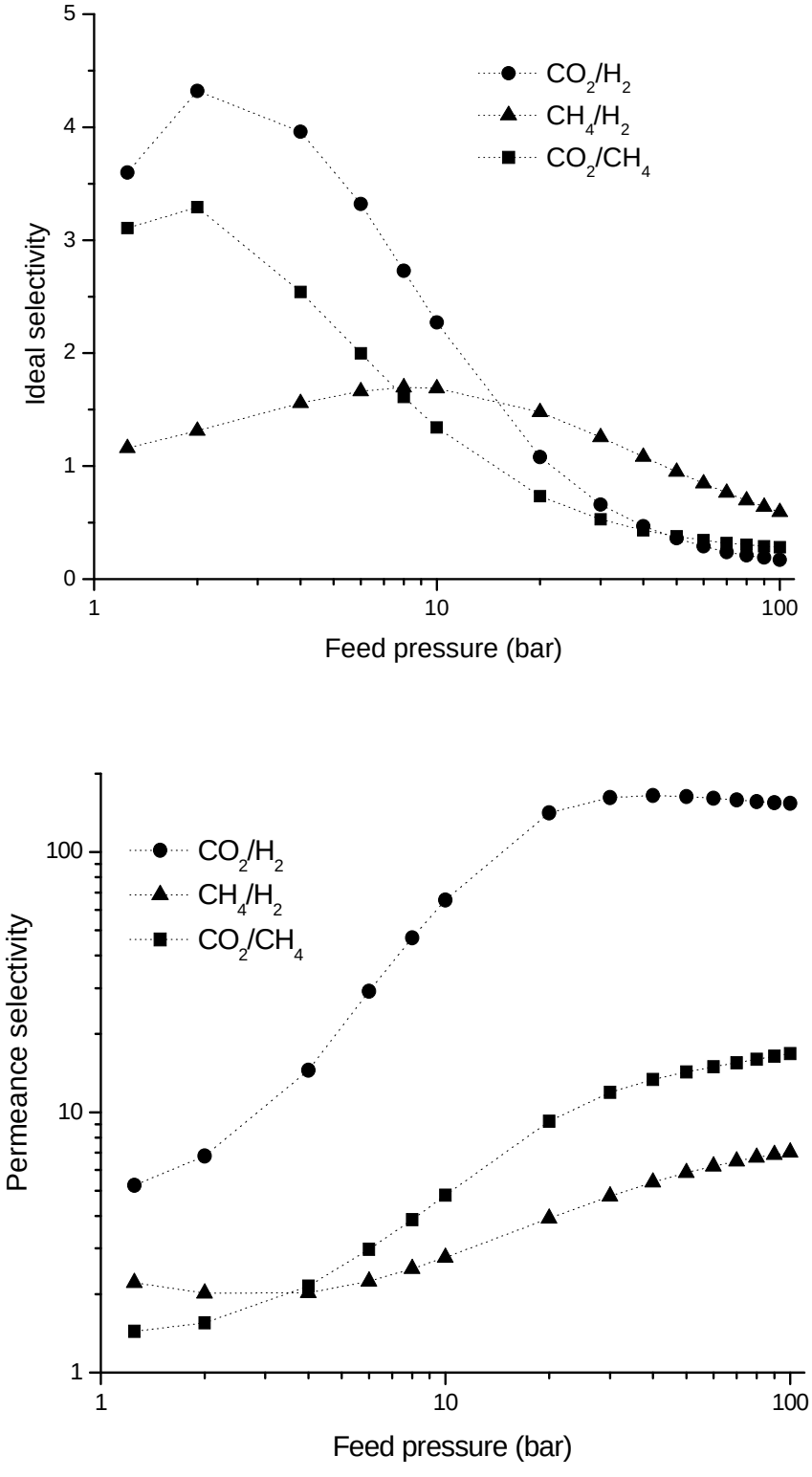

Figure 4.1 Predicted (a) ideal selectivity (b) mixture selectivity of mixtures through CuBTC membrane. The first species in the label indicates the component selected.

The mixture selectivity is enormously different from the ideal selectivity, as observed before for mixtures of H_2/CH_4, CO_2/CH_4 and CO_2/H_2 in an IRMOF-1 membrane under similar conditions. The difference between the selectivities can be attributed to the multi-component effects in the diffusing mixtures as previously discussed in Chapter 3. For H_2/CH_4 and CO_2/H_2 mixtures, the mixture selectivity at the lowest pressure shown in Figure 4.1b is higher than the ideal selectivity. The strongly adsorbing gas component, that is, CO_2 (CH_4) in the CO_2/H_2 (CH_4/H_2) mixture, reduces the concentration gradient across the membrane of the weakly adsorbed gas component, H_2. Furthermore, the strongly adsorbing component reduces the diffusion rate of the more mobile species, H_2. As a result of these two effects, the mixture selectivity for the strongly adsorbing component over H_2 is higher than the ideal selectivity.

These effects become more significant at higher loadings. For example, the ideal selectivity of CO_2 from an equimolar CO_2/H_2 mixture is about 0.5 for a pressure range of 30-100 bar, suggesting that CuBTC is weakly selective for H_2 (Figure 4.1a). On the other hand, the mixture selectivity is predicted to be 150 for separation of CO_2, indicating that CuBTC is a very selective membrane for this mixture (Figure 4.1b). The behavior for the CO_2/CH_4 mixture is more complicated. At low pressures, the mixture selectivity is lower than the ideal selectivity since both gas components compete for adsorption. At higher pressures shown in Figure 4.1b, the net CO_2 concentration gradient across the membrane is positive, meaning that, net transport of CO_2 through CuBTC membrane only occurs due to the multi-component effects.

We can compare CuBTC and IRMOF-1 membranes based on their adsorption selectivity, diffusion selectivity and mixture selectivity. Adsorption selectivities are

calculated as the ratio of concentrations of the two species in the adsorbed phase normalized by their bulk phase gas composition. The diffusion selectivity is defined as the ratio of the diagonal Fickian diffusivities computed by the SSK method. The binary mixture Fickian diffusion matrix is composed of two diagonal (D_{11} and D_{22}) and two off-diagonal diffusivity coefficients (D_{12} and D_{21}). The diagonal (off-diagonal) diffusivity coefficients relate the concentration gradient of each species with the steady state flux of the same (opposite) species. The ratio of diagonal Fickian diffusivities is analogous to the ratio of single component transport diffusivities, a quantity that describes the influence of single component diffusion on a membrane's ideal selectivity. The diffusion selectivity is therefore indicative of the contribution of diffusion to the overall selectivity of a membrane in situations where transport is dominated by the diagonal components of the Fickian diffusion matrix. Mixture selectivities are calculated from the full treatment of the membrane under steady state conditions described above. For both IRMOF-1 and CuBTC membranes, all the selectivities are calculated for a situation where the feed gas was an equimolar mixture and the transmembrane pressure drop was 80% of the feed pressure.

Figure 4.2 shows that CuBTC has a higher adsorption selectivity than IRMOF-1 for all mixtures that we studied. At 10 bar, for example, the adsorption selectivity of CO_2 from H_2 is about 15 and 150 in IRMOF-1 and CuBTC crystals, respectively. The adsorption selectivity also differs significantly for H_2/CH_4 and CO_2/CH_4 mixtures in the two MOFs. This result is consistent with previous data on mixture adsorption in these materials.[4] The high adsorption selectivity of CuBTC can be attributed to two effects: the presence of open metal sites in CuBTC and the relatively small pore size of CuBTC.

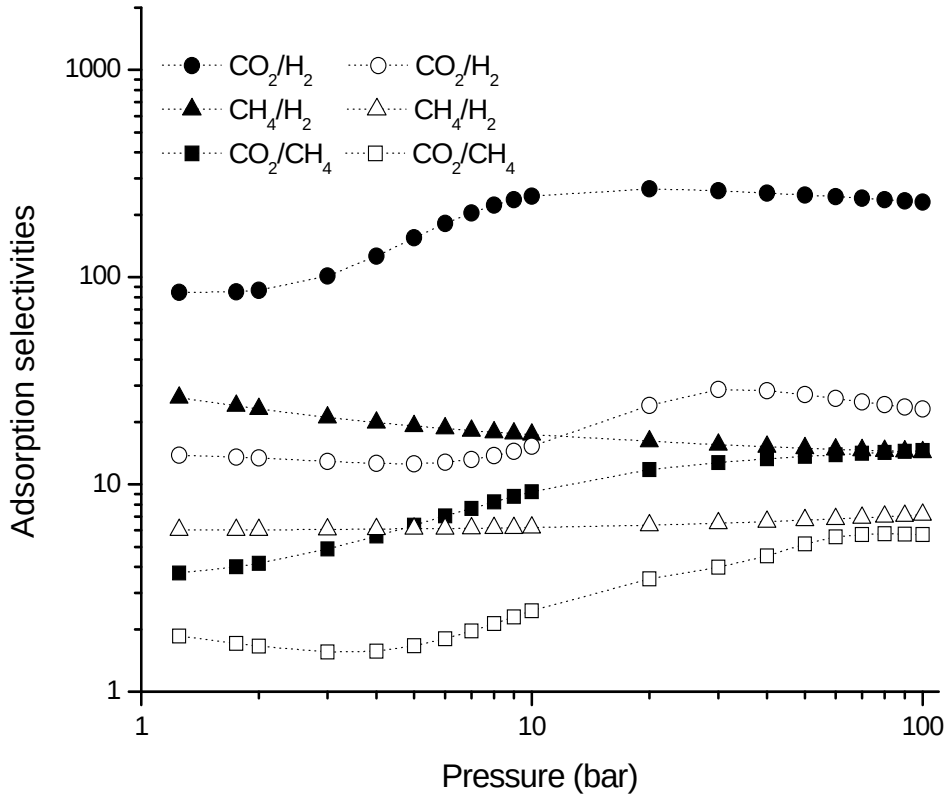

Figure 4.2 Adsorption selectivity of mixtures in CuBTC (closed symbols) and IRMOF-1 (open symbols). The first species in the label indicates the component selected.

The open metal sites of CuBTC provide strong electrostatic interactions with CO_2 molecules and enhance the adsorption selectivity of CO_2. This effect has been discussed in the literature[30] and it contributes strongly to the enhanced adsorption selectivity of CO_2 from H_2 or CH_4 in CuBTC relative to IRMOF-1. CuBTC has small tetrahedral pockets of ~5 Å in diameter in addition to a channel that is ~9 Å in diameter, whereas IRMOF-1 has a cubic main channel with a pore diameter > 10 Å. The diameters of both the main channels and small pockets of CuBTC are smaller than the channel diameter of IRMOF-1, providing a stronger confinement of at least some guest molecules in CuBTC. The degree of confinement of H_2 molecules in the channels of IRMOF-1 and the pores of

CuBTC can be thought as being similar, because in both cases the molecule is small relative to the pore size, giving similar adsorption strength for H_2. CH_4 molecules, in contrast, experience stronger confinement in narrow pores of CuBTC than in the large pores of IRMOF-1, resulting in an enhancement of CH_4 adsorption in CuBTC compared to IRMOF-1. This effect also contributes to the adsorption of CO_2 in CuBTC.

The ratios of diagonal Fickian diffusivities for the three adsorbed mixtures in IRMOF-1 and CuBTC are shown in Figure 4.3. This ratio tends to decrease with pressure, since at higher loadings the slowly diffusing species reduce the diffusivity of a more mobile species in an adsorbed mixture.[22,23,31]

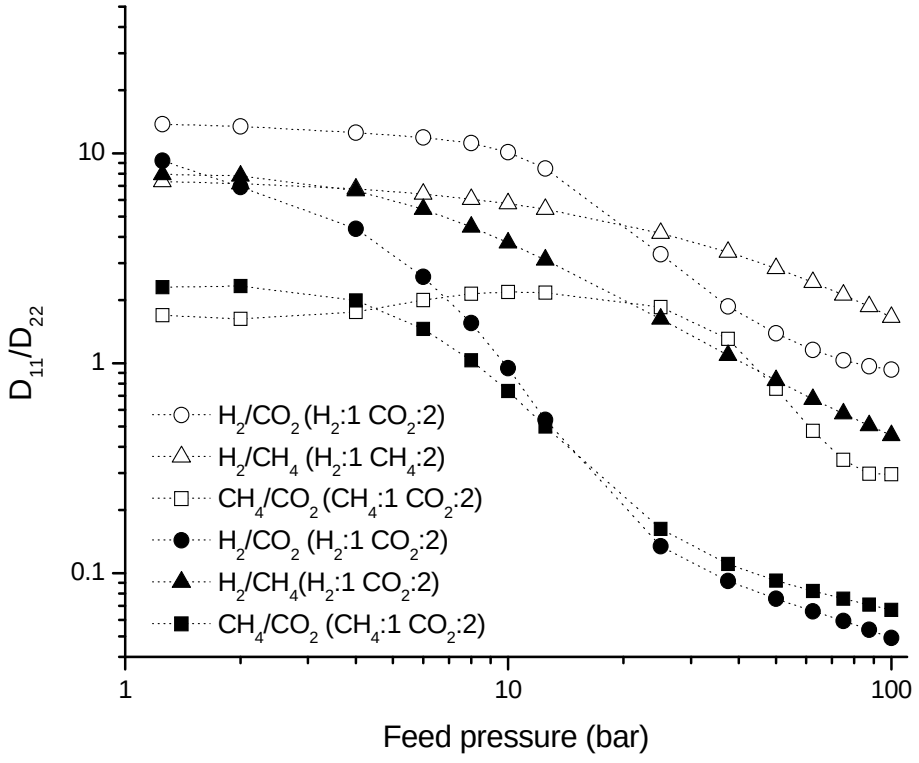

Figure 4.3 Diffusion selectivity of mixtures in CuBTC (closed symbols) and IRMOF-1 (open symbols). The first species in the label indicates the component selected.

The H_2/CH_4 mixture is a good example to understand the effect of diffusion rates on overall membrane performance. Diffusion selectivity favors H_2 over CH_4 in their binary mixture at low pressures both in IRMOF-1 and CuBTC, since H_2 is more mobile than CH_4. IRMOF-1 and CuBTC exhibits almost same diffusion selectivity for H_2 over CH_4 (around 8) up to a feed pressure of ~6 bar. If we look at the mixture selectivity for this mixture under the same pressure condition in Figure 4.4, however, IRMOF-1 and CuBTC demonstrate rather different mixture selectivities. At 6 bar, CuBTC favors CH_4 over H_2 with a mixture selectivity of 2 whereas IRMOF-1 favors H_2 over CH_4 with a selectivity of 1.25. In this example, the adsorption selectivity is the dominant factor determining the overall membrane selectivity.

Comparing the diffusion selectivity and adsorption selectivity for CO_2/CH_4 and CO_2/H_2 mixtures indicates that the overall performance of CuBTC and IRMOF-1 membranes for these mixtures is dominated by the selectivity of adsorption. For feed pressures up to 10 bar, diffusion selectivity favors H_2 over CO_2 both in CuBTC and IRMOF-1 membranes, while adsorption selectivity strongly favors CO_2 over H_2. Figure 4.4 shows that both CuBTC and IRMOF-1 membranes are CO_2 selective in this regime. At pressures higher than 10 bar, CO_2 slows down H_2 so much that diffusion selectivity also favors CO_2 over H_2 when CuBTC is used as a membrane.

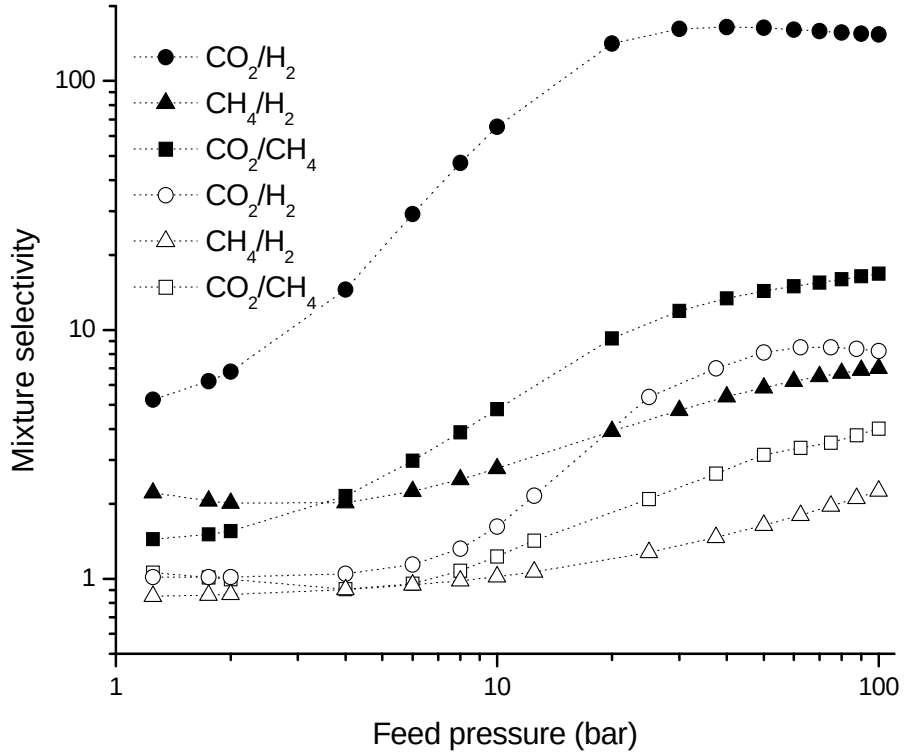

Figure 4.4 Mixture selectivity of mixtures in CuBTC (closed symbols) and IRMOF-1 (open symbols). The first species in the label indicates the component selected.

Figure 4.5 and 4.6 shows the 'selectivity maps' that we created to investigate mixture selectivities for H_2/CH_4, CO_2/CH_4 and CO_2/H_2, respectively in CuBTC membrane under different operating conditions. We showed similar selectivity maps for the binary mixtures of CH_4, CO_2 and H_2 for IRMOF-1 membranes in the previous chapter. The mixture selectivities calculated for a CuBTC membrane are higher than the values calculated for IRMOF-1 membrane, but the qualitative structure of the selectivity maps for the two materials are similar to each other.

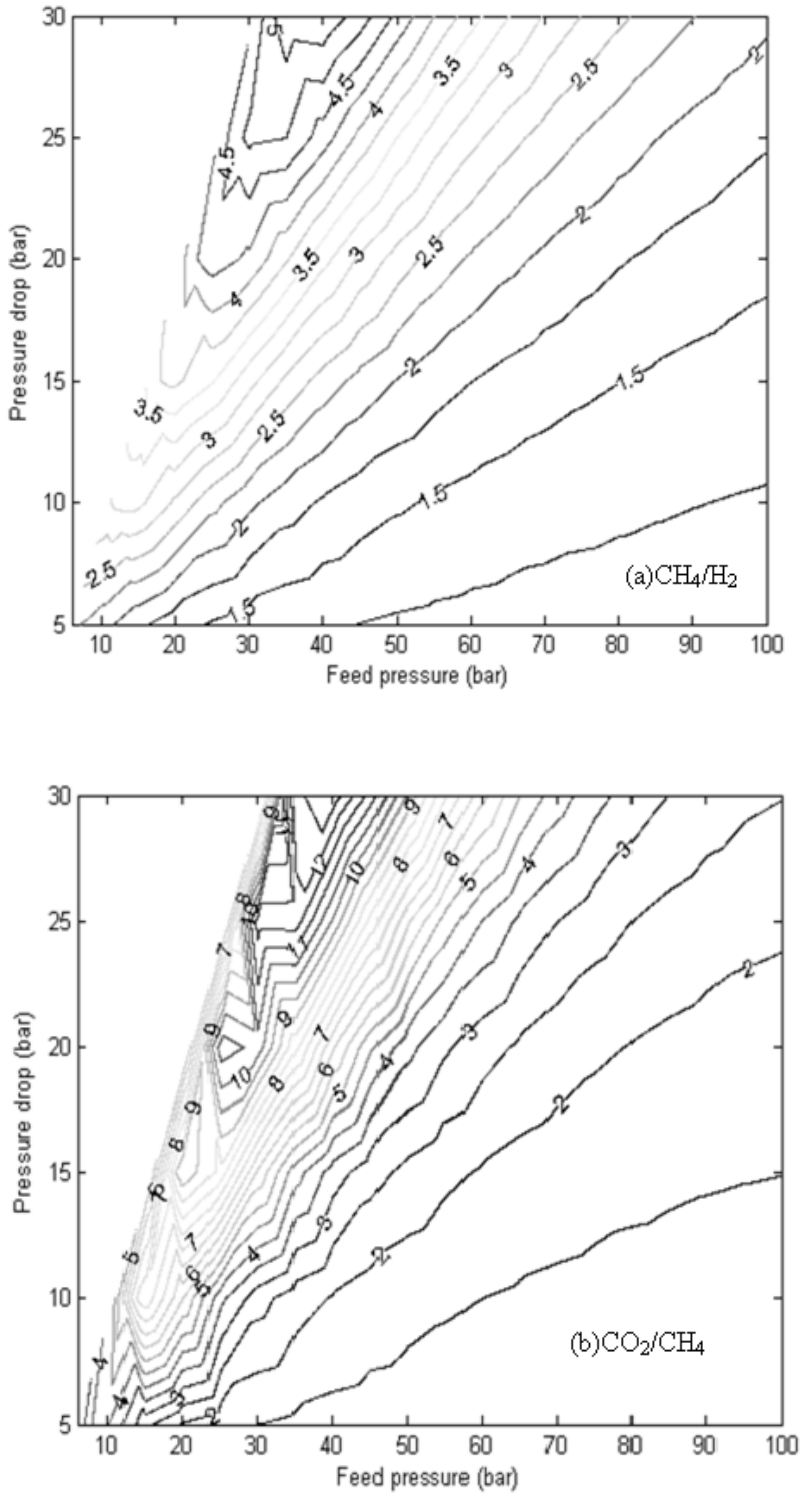

Figure 4.5 Selectivity of (a) CH_4 from equimolar CH_4/H_2 mixture (b) CO_2 from equimolar CO_2/CH_4 mixture through CuBTC membrane at 298 K as a function of feed pressure and pressure drop.

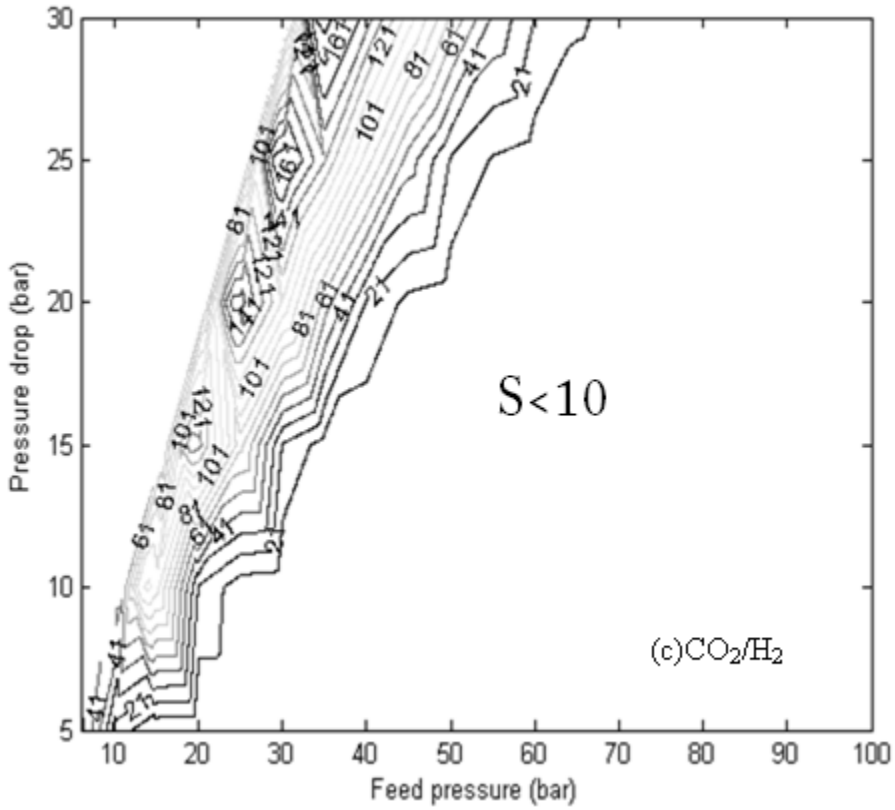

Figure 4.6 Selectivity of CO_2 from equimolar CO_2/H_2 mixture through CuBTC membrane at 298 K as a function of feed pressure and pressure drop. S<10 indicates the area where selectivity of CO_2 from CO_2/H_2 mixture is less than 10.

Figure 4.6 demonstrates that CuBTC exhibits a CO_2 selectivity as high as ~160 from equimolar CO_2/H_2 mixture. The highest selectivity of CO_2 from equimolar CO_2/H_2 mixture was found to be about ~8 in IRMOF-1 membrane calculations. The predicted selectivity for CuBTC membranes for CO_2/H_2 mixtures is up to 20 times higher than for IRMOF-1 membranes. These results are the first specific example of the idea that varying the structure of a MOF can lead to large changes in the performance of a MOF-based membrane. Most of this increase in performance is associated with the higher adsorption

selectivity of CuBTC. Changes in the characteristics of molecular diffusion between the two materials also contribute to the variation in membrane performance, but it appears that focusing attention on adsorption selectivity will be a useful path forward for selecting MOFs suitable as membranes. This is a useful observation because the design or selection of materials with enhanced adsorption selectivity is a conceptually easier problem than the analogous task for diffusion-based selectivity.

4.3 Conclusions

To summarize, we have showed that there is a considerable difference between ideal selectivity and mixture selectivity of a CuBTC membrane, a conclusion that is similar to previous calculations for IRMOF-1 membranes. This conclusion reiterates the observation from previous chapter that it is crucial to characterize MOF membranes based on their performance for mixed gas feeds rather than extrapolating their performance from results with single gases.

Our calculations describe idealized membranes that are made from defect-free single crystals of MOFs. This situation is, of course, not practical to consider for the fabrication of real membranes for practical applications. Understanding the properties of these idealized materials, however, is useful for considering what MOFs from among the huge numbers of MOFs that have been synthesized would be worthwhile targets for experimental efforts based on either polycrystalline thin films or in mixed matrix membranes in which MOF crystals are embedded within a permeable polymer matrix.

4.4 References

(1) Wang, Q. M.; Shen, D. M.; Bulow, M.; Lau, M. L.; Deng, S. G.; Fitch, F. R.; Lemcoff, N. O.; Semanscin, J. *Micropor. Mesopor. Mater.* **2002**, *55*, 217.

(2) Millward, A. R.; Yaghi, O. M. *J. Am. Chem. Soc.* **2005**, *127*, 17998.

(3) Yang, Q.; Zhong, C. *Chem. Phys. Chem.* **2006**, *7*, 1417.

(4) Yang, Q.; Zhong, C. *J. Phys. Chem. B* **2006**, *110*, 17776.

(5) Yang, Q.; Chunyu, X.; Zhong, C.; Chen, J.-F. *AIChE J.* **2007**, *53*, 2832.

(6) Liu, J.; Culp, J. T.; Natesakhawat, S.; Bockrath, B. C.; Zande, B.; Sankar, S. G.; Garberoglio, G.; Johnson, J. K. *J. Phys. Chem. C* **2007**, *111*, 9305.

(7) Garberoglio, G.; Skoulidas, A. I.; Johnson, J. K. *J. Phys. Chem. B* **2005**, *109*, 13094.

(8) Wang, S. *Energy & Fuels* **2007**, *21*, 953.

(9) Vishnyakov, A.; Ravikovitch, P. I.; Neimark, A. V.; Bulow, M.; M.Wang, Q. *Nano Letters* **2003**, *3*, 713.

(10) Krungleviciute, V., K. Lask, L. Heroux, A. D. Migone, J.-Y. Lee, J. Li, and; Skoulidas, A. *Langmuir* **2007**, *23*, 3106.

(11) Chui, S. S.-Y.; Lo, S. M.-F.; Charmant, J. P. H.; Orpen, A. G.; Williams, I. D. *Science* **1999**, *283*, 1148.

(12) Rappe, A. K.; Casewit, C. J.; Colwell, K. S.; Goddard, W. A.; Skiff, W. M. *J. Am. Chem. Soc.* **1992**, *114*, 10024.

(13) Harris, J. G.; Yung, K. H. *J. Phys. Chem. B* **1995**, *99*, 12021.

(14) Buch, V. *J. Chem. Phys.* **1994**, *100*, 7610.

(15) Jiang, S. Y., K.E. Gubbins, and J.A. Zollweg. *Mol. Phys.* **1993**, *80*, 103.

(16) Potoff, J. J.; Siepmann, J. I. *AIChE J.* **2001**, *47*, 1676.

(17) Skoulidas, A. I.; Sholl, D. S. *J. Phys. Chem. B* **2005**, *109*, 15760.

(18) Frenkel, D.; Smit, B. *Understanding Molecular Simulation: From Algorithms to Applications*, 2nd ed.; Academic Press: San Diego, 2002.

(19) Allen, M. P.; Tildesley, D. J. *Computer Simulation of Liquids*; Oxford University Press: New York, 1987.

(20) Chen, H.; Sholl, D. S. *J. Membr. Sci.* **2006**, *269*, 152.

(21) Sanborn, M. J.; Snurr, R. Q. *Sep. Purif. Technol.* **2000**, *20*, 1.

(22) Skoulidas, A. I.; D. S. Sholl; Bowen, T. C.; Doelling, C.; Falconer, J. L.; Noble, R. D. *J. Membr. Sci.* **2003**, *227*, 123.

(23) Sholl, D. S. *Acc. Chem. Res.* **2006**, *39*, 403.

(24) Skoulidas, A. I.; Sholl, D. S.; Krishna, R. *Langmuir* **2003**, *19*, 7977.

(25) Keskin, S.; Liu, J.; Johnson, J. K.; Sholl, D. S. *Langmuir* **2008**, *24*, 8254.

(26) Newsome, D. A.; Sholl, D. S. *J. Phys. Chem. B* **2005**, *109*, 7237.

(27) Newsome, D. A.; Sholl, D. S. *Nano Lett.* **2006**, *6*, 2150.

(28) Keskin, S.; Sholl, D. S. *J. Phys. Chem. C* **2007**, *111*, 14055.

(29) Keskin, S.; Sholl, D. S. *Ind. Eng. Chem. Res.* **2009**, *48*, 914.

(30) Karra, J. R.; Walton, K. S. *Langmuir* **2008**, *24*, 8620.

(31) Heuchel, M.; Snurr, R. Q.; Buss, E. *Langmuir* **1997**, *13*, 6795.

CHAPTER 5

TESTING THE ACCURACY OF MIXING THEORIES IN METAL ORGANIC FRAMEWORKS

Mass transport of chemical mixtures in nanoporous materials is important in applications of these materials, but measuring diffusion of mixtures experimentally is challenging. Methods that can predict multi-component diffusion coefficients from single component data can be extremely useful if these methods are known to be accurate. In this chapter, we present the first test of a method of this kind for molecules adsorbed in a metal organic framework (MOF). Specifically, we examine the method proposed by Skoulidas, Sholl, and Krishna[1] (SSK) by comparing predictions made with this method to molecular simulations of mixture transport of H_2/CH_4 in CuBTC. These calculations provide the first direct information on mixture transport of any species in a MOF. The predictions of the SSK approach are in good agreement with our direct simulations of mixture diffusion, suggesting that this approach may be a powerful one for examining multi-component diffusion in MOFs. We also use our molecular simulation data to test two well known methods for predicting binary adsorption isotherms and mixture self diffusion coefficients.

5.1 Predicting Mixture Properties from Single Component Data

In many applications that are envisioned for MOFs, the behavior of mixtures of adsorbed species is of paramount importance. Although the adsorption of single component gases in MOFs has been examined in a large number of experiments,[2-7] much

less information is available about the properties of adsorbed mixtures in MOFs. This situation is more striking when the transport properties of adsorbed mixtures are considered. The diffusion of single component adsorbates in MOFs have been probed in a limited number of simulation studies[8-14] and an even smaller number of experimental studies.[15-19] To date, no information at all is available on the diffusion of multi-component adsorbed mixtures in MOFs. This lack of information strongly limits the kinds of applications for which MOFs can be considered. Membrane-based separations, for example, intrinsically rely on both adsorption and diffusion, so knowledge of how species in adsorbed mixtures diffuse is a prerequisite for considering MOFs in these applications.[20] Kinetic-based separations are widely practiced industrially with established nanoporous adsorbents;[21] these kinds of processes cannot be evaluated for MOFs without information on diffusion rates.

Because measuring mixture diffusion in nanoporous materials experimentally is challenging, molecular simulations can play a useful role by providing highly detailed information about specific examples of interest. Simulations of this kind have been used in recent years to examine a variety of nanoporous materials, including zeolites[22-25] and carbon nanotubes.[26-31] The prediction of transport properties in chemical mixtures using data taken from single component studies has been a longstanding goal in describing mass transport in complex materials.[32] The validation of methods for this task can have great practical significance, but this type of validation can only be considered when high quality mixture diffusion data is available. In this chapter, we use MD data of adsorbed gas mixtures in CuBTC to test the validity of three correlations that have been proposed to predict mixture properties from single component data. To describe the matrix of

diffusion coefficients relevant to macroscopic mass transport in adsorbed mixtures, we use the correlation developed by Skoulidas, Sholl, and Krishna (SSK).[33] This approach has previously been tested via comparison with molecular simulation data for a variety of chemical mixtures in mordenite,[34] silicalite,[25,35] faujasite[36-38] and single walled carbon nanotubes.[28,31,39] For self diffusion in binary mixtures, we use a correlation suggested by Paschek and Krishna.[40] Finally, we examine the accuracy of Ideal Adsorbed Solution Theory[41] for predicting the binary adsorption isotherm of the mixtures we considered. In each case, we find that these approaches accurately predict the mixture properties. These observations suggest that these methods may have great utility in describing the properties of adsorbed mixtures in MOFs in a way that will allow these fascinating materials to be screened for practical applications.

5.2 Computational Details

Our molecular simulations of CH_4/H_2 mixtures in CuBTC used similar methods to earlier simulations of single component gas adsorption and diffusion in this material.[8,42] Both adsorption and diffusion simulations were performed at 298 K. In these simulations, a rigid CuBTC structure with a unit cell dimension of 26.343 Å was used. The atomic positions of CuBTC were obtained from X-ray diffraction data,[43] from which we removed the atoms belonging to the solvent molecules. We used the universal force field (UFF)[44] for the framework atoms in our simulations. A spherical Lennard-Jones (LJ) 12-6 potential was used to model adsorbed H_2 and CH_4 molecules.[45,46] The fluid-fluid interaction potential parameters used in our simulations are reported in Table 5.1. The Lorentz-Berthelot mixing rules were employed to calculate the fluid-solid LJ cross interaction parameters. The fluid-fluid and fluid-solid intermolecular potentials were

truncated at 17 Å for adsorption simulations and no long-range corrections were applied. Fluid-fluid and fluid-solid intermolecular potentials were truncated at 13 Å for diffusion simulations, with long-range corrections applied. We have verified that diffusivities calculated using a cut-off radius of 13 Å with long-range corrections gives results that are indistinguishable from calculations using a truncation of 17 Å without long-range corrections. For adsorption simulations, we used a simulation box of 2×2×2crystallographic unit cells whereas for diffusion the size of the simulation box was 1×1×1.

Table 5.1 Lennard-Jones potential parameters for adsorbate molecules used in this work.

Adsorbate	Reference	σ (Å)	ε/*k* (K)
H_2	45	2.960	34.20
CH_4	46	3.812	148.20

We used the conventional GCMC technique in this work to compute adsorption isotherms.[47,48] The details of GCMC simulations for binary mixture adsorption are given in the previous chapter. Equilibrium MD simulations were used to compute the self and corrected diffusivities for pure adsorbates and mixture self diffusion coefficients and Onsager transport coefficients for adsorbed mixtures with a 75/25, 50/50, and 25/75 ratio of H_2/CH_4 in CuBTC. The details of using EMD simulations to obtain these diffusion coefficients once the interaction parameters for adsorbates in a nanoporous adsorbent have been defined have been described in previous studies of zeolites and carbon nanotubes.[8,23,25,28,49] We used a Nosé-Hoover thermostat in NVT-MD simulations and

performed 40 independent MD simulations, each having a simulation length of 20-30 ns, for each loading and/or composition we considered. Using a large number of independent trajectories is vital in order to compute the corrected diffusivities (for pure fluids) and Onsager coefficients (for mixtures). After creating initial states with the appropriate loading using GCMC, each system was first equilibrated with EMD for about 20 ps prior to taking data.

Below, we discuss the results from our molecular simulations of binary adsorption and diffusion of H_2/CH_4 mixture in CuBTC in the context of predicting these mixture properties using single component data. For each property of interest, we introduce a method that has been proposed for predicting mixture properties and then compare the outcomes of this method with data obtained directly from our molecular simulations of adsorbed mixtures.

5.2.1 Macroscopic Diffusion Coefficients

We tested the accuracy of the method of Skoulidas, Sholl, and Krishna (SSK)[33] for predicting the binary matrix of Fickian diffusivities of H_2/CH_4 mixtures in CuBTC. To apply this method, it is necessary to first describe adsorption and diffusion of each species in the mixture as a single component. We first obtained single component adsorption isotherms from GCMC simulations. Dual-site Langmuir isotherms (defined in Equation 3.1 in Chapter 3) were fitted to each single component isotherm. At low pressures (between 0.001 bar and 1 bar), the adsorption isotherm of H_2 was fitted to Henry's law, whereas adsorption isotherm of CH_4 was fitted to an independent dual site Langmuir isotherms. The parameters of these models are defined in Table 5.2, where H_{H2} represents the Henry's constant of H_2. These models were used to define the saturation

loading of each adsorbed species. Room temperature single component adsorption isotherms of H_2 and CH_4 in CuBTC are shown in Figure 5.1.

Table 5.2 Values and units of single component isotherm parameters.

Parameters at pressures > 1 bar	Units	Values
a	molecules/unit cell	161.16
b	bar	1170.8
c	molecules/unit cell	113.24
d	bar	245.79
e	molecules/unit cell	50.882
f	bar	252.77
g	molecules/unit cell	126.57
h	bar	12.538
Parameters at pressures ≤ 1 bar	Units	Values
H_{H2}	molecules/unit cell/bar	0.6054
e	molecules/unit cell	46.296
f	bar	4.8481
g	molecules/unit cell	5.4074
h	bar	0.3582

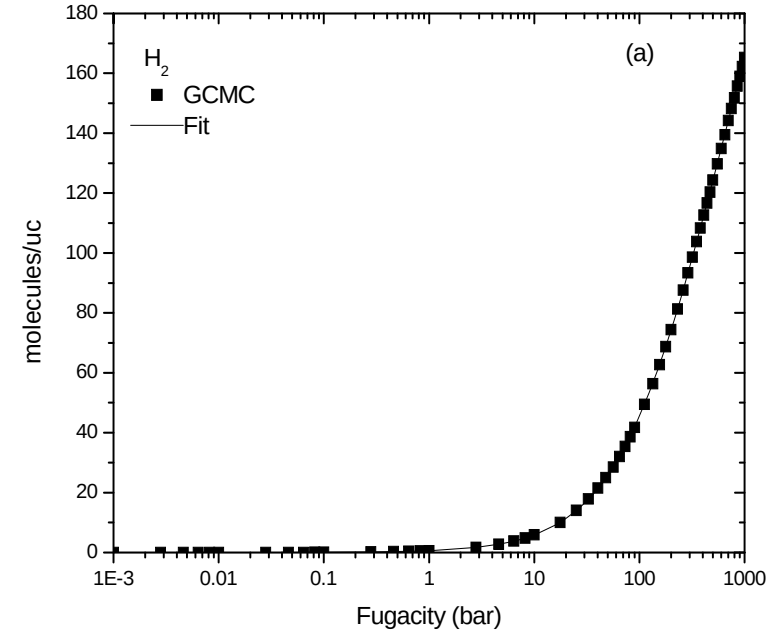

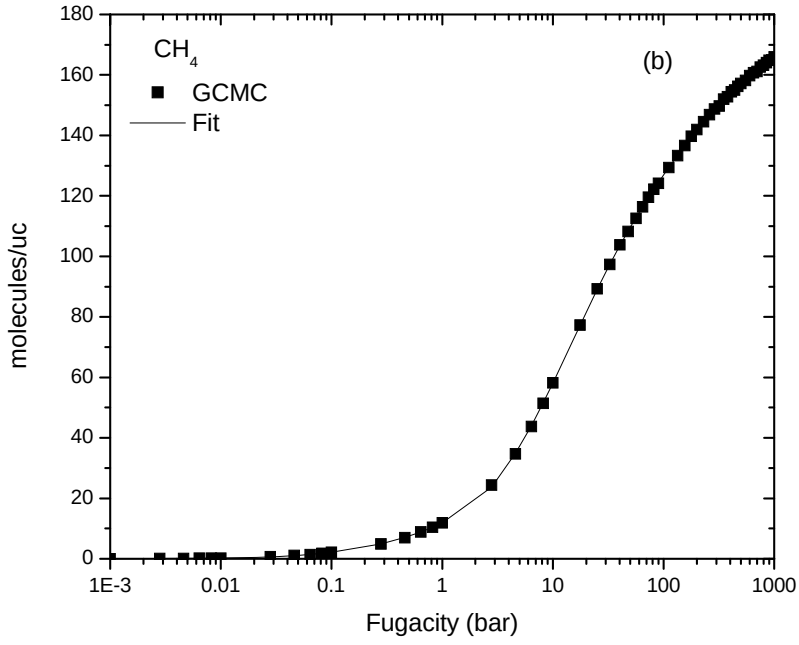

Figure 5.1 Single-component adsorption isotherm of (a) H_2 (b) CH_4 in CuBTC.

In order to use the SSK approach to describe mixture diffusion, continuous functions describing the pure component self and corrected diffusivities are required. Single component self and corrected diffusivities, $D_{self,i}$ and $Đ_i$, respectively, of H_2 and CH_4 in CuBTC were computed by MD as explained in Chapter 2. The corrected diffusivity, $Đ_i$, of H_2 and CH_4 was fitted to a second order and fifth order polynomial, respectively. An exponential function was used to describe the self diffusivity of H_2 whereas a fifth order polynomial was fitted for self diffusivity of CH_4:

$$Đ_{H_2} = A_1 + A_2\theta_{H_2} + A_3{\theta_{H_2}}^2 \tag{5.1}$$

$$Đ_{CH_4} = B_1 + B_2\theta_{CH_4} + B_3{\theta_{CH_4}}^2 + B_4{\theta_{CH_4}}^3 + B_5{\theta_{CH_4}}^4 + B_6{\theta_{CH_4}}^5 \tag{5.2}$$

$$D_{self,H_2} = R_1 \exp(-\theta_{H_2} / R_2) + R_3 \tag{5.3}$$

$$D_{self,CH_4} = S_1 + S_2\theta_{CH_4} + S_3{\theta_{CH_4}}^2 + S_4{\theta_{CH_4}}^3 + S_5{\theta_{CH_4}}^4 + \mathrm{S}_6{\theta_{CH_4}}^5 \tag{5.4}$$

These two diffusivities were fitted to continuous functions subject to two constraints. At zero loading, the functions describing the corrected diffusivities were constrained to give the observed self diffusion coefficients. As mentioned in this section, the two diffusivities must coincide at this loading. At the saturation loadings defined by the dual-site Langmuir single component isotherms, each diffusivity coefficient was constrained to be zero (see Figures 5.2 and 5.3). The fitted diffusivities were written as a function of fractional loading $\theta_i = \Theta_i / \Theta_{i,sat}$ in which Θ_i and $\Theta_{i,sat}$ represent the loading of species *i* and the saturation loading of species *i*, respectively. The fitted parameters for the functions describing each single component diffusivity coefficients are given in Table 5.3.

Table 5.3 Values and units of parameters in fitting functions for diffusivities.

Parameters	Values	Units	Parameters	Values	Units
A_1	0.00151	cm^2/s	R_1	-0.00139	cm^2/s
A_2	0.00094	cm^2/s	R_2	-1.36042	-
A_3	-0.02480	cm^2/s	R_3	0.00290	cm^2/s
B_1	6.67E-5	cm^2/s	S_1	6.67E-5	cm^2/s
B_2	0.00136	cm^2/s	S_2	0.00129	cm^2/s
B_3	-0.00568	cm^2/s	S_3	-0.00524	cm^2/s
B_4	0.01495	cm^2/s	S_4	0.00852	cm^2/s
B_5	-0.01928	cm^2/s	S_5	-0.00643	cm^2/s
B_6	0.00860	cm^2/s	S_6	0.00179	cm^2/s

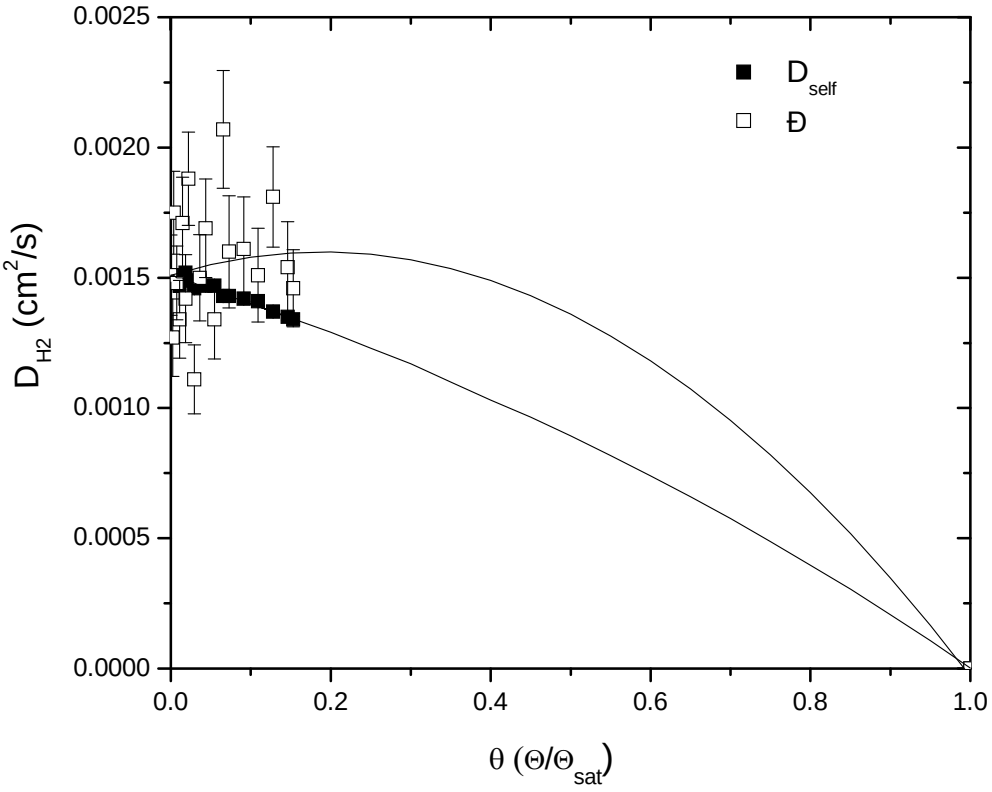

Figure 5.2 Self and corrected diffusion coefficients of H_2 in CuBTC at 298 K. Symbols show the data from the MD simulations, while curves show the fitting functions defined in the text.

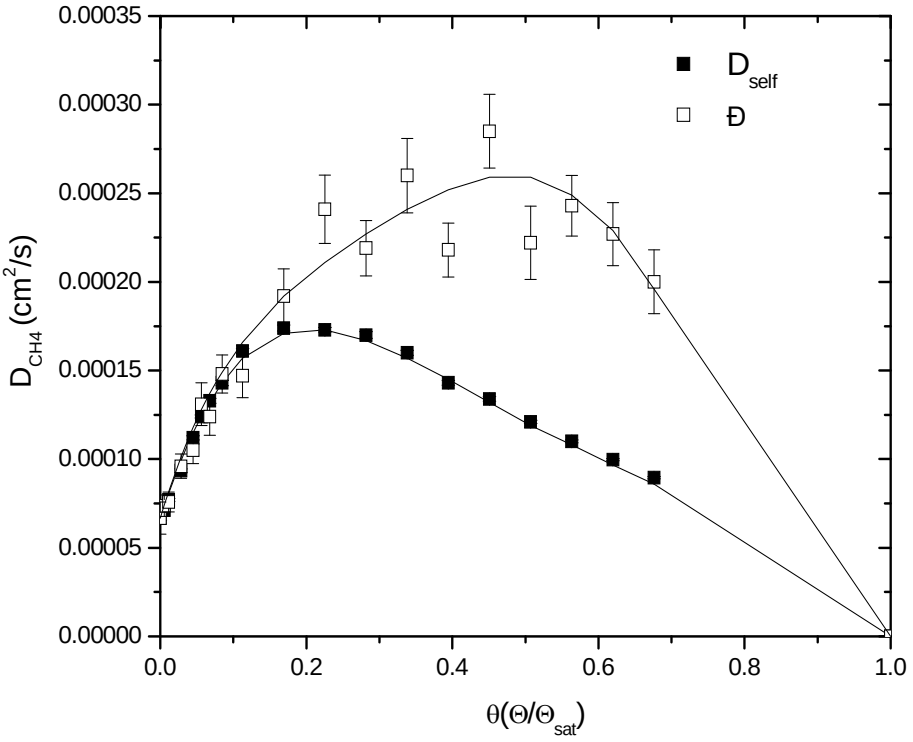

Figure 5.3 Self and corrected diffusion coefficients of CH_4 in CuBTC at 298 K. Symbols show the data from the MD simulations, while curves show the fitting functions defined in the text.

When diffusion of a binary mixture is considered, the self and corrected diffusivity values can still be defined, and they depend in general, on the loading of all adsorbed species, so $D_{i,self} = D_{i,self}(\Theta_1,\Theta_2)$ and $Đ_i = Đ_i(\Theta_1,\Theta_2)$. In an adsorbed mixture, two additional diffusion coefficients define the correlation effects,[33] the self-exchange diffusivity, $Đ_{ii}^{corr}$, and the binary-exchange diffusivity, $Đ_{ij}^{corr}$. Correlation effects can be affected by the topology of the adsorbent or momentum transfer between sorbed molecules[24] or the concerted motions of clusters of sorbed molecules.[22,50] To predict these two diffusivities, the SSK approach replaces the fractional single component

occupancy, θ, with the fractional total occupancy, $(\theta_1+\theta_2)=(\Theta_1/\Theta_{1,sat},\Theta_2/\Theta_{2,sat})$ and estimates the so-called self exchange diffusivities, $Đ_{ii}^{corr}$, using

$$D_{i,self}(\theta)=\frac{1}{\frac{1}{Đ_i(\theta)}+\frac{\theta}{Đ_{ii}^{corr}(\theta)}} \tag{5.5}$$

In a similar way, the binary-exchange coefficients, $Đ_{ij}^{corr}$, are estimated by[33]

$$\Theta_{j,sat}Đ_{ij}^{corr}(\theta)=\left[\Theta_{j,sat}Đ_{ii}^{corr}(\theta)\right]^{\theta_i/\theta_i+\theta_j}\left[\Theta_{i,sat}Đ_{jj}^{corr}(\theta)\right]^{\theta_j/\theta_i+\theta_j} \tag{5.6}$$

To calculate the matrix of Fickian diffusivities from these quantities, we need to calculate two matrices, the correlation matrix [B], with elements

$$B_{ii}=\frac{1}{Đ_i}+\sum_{j=1,j\neq i}^{n}\frac{\theta_j}{Đ_{ij}^{corr}}\ ,\qquad B_{ij}=\frac{-\theta_i}{Đ_{ij}^{corr}},\qquad i,j=1,2 \tag{5.7}$$

and the matrix of thermodynamic correction factors [Γ], with elements

$$\Gamma_{ij}=\left(\frac{\Theta_{j,sat}}{\Theta_{i,sat}}\right)\frac{\Theta_i}{p_i}\frac{\partial p_i}{\partial\Theta_j}=\frac{\theta_i}{\theta_j}\frac{\partial\ln p_i}{\partial\ln\theta_j},\quad i,j=1,2 \tag{5.8}$$

Here, p_i is the partial pressure of species i in the bulk phase in equilibrium with the adsorbed phase.

To evaluate the thermodynamic correction factors defined above, we computed the binary adsorption isotherm of H_2/CH_4 mixtures in CuBTC using GCMC simulations. These simulations were performed for mixture compositions from 0.1 to 0.9 at 9 different

compositions and total pressures from 0.001 bar to 90 bar at 31 different pressures. We then fitted our GCMC data to an extended dual-site Langmuir model as described in Equations 3.3 and 3.4 of Chapter 3. The parameters of this model are tabulated in Table 5.4. A comparison of the agreement between the fitted isotherms and our GCMC data is shown in Figure 5.4. All thermodynamic correction factors used in our prediction of the binary diffusivities below were calculated from the extended dual-site Langmuir model.

Table 5.4 Values of parameters used in fitting the binary adsorption of CH_4/H_2 mixtures.

Parameters	Values	Parameters	Values	Units
a_1	0.013574	b_1	11.083189	molecules/unit cell
a_2	0.000140	b_2	0.033765	-
a_3	0.002532	b_3	2.467720	-
a_4	0.051036	b_4	0.546420	bar
a_5	0.013574	b_5	4.392285	molecules/unit cell
a_6	0.000140	b_6	0.001781	-
a_7	0.002532	b_7	0.031440	-
a_8	0.051036	b_8	0.511919	bar

The approach defined above for computing the adsorbed mixture's thermodynamic correction factors does not strictly follow the idea of predicting mixture diffusivities using only single component data. To achieve this goal, we would need to predict the binary adsorption isotherm using only single component data. We discuss the use of Ideal Adsorbed Solution Theory (IAST) for this purpose in section 5.2.3.

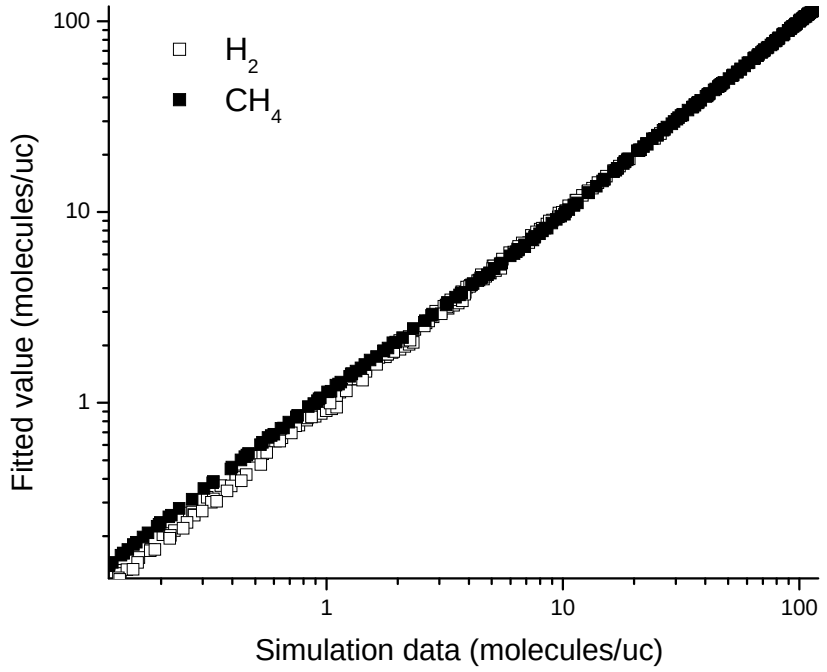

Figure 5.4 A comparison of the binary adsorption isotherms determined from GCMC simulations and calculated using the fitting functions described in the text at all state points.

Finally, with the knowledge of correlation factors [B] and thermodynamic correction factors [Γ], an explicit expression exists for the Fickian matrix [D]:

$$[D] = [B]^{-1}[\Gamma], \quad [D] = \begin{pmatrix} D_{11} & D_{12} \\ D_{21} & D_{22} \end{pmatrix}. \qquad 5.9$$

Our MD simulations calculated Onsager coefficients, L_{ij}, rather than Fickian diffusivities.[25,28] These Onsager coefficients and the matrix of Fickian coefficients are mathematically equivalent and they are related to each other without approximation by expressions involving derivatives of the mixture adsorption isotherm for the adsorbed

species as discussed in Chapter 2.[33] We converted the Onsager coefficients from our MD simulations into Fickian diffusion coefficients using Equation 2.14 of Chapter 2.

The predictions of the SSK mixing theory for various compositions of adsorbed H_2/CH_4 mixtures in CuBTC are compared with our MD data in Figures 5.5, 5.6 and 5.7. Here and below subscripts 1 (2) refers to H_2 (CH_4). As shown in these figures, the general agreement between the SSK approach and MD simulations is good. Although the predictions of SSK theory are not perfect, they capture the quantitative trends of MD simulations.

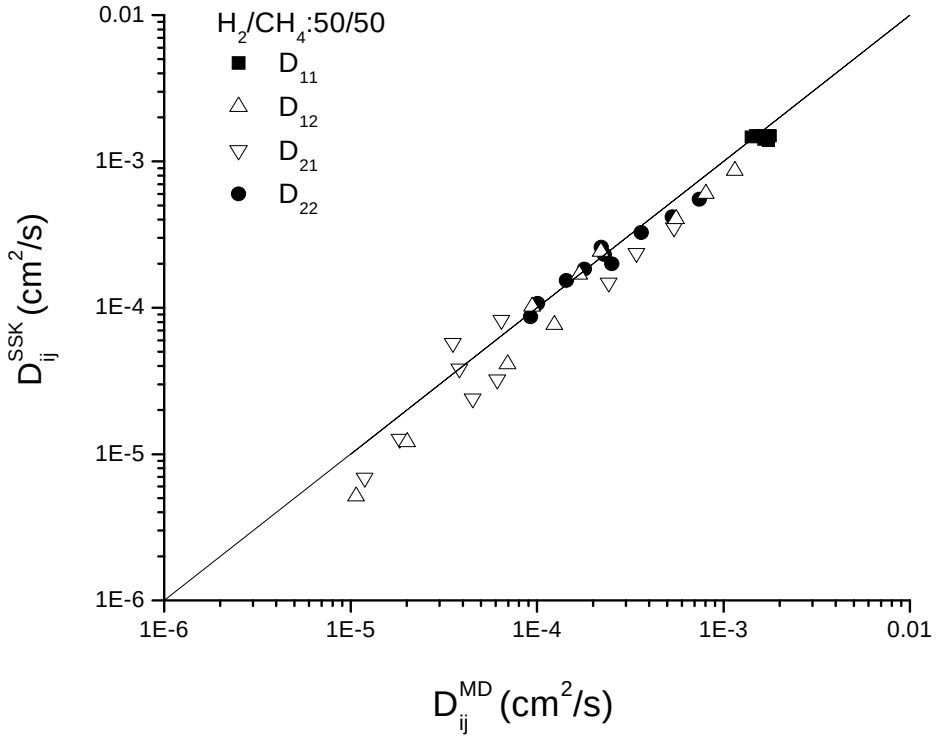

Figure 5.5 A comparison of the Fickian diffusivity matrix elements computed using EMD (horizontal axis) with the predictions of SSK theory (vertical axis) for H_2/CH_4 mixture compositions of 50/50.

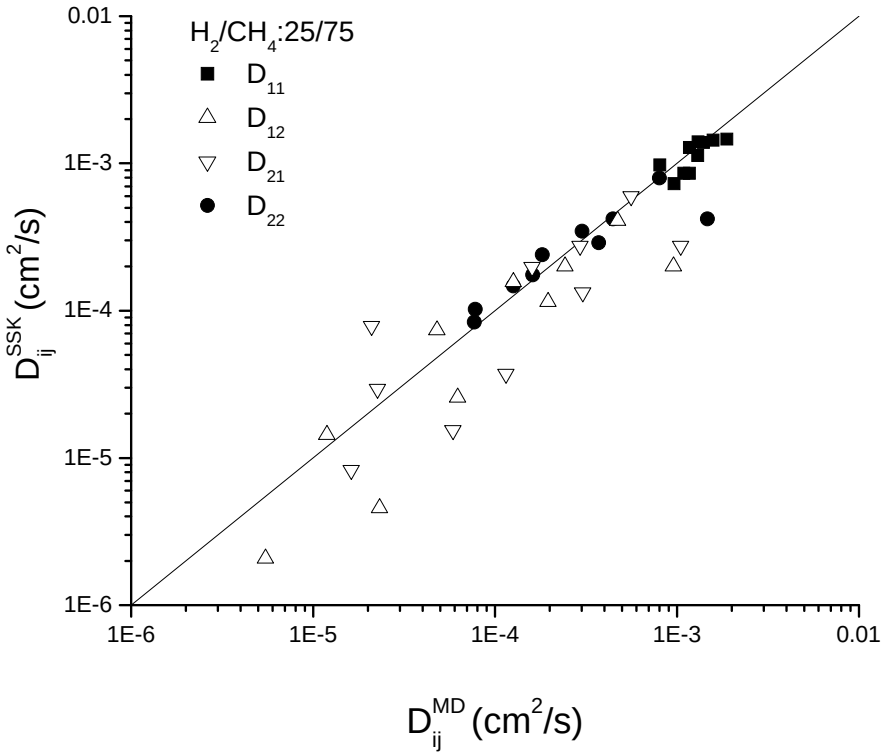

Figure 5.6 A comparison of the Fickian diffusivity matrix elements computed using EMD (horizontal axis) with the predictions of SSK theory (vertical axis) for H_2/CH_4 mixture compositions of 25/75.

This theory has been tested before for several different systems. Krishna and co-workers used MD simulations to compare mixture diffusion data of hexane/butane isomers in mordenite,[34] linear alkanes in silicalite[35] and faujasite[36,37] and in single walled carbon nanotube.[39] In all of these cases, the SSK approach was observed to give accurate predictions. Our current results have a similar level of agreement with these earlier tests of this approach. The one example where the SSK approach is known to give inaccurate results comes from calculations by Sholl[51] for four lattice models with different levels of site energy heterogeneity. In models with strongly heterogeneous site energy distributions, the predictions of the SSK approach were found to be quite inaccurate.

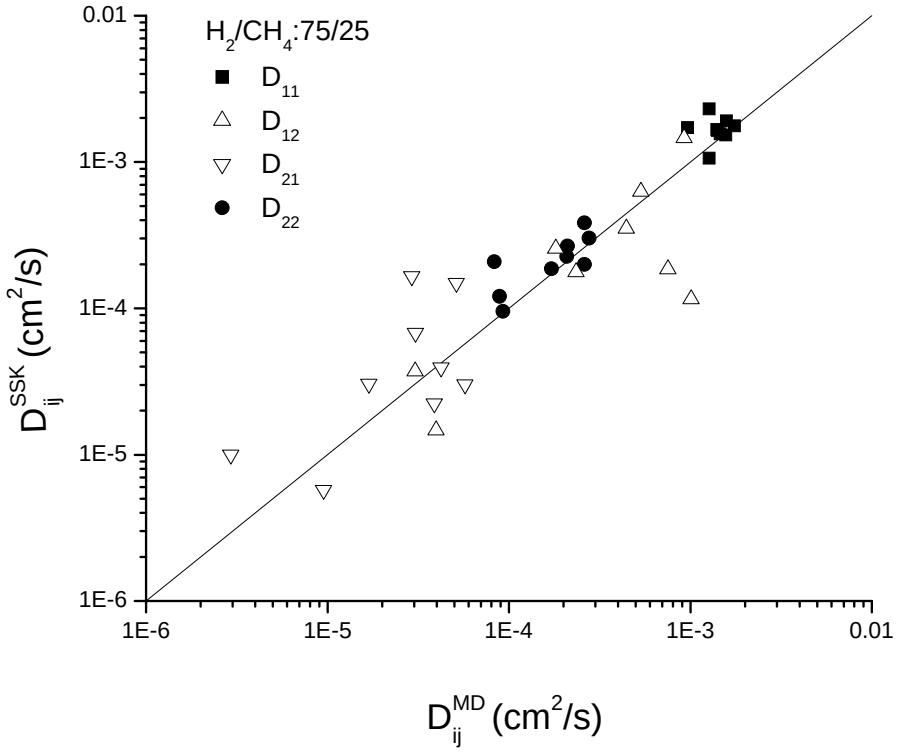

Figure 5.7 A comparison of the Fickian diffusivity matrix elements computed using EMD (horizontal axis) with the predictions of SSK theory (vertical axis) for H_2/CH_4 mixture compositions of 75/25.

Several statistics characterizing the agreement (or lack thereof) between the SSK-based predictions and our MD data are summarized in Table 5.5. The predictions of the mixing theory are generally more accurate for the diagonal diffusivities than the off-diagonal diffusivities. It is important to note that there are many state points shown in Figure 5.5, 5.6 and 5.7 where the off-diagonal diffusion coefficients, D_{12} and D_{21}, are comparable in magnitude to the diagonal diffusion coefficients.

Table 5.5 Statistics summarizing the comparison between mixture diffusion coefficients predicted by SSK method, D_{ij}^{SSK} and the mixture diffusion coefficients calculated by EMD simulations, D_{ij}.

composition (H_2/CH_4)	mean	standard deviation	maximum	minimum
50/50				
D_{11}^{SSK}/D_{11}	0.90	0.09	1.04	0.79
D_{12}^{SSK}/D_{12}	0.77	0.22	1.10	0.48
D_{21}^{SSK}/D_{21}	0.82	0.37	1.62	0.52
D_{22}^{SSK}/D_{22}	0.95	0.14	1.18	0.74
25/75				
D_{11}^{SSK}/D_{11}	0.96	0.15	1.21	0.73
D_{12}^{SSK}/D_{12}	0.80	0.48	1.54	0.20
D_{21}^{SSK}/D_{21}	1.09	1.15	3.75	0.26
D_{22}^{SSK}/D_{22}	1.10	0.18	1.32	0.29
75/25				
D_{11}^{SSK}/D_{11}	1.28	0.34	1.82	0.97
D_{12}^{SSK}/D_{12}	0.95	0.48	1.57	0.25
D_{21}^{SSK}/D_{21}	1.97	1.80	5.64	0.53
D_{22}^{SSK}/D_{22}	1.32	0.53	2.51	0.77
all data				
D_{11}^{SSK}/D_{11}	1.02	0.27	1.82	0.73
D_{12}^{SSK}/D_{12}	0.81	0.40	1.57	0.20
D_{21}^{SSK}/D_{21}	1.23	1.24	5.64	0.26
D_{22}^{SSK}/D_{22}	1.09	0.37	2.51	0.29

For 50/50 adsorbed mixtures of H_2/CH_4, the mixing theory underestimates all four coefficients on average. D_{11} was underestimated by ~10% on average whereas D_{22} was underpredicted by ~5% on average. For the state points that showed the poorest

agreement between the MD data and the mixing theory for this composition, the diagonal diffusivities were underpredicted by ~20%. The off-diagonal coefficients were underestimated by ~20% on average, and in the worst case example, D_{21} was overestimated by ~60%.

In mixtures with a 25/75 composition of adsorbed H_2/CH_4, D_{11} and D_{12} were underestimated whereas D_{21} and D_{22} were overestimated. The average deviations between the mixing theory and the MD data for D_{11} and D_{22} for this composition were ~4% and ~10%, respectively. For the off-diagonal diffusivities, the average deviations were found to be higher, ~20% and ~9% for D_{12} and D_{21}. In the worst case scenario, D_{21} was overestimated by almost a factor of 4. Similarly, in a composition of H_2/CH_4:75/25, the predictions for D_{21} were less accurate than the other diffusion coefficients. For the worst example, this coefficient was overestimated by a factor of 5. The diagonal coefficients were overestimated by ~30% on average for this mixture composition.

Both diagonal and off-diagonal diffusivity coefficients were predicted more accurately for the 50/50 adsorbed mixture of H_2/CH_4 than those of 25/75 or 75/25 mixtures. This observation is consistent with previous applications of the SSK theory in other nanoporous materials. The predictions of the mixing theory for CH_4/CF_4 mixtures in silicalite were compared with MD simulations of same mixture in an earlier work and the mixing theory was found to be somewhat inaccurate for the highest concentrations of CH_4/CF_4 mixtures.[23]

It is interesting to consider how well mixture transport diffusivities can be predicted as the composition of the adsorbed phase is varied. The nature of the EMD simulations used to directly examine binary diffusion may play a role in this observation,

as it is intrinsically more difficult to accumulate accurate statistics for species-species interactions when one species is present at low concentrations. Despite this issue, our results support the idea that the SSK approach for predicting mixture transport diffusivities in the examples we have explored is greater for equimolar adsorbed mixtures than for adsorbed mixtures with 25/75 or 75/25 compositions. Adsorbed mixtures with highly asymmetric compositions can be relevant in a variety of practical applications, so it would be helpful to develop information in future studies of this kind on the applicability of the SSK approach to compositions of this kind.

5.2.2 Mixture Self Diffusion Coefficients

We now turn to the self diffusion of each species in adsorbed mixtures in CuBTC. Molecular simulations of self diffusion in adsorbed mixtures in zeolites has played an important role in understanding this phenomena, and several studies have made careful comparisons between simulated and measured mixture self diffusivities.[52-54] No previous experimental or simulation data for mixture self diffusion in MOFs is available.

Krishna and Paschek[55] introduced the following model in order to predict the self diffusion coefficients in a mixture from single component data:

$$D_{i,self} = \frac{1}{\frac{1}{Đ_i} + \frac{\theta_i}{Đ_{ii}^{corr}} + \frac{\theta_j}{Đ_{ij}^{corr}}}, \quad D_{j,self} = \frac{1}{\frac{1}{Đ_j} + \frac{\theta_i}{Đ_{ji}^{corr}} + \frac{\theta_j}{Đ_{jj}^{corr}}} \qquad 5.10$$

This model has been tested in carbon nanotubes[39] and MFI zeolite,[33] where the predictions of the model were found to be in good agreement with MD simulations of

mixture diffusion. In this model, $D_{i,self}$ is the self diffusivity of species *i* in a binary mixture with species *j*, $Đ_i$ is the pure component Maxwell-Stefan diffusivity (also known as corrected diffusivity, as discussed above) , $Đ_{ii}$ and $Đ_{ij}$ are the self-exchange and binary-exchange diffusivities and θ_i is the fractional loading of species *i*. In application of this expression, it is important to remember that since we have a binary mixture, the corrected diffusivities are actually evaluated at the total fractional loading, not at the pure component fractional loading.

Here, we compare predictions made using Krishna and Paschek's approach with our direct MD simulations of adsorbed mixtures. Self diffusivities, $D_{self,i}$, for single component adsorbates and mixtures and single component corrected diffusivities, $Đ_i$, were computed using MD simulations as described in Chapter 2 and exchange coefficients were computed as explained in section 5.2.1. Mixture self diffusivity predictions given by Krishna and Paschek's correlation and EMD simulations are compared for H_2/CH_4 in CuBTC at room temperature in Figure 5.8. This figure shows the data for adsorbed mixtures of H_2/CH_4 with three different compositions: 50/50, 25/75 and 75/25. The predictions for self diffusivities in a mixture are in a good agreement with the results of MD simulations.

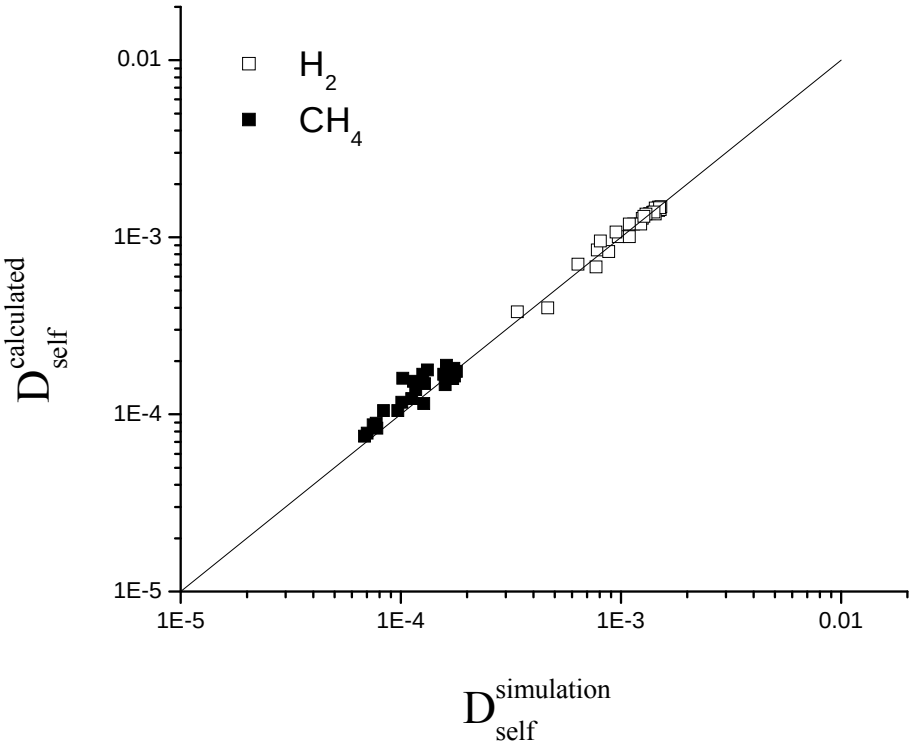

Figure 5.8 A comparison of the binary self diffusion coefficients computed using EMD and calculated using correlation of Paschek and Krishna described in the text.

A comparison of the binary self diffusion coefficients as a function of total loading for these three mixture compositions is given in Figure 5.9. Each figure demonstrates that the self diffusivity of the fast species, H_2, becomes slower due to the slow CH_4 molecules, whereas the diffusivity of slow species, CH_4, increases in the presence of the fast species. The observation that a slowly diffusing species strongly reduces the diffusivity of a faster diffusing species in an adsorbed mixture is a common one.[23]

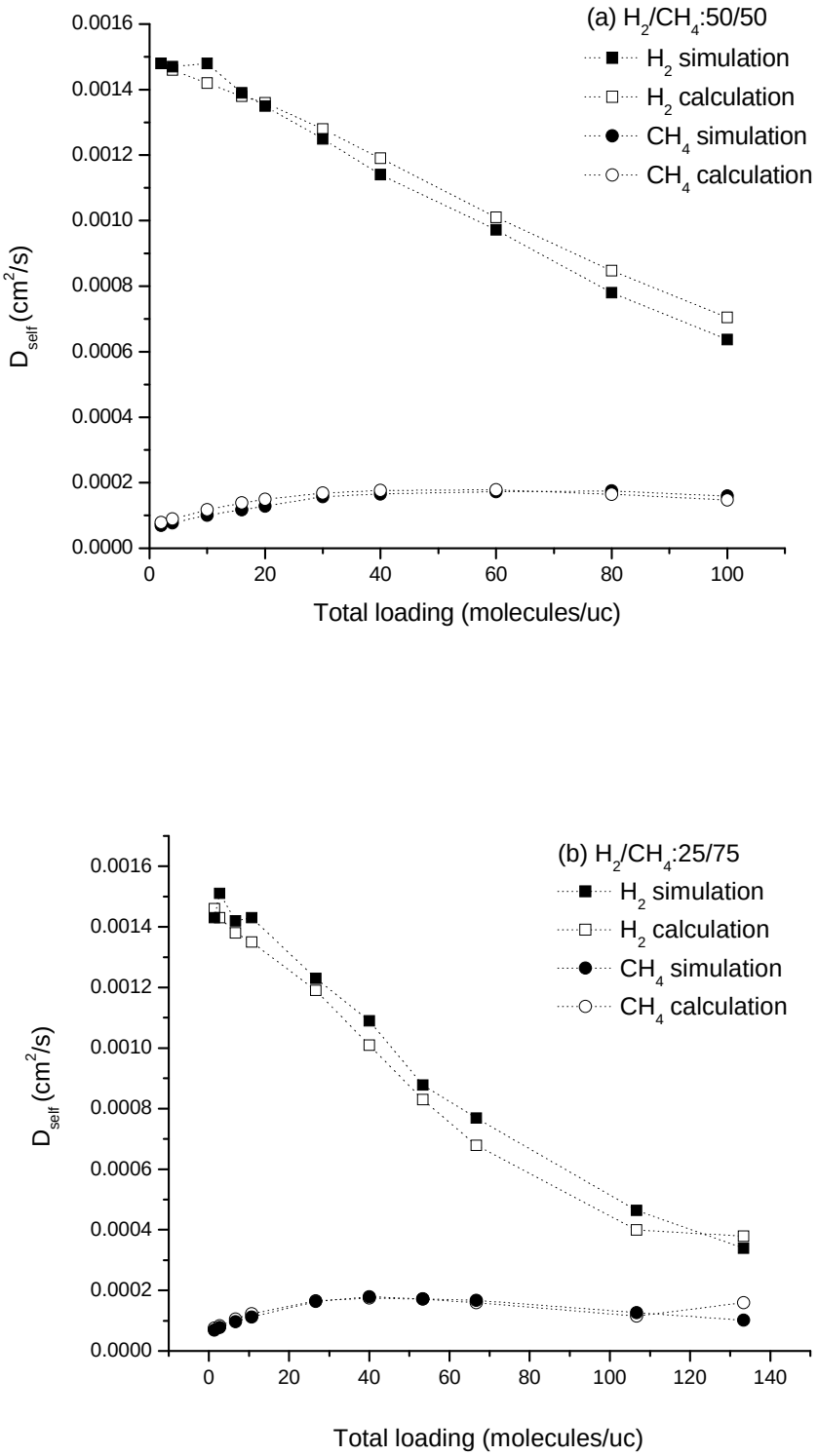

Figure 5.9 A comparison of the binary self diffusion coefficients computed using EMD and calculated using the Krishna's models as a function of total loading for H_2/CH_4 mixture compositions of (a) 50/50, (b) 25/75, (c) 75/25.

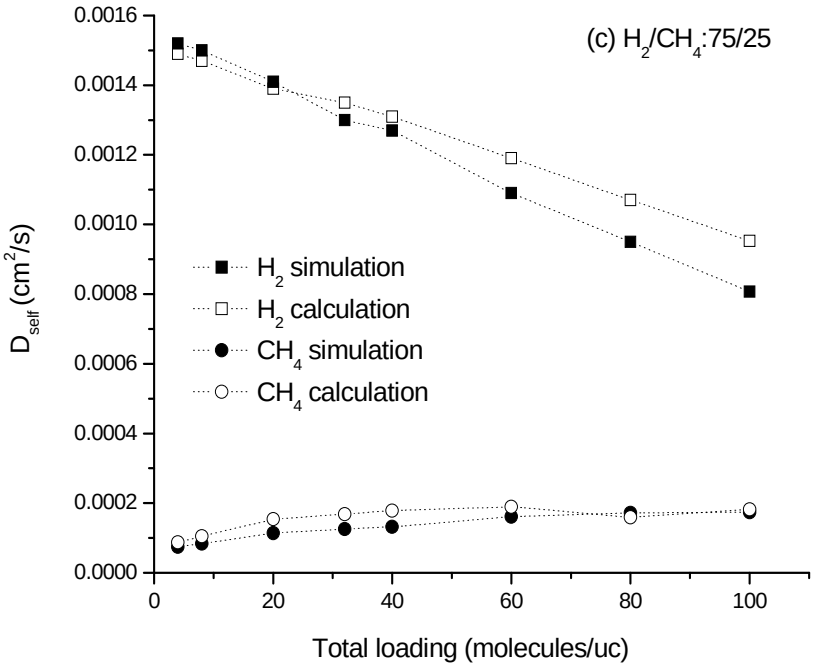

Figure 5.9 Continued

5.2.3 Binary Adsorption Isotherms

In the calculations above, we performed GCMC simulations of mixture adsorption and fitted the resulting simulation data to continuous models in order to calculate thermodynamic correction factors numerically. In cases where binary adsorption data is not available, Ideal Adsorbed Solution Theory (IAST)[41] can be used to predict binary adsorption isotherms. Therefore, we also examined the accuracy of IAST for H_2/CH_4 mixtures in CuBTC by using the single component adsorption data obtained from GCMC simulations. IAST is a well developed technique to describe the calculation of the adsorption equilibria for components in a gaseous mixture, using only data for the pure component adsorption equilibria at the same temperature and on the same adsorbent.[41] This theory is known to work accurately in many nanoporous materials

except in materials which have strong energetic or geometric heterogeneity.[56,57] It has been pointed out that IAST becomes less accurate at high densities of the adsorbed species, even for mixtures that are relatively ideal and therefore other approaches have been also proposed to deal with the nonideality.[56,58-62] Furthermore, IAST has been tested recently for adsorption of light gases in MOF-5 and CuBTC by comparing the results of binary molecular simulations and the predictions of theory.[63-65] The agreement between IAST predictions and binary mixture adsorption simulation results in these examples was generally found to be good.

In Figure 5.10, we compare the predictions of IAST with our direct GCMC simulation results for adsorption of H_2/CH_4 mixture in CuBTC. Overall, the IAST predictions are in a good agreement with the simulation data. The one collection of data that shows some systematic inaccuracy in the IAST predictions corresponds to adsorption predictions for CH_4 in a gas phase mixture composition of H_2/CH_4:0.9/0.1. In this limit, the single component isotherm for H_2 must be integrated to extremely high fugacities to apply IAST, a situation that introduces imprecision into IAST. A detailed discussion of the sources of inaccuracies in applying IAST was given by Chen and Sholl.[56]

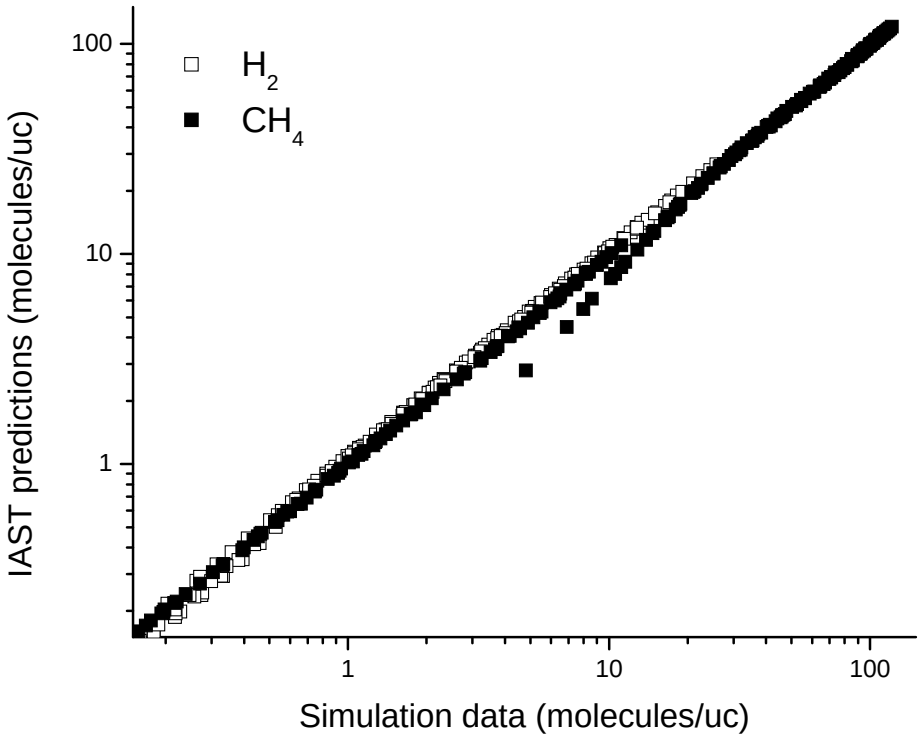

Figure 5.10 A comparison of the binary adsorption isotherms determined from GCMC simulations and predicted using IAST at all state points.

We noted earlier in this chapter that our application of the SSK approach to predict binary diffusion made use of information from the binary adsorption isotherm. If IAST is used instead of the binary adsorption isotherm data, then the SSK approach can be used with only single component data. To examine what impact using IAST would have in this process, we repeated the calculations using IAST to generate data equivalent to that in Figure 5.4 for fitting a continuous model for the binary isotherm. This revised isotherm was then used along with the same information on single component diffusion as before to predict the binary Fickian diffusivities for all state points we examined using binary EMD. The statistics summarizing these calculations are listed in Table 5.6.

Table 5.6 Statistics summarizing the comparison between mixture diffusion coefficients predicted by SSK method, D_{ij}^{SSK} and the mixture diffusion coefficients calculated by EMD simulations, D_{ij} (calculations performed with IAST generated binary isotherms).

composition (H_2/CH_4)	mean	standard deviation	maximum	minimum
50/50				
D_{11}^{SSK}/D_{11}	0.90	0.09	1.04	0.80
D_{12}^{SSK}/D_{12}	0.79	0.20	1.09	0.52
D_{21}^{SSK}/D_{21}	0.85	0.34	1.58	0.54
D_{22}^{SSK}/D_{22}	0.95	0.14	1.18	0.74
25/75				
D_{11}^{SSK}/D_{11}	1.19	0.31	1.83	0.78
D_{12}^{SSK}/D_{12}	1.57	1.02	3.56	0.39
D_{21}^{SSK}/D_{21}	0.56	0.36	1.25	0.19
D_{22}^{SSK}/D_{22}	0.98	0.25	1.29	0.33
75/25				
D_{11}^{SSK}/D_{11}	1.05	0.22	1.57	0.85
D_{12}^{SSK}/D_{12}	0.90	0.29	1.36	0.45
D_{21}^{SSK}/D_{21}	0.97	0.44	1.63	0.35
D_{22}^{SSK}/D_{22}	1.46	0.59	2.87	1.05
all data				
D_{11}^{SSK}/D_{11}	1.06	0.24	1.83	0.78
D_{12}^{SSK}/D_{12}	1.06	0.65	3.56	0.39
D_{21}^{SSK}/D_{21}	0.77	0.40	1.63	0.19
D_{22}^{SSK}/D_{22}	1.07	0.44	2.87	0.33

Overall, the statistics for the IAST-based calculations in Table 5.6 are quite similar to those in Table 5.5. This is not surprising; it simply reflects the fact that IAST provides a good description of mixture adsorption in this material. The statistics in Table 5.6 for

the diagonal diffusivities are essentially equivalent to the statistics in Table 5.5. For D_{12}^{SSK}/D_{12}, the mean when IAST is used (Table 5.6) is slightly closer to one than for the data in table 5.5, but the IAST data show more scatter. For D_{21}^{SSK}/D_{21}, the statistics for the IAST based calculations are somewhat better than the data in Table 5.5, but we believe that this result stems from fortuitous cancelation of errors rather than any genuine physical effect. For adsorbed compositions at high concentrations that are dominated by H_2, the use of IAST introduces inaccuracies in the calculated thermodynamic correction factors, and these result in a reduction of the accuracy of the diffusion coefficients predicted with the SSK approach. In principle, these inaccuracies could be reduced while still using only single-component data by using mixing theories for adsorption that go beyond IAST.[56] For our example, the uncertainty introduced by using IAST appears to be considerably smaller than the uncertainty associated with the predictions of the SSK approach, so using more elaborate mixing theories does not seem justified in this case.

5.3 Conclusions

To summarize, we present the first examination of diffusion of a mixture of adsorbed molecules in a MOF material in this chapter. Specifically, we use molecular simulations to examine mixture adsorption and diffusion of H_2/CH_4 mixture in CuBTC. The data from these simulations made it possible to test several correlations that have been proposed previously to predict mixture transport and adsorption properties in nanoporous materials. The main conclusion from these calculations is that for H_2/CH_4 mixtures in CuBTC it is possible to predict mixture properties from single component data with a high degree of accuracy. This conclusion has important implications for predicting the possible utility of MOFs in chemical separations, especially in applications

that rely on mass transport of adsorbed species. By using these correlations, it is possible to rapidly examine a large range of potential operating conditions for chemical mixtures as soon as information on each species in the MOF of interest is known. If methods equivalent to the correlations we have explored were not available, the performance of MOFs for chemical mixtures could only be tested by accumulating detailed mixture diffusion and adsorption data at every state point relevant to the macroscopic process being examined. An example of using the correlations we have tested here for predicting the performance of MOF-5 and CuBTC in membrane-based separations of gas mixtures has been given in Chapter 3 and Chapter 4 and our current results give good support for the validity of those calculations.

An important issue that we cannot directly address with our current results is the generality of our conclusion that the properties of adsorbed mixtures in MOFs can be predicted from single component data. We can speculate about this issue from two perspectives. First, could similar levels of agreement be expected for H_2/CH_4 mixtures in other MOFs? The answer to this question seems likely to be yes, since CuBTC does not have any structural characteristics that suggest it defines a potential energy surface for these adsorbed species that differs greatly in character from other MOFs. This idea is supported by the observation that qualitative aspects of molecular diffusion in MOFs have been found to be similar to diffusion in noncationic zeolites,[8] and the same correlations that we have used here have been shown to work well in a variety of noncationic zeolites. We also show examples where these correlations are successful to predict adsorption and diffusion of H_2/CH_4 mixtures in other MOFs in the next chapter.

Second, how well would these correlations perform for a more chemically complex adsorbed mixture in CuBTC or some other MOF? Previous tests of these methods for a variety of mixtures of nonpolar species in noncationic zeolites have yielded good results,[37,66] and we speculate the similar outcomes will be found for MOFs. To date, however, there have not been extensive tests of these approaches for mixtures involving polar species. We also show and discuss the results of using correlations to predict mixture self diffusivities and adsorption isotherms for CO_2/H_2 mixture in several different types of MOF structures in the next chapter.

It is important to note in closing that our analysis of mixture diffusion in MOFs is entirely based on results of our molecular simulations for these phenomena. This state of affairs inevitably introduces issues related to the fidelity of simulations of this kind to the properties of real materials. In our MD simulations, to give just an example of an issue of this type, the MOF framework was treated as being rigid; this is clearly not the situation in a real MOF. It would of course be very interesting to compare the predictions of our calculations against detailed experimental measurements of molecular diffusion in MOFs, and we hope that this work motivates future experimental work of this kind.

5.4 References

(1) Skoulidas, A. I.; Sholl, D. S.; Krishna, R. *Langmuir* **2003**, *19*, 7977.

(2) Lee, J. Y.; Li, J.; Jagiello, J. *J. Solid State Chem.* **2005**, *178*, 2527.

(3) Zhou, W.; Wu, H.; Hartman, M. R.; Yildirim, T. *J. Phys. Chem. C* **2007**, *111* 16131.

(4) Millward, A. R.; Yaghi, O. M. *J. Am. Chem. Soc.* **2005**, *127*, 17998.

(5) Garberoglio, G.; Skoulidas, A. I.; Johnson, J. K. *J. Phys. Chem. B* **2005**, *109*, 13094.

(6) Eddaoudi, M.; Li, H.; Yaghi, O. M. *J. Am. Chem. Soc.* **2000**, *122*, 1391.

(7) Wong-Foy, A. G.; Matzger, A. J.; Yaghi, O. M. *J. Am. Chem. Soc.* **2006**, *128*, 3494.

(8) Skoulidas, A. I.; Sholl, D. S. *J. Phys. Chem. B* **2005**, *109*, 15760.

(9) Skoulidas, A. I. *J. Am. Chem. Soc.* **2004**, *126*, 1356.

(10) Amirjalayer, S.; Tafipolsky, M.; Schmid, R. *Angew. Chem. Int. Ed.* **2007**, *46*, 463.

(11) Düren, T.; Snurr, R. Q. *J. Phys. Chem. B* **2004**, *108*, 15703.

(12) Yang, Q.; Zhong, C. *J. Phys. Chem. B* **2005**, *109*, 11862.

(13) Liu, B.; Yang, Q.; Xue, C.; Zhong, C.; Smit, B. *Phys. Chem. Chem. Phys.* **2008**, *10*, 3244.

(14) Liu, J.; Lee, J. Y.; Pan, L.; Obermyer, R. T.; Simizu, S.; Zande, B.; Li, J.; Sankar, S. G.; Johnson, J. K. *J. Phys. Chem. C* **2008**, *112*, 2911.

(15) Stallmach, F.; Groger, S.; Kunzel, V.; Kärger, J.; Yaghi, O. M.; Hesse, M.; Muller, U. *Angew. Chem. Int. Ed.* **2006**, *45*, 2123.

(16) Salles, F.; Jobic, H.; Maurin, G.; Koza, M. M.; Llewellyn, P. L.; Devic, T.; Serre, C.; Ferey, G. *Phys. Rev. Lett.* **2008**, *100*, 245901.

(17) Rosenbach, N.; Jobic, H.; Ghoufi, A.; Salles, F.; Maurin, G.; Bourrrelly, S.; Llewellyn, P. L.; Devic, T.; Serre, C.; Ferey, G. *Angew. Chem. Int. Ed.* **2008**, *47*, 6611.

(18) Greathouse, J. A.; Allendorf, M. D. *J. Phys. Chem. C* **2008**, *112*, 5795.

(19) Chmelik, C.; Kärger, J.; Wiebcke, M.; Caro, J.; van Baten, J. M.; Krishna, R. *Micropor. Mesopor. Mater.* **2009**, *117*, 22.

(20) Keskin, S.; Sholl, D. S. *J. Phys. Chem. C* **2007**, *111*, 14055.

(21) Yang, R. T. *Gas Separation by Adsorption Processes*; Butterworths: Boston, 1987.

(22) Sholl, D. S. *Ind. Eng. Chem. Res.* **2000**, *39*, 3737.

(23) Sholl, D. S. *Acc. Chem. Res.* **2006**, *39*, 403.

(24) Skoulidas, A. I.; Sholl, D. S. *J. Phys. Chem. B* **2002**, *106*, 5058.

(25) Skoulidas, A. I.; Sholl, D. S.; Bowen, T. C.; Doelling, C.; Falconer, J. L.; Noble, R. D. *J. Membrane Sci.* **2003**, *227*, 123.

(26) Skoulidas, A. I.; Sholl, D. S.; Johnson, J. K. *J. Chem. Phys.* **2006**, *124*, 054708.

(27) Skoulidas, A. I.; Ackerman, D. M.; Johnson, J. K.; Sholl, D. S. *Phys. Rev. Lett.* **2002**, *89*, 185901.

(28) Chen, H.; Sholl, D. S. *J. Membrane Sci.* **2006**, *269*, 152.

(29) Chen, H.; Johnson, J. K.; Sholl, D. S. *J. Phys. Chem. B* **2006**, *110*, 1971.

(30) Jakobtorweihen, S.; Verbeek, M. G.; Lowe, C. P.; Keil, F. J.; Smit, B. *Phys. Rev. Lett.* **2005**, *95*, 044501.

(31) Chen, H.; Sholl, D. S. *J. Am. Chem. Soc.* **2004**, *126*, 7778.

(32) Wesselingh, J. A.; Krishna, R. *Mass Transfer in Multicomponent Mixtures*; Delft University Press: Delft, 2000.

(33) Skoulidas, A. I.; Sholl, D. S.; Krishna, R. *Langmuir* **2003**, *19*, 7977.

(34) van Baten, J. M.; Krishna, R. *Micro. Meso. Mat.* **2005**, *84*, 179.

(35) Krishna, R.; van Baten, J. M. *Chem. Phys. Lett.* **2005**, *407*, 159.

(36) Krishna, R.; van Baten, J. M. *J. Phys. Chem. B* **2005**, *109*, 6386.

(37) Chempath, S.; Krishna, R.; Snurr, R. Q. *J. Phys. Chem. B* **2004**, *108*, 13481.

(38) Sanborn, M. J.; Snurr, R. Q. *AIChE Journal* **2001**, *47*, 2032.

(39) Krishna, R.; van Baten, J. M. *Ind. Eng. Chem. Res.* **2006**, *45*, 2084.

(40) Krishna, R.; Paschek, D. *Phys. Chem. Chem. Phys.* **2002**, *4*, 1891.

(41) Myers, A. L., and J.M. Prausnitz. *AIChE Journal* **1965**, *11*, 121.

(42) Liu, J.; Culp, J. T.; Natesakhawat, S.; Bockrath, B. C.; Zande, B.; Sankar, S. G.; Garberoglio, G.; Johnson, J. K. *J. Phys. Chem. C* **2007**, *111*, 9305.

(43) Chui, S. S. Y.; Lo, S. M. F.; Charmant, J. P. H.; Orpen, A. G.; Williams, I. D. *Science* **1999**, *283*, 1148.

(44) Rappe, A. K.; Casewit, C. J.; Colwell, K. S.; Goddard, W. A.; Skiff, W. M. *J. Am. Chem. Soc.* **1992**, *114*, 10024.

(45) Buch, V. *J. Chem. Phys.* **1994**, *100*, 7610.

(46) Jiang, S. Y.; Gubbins, K. E.; Zollweg, J. A. *Mol. Phys.* **1993**, *80*, 103.

(47) Allen, M. P.; Tildesley, D. J. *Computer Simulation of Liquids*; Oxford University Press: New York, 1987.

(48) Frenkel, D.; Smit, B. *Understanding Molecular Simulation: From Algorithms to Applications*; Academic Press: London, 1996.

(49) Sanborn, M. J.; Snurr, R. Q. *Sep. Purif. Technol.* **2000**, *20*, 1.

(50) Sholl, D. S.; Lee, C. K. *J. Chem. Phys.* **2000**, *112*, 817.

(51) Sholl, D. S. *Langmuir* **2006**, *22*, 3707.

(52) Jost, S.; Bär, N.; Fritzsche, S.; Haberlandt, R.; Kärger, J. *J. Phys.Chem. B* **1998**, *102*, 6375.

(53) Gergidis, L. N.; Theodorou, D. N.; Jobic, H. *J. Phys. Chem. B* **2000**, *104*, 5541.

(54) Paschek, D.; Krishna, R. *Langmuir* **2001**, *17*, 247.

(55) Krishna, P.; Paschek, D. *Phys. Chem. Chem. Phys.* **2002**, *4*, 1891.

(56) Chen, H.; Sholl, D. S. *Langmuir* **2007**, *23*, 6431.

(57) Murthi, M.; Snurr, R. Q. *Langmuir* **2004**, *20*, 2489.

(58) Dunne, J.; Myers, A. L. *Chem. Eng. Sci.* **1994**, *49*, 2941.

(59) Murthi, M.; Snurr, R. Q. *Langmuir* **2004**, *20*, 2489.

(60) Akten, E. D.; Siriwardane, R.; Sholl, D. S. *Energy Fuel* **2003**, *17*, 977.

(61) Costa, E.; Sotelo, J. L.; Calleja, G.; Marro´n, C. *AIChE* **1981**, *27*, 5.

(62) Goj, A.; Sholl, D. S.; Akten, E. D.; Kohen, D. *J. Phys. Chem. B* **2002**, *106*, 8367.

(63) Yang, Q.; Zhong, C. *J. Phys. Chem. B* **2006**, *110*, 17776.

(64) Wang, S.; Yang, Q.; Zhong, C. *J. Phys. Chem. B* **2006**, *110*, 20526.

(65) Babarao, R.; Hu, Z.; Jiang, J.; Chempath, S.; Sandler, S. I. *Langmuir* **2007**, *23*, 659.

(66) van Baten, J. M.; Krishna, R. *Micro. Meso. Mat* **2005**, *84*, 179.

CHAPTER 6

EFFICIENT METHODS FOR SCREENING METAL ORGANIC FRAMEWORK MEMBRANES

We presented atomically-detailed calculations to predict the performance of MOFs for membrane-based separations of gases in the previous chapters. However, these calculations require considerable computational resources and time. In this chapter, we introduce an efficient approximate method for screening MOFs based on atomistic models that will accelerate the modeling of membrane applications. The validity of this approximate method is examined by comparison with detailed calculations for CH_4/H_2, CO_2/CH_4 and CO_2/H_2 mixtures at room temperature permeating through IRMOF-1 and CuBTC membranes. These results allow us to hypothesize a connection between two computationally efficient correlations predicting mixture adsorption and mixture self diffusion properties and the validity of our approximate screening method. We then apply our model to six additional MOFs, IRMOF-8, -9, -10 and -14, $Zn(bdc)(ted)_{0.5}$, and COF-102, to examine the effect of chemical diversity and interpenetration on the performance of MOF membranes for light gas separations.

6.1 Necessity for a Screening Model

The enormous number of distinct MOFs that are known presents both a challenge and an opportunity for development of MOF-based membranes. The wide range of available pore sizes, topologies, and functionalities strongly suggests that existing MOFs will have useful properties as membranes for separations of practical interest. The considerable resources that are necessary to fabricate membranes from new crystalline

materials, however, mean that it is impractical to consider screening large numbers of potential materials experimentally. This situation suggests that quantitative computational modeling can play a useful role in selecting materials that deserve experimental development.[1]

We have previously developed methods suitable for using atomistic models to predict the permeability and selectivity of MOF membranes for gas separations by examining CH_4/H_2, CO_2/CH_4 and CO_2/H_2 mixtures at room temperature permeating through IRMOF-1 and CuBTC membranes.[2-4] These methods provide useful insight into the mixture effects that can dominate membrane performance at moderate and high pressure conditions. Unfortunately, the computational requirements for applying these methods make it impractical to consider using them to screen a large number of MOFs, although they can certainly be of value for making detailed predictions about specific materials of interest.

In this chapter, we describe, validate, and apply an approximate modeling strategy based on atomistic simulations that can be used to accelerate the screening of MOFs for membrane applications. This approximate approach is motivated by our earlier detailed studies of IRMOF-1 and CuBTC membranes,[2-4] and we use detailed calculations from these two MOFs to probe the validity of the approximate approach. We find that the approximate approach is valid in many but not all cases, and we propose a computationally efficient strategy for identifying the latter cases using two well-known correlations for mixture adsorption and mixture self diffusivities.

Having introduced our new method, we apply it to eight MOFs, IRMOF-1,-8, -9, -10 and -14, CuBTC, $Zn(bdc)(ted)_{0.5}$, and COF-102 (see Figures 1.2, 1.3 and 6.1). The

IRMOF materials share the same octahedral $Zn_4O(CO)_2$ clusters linked by different organic dicarboxylate linkers, so they provide an example of how varying the pore size influences membrane performance. IRMOF-9 is a catenated version of IRMOF-10,[5] so including these two materials gives an example of the influence of catenation on the membrane performance. In a catenated material, two independent frameworks self-assemble in an interpenetrated manner.[5-8] The possible utility of using catenation to enhance gas adsorption has been discussed by Snurr and co-workers, who observed that the influence of catenation depends on the physical conditions of the targeted application.[6] IRMOF-1, -8, -10 and 14 are three dimensional cubic structures with pore sizes 10.9/14.3, 12.5/17.1, 16.7/20.2, 14.7/20.1 Å in diameter, respectively.[5] IRMOF-9 is a cubic catenated structure with four different pores 4.5/6.3/8.1/10.7 Å in diameter. CuBTC, also known as HKUST-1, has main channels 9 Å in diameter, surrounded by tetrahedral pockets with diameters of 5 Å and windows 3.5 Å wide.[9] $Zn(bdc)(ted)_{0.5}$ and COF-102 were chosen to represent MOFs with somewhat smaller pore sizes. $Zn(bdc)(ted)_{0.5}$ is a tetragonal structure with one channel having cross section of 7.5×7.5 Å and a smaller channel with a cross section of 4.8×3.2 Å.[10] COF-102 is a covalent organic framework that consists of organic linkers covalently bonded with boron oxide clusters. The largest cavity in the center of COF-102 is around 5.6 Å from the nearest hydrogen atoms.[11] For each material, we considered CH_4/H_2, CO_2/CH_4 and CO_2/H_2 mixtures at room temperature. CH_4/H_2 mixtures are important in the process of purification of synthetic gas obtained from steam reforming of natural gas. Removal of CO_2 from CO_2/CH_4 and CO_2/H_2 mixtures are relevant for upgrading natural gas and purifying hydrogen.

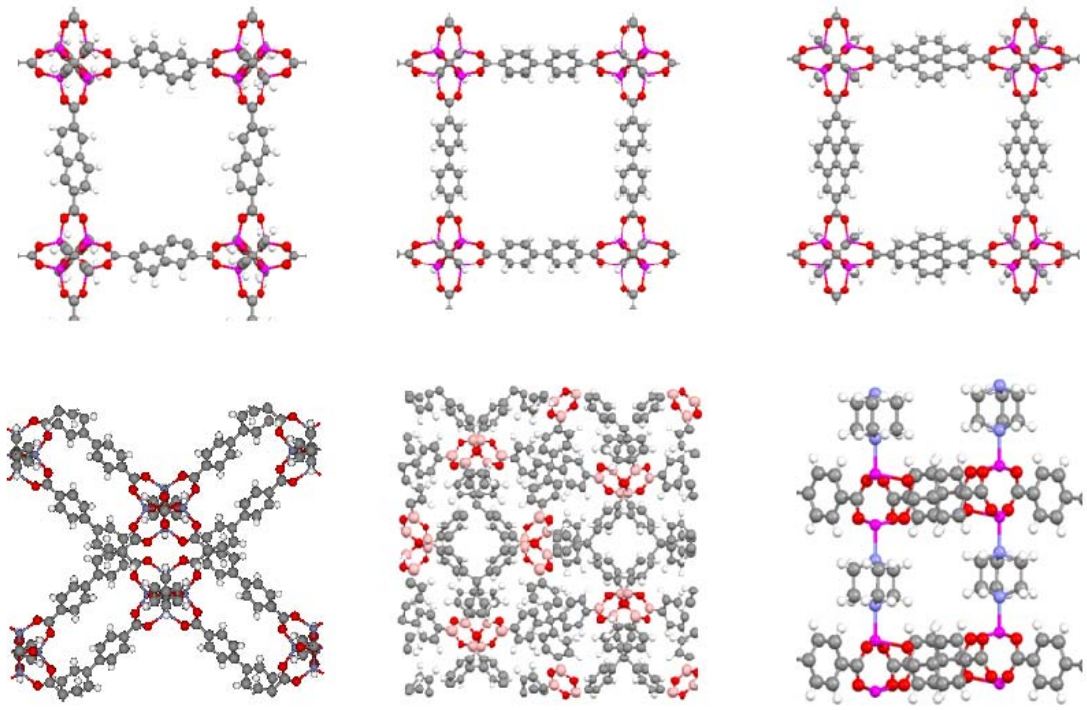

Figure 6.1 Unit cell structures of MOFs considered as membrane materials: From left to right: IRMOF-8, IRMOF-10, IRMOF-14 (top line), IRMOF-9, COF-102, $Zn(bdc)(ted)_{0.5}$ (bottom line). Zn: violet, O: red, C: gray, B: pink, N: purple and H: white.

The materials that we listed above have already been studied by several groups using molecular modeling. Babarao and Jiang reported a molecular simulation study for CO_2 storage in IRMOF-1, IRMOF-14 and COF-102.[12] Yang et al. used molecular simulations to investigate the properties of CO_2 adsorption and diffusion in IRMOF-1, -8, -10 and CuBTC.[13] Liu et al. studied adsorption and diffusion of H_2 in $Zn(bdc)(ted)_{0.5}$ using molecular simulations.[10] Although most previous modeling examined non-catenated IRMOFs, studies on catenated MOFs have only started more recently. Liu and co-workers studied the interpenetrated MOFs IRMOF-9, -11 and -13 for adsorption-based separation of CH_4/H_2 mixture using molecular simulations.[14] Liu et al. also investigated the effect of hydrogen diffusion in the same interpenetrated MOFs.[15] These

studies have investigated single component and mixture gas adsorption and single component gas diffusion but they do not give information about the potential of MOFs in membrane applications. Here, we use molecular modeling to report the first intrinsic information of these materials as membranes.

6.2 Computational Details

In the earlier chapters of this thesis, we described a method that combines atomistic and continuum modeling to estimate the intrinsic properties of single crystal MOF membranes.[2-4] Throughout the remainder of this chapter we will refer to this method as a "detailed calculation" for a MOF membrane. In these calculations, as in the approximate method defined below, we assume that the crystal structure of the MOF is known from experiment and that interatomic potentials for interactions between adsorbed molecules and the MOF are available. Our methods are suitable for simulations in which the MOF framework is allowed to be flexible[16] but all of the calculations we report below treat the framework as rigid. This assumption, which is reasonable in many cases, means that interatomic potentials defining the degrees of freedom within the MOF framework do not need to be specified.

To motivate our new computationally efficient approximate method, it is useful to summarize the key steps within a detailed calculation:[2-4]

(1) A set of continuous functions that quantifies mixture adsorption at all bulk compositions and pressures of interest must be developed. This task can be accomplished by performing mixture Grand Canonical Monte Carlo (GCMC) simulations at a large number of bulk phase conditions and then developing functions that fit this data.

(2) Equilibrium Molecular Dynamics (MD) simulations are used to calculate the loading-dependent single component self and corrected diffusivities for each adsorbed species of interest. Self diffusivities describe the motion of individual molecules, whereas the corrected diffusivity (also known as the Maxwell-Stefan diffusivity) incorporates information about the collective motion of multiple adsorbed molecules.[17-22] These diffusivities must be calculated for the full range of molecular loadings that is available in the MOF (as defined by the single component adsorption isotherm). Calculating corrected diffusivities using MD is computationally demanding since the collective nature of this property requires >20 independent MD simulations at each state point.[17,20,21,23]

(3) To describe mixture permeation, information about macroscopic mixture diffusion is required. In principle, this information can be obtained via equilibrium MD simulations at a large number of state points, but this approach is extremely computationally intensive.[18-21,23-26] In practice, we avoid this difficulty by using a correlation introduced by Skoulidas, Sholl and Krishna (SSK)[26] for predicting mixture diffusivities from the data available from steps (1) and (2) above. To apply the SSK method, functions describing the single component self and corrected diffusivities of each species as a function of their loadings are needed.

(4) Once both mixture adsorption and diffusion data is available, a straightforward continuum model is used to predict the steady state permeance of gas mixtures through a membrane. These calculations are based on a shell model, which assumes the matrix of Fickian diffusivities for the adsorbed components is constant throughout the membrane at the concentration defined by the mean of feed and permeate side concentrations.[27]

The overall computational effort associated with this approach is dominated by the calculation of the single component corrected diffusivities. As noted above, the calculation of this quantity at each state point requires tens of independent MD trajectories. From the standpoint of practical implementation, the curve fitting that is required in steps (1) and (3) also creates a barrier to efficiently adapting this overall calculation to new materials. Below, we describe an approximate method for characterizing the performance of a MOF membrane from an atomically-detailed model of the material that avoids both of these undesirable features of our previous method.

To introduce our new method, it is important to describe in more precise terms what we mean by characterizing the performance of a MOF membrane. Both the permeability and selectivity of membranes are important performance metrics. The MOF membranes that we have examined previously have all had high permeability but relatively low selectivity,[2-4] indicating that the latter property is of more importance than the former in searching for materials with attractive prospects for practical implementation. We therefore aim to screen membrane materials based on their selectivity for mixture permeation. In principle, a membrane's selectivity is a function of the feed pressure, feed composition, and transmembrane pressure drop. The selectivity is typically a relatively weak function of the feed composition, so it is acceptable for screening purposes to choose any feed composition that is convenient. On this basis, we have reported extensive calculations of membrane selectivities as functions of feed pressure and pressure drop.[2-4] A key observation from these detailed calculations is that the maximum selectivity at a fixed feed pressure is observed for a pressure drop close to total feed pressure. In other words, choosing the permeate side to be a vacuum is a useful

approximation for estimating the maximum membrane selectivity. These observations reduce the task of characterizing the membrane selectivity to understanding the selectivity as a function of single parameter, the feed pressure, at a well defined feed composition and pressure drop. It is important in this context to note that we intend that the calculations we describe below will be used in the context of materials screening, meaning that when materials with promising properties are found they can be characterized more accurately using detailed calculations at the full range of operating conditions of interest.

Recently, Krishna and van Baten suggested that the selectivity of zeolite membranes under conditions where the permeate side was a vacuum could be approximated by[28]

$$\alpha_{perm,1/2} = \frac{D_{1,self}}{D_{2,self}} \cdot \frac{q_1}{q_2} = \alpha_{diff} \cdot \alpha_{sorp} \qquad 6.1$$

where $\alpha_{perm,1/2}$, α_{sorp} and α_{diff} represents the permeation selectivity of species 1 over species 2, the sorption selectivity and diffusion selectivity, respectively. In this approximate expression, the diffusion selectivity is defined as the ratio of self diffusivities in a binary mixture, $D_{i,self}$ whereas the sorption selectivity is described as the ratio of adsorbed molar loadings, q_i. This expression differs from simpler expressions that are widely used in the membrane literature that define an "ideal" selectivity based on ratios of single component quantities. When mixture effects are important, the ideal selectivity of a membrane often differs significantly from the more important situation of a permeating mixture.[2]

To apply this expression, the conditions under which the diffusion selectivity and adsorption selectivity are evaluated must be specified. Krishna and van Baten determined adsorbed loadings using GCMC simulations with equimolar bulk mixtures, and determined the self diffusivity data in Equation 6.1 from MD simulations of equimolar adsorbed mixtures. In some cases, MD simulations were performed at 3:1 or 10:1 adsorbed molar loadings to reflect the adsorption selectivities of these zeolites. A disadvantage of this approach was that the loadings used for the calculation of the diffusion selectivities did not necessarily match the loadings that would be expected in the crystal on the feed side of the membrane. Babarao and Jiang[29] recently used this approach to predict the permselectivity of IRMOF-1 as a function of total loading based on the adsorption of equimolar mixture.

We modified Krishna and van Baten's formulation in two simple ways to make it more suitable for describing membranes under arbitrary conditions. First, we allow the adsorption selectivity to be defined for an arbitrary bulk phase composition,

$$\alpha_{sorp} = \frac{(q_1 / q_2)}{(y_1 / y_2)} \tag{6.2}$$

where y_i is the mole fraction of component i in the bulk phase. Second, we use MD to evaluate the mixture self diffusivities directly at the corresponding adsorbed composition (q_1 and q_2). This replaces Equation 6.1 with

$$\alpha_{perm,1/2} = \frac{D_{1,self}(q_1, q_2)}{D_{2,self}(q_1, q_2)} \cdot \frac{q_1 / q_2}{y_1 / y_2} = \alpha_{diff} \cdot \alpha_{sorp} \tag{6.3}$$

Equation 6.3 predicts the membrane's selectivity at a specified feed pressure and composition based on a single mixture GCMC simulation and an MD simulation performed at the loadings determined from this GCMC calculation.

It is important to understand why (and when) this approximate expression is reasonable. One way to do this is to compare it analytically with the selectivity derived from our detailed calculations. The aim of this derivation is to present how our screening model approximates the selectivity of a membrane compared to the more detailed calculations of this quantity. First, we show a derivation for the selectivity of a membrane calculated by a method that uses the SSK correlation[26] to calculate the binary Fickian diffusivities. In these detailed calculations,[2-4] we define a membrane's selectivity, $S^{\det}$ for an equimolar feed mixture as the ratio of fluxes, J_i of each species where D_{ij} is an element of the matrix of Fickian diffusivities and ∇c_i is the concentration gradient of species *i*:

$$S^{\det} = \frac{J_1}{J_2} = \frac{D_{11} \cdot \nabla c_1 + D_{12} \cdot \nabla c_2}{D_{21} \cdot \nabla c_1 + D_{22} \cdot \nabla c_2} \qquad 6.4$$

In the shell model that is used in our detailed calculations, the diffusivities are evaluated at the concentrations in the center of the membrane.[27,30] When the permeate site of the membrane is kept under vacuum, the concentration gradient of each species can be written as follows:

$$\nabla c_1 = \frac{c_1^{feed} - c_1^{permeate}}{L} \simeq \frac{c_1^{feed}}{L} \quad , \nabla c_2 \simeq \frac{c_2^{feed}}{L} \qquad 6.5$$

The adsorption selectivity, α_{sorp} is defined as the ratio of adsorbed amounts of each species at the feed side for an equimolar bulk mixture. In case of a non-equimolar feed mixture, the adsorption selectivity is normalized by the bulk gas compositions, y_i of the mixture:

$$\alpha_{sorp} = \frac{c_1^{feed} / c_2^{feed}}{y_1 / y_2} \tag{6.6}$$

Using these expressions, Equation 6.4 becomes:

$$S^{\det} = \frac{D_{11} \cdot \nabla c_1 / \nabla c_2 + D_{12}}{D_{21} \cdot \nabla c_1 / \nabla c_2 + D_{22}} = \frac{D_{11} \cdot (c_1^{feed} / c_2^{feed}) + D_{12}}{D_{21} \cdot (c_1^{feed} / c_2^{feed}) + D_{22}} = \alpha_{sorp} \cdot \frac{D_{11} + \dfrac{D_{12}}{\alpha_{sorp}}}{D_{21} \cdot \alpha_{sorp} + D_{22}} \tag{6.7}$$

This result emphasizes the fact that the full Fickian diffusivity matrix needs to be known, in general, to define the overall membrane selectivity. The Fickian diffusivity matrix can be written in terms of corrected diffusivities, self-exchange and binary-exchange diffusion coefficients, fractional loadings and thermodynamic corrections factors without approximation as explained in Chapter 5:[26]

$$\begin{pmatrix} D_{11} & D_{12} \\ D_{21} & D_{22} \end{pmatrix} = \begin{pmatrix} B_{11} & B_{12} \\ B_{21} & B_{22} \end{pmatrix}^{-1} \cdot \begin{pmatrix} \Gamma_{11} & \Gamma_{12} \\ \Gamma_{21} & \Gamma_{22} \end{pmatrix} = \begin{pmatrix} \dfrac{1}{Đ_1(\theta_T)} + \dfrac{\theta_2}{Đ_{12}^{corr}(\theta_T)} & -\dfrac{\theta_1}{Đ_{12}^{corr}(\theta_T)} \\ -\dfrac{\theta_2}{Đ_{21}^{corr}(\theta_T)} & \dfrac{1}{Đ_2(\theta_T)} + \dfrac{\theta_1}{Đ_{21}^{corr}(\theta_T)} \end{pmatrix}^{-1} \cdot \begin{pmatrix} \Gamma_{11} & \Gamma_{12} \\ \Gamma_{21} & \Gamma_{22} \end{pmatrix} \tag{6.8}$$

After some algebra, Equation 6.7 becomes:

$$S^{det} = \alpha_{sorp} \cdot \frac{\frac{1}{Đ_2(\theta_T)} \cdot \left(\Gamma_{11} + \frac{\Gamma_{12}}{\alpha_{sorp}} \right) + \frac{\theta_1}{Đ_{21}^{corr}(\theta_T)} \cdot \left(\Gamma_{11} + \frac{\Gamma_{12}}{\alpha_{sorp}} + \frac{\theta_2^{sat}}{\theta_1^{sat}} \cdot \left(\Gamma_{21} + \frac{\Gamma_{22}}{\alpha_{sorp}} \right) \right)}{\frac{1}{Đ_1(\theta_T)} \cdot \left(\Gamma_{22} + \Gamma_{21} \cdot \alpha_{sorp} \right) + \frac{\theta_2}{Đ_{12}^{corr}(\theta_T)} \cdot \left(\Gamma_{22} + \Gamma_{21} \cdot \alpha_{sorp} + \frac{\theta_1^{sat}}{\theta_2^{sat}} \cdot \left(\Gamma_{12} + \Gamma_{11} \cdot \alpha_{sorp} \right) \right)} \qquad 6.9$$

In practice, we have used the SSK correlation to relate the self-exchange diffusion coefficients, which can be determined from single-component MD simulations, with the binary-exchange diffusion coefficients that appear in Equation 6.9. Equation 6.10 shows the approximate logarithmic interpolation formula used within the SSK correlation to define the relationship between these exchange diffusion coefficients. After using Equation 6.10 and introducing the terms in Equation 6.11, we can rewrite Equation 6.9 as Equation 6.12:

$$\theta_{j,sat} Đ_{ij}^{corr} = \left[\theta_{j,sat} Đ_{ii}^{corr} \right]^{\Theta_i / (\Theta_i + \Theta_j)} \left[\theta_{i,sat} Đ_{jj}^{corr} \right]^{\Theta_j / (\Theta_i + \Theta_j)} \qquad 6.10$$

$$\Gamma_{11} + \frac{\Gamma_{12}}{\alpha_{sorp}} = m \qquad \Gamma_{22} + \Gamma_{21} \cdot \alpha_{sorp} = n \qquad 6.11$$

$$S^{det} = \alpha_{sorp} \cdot \left[\frac{m}{n} \right] \cdot \frac{\frac{1}{Đ_2(\theta_T)} + \frac{\theta_1}{Đ_{21}^{corr}(\theta_T)} + \frac{\theta_2}{Đ_{22}^{corr}(\theta_T)} \cdot \left[\left(\frac{Đ_{22}^{corr}(\theta_T)}{Đ_{11}^{corr}(\theta_T)} \right)^{\frac{\theta_1 \cdot \theta_1^{sat}}{\theta_1 \cdot \theta_1^{sat} + \theta_2 \cdot \theta_2^{sat}}} \cdot \left(\frac{\theta_2^{sat}}{\theta_1^{sat}} \right)^{\frac{\theta_2 \cdot \theta_2^{sat}}{\theta_1 \cdot \theta_1^{sat} + \theta_2 \cdot \theta_2^{sat}}} \cdot \frac{n}{m} \right]}{\frac{1}{Đ_1(\theta_T)} + \frac{\theta_2}{Đ_{12}^{corr}(\theta_T)} + \frac{\theta_1}{Đ_{11}^{corr}(\theta_T)} \cdot \left[\left(\frac{Đ_{11}^{corr}(\theta_T)}{Đ_{22}^{corr}(\theta_T)} \right)^{\frac{\theta_2 \cdot \theta_2^{sat}}{\theta_1 \cdot \theta_1^{sat} + \theta_2 \cdot \theta_2^{sat}}} \cdot \left(\frac{\theta_1^{sat}}{\theta_2^{sat}} \right)^{\frac{\theta_1 \cdot \theta_1^{sat}}{\theta_1 \cdot \theta_1^{sat} + \theta_2 \cdot \theta_2^{sat}}} \cdot \frac{m}{n} \right]} \qquad 6.12$$

Equation 6.12 shows the membrane's selectivity for an equimolar feed mixture with a vanishingly small total pressure on the permeate side as calculated with our SSK-based detailed calculations.

The approximate model that we suggested, Equation 6.3, defines the membrane's selectivity as a product of the adsorption selectivity and the ratio of self diffusivities. This model is evaluated at the feed side of the membrane. In our application of Equation 6.3, we used molecular simulations to calculate the self diffusivities at these loadings. Since the shell model described above uses the average loadings at the center of the membrane and the permeate side is under vacuum, the fractional loadings at the feed side are double the loadings in the center of the membrane. In examples where Krishna and Paschek's self diffusion correlation is accurate (that is, it agrees with direct molecular simulations of mixture self diffusion), the self diffusivities in the mixture can be expressed using this correlation. If this is done, the selectivity predicted by Equation 6.3 can be written after some algebra as:

$$S^{\text{model}} = \alpha_{sorp} \cdot \alpha_{diff} = \alpha_{sorp} \cdot \frac{D_{1,self}}{D_{2,self}} = \alpha_{sorp} \cdot \frac{\dfrac{1}{2Đ_2(2\theta_T)} + \dfrac{\theta_1}{Đ_{21}^{corr}(2\theta_T)} + \dfrac{\theta_2}{Đ_{22}^{corr}(2\theta_T)}}{\dfrac{1}{2Đ_1(2\theta_T)} + \dfrac{\theta_2}{Đ_{12}^{corr}(2\theta_T)} + \dfrac{\theta_1}{Đ_{11}^{corr}(2\theta_T)}} \qquad 6.13$$

Here, the fractional loadings, θ_i, are the loadings at the center of the membrane as defined in the shell model for permeation, and the loadings at which the diffusivities are evaluated to apply the approximate model are explicitly noted. As we can see by comparing Equation 6.12 and 6.13 (or equivalently, Equation 6.3), Equation 6.13 is an

approximation to the selectivity predicted by the more detailed calculation. The model in Equation 6.13 is different than Equation 6.12 in three ways:

a) Our model calculates the corrected diffusivities and correlation diffusivities at fractional loadings that are different from the loadings used in detailed calculations. This fact leads to the factors of 2 in Equation 6.13 that do not appear in Equation 6.12.

b) Our approximate model neglects the terms given in square parentheses in Equation 6.12 that multiply the third term in both the numerator and denominator of Equation 6.12.

c) The approximate model neglects the factor of (m/n) that multiplies the entire result in Equation 6.12.

One use of the equations above is to examine the validity of our approximate method in the limit of low pressures. At sufficiently low pressures, the fractional loadings tend to approach zero, so the second and third terms in the numerator and denominator of Equation 6.12 vanish. As a result, the terms in square parentheses in Equation 6.12 that do not appear in Equation 6.13 vanish in this limit. At low pressures the corrected diffusivities are almost independent of concentration, so the differences in concentration between Equation 6.12 and 6.13 are unimportant. The term (m/n) in Equation 6.12 approaches one at low loadings because the diagonal (off-diagonal) thermodynamic corrections factors approach unity (zero) in the limit of low pressures. The fact that these methods coincide at low pressures is not surprising, but it is useful to confirm this expectation explicitly.

Another use of the equations above is to consider the accuracy of our approximate method at pressures corresponding to non-dilute loadings in the MOF membrane. The model in Equation 6.13 gives better approximations at higher loadings if:

a) each of the terms in square parentheses in Equation 6.12 are close to one in magnitude.

b) the corrected and exchange diffusivities evaluated at $2 \cdot \theta_T$ in Equation 6.13 are similar to the ones evaluated at θ_T in Equation 6.12.

Here, we briefly discuss conditions at which the situations described in (a) and (b) may hold. The terms in square parentheses in Equation 6.12 includes a factor of (*m/n*), the ratio of saturation loadings of each species and the ratio of self-exchange diffusivity coefficients. Figure 6.2 shows the values of the term (*m/n*) for three different adsorbed mixtures in CuBTC as a function of the bulk pressure, assuming an equimolar bulk mixture. The term (*m*/*n*) is close to unity at low loadings as we discussed above. The value of this term deviates from unity at higher loadings since both the diagonal and off-diagonal thermodynamic correction factors increase at higher loadings. This deviation is more pronounced if the adsorption selectivity is high for a given system. Specifically, for the systems such as CO_2/H_2 or CO_2/CH_4 (CH_4/H_2) in which adsorption selectivity increases (decreases) as the loading increases due to energetic (entropic) effects, the term (*m/n*) becomes less (more) than unity.

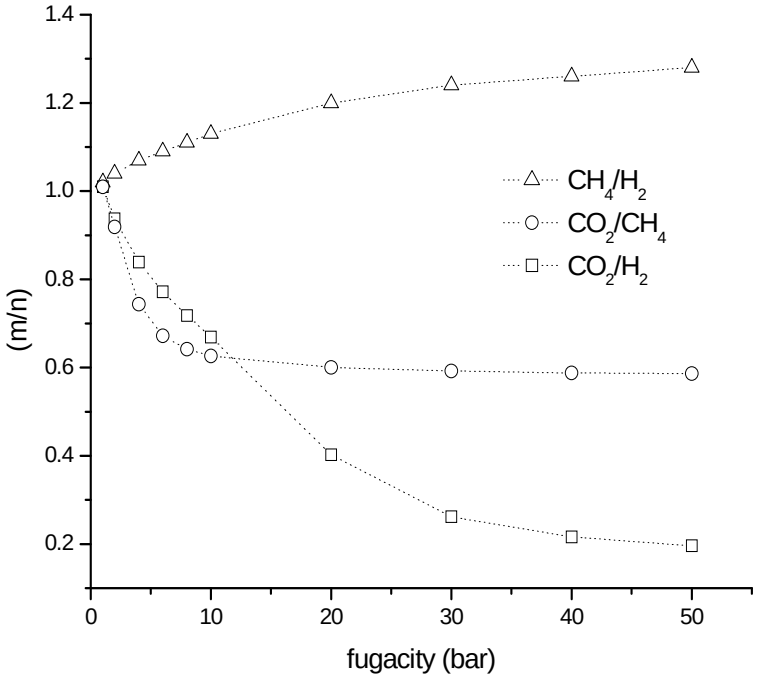

Figure 6.2 The values of *(m/n)* for adsorbed CH_4/H_2, CO_2/CH_4 and CO_2/H_2 mixtures in equilibrium with equimolar bulk mixtures at the specified fugacities at room temperature in CuBTC.

The degree of deviation from unity in (*m/n*) is also related to the magnitude of the adsorption selectivity. For example, this deviation is more significant for CO_2/H_2 than the other gas pairs in Figure 6.2 because the adsorption selectivity for the former system is much larger than the others. The ratio of saturation loadings will be close to one in cases where the two species are similar in chemistry and size, but will differ strongly from one if the two species are strongly dissimilar. For example, the ratio is not close to unity for CO_2/H_2 mixtures, since both the chemistry and size of these species are very different from each other. The self-exchange diffusivity coefficient provides a measure of vacancy and geometry correlations for the particular adsorbate–adsorbent topology. The ratio of self-exchange diffusivity coefficients will be close to one if the two species exhibit

similar correlation effects when considered as single components. Finally, the corrected and exchange diffusivities evaluated at different fractional total loadings in Equations 6.12 and 6.13 will be similar if the corrected diffusivities vary linearly with the fractional coverage and the exchange diffusion coefficients are not strongly dependent on fractional loading in the systems studied. However, this is not true for all the systems we have considered.

We emphasize that the discussion above only applies to systems in which the SSK correlation and Krishna and Paschek's correction for mixture self diffusion are both valid. If these two correlations are not accurate for a system of interest, then Equation 6.8 is still valid, but Equation 6.12 and 6.13 cannot be used with confidence.

Using Equation 6.3 for our screening purposes avoids the need to calculate single component corrected diffusivities and the complications that arise from fitting smooth functions to adsorption and diffusion data. It also avoids the need to apply the SSK correlation to predict mixture diffusion coefficients at arbitrary loadings. The computational efficiency of using Equation 6.3 relative to our detailed calculations can be illustrated by briefly listing the calculations needed for each method. Application of our detailed method to a binary gas mixture requires ~100-200 mixture GCMC simulations and ~20-30 calculations of single component corrected diffusivities. Each of the latter requires 20-30 MD trajectories, so 400-900 independent MD trajectories are needed in total. In contrast, Equation 6.3 can be applied over a full range of feed pressures using ~10 mixture GCMC simulations and a smaller number of MD trajectories at each of these state points; an enormous savings of computational effort. We reiterate that Equation 6.3 is approximate; and cannot give information about all possible operating conditions of

interest. More detailed and accurate calculations can be performed for the materials that show the greatest promise characterized by Equation 6.3.

In order to apply Equation 6.3 we first define the bulk composition and pressure of the gas mixture fed to the membrane. In all of our calculations, the bulk phase composition is specified in terms of fugacity. The differences between fugacity and pressure for H_2 and CH_4 for the conditions we consider are small. For CO_2, an appropriate equation of state should be used to correctly interpret the fugacities defined in our calculations as physical pressures for the highest fugacities we consider below. We have only considered conditions under which the bulk phase is a gas. For convenience of presentation, our membrane results are typically described in terms of feed pressure, although it would be more precise to state this quantity as fugacity. Mixture adsorption is examined using GCMC simulations at the pressure of interest at room temperature. MD simulations are performed to assess the self diffusivities of each species at the mixture concentrations calculated from GCMC. The details of GCMC and MD calculations and the potential parameters for adsorbate molecules in IRMOF-1 and CuBTC can be found in earlier chapters.[2,3,22,31] The atomic partial charges for atoms of IRMOF-8, -9, -10, -14 and COF-102 are taken from previous studies in the literature.[12,13]

6.3 Model Validation

We can examine the accuracy of the approximate method defined above by comparing results from this method with our previous detailed calculations for IRMOF-1 and CuBTC presented in Chapter 3 and Chapter 4. We performed these comparisons for CH_4/H_2, CO_2/CH_4 and CO_2/H_2 mixtures at room temperature. In each case, we set the transmembrane pressure drop to be equal to the total feed pressure. These comparisons

are shown in Figure 6.3. In this figure, the uncertainties on the results from the approximate method arise from observed uncertainties in the GCMC and MD simulations used to apply Equation 6.3. The approximate model accurately predicts the membrane selectivity for CH_4/H_2 mixtures permeating through IRMOF-1. The predictions of the approximate model are less accurate for the same mixture in CuBTC, although the approximate result certainly captures the trend found in detailed calculations of this selectivity. The largest deviation between the approximate model's predictions and the detailed calculation for this mixture is around ~25% for CH_4/H_2 in CuBTC. As we observed before, the selectivity of these membranes for this mixture is not high enough to make either material attractive in practical applications.

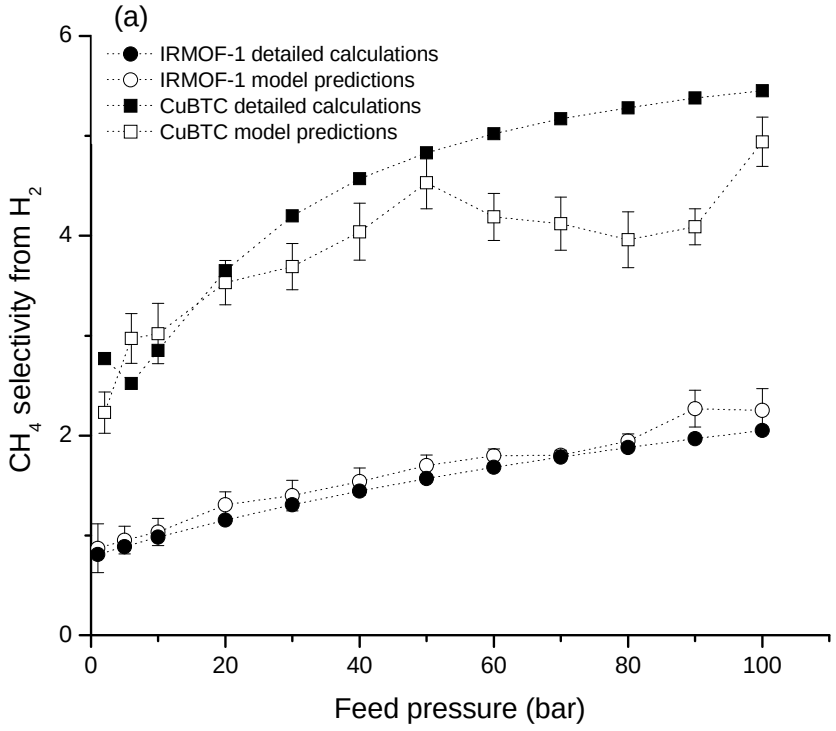

Figure 6.3 Predicted membrane selectivity of IRMOF-1 and CuBTC for separation of (a) CH_4/H_2, (b) CO_2/CH_4 and (c) CO_2/H_2 mixtures. The feed gas composition is CO_2/H_2:10/90 and equimolar in all other cases.

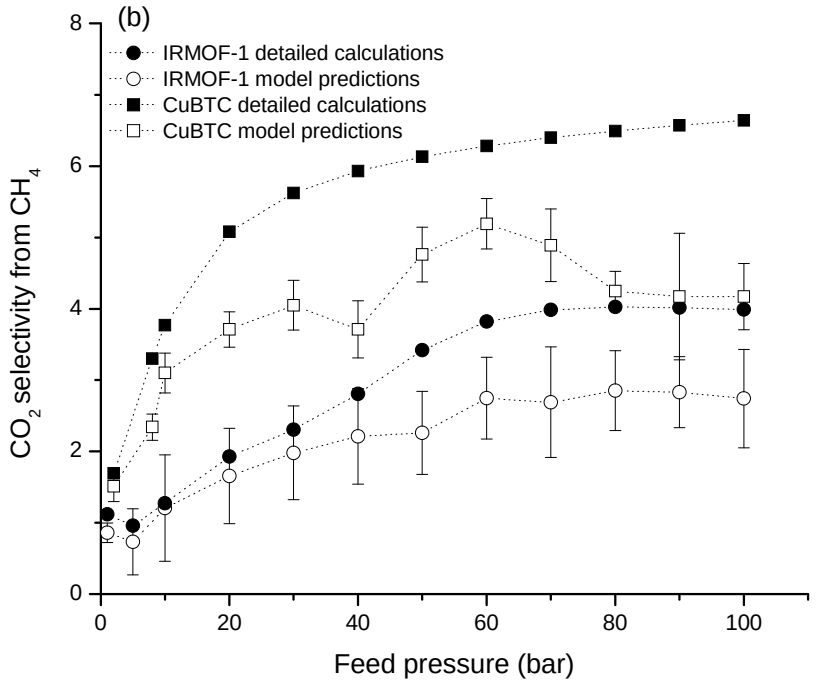

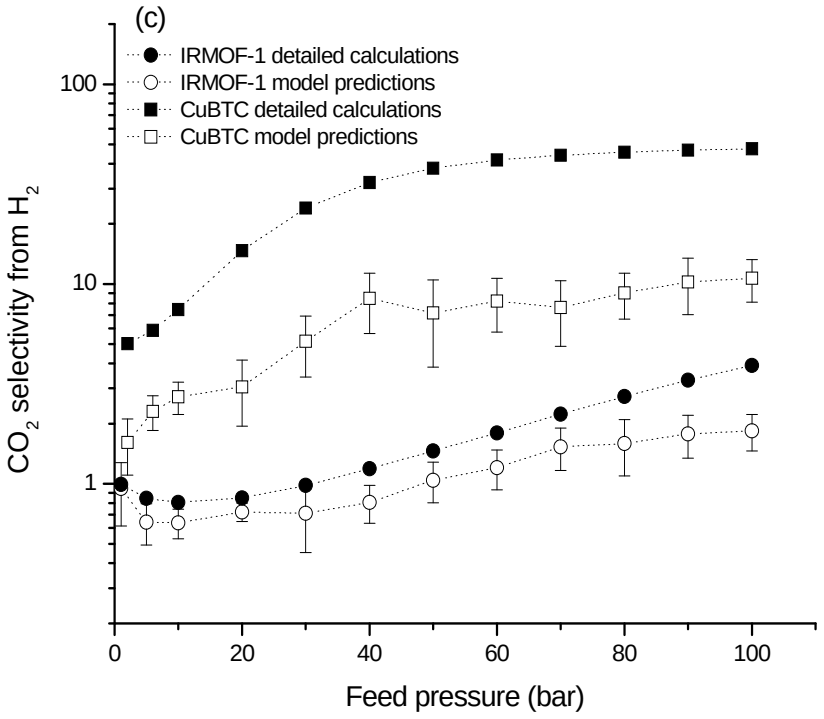

Figure 6.3 Continued

The approximate model underestimates the membrane selectivity for CO_2/CH_4 mixtures in both IRMOF-1 and CuBTC (Figure 6.3b). The poorest agreement between the model predictions and detailed calculations for the CO_2/CH_4 selectivity is ~34% and ~37% in IRMOF-1 and CuBTC membranes, respectively. The approximate model performs acceptably for CO_2/H_2 mixtures in IRMOF-1, underestimating the selectivity by ~4-52%. For the same mixture in a CuBTC membrane, however, the approximate model performs poorly; the approximate calculation underestimates the selectivity by factor of 2.5-6 over the entire range of conditions we examined (Figure 6.3c). Overall, the case of CO_2/H_2 in CuBTC system was the only example among the six cases that we tested where the approximate model shows a poor agreement with our previous detailed calculations in describing the qualitative properties of the membrane. Below, we explore two different ideas to understand the reasons behind this disagreement and discuss how calculations related to these ideas can be used as diagnostic tools for our screening model.

As discussed above, Equation 6.3 is an approximation to the detailed calculation approach that we have used earlier. In a full treatment of mixture permeation, diffusion should be described by a matrix of macroscopic diffusion coefficients. This approach could use a Fickian, Maxwell-Stefan, or Onsager formulation of mixture transport, as the three approaches are mathematically equivalent.[19] As defined above, our detailed calculations used the SSK correlation to predict these mixture macroscopic diffusivities. It is crucial to note that this step is necessarily approximate, so our "detailed calculations" are only correct in situations where this correlation is accurate. Previous studies have shown that predictions of the SSK approach are accurate for several simple gas mixtures

in MOFs as well as adsorbed mixtures in zeolites and carbon nanotubes.[23,26,31,32] However, the SSK correlation can fail in systems with strongly heterogeneous potential energy surfaces.[33] It is useful to note that in examples where strong heterogeneity exists for adsorbed mixtures, two other methods for predicting mixture properties from single component data are known to fail: Ideal Adsorbed Solution Theory (IAST)[34] for predicting binary adsorption isotherms and a correlation proposed by Krishna and Paschek[35] for predicting mixture self diffusivities. Motivated by these observations, we have tested IAST and the Krishna/Paschek self diffusivity correlation for CH_4/H_2, CO_2/CH_4 and CO_2/H_2 mixtures in IRMOF-1 and CuBTC.

IAST is a well developed technique to describe the adsorption equilibria for components in a gaseous mixture using pure component adsorption data at the same temperature.[34] We examined the accuracy of IAST for CH_4/H_2, CO_2/CH_4 and CO_2/H_2 mixtures in IRMOF-1 and CuBTC by using single component adsorption data obtained from GCMC simulations. Initially single component GCMC simulation data is collected up to 100 bar for each species. The single component isotherms are then fitted using a dual site Langmuir (Langmuir-Freundlich) isotherm for H_2 and CH_4 (CO_2). In the case of some mixtures such as CO_2/H_2, we need to extrapolate the single component isotherm data to very high fugacities to apply IAST. For these cases, we have extended our single component GCMC data by collecting data up to 1000 bar to generate smooth isotherms that more reliably reproduce the ideal of having perfect information about the single component isotherm.

We compare the predictions of IAST with our direct mixture GCMC simulation results for adsorption selectivities in Figure 6.4. The ratio of adsorption selectivity

calculated by GCMC to the adsorption selectivity calculated by IAST is plotted as a function of bulk gas pressure in each case. If IAST works accurately, this ratio is of course around 1. Overall, the IAST predictions are in a good agreement with the mixture GCMC simulation data for all mixtures in IRMOF-1, as demonstrated earlier by others.[36] IAST becomes less accurate at high densities of the adsorbed species, even for mixtures that are relatively ideal. One mixture in IRMOF-1 that shows some systematic inaccuracy in the IAST is CO_2/H_2. For this mixture, the single component isotherm for H_2 must be integrated to extremely high fugacities to apply IAST, a situation that introduces imprecision into IAST. A detailed discussion of this and other sources of inaccuracies in applying IAST was given by Chen and Sholl.[37]

The agreement between IAST and GCMC is good for CH_4/H_2 and CO_2/CH_4 mixtures in CuBTC in Figure 6.4. This result is not new.[31,36] The one example from the six cases we examined where IAST deviates strongly from the true mixture properties is CO_2/H_2 in CuBTC. This situation was noted earlier by Yang and Zhong,[36] who attributed this failure to the complex pore structure of CuBTC and the significant difference in size and chemistry of CO_2 and H_2 molecules. From a molecular point of view, the open metal sites of CuBTC provide strong interactions with CO_2 molecules, whereas H_2 is barely adsorbed on CuBTC.[38] Moreover, the smaller pores present in CuBTC causes a strong confinement of CO_2 molecules but they do not have the same effect on the smaller H_2 molecules. It is therefore not completely unexpected that IAST cannot accurately predict the mixture isotherms for this example.

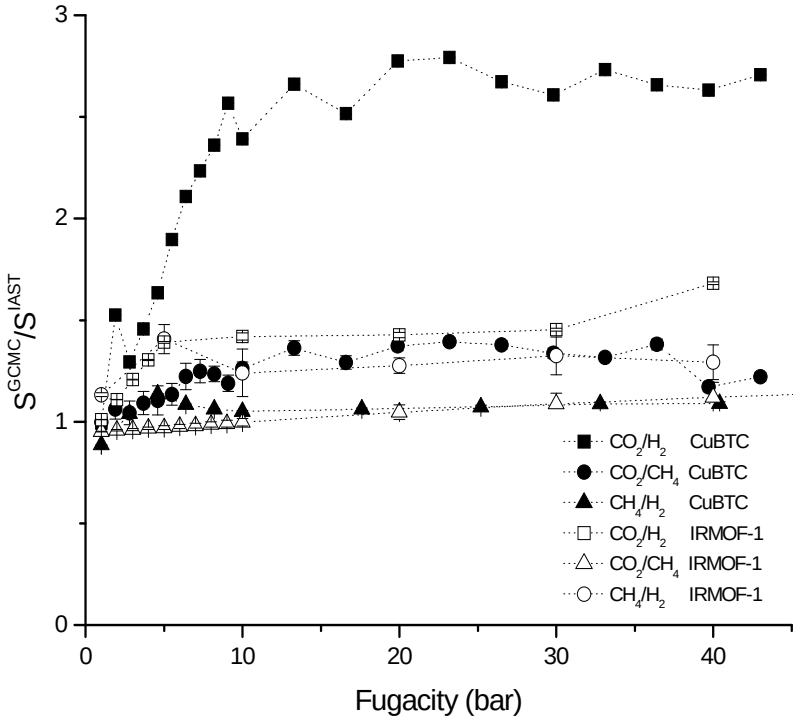

Figure 6.4 The ratio of adsorption selectivities calculated by mixture GCMC simulations to the one calculated by IAST for CH_4/H_2, CO_2/CH_4 and CO_2/H_2 mixtures in IRMOF-1 and CuBTC. The bulk mixture is equimolar in all cases. The first species listed in the labels indicates the species that is selectively adsorbed.

The second theory that we examined on is Krishna and Paschek's correlation[35] for predicting the self diffusion coefficients in a mixture from single component diffusivities. In this correlation, the self diffusivity coefficients in a mixture are calculated based on the pure component Maxwell-Stefan diffusivity (also referred as corrected diffusivities above), the self-exchange and binary-exchange diffusivities and the fractional loadings. The self and binary-exchange diffusivities reflect correlation effects in a mixture. All of this information is available from single component diffusivity calculations. This theory

has been tested in zeolites and carbon nanotubes, where the predictions of the model found to be in a good agreement with direct MD simulations of mixture diffusion.[26,39]

Figure 6.5 shows the ratio of self diffusivity coefficients predicted by Krishna and Paschek's correlation to accurate results from mixture MD simulations for CH_4/H_2, CO_2/CH_4 and CO_2/H_2 mixtures in IRMOF-1 and CuBTC. The correlation works well for all adsorbed mixtures in IRMOF-1, giving maximum deviations of around 25%. As we previously reported, the correlation agrees well with the MD data for adsorbed mixtures of CH_4/H_2 and CO_2/CH_4 in CuBTC.[31] However, the correlation performs poorly for CO_2/H_2 mixtures in CuBTC. In this mixture, the correlation agrees with the MD data only in the limit of low loadings, where the correlation is known to be exact. If we consider the ratio of self diffusivity of CO_2 to H_2 in their binary mixture, the correlation overestimates this ratio by a factor of ~4 compared to the actual ratio established with the mixture MD simulations.

To summarize our results so far, we have tested our approximate screening model, IAST and the Krishna/Paschek correlation for three gas mixtures in two different MOFs. From these six examples, it is only CO_2/H_2 mixtures in CuBTC for which these three methods perform poorly. These validation calculations indicate that we can potentially use IAST or the Krishna/Paschek correlation to examine the reliability of our approximate screening calculations (although the screening model given in Equation 6.3 does not invoke either of these correlations).

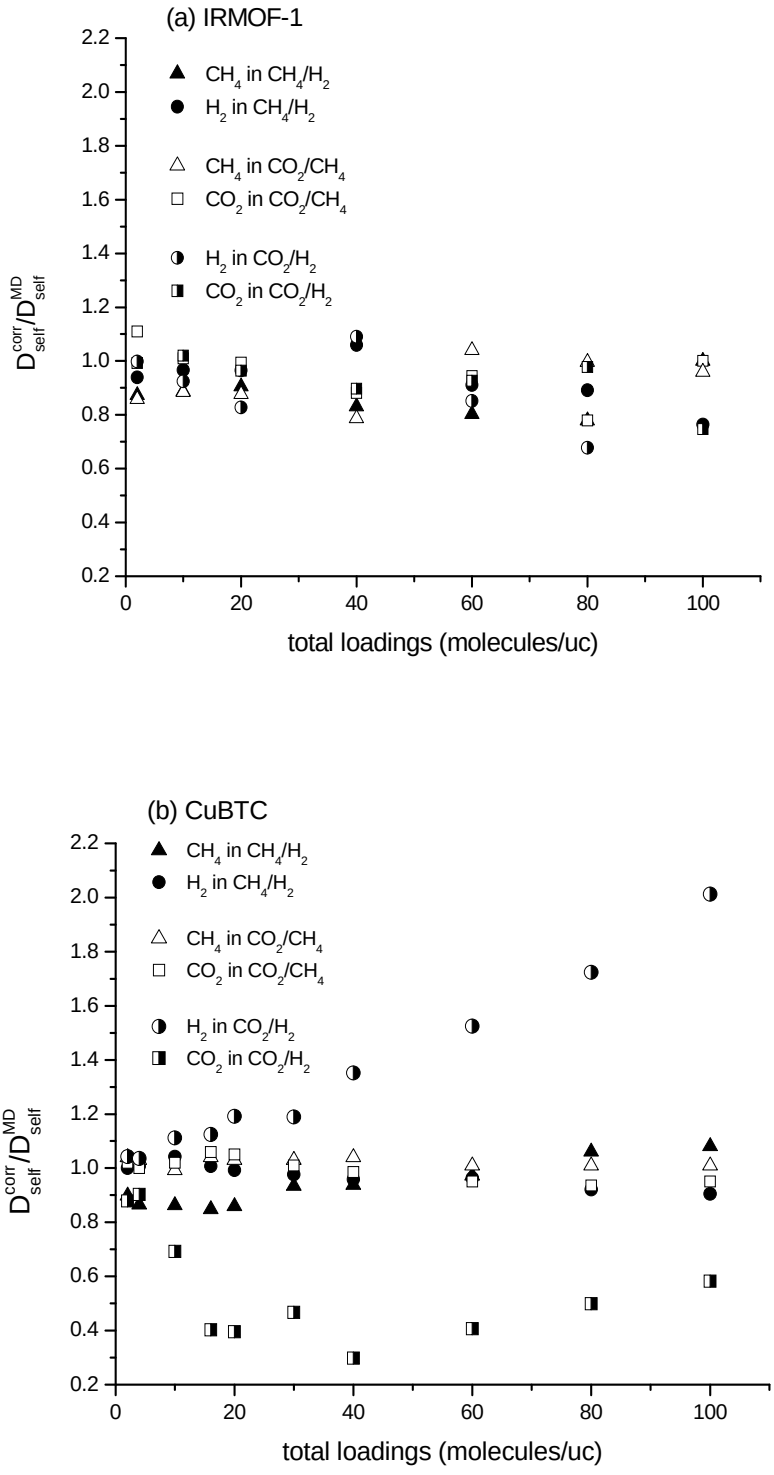

Figure 6.5 The ratio of self diffusivities predicted by Krishna/Paschek correlation to the result of mixture MD simulations for CH_4/H_2, CO_2/CH_4 and CO_2/H_2 mixtures in (a) IRMOF-1 and (b) CuBTC. The adsorbed mixtures are equimolar in all cases.

Using IAST requires the availability of single component adsorption isotherms, which can be rapidly calculated using GCMC. In contrast, the Krishna/Paschek correlation requires knowledge of the loading-dependent single component corrected diffusivities. Avoiding the calculation of these quantities was one of the main advantages of our approximate screening method, so using the Krishna/Paschek correlation in this way is not ideal for our purposes. We therefore propose the following rule of thumb for our approximate screening of MOF membranes: if IAST accurately predicts the mixture isotherm for the adsorbed mixture of interest, then our approximate membrane screening is expected to give results that are accurate enough to be used in materials screening. Conversely, if IAST does not give accurate predictions, then we are not able to judge the reliability of our approximate model.

It is important to note that in situations where IAST does not make accurate predictions, it is also reasonable to expect the SSK correlation's predictions of binary diffusivities to be inaccurate. The SSK predictions are used in a central way in the detailed membrane calculations that we outlined above.[3,4,26] The crucial conclusion from this line of reasoning is that if IAST does not make accurate predictions, then we cannot expect results from the detailed calculation approach defined earlier to be reliable. That is, there are some membrane material/gas mixture combinations for which we cannot predict the 'correct' answer for membrane selectivity using detailed calculations as we have defined them. Of the six examples we introduced above, only CO_2/H_2 permeation through CuBTC membranes falls into this category. Accurate modeling of materials falling in this category requires modeling approaches that do not rely on correlations for the mixture diffusivities such as the SSK method. At present, the only way that this

situation can be tackled is to determine mixture transport diffusivities at a wide range of loadings using MD and to predict permeation based on continuous functions fitted to the calculated diffusivities.[32,40-42] Unfortunately, this approach is extremely computationally demanding, so it can only be contemplated for materials that are expected to have very interesting properties. We return to this important issue in the next chapter.

6.4 Screening of New MOF Membranes

In this section, we compare a series of MOF materials based on their adsorption-based selectivity calculated using mixture GCMC simulations and membrane-based selectivity calculated using the approximate model given in Equation 6.3. Our screening strategy is to apply IAST as the basis for deciding whether the membrane results are meaningful. For each mixture, we first compare the mixture isotherm of each species calculated by GCMC with predictions from IAST. If IAST accurately predicts the mixture isotherm for the adsorbed mixture of interest, then we apply our approximate membrane screening method to predict the membrane-based selectivity.

We applied IAST to predict mixture isotherms at bulk pressures of 1-100 bar for CH_4/H_2, CO_2/CH_4 and CO_2/H_2 mixtures at room temperature in each MOF. The mixtures containing CO_2 were not examined in $Zn(bdc)(ted)_{0.5}$ because an interatomic potential for this system is not currently available. The ratios of adsorption selectivities calculated by GCMC to the predictions of IAST at a pressure of 60 bar are listed in Table 6.1. The IAST predictions are accurate for CH_4/H_2 and CO_2/CH_4 mixtures in all the MOFs we examined. This lets us use our approximate screening method for these systems.

Table 6.1 The ratio of adsorption-based selectivities calculated by GCMC to the one calculated by IAST at 60 bar at room temperature for equimolar bulk mixtures. *In these cases, the bulk composition of CO_2/H_2 or CH_4/H_2 is 0.1/0.9.

MOF	CH_4/H_2 GCMC/IAST	CO_2/CH_4 GCMC/IAST	CO_2/H_2* GCMC/IAST
IRMOF-1	1.15	1.11	1.25
IRMOF-8	1.18	1.23	0.98
IRMOF-9	1.06	1.18	**1.15**
IRMOF-10	1.13	1.14	1.23
IRMOF-14	1.13	1.03	1.15
COF-102	1.15	1.14	**2.25**
$Zn(bdc)(ted)_{0.5}$	1.01*	N/A	N/A

Figure 6.6 shows the ratio of adsorption selectivity calculated by GCMC to the one predicted by IAST for CO_2/H_2 mixtures in each MOF. IAST accurately predicts the CO_2/H_2 mixture isotherms for IRMOF-1, -8, -10 and -14, giving maximum deviations from GCMC results around 25%. There are two cases where IAST predictions strongly deviate from GCMC data: CO_2/H_2 in COF-102 and IRMOF-9. For COF-102, the predictions of IAST are in a reasonable agreement with GCMC up to 20 bar, but IAST underestimates (overestimates) the adsorption isotherm of CO_2 (H_2) at higher pressures. Therefore, IAST predictions underestimate the adsorption selectivity of CO_2 by a factor of ~2-2.5 in COF-102. For IRMOF-9, the situation is more complicated. Although IAST predictions agrees with the simulation data at 60 bar, the general trend of the selectivity curve is not good even at low pressures (see Table 6.1 and Figure 6.8a). Because IAST is

not accurate for CO_2/H_2 mixture adsorption in COF-102 and IRMOF-9, our approximate model to estimate membrane selectivity cannot be used with confidence for these systems. The results showing the predicted membrane selectivity of CO_2 from CO_2/H_2 mixture in IRMOF-9 and COF-102 membranes are omitted for this reason. We return to these two examples in the next chapter. Below, we demonstrate the performance of IRMOF-8, -9, -10, -14, $Zn(bdc)(ted)_{0.5}$ and COF-102 for adsorption-based and membrane-based separations of CH_4/H_2, CO_2/CH_4 and CO_2/H_2 mixtures at room temperature. For each case, we have also presented the data for IRMOF-1 to make comparisons.

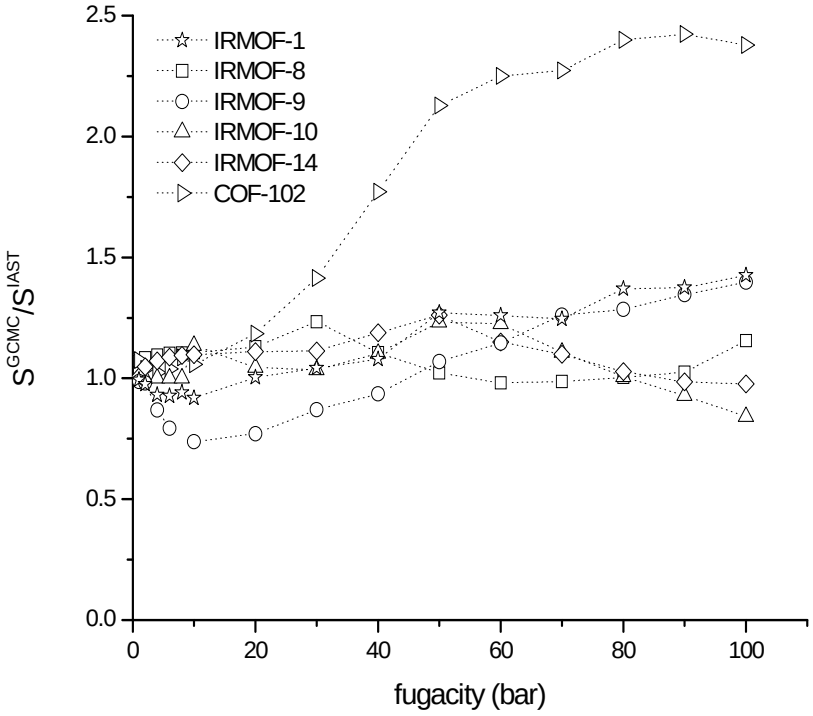

Figure 6.6 The ratio of adsorption selectivities calculated by mixture GCMC simulations to the one calculated by IAST for CO_2/H_2 mixtures. The bulk mixture is CO_2/H_2:10/90 in all cases.

Figure 6.7 shows the adsorption-based and predicted membrane-based selectivity for separation of CH_4/H_2 mixtures in a range of MOFs. Adsorption selectivity favors CH_4 in all MOFs at low pressures, since CH_4 is energetically preferred over H_2. At higher pressures, the adsorption selectivity of CH_4 from H_2 slightly decreases since entropic effects come into play and favor H_2 adsorption (see Figure 6.7a). The adsorption selectivity at low pressures from the highest to the lowest is $Zn(bdc)(ted)_{0.5}$ > IRMOF-9 > COF-102 > non-catenated IRMOFs. This is consistent with the idea that smaller pores provide stronger adsorption selectivity.

The effect of catenation on adsorption can be observed by comparing IRMOF-10 and its catenated version, IRMOF-9. The adsorption-based selectivity of IRMOF-9 for CH_4 is almost four times higher than its non-catenated counterpart. Liu and coworkers also reported the enhanced adsorption selectivity of CH_4/H_2 mixture in IRMOF-9 as a result of additional small pores and adsorption sites formed by the interpenetration of framework.[14]

One striking feature of Figure 6.7b is that membrane selectivities are smaller than adsorption-based selectivities in every material. Our approximate method predicts the membrane's selectivity as the product of adsorption selectivity and diffusion selectivity (see Equation 6.3). Although adsorption selectivity favors CH_4 at all loadings, diffusion selectivity favors H_2 since it moves more quickly than CH_4. At higher loadings, however, CH_4 reduces the diffusivity of the faster diffusing species, H_2, in their adsorbed mixture. This effect causes higher diffusion selectivities towards CH_4 and therefore enhances membrane selectivity at higher pressures.

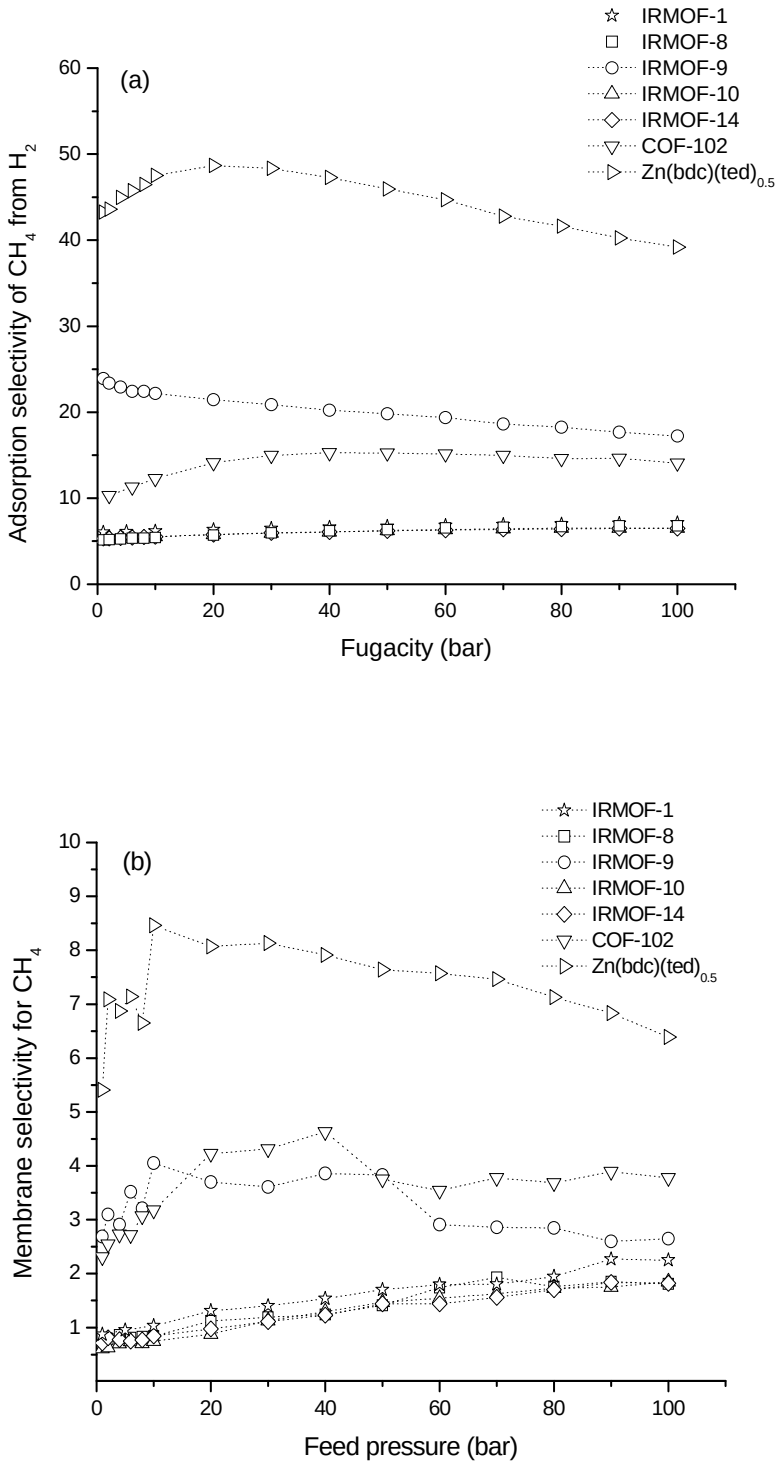

Figure 6.7 (a) Adsorption-based selectivity (b) membrane-based selectivity of IRMOF-1, -8, -9, -10, -14, COF-102, $Zn(bdc)(ted)_{0.5}$ for separation of CH_4/H_2 mixture. The feed gas composition is CH_4/H_2:10/90 in $Zn(bdc)(ted)_{0.5}$ and equimolar in all other cases.

Figure 6.8 shows the adsorption-based selectivity and predicted membrane-based selectivity of IRMOF-1, -8, -9, -10, -14 and COF-102 for CO_2/CH_4 mixtures. Again, the predictions of IAST are in reasonable agreement with mixture GCMC data, allowing us to apply our approximate model to all of these materials. In contrast to what we have observed for CH_4/H_2 mixtures, the adsorption-based selectivities are low for CO_2/CH_4 mixtures for all the MOFs studied. COF-102 and IRMOF-9 have the highest adsorption selectivities due to their relatively smaller pores providing a stronger confinement of at least some guest molecules. We note that CuBTC showed higher adsorption-based and membrane-based selectivities (Figure 6.3b) than the MOFs shown in Figure 6.8 because CuBTC has strong electrostatic interactions with CO_2 due to the existence of open metal sites. The adsorption selectivities of CO_2 from CO_2/CH_4 mixtures for the non-catenated IRMOFs follows the order IRMOF-1 > IRMOF-8 > IRMOF-10 > IRMOF-14. This order is same with the increasing number of carbons on the linker of MOFs. Given the strong interaction between CO_2 molecules and the metal clusters of MOFs, increased number of carbons on the linker provides additional adsorption sites for CH_4 and causes a decrease in adsorption selectivity towards CO_2.

The main observation from Figure 6.8b is that none of the MOFs that we have examined are promising membrane materials for separation of CO_2/CH_4 mixtures. At low feed pressures, adsorption slightly favors CO_2 over CH_4 in non-catenated IRMOFs, but these membranes are slightly selective for CH_4 due to the rapid diffusion of CH_4. At higher pressures, the maximum CO_2 selectivity is ~4 due to the competitive adsorption and diffusion behavior of CO_2 and CH_4.

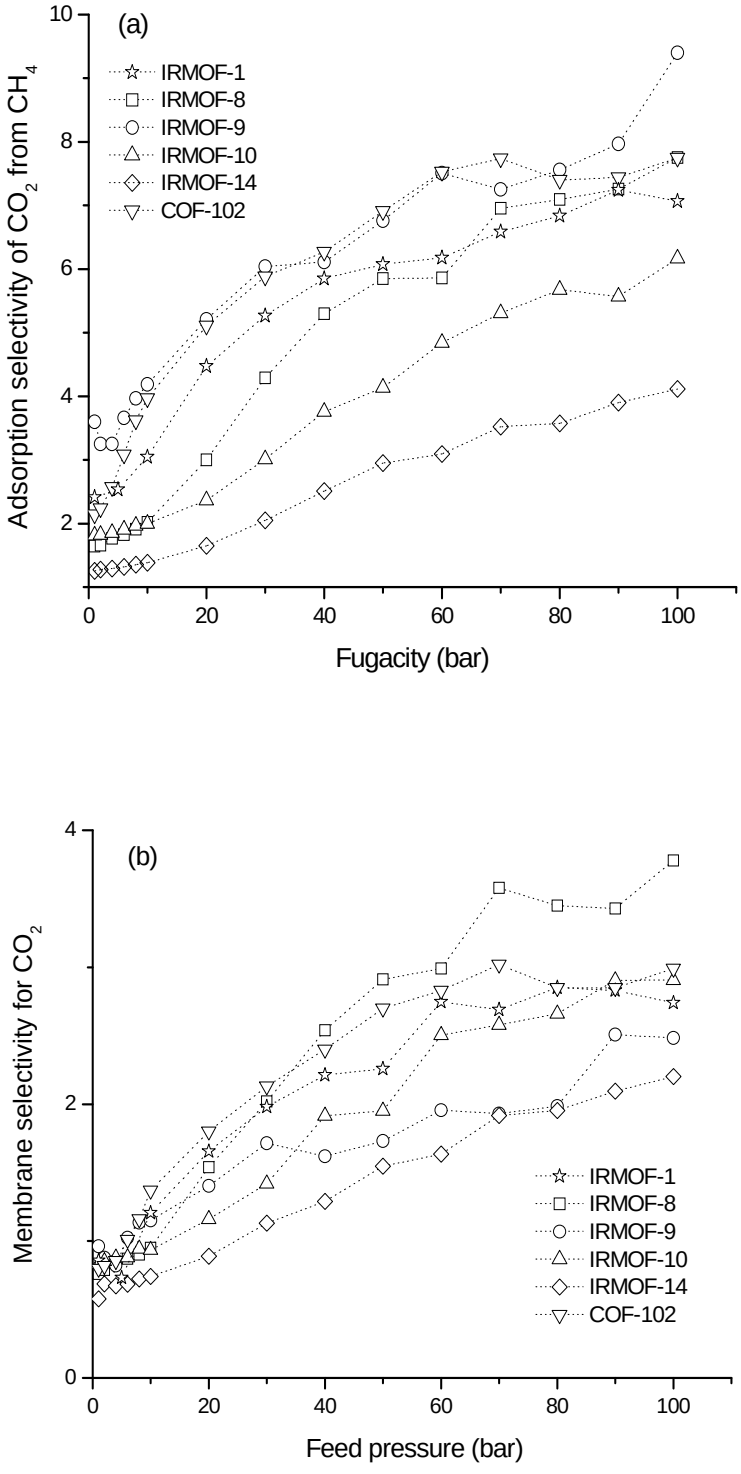

Figure 6.8 (a) Adsorption-based selectivity (b) membrane-based selectivity of IRMOF-1, -8, -9, -10, -14, COF-102 for separation of CO_2/CH_4 mixture. The feed gas mixture is equimolar in all cases.

It is interesting to compare the membrane performances of IRMOF-10 and its catenated counterpart IRMOF-9. The existence of small pores in IRMOF-9 enhances the adsorption selectivity of CO_2 compared to IRMOF-10. However, CO_2 diffusion is faster in IRMOF-10 due to the higher available free volume of this material. Therefore, IRMOF-10 exhibits higher CO_2 selectivity than its catenated version.

Figure 6.9a shows the adsorption-based selectivity of IRMOF-1, -8, -9, -10, -14 and COF-102 for separation of CO_2/H_2 mixtures. CO_2 is very strongly preferred over H_2 at all loadings and therefore, the adsorbed mixture is very CO_2 dominant in all of these MOFs. Since it is statistically not very accurate to measure self diffusivities when one of the components is only present in small quantities, we performed all GCMC and MD simulations used in the application of Equation 6.3 at a bulk gas composition of CO_2/H_2:10/90. We have also shown the predicted adsorption selectivity of CO_2 from CO_2/H_2 mixture by IAST for COF-102 and IRMOF-9 on Figure 6.9a. As we discussed above, IAST fails to accurately predict the mixture isotherm for these two materials. It is important to note that these failures cannot be attributed solely to the MOF structures. Figure 6.9b shows that IAST predicts the adsorption selectivities for CH_4/H_2 and CO_2/CH_4 mixture in COF-102 and IRMOF-9 with reasonable accuracy. The applicability of IAST to CH_4/H_2 in IRMOF-9 system was also shown before by others.[14]

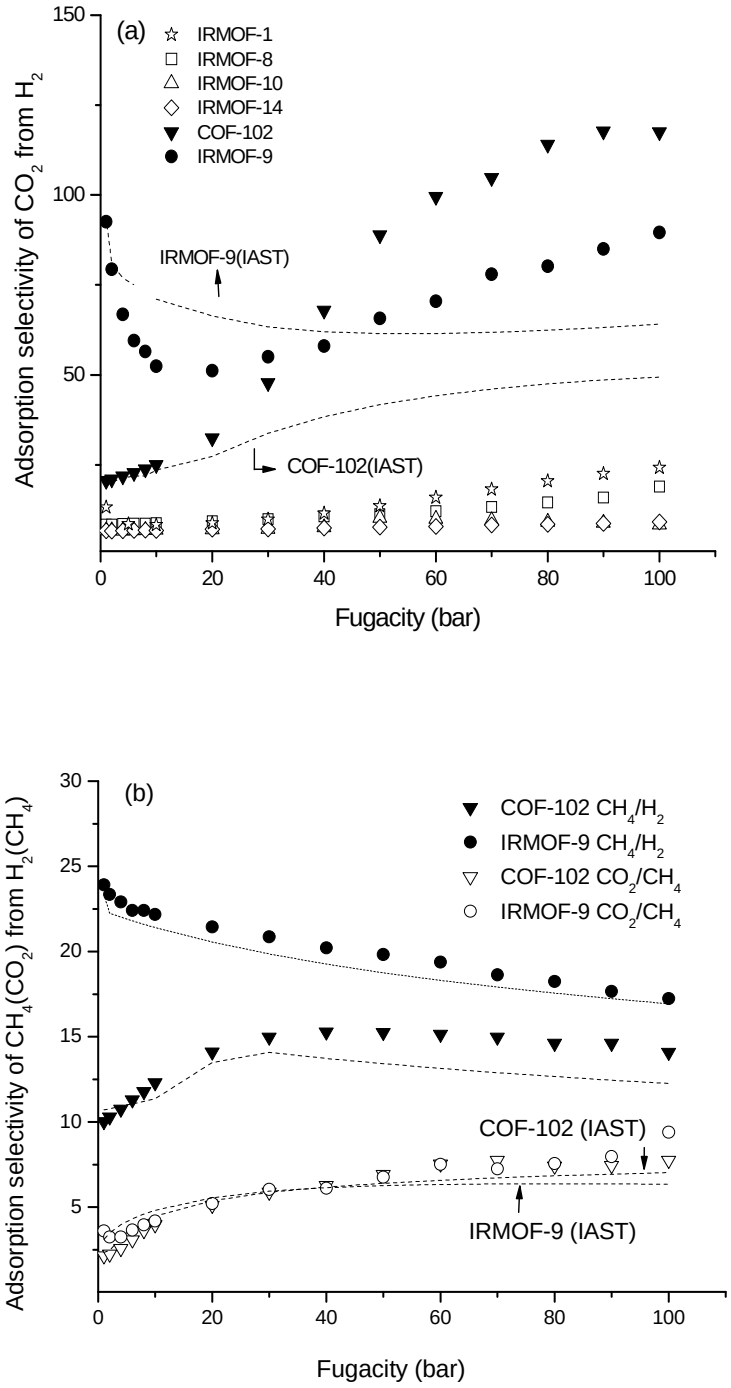

Figure 6.9 (a) Adsorption-based selectivity of IRMOF-1, -8, -9, -10, -14 and COF-102 for separation of CO_2/H_2 mixture. The composition of the feed gas is CO_2/H_2:10/90 in all cases. (b) Adsorption-based selectivity of IRMOF-9 and COF-102 for separation of CH_4/H_2 and CO_2/CH_4 mixture. The composition of the feed gas is equimolar. The dashed lines show the predictions of IAST both on (a) and (b).

The adsorption selectivity of CO_2 from CO_2/H_2 mixtures is the highest in IRMOF-9 and COF-102. Similar to the argument that we made for CuBTC, the MOFs with small pores provide stronger confinement of CO_2 molecules. The degree of confinement of H_2 molecules in MOFs with small pores and MOFs with large pores can be thought as being similar, because in both cases the molecule is small relative to the pore size, giving similar adsorption strength for H_2. The stronger confinement of CO_2 in narrow pore MOFs than in the large pore MOFs results in an enhancement of CO_2 adsorption over H_2.

The predicted membrane selectivities of IRMOF-1, -8, -10 and -14 for separation of CO_2/H_2 mixture are shown in Figure 6.10. The membrane selectivities of COF-102 and IRMOF-9 are not shown in this figure. Since IAST is inaccurate for these two cases, the approximate model we have used to estimate membrane selectivity is not valid for these systems. The membrane-based selectivity of CO_2 is low (less than 2) in all MOFs shown in Figure 6.10 at all pressures that we studied. At pressures up to 50 bar, the membrane is selective for H_2 due to the rapid diffusion of H_2. At this pressure regime, adsorption-based selectivities for CO_2 are less than 10 for all non-catenated MOFs (see Figure 6.9a). However, at these loadings, the self diffusivity of H_2 is much higher than CO_2, compensating the adsorption selectivity and making membranes selective for H_2. Since IRMOF-1 and -8 exhibit higher adsorption selectivity toward CO_2 at higher loadings (see Figure 6.9a), this effect is less significant for them than for IRMOF-10 and IRMOF-14.

It is also useful to compare the properties of MOF membranes with other nanoporous membranes. Separation of equimolar mixtures of H_2 and CH_4 hydrogen has been performed with a variety of materials at room temperature and moderate pressures.

A selectivity of 8 has been reported with a SAPO-34 membrane,[43] while the selectivity reported for a microporous SSF membrane was 2.[44] Theoretical modeling of carbon nanotubes has predicted a membrane selectivity of 13 for this separation.[41] Separation of equimolar mixtures of CH_4 and CO_2 has been reported using SAPO-34 membranes at room temperature at a feed pressure of 222 kPa and a permeate pressure of 84 kPa with selectivities exceeding 100.[45] Robeson reviewed data from a large number of polymeric membranes, where CO_2 selectivities from equimolar CO_2/CH_4 mixtures vary between 2 and 100.[46]

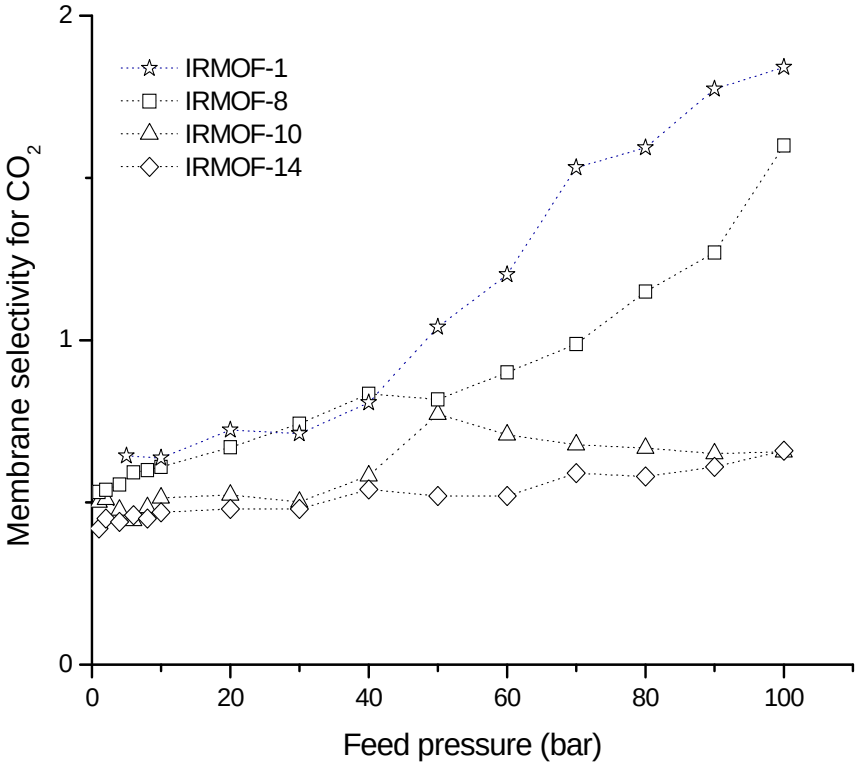

Figure 6.10 Predicted membrane-based selectivity of IRMOF-1, -8, -10, -14 for separation of CO_2/H_2 mixture. The composition of the feed gas is CO_2/H_2:10/90 in all cases.

6.5 Conclusions

In this chapter, we have introduced an approximate method based on information from molecular simulations to predict the properties of MOF-based membranes for separation of gas mixtures. We have checked the validity of this method by comparing the predictions of the method with our previous detailed calculations for CH_4/H_2, CO_2/CH_4 and CO_2/H_2 mixtures permeating through IRMOF-1 and CuBTC membranes. This validation lets us to hypothesize a connection between our model and two computationally efficient correlations, IAST and Krishna and Paschek's correlation for mixture self diffusion. We hypothesize that if IAST (Krishna and Paschek's diffusion correlation) accurately predicts the mixture isotherm (self diffusion) for the adsorbed mixture of interest, then our approximate membrane screening is expected to give results that are accurate enough to be used in materials screening. If these theories do not give accurate predictions, further methods are required to judge the reliability of our approximate membrane screening. Since application of IAST is more straightforward and computationally efficient than Krishna and Paschek's diffusion correlation, we use IAST as a diagnostic tool to determine if membrane properties can be predicted by our approximate method. Among the six examples for which we tested our approximate model, it is only CO_2/H_2 mixtures in CuBTC for which there is a poor agreement between the proposed correlations and direct molecular simulations. We emphasize that in cases where IAST and Krishna and Paschek's diffusion correlation fail to make accurate predictions, it is reasonable to expect that the SSK correlation would give inaccurate predictions for diffusivity coefficients. Since we applied the SSK correlation in our detailed calculations for CO_2/H_2 permeation through CuBTC membranes, we are unable

to judge the validity of these detailed calculations for this specific system. In cases where IAST and Krishna and Paschek's diffusion correlation fail, it is reasonable to say that it is not possible to predict the 'correct' answer for membrane selectivity based on these detailed calculations. We return to this point in the next chapter.

After validation of our approach, we have studied several MOFs, IRMOF -8, -9, -10, -14 and a covalent organic framework, COF-102, to examine the effect of chemical diversity and interpenetration on the performance of MOF-based membranes. We first applied IAST as the basis for deciding whether the membrane results are meaningful. Since the IAST predictions are found to be accurate for CH_4/H_2 and CO_2/CH_4 mixtures in all of these MOFs, we used our approximate model to predict the membrane selectivity for these mixtures in all MOFs. Our results indicated, as might be expected, that MOFs with smaller pores such as COFs or catenated structures are better choices to fabricate a membrane for separation of CH_4/H_2 mixtures since they exhibit higher adsorption-based and membrane-based selectivities. The separation of CO_2 from CH_4 or H_2 using a MOF membrane is not favorable in any of the materials we examined due to low CO_2 selectivities. We identified two cases where IAST fails to predict mixture isotherms accurately: CO_2/H_2 in COF-102 and IRMOF-9. We did not use our screening method to predict the membrane selectivity of these two MOFs. However, our results suggest that these MOFs would potentially be useful in adsorption-based separation of CO_2. Overall, MOFs with relatively small pores such as IRMOF-9, COF-102 and CuBTC exhibit higher adsorption selectivities for CO_2 over H_2. It is interesting that the materials with the most physically interesting adsorption selectivity are the ones for which IAST performs with the least accuracy.

This work highlights the fact that understanding membrane-based separation requires a detailed understanding of both molecular adsorption and diffusion. For all of the MOFs studied in this chapter, we have observed higher adsorption-based selectivities than membrane-based selectivities. This observation signifies that in the mixtures that we studied adsorption selectivity is compensated by the low diffusion selectivities since strongly adsorbed species diffuse more slowly than the weakly adsorbed species. Finding examples of mixture/MOF systems where adsorption and diffusion do not compensate each other would be very interesting for our screening calculations. At least one example with this attractive combination of properties is known from studies of small pore zeolites, demonstrating that it is possible to find nanoporous materials with these properties.[47]

Although our results are somewhat negative in the sense that most of the MOFs we have examined are not good candidates for making highly selective membranes, these results underline the importance of screening large numbers of MOFs to find materials with high performance before investigating a large amount of time and resources into fabricating a membrane. We reiterate that the predictions of our model are approximate and can only give information at permeate pressures close to vacuum condition. Although selectivity is a very important property to characterize the performance of a membrane, a membrane with a high selectivity but a low flux is economically unattractive. Our predictions do not give a direct insight to the flux or permeability of gas mixtures through the membrane but provides an approximation for the ratio of fluxes. More detailed calculations[2-4,41] should be performed for the MOFs showing the greatest promise characterized by our model to examine the permeability.

6.6 References

(1) Hao, S.; Sholl, D. S. *Energy and Environ. Sci.* **2008**, *1*, 175.

(2) Keskin, S.; Sholl, D. S. *J. Phys. Chem. C* **2007**, *111*, 14055.

(3) Keskin, S.; Sholl, D. S. *Ind. Eng. Chem. Res.* **2009**, *48*, 914.

(4) Keskin, S.; Liu, J.; Johnson, J. K.; Sholl, D. S. *Micropor. Mesopor. Mater.* **2009**, *125*, 101.

(5) Eddaoudi, M.; Kim, J.; Rosi, N.; Vodak, D.; Wachter, J.; O'Keeffe, M.; Yaghi, O. M. *Science* **2002**, *295*, 469.

(6) Ryan, P.; Broadbelt, L. J.; Snurr, R. Q. *Chem. Commun.* **2008**, 4132.

(7) Jung, D.; Kim, D.; Lee, T. B.; Choi, S. B.; Yoon, J. H.; Kim, J.; Choi, K.; Choi, S.-H. *J. Phys. Chem. B* **2006**, *110*, 22987.

(8) Yaghi, O. M.; O'Keeffe, M.; Ockwig, N. W.; K.Chae, H.; Eddaoudi, M.; Kim, J. *Nature* **2003**, *423*, 705.

(9) Chui, S. S.-Y.; Lo, S. M.-F.; Charmant, J. P. H.; Orpen, A. G.; Williams, I. D. *Science* **1999**, *283*, 1148.

(10) Liu, J.; Lee, J. Y.; Pan, L.; Obermyer, R. T.; Simizu, S.; Zande, B.; Li, J.; Sankar, S. G.; Johnson, J. K. *J. Phys. Chem. C* **2008**, *112*, 2911.

(11) El-Kaderi, H. M.; Hunt, J. R.; Mendoza-Cortés, J. L.; A.P. Côté; Taylor, R. E.; M.O'Keeffe; Yaghi, O. M. *Science* **2007**, *316*, 268.

(12) Babarao, R.; Jiang, J. *Langmuir* **2008**, *24*, 6270.

(13) Yang, Q.; C. Zhong; Chen, J.-F. *J. Phys. Chem. C* **2008**, *112*, 1562.

(14) Liu, B.; Yang, Q.; Xue, C.; C. Zhong; Chen, B.; Smit, B. *J. Phys. Chem. C* **2008**, *112*, 9854.

(15) Liu, B.; Yang, Q.; Xue, C.; Zhong, C.; Smit, B. *Phys. Chem. Chem. Phys.* **2008**, *10*, 3244.

(16) Tafipolsky, M.; Amirjalayer, S.; Schmid, R. *J. Comput. Chem.* **2007**, *28*, 1169.

(17) Kärger, J.; Ruthven, D. *Diffusion in Zeolites and Other Microporous Materials*; John Wiley & Sons: New York, 1992.

(18) Keil, F. J.; Krishna, R.; Coppens, M. O. *Rev. Chem. Eng.* **2000**, *16*, 71.

(19) Sholl, D. S. *Acc. Chem. Res.* **2006**, *39*, 403.

(20) Skoulidas, A. I.; Sholl, D. S. *J. Phys. Chem. B* **2002**, *106*, 5058.

(21) Skoulidas, A. I.; Sholl, D. S. *J. Phys. Chem. A* **2003**, *107*, 10132.

(22) Skoulidas, A. I.; Sholl, D. S. *J. Phys. Chem. B* **2005**, *109*, 15760.

(23) Skoulidas, A. I.; D. S. Sholl; Bowen, T. C.; Doelling, C.; Falconer, J. L.; Noble, R. D. *J. Membr. Sci.* **2003**, *227*, 123.

(24) Krishna, R.; van Baten, J. M. *Chem. Eng. Sci.* **2008**, *63*, 2130.

(25) Goj, A.; Sholl, D. S.; Akten, E. D.; Kohen, D. *J. Phys. Chem. B* **2002**, *106*, 8367.

(26) Skoulidas, A. I.; Sholl, D. S.; Krishna, R. *Langmuir* **2003**, *19*, 7977.

(27) Wesselingh, J. A.; Krishna, R. *Mass Transfer in Multicomponent Mixtures*; Delft University Press: Delft, 2000.

(28) Krishna, R.; van Baten, J. M. *Chem. Eng. J.* **2007**, *133*, 121.

(29) Babarao, R.; Jiang, J. *Langmuir* **2008**, *24*, 5474.

(30) Newsome, D. A.; Sholl, D. S. *Nano Lett.* **2006**, *6*, 2150.

(31) Keskin, S.; Liu, J.; Johnson, J. K.; Sholl, D. S. *Langmuir* **2008**, *24*, 8254.

(32) Chempath, S.; Krishna, R.; Snurr, R. Q. *J. Phys. Chem. B* **2004**, *108*, 13481.

(33) Sholl, D. S. *Langmuir* **2006**, *22*, 3707.

(34) Myers, A. L.; Prausnitz, J. M. *AIChE J.* **1965**, *11*, 121.

(35) Krishna, R.; Paschek, D. *Phys. Chem. Chem. Phys.* **2002**, *4*, 1891.

(36) Yang, Q.; Zhong, C. *J. Phys. Chem. B* **2006**, *110*, 17776.

(37) Chen, H.; Sholl, D. S. *Langmuir* **2006**, *22*, 709.

(38) Karra, J. R.; Walton, K. S. *Langmuir* **2008**, *24*, 8620.

(39) Krishna, R.; van Baten, J. M. *Ind. Eng. Chem. Res.* **2006**, *45*, 2084.

(40) Sanborn, M. J.; Snurr, R. Q. *AIChE J.* **2001**, *47*, 2032.

(41) Chen, H.; Sholl, D. S. *J. Membr. Sci.* **2006**, *269*, 152.

(42) Chen, H.; Sholl, D. S. *J. Am. Chem. Soc.* **2004**, *126*, 7778.

(43) Poshusta, J. C.; Tuan, V. A.; Pape, E. A.; Noble, R. D.; Falconer, J. L. *AIChE J.* **2000**, *46*, 779.

(44) Vieira-Linhares, A. M.; Seaton, N. A. *Chem. Eng. Sci.* **2003**, *58*, 4129.

(45) Li, S. G.; Falconer, J. L.; Noble, R. D. *Adv. Mat.* **2006**, *18*, 2601.

(46) Robeson, L. M. *J. Membr. Sci.* **1991**, *62*, 165.

(47) Jee, S.-E.; Sholl, D. S. *J. Am. Chem. Soc.* **2009**, *131* 7896.

CHAPTER 7

COMPARISON OF VARIOUS METHODS TO PREDICT SELECTIVITY OF METAL ORGANIC FRAMEWORK MEMBRANES

In Chapters 3 and 4, we described a detailed calculation approach in which the SSK (Skoulidas, Sholl, Krishna) method is used in a central way to predict the selectivity of metal organic framework (MOF) membranes for separation of binary gas mixtures. We then described in Chapter 6 an efficient approximate modeling strategy based on atomistic simulations that can be used instead of detailed calculations to accelerate the screening of MOF membranes. One conclusion from all these calculations was that there are some membrane material/gas mixture combinations for which we can neither predict the 'correct' answer for membrane selectivity using the detailed calculation approach nor judge the validity of our approximate method. CO_2/H_2 mixtures in CuBTC, COF-102 and IRMOF-9 are the cases which fall in this category. Accurate modeling of these cases requires determining mixture transport diffusivities at a wide range of loadings using molecular dynamics (MD) simulations and predicting mixture permeation based on these calculated diffusivities; this approach is very computationally demanding. In this chapter, we use this approach to predict the selectivity of CuBTC, COF-102 and IRMOF-9 for separation of CO_2/H_2 mixtures. We then compare these direct MD simulations with the methods introduced previously for membrane selectivity and discuss the accuracy and efficiency of these different methods. Finally, we suggest a robust screening strategy to study MOF materials for membrane-based gas separations.

7.1 Computational Details

We described the detailed calculation approach and our approximate method in Chapter 3 and Chapter 6, respectively.[1,2] Here, we only consider predicting the selectivity of MOF membranes by evaluating the transport diffusivities via MD simulations in the special case where the permeate pressure is a vacuum. This specific operating condition is the same as was analyzed extensively in Chapter 6. The crucial feature of the method described below is that no assumptions are invoked about the diffusion coefficients in the adsorbed mixture. Instead, the mixture diffusion coefficients relevant to the mass transport are determined directly from molecular simulations.

We first define the bulk gas composition and pressure of the gas mixture fed to membrane. The adsorbed loadings of each species at the feed side of the membrane were then evaluated using mixture GCMC simulations under the defined feed pressure and composition. Since the permeate side of the membrane was assumed to be vacuum, the average loading of each species at the center of the membrane is equal to the half of the adsorbed loadings at the feed side of the membrane within a shell model description. We then use MD simulations to calculate the Onsager coefficients of the mixture at these adsorbed loadings of each species at the center of the membrane. The details of using MD simulations to obtain Onsager coefficients once the interaction parameters for adsorbates in a nanoporous adsorbent have been defined was described in Chapter 2.[3-5] We performed 20 independent MD simulations, each having a simulation length of 20-30 ns for each loading we considered, since using a large number of independent trajectories is vital in order to compute the Onsager coefficients.[6,7]

The Onsager coefficients calculated using MD were converted to Fickian diffusivities through Equation 2.12. The conversion of Onsager coefficients to Fickian diffusivities requires computing the thermodynamic correction factors associated with the adsorbed mixture. To evaluate these, we fitted a mixture isotherm for all adsorbed loadings from an extensive set of GCMC simulations. Specifically, GCMC simulations were performed for bulk phase mixture compositions from 0.1 to 0.9 at 9 different compositions and at 32 different total pressures. This GCMC data was used to fit a combined Langmuir-Freundlich model as described in Equations 3.5 and 3.6 of Chapter 3. All thermodynamic correction factors used in our prediction of the binary diffusivities below were calculated from the combined Langmuir-Freundlich model. A comparison of the agreement between the fitted isotherms and our direct mixture GCMC data for the three MOFs we considered is shown in Figure 7.1. Finally, the flux of each species was calculated using Equation 2.7 of Chapter 2.

The adsorption of CO_2 is very strongly preferred over H_2 in all of the MOFs we considered and therefore the adsorbed mixture is very CO_2 dominant. It is computationally challenging to accurately measure the Onsager coefficients when one of components is present only at dilute concentrations. For this reason, we only applied the method described above to study conditions where the feed is a 10/90 mixture of CO_2/H_2.

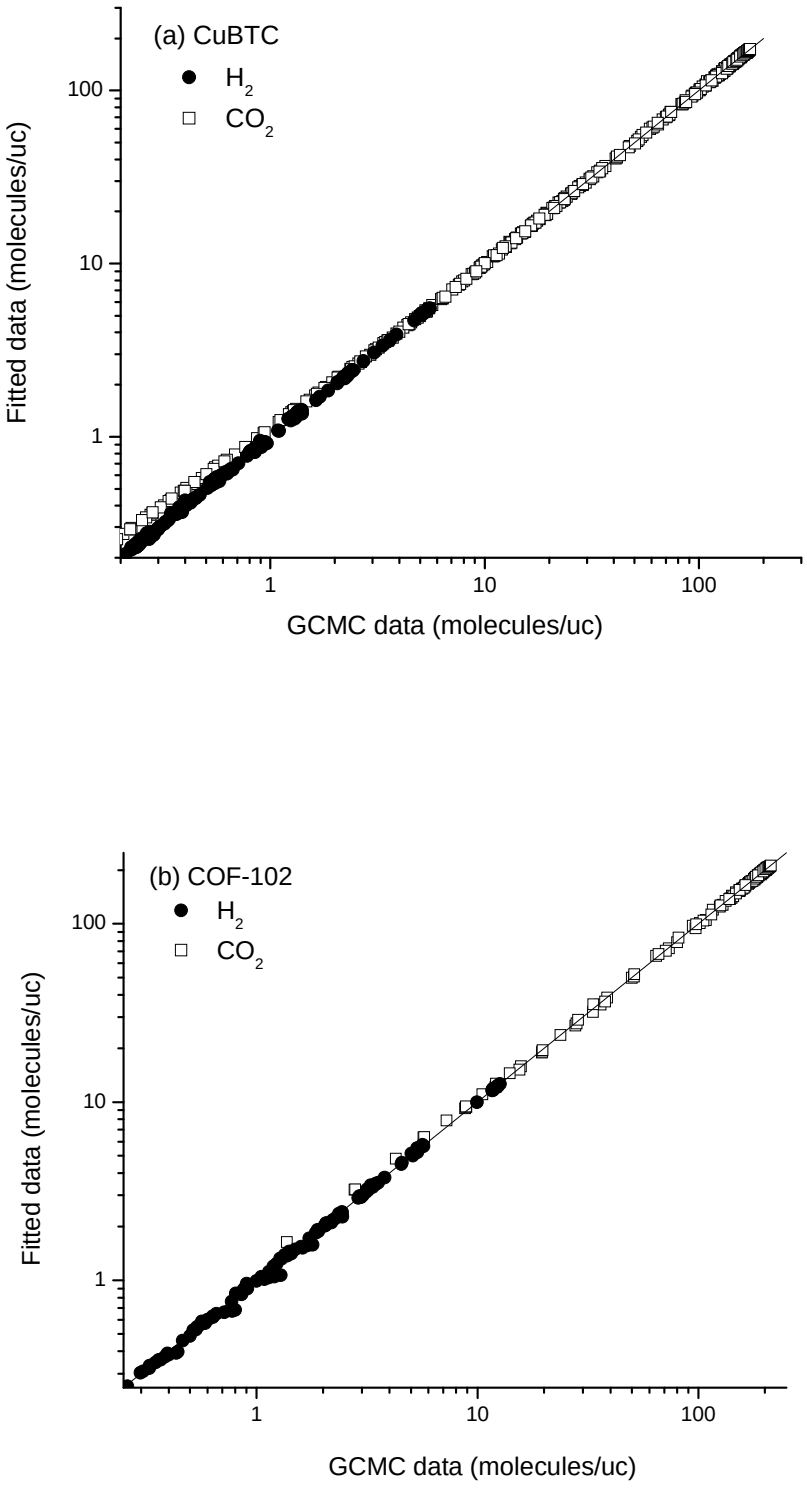

Figure 7.1 A comparison of the room temperature binary adsorption isotherms determined from GCMC simulations and calculated using fitted isotherms for CO_2/H_2 mixtures in (a) CuBTC (b) COF-102 (c) IRMOF-9.

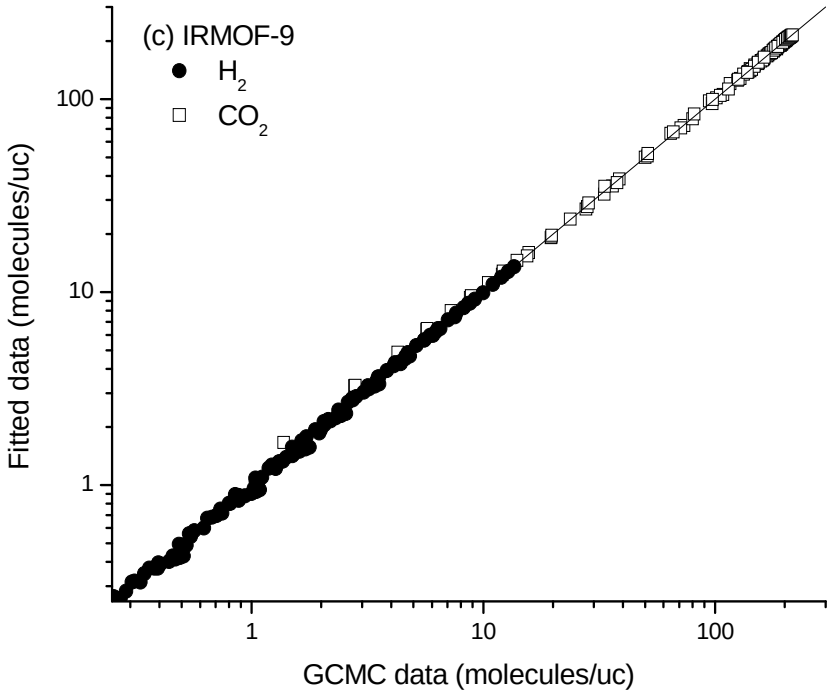

Figure 7.1 Continued

7.2 Comparison of Methods

We first examined the separation of CO_2 from H_2 using a CuBTC membrane. Figure 7.2 compares the predictions of the calculation approach where the SSK method is used in a central way (Chapter 4), our approximate method (Chapter 6) and the direct MD simulations for selectivity of CO_2. We reiterate that the latter method is the only one that gives a result free of assumptions about the values of the binary diffusion coefficients, so it should be viewed as giving the correct results.

The most striking result from Figure 7.2 is that the SSK-based calculations dramatically overpredict the CO_2 selectivity compared to direct MD calculations. The disagreement between the two methods for the membrane selectivity indicates that the

SSK theory failed to predict the mixture macroscopic transport diffusivities accurately. To directly assess this statement, we compared the Fickian diffusivity matrix elements computed using direct MD simulations with the predictions of the SSK theory for CO_2/H_2 mixtures in CuBTC in Figure 7.3. SSK overpredicts (underpredicts) the Fickian diffusivities, D_{11} and D_{21} (D_{22} and D_{12}). As noted in Figure 7.3, subscripts 1 and 2 here refer to CO_2 and H_2, respectively. In terms of the performance of the membrane, the magnitude of D_{21} means that this diffusivity can be neglected compared to the others. Overpredicting D_{11} and underpredicting D_{12} and D_{22} means that the net CO_2 (H_2) flux was overestimated (underestimated), leading to the overestimation of selectivity for CO_2 in the membrane calculations.

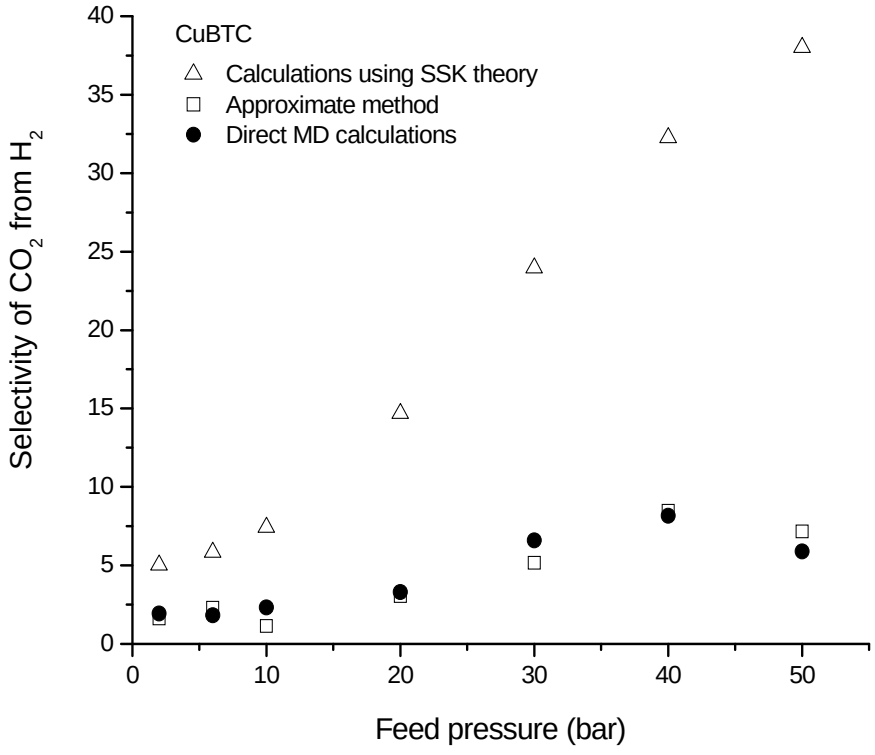

Figure 7.2 Predicted membrane selectivity of CuBTC for separation of CO_2/H_2 mixture. The feed gas composition is CO_2/H_2:10/90. The permeate side is a vacuum.

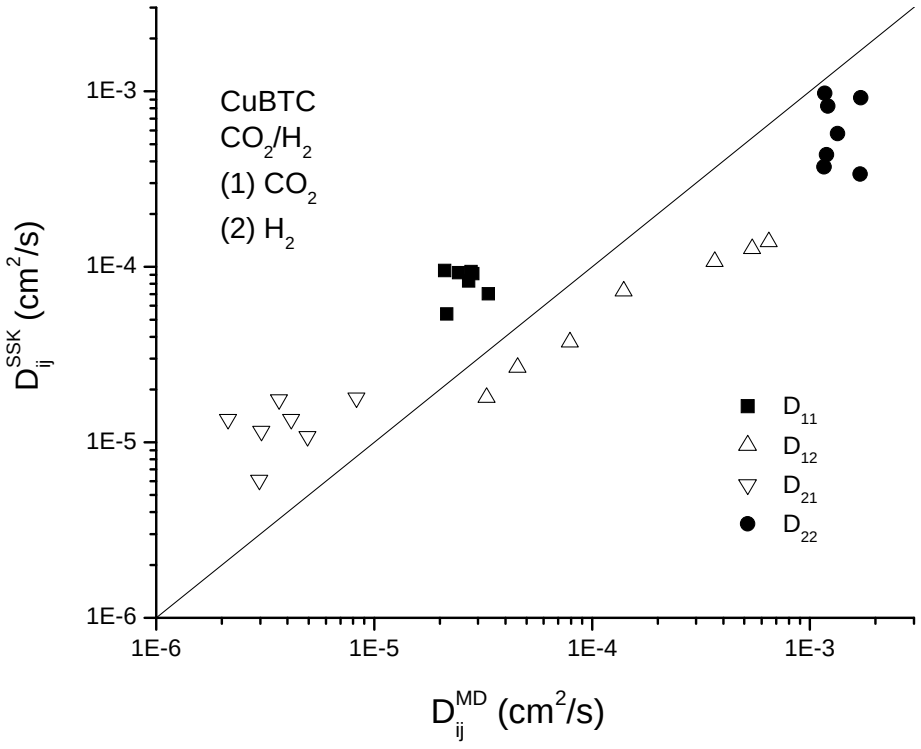

Figure 7.3 A comparison of the Fickian diffusivity matrix elements computed using MD (horizontal axis) with the predictions of the SSK theory (vertical axis) for CO_2/H_2 mixture with a bulk composition of 10/90.

A surprising feature of Figure 7.2 is that the predictions of our approximate method from Chapter 6 agree well with the direct MD simulations. That gives an example in which the approximate method from Chapter 6 makes accurate predictions for membrane selectivity in a case where IAST performs poorly, a situation where we had previously argued that we could not judge the accuracy of our approximate method.

The good agreement between the approximate method and the direct MD calculations suggests that the mixture self diffusivities that are the basis of our approximate method are able to capture the trend and magnitude of the mixture's Fickian transport diffusivities. Figure 7.4 shows the mixture self diffusivities and Fickian

diffusivities, all of which were computed using MD simulations, for adsorbed CO_2/H_2 mixtures in CuBTC. The mixture self diffusivities of CO_2 and H_2 match well with the diagonal Fickian diffusivities. The term D_{21} is small compared to the diagonal terms and therefore it is reasonable to neglect the effect of this term on the selectivity. The same is not true, however, for the other off-diagonal term, D_{12}, which has a higher value than D_{11} at high loadings. By definition, D_{12} governs the effect of the concentration gradient of species 2 (H_2) on the flux of species 1 (CO_2):

$$J_1 = J_{11} + J_{12} = D_{11} \cdot \nabla c_1 + D_{12} \cdot \nabla c_2 \qquad 7.1$$

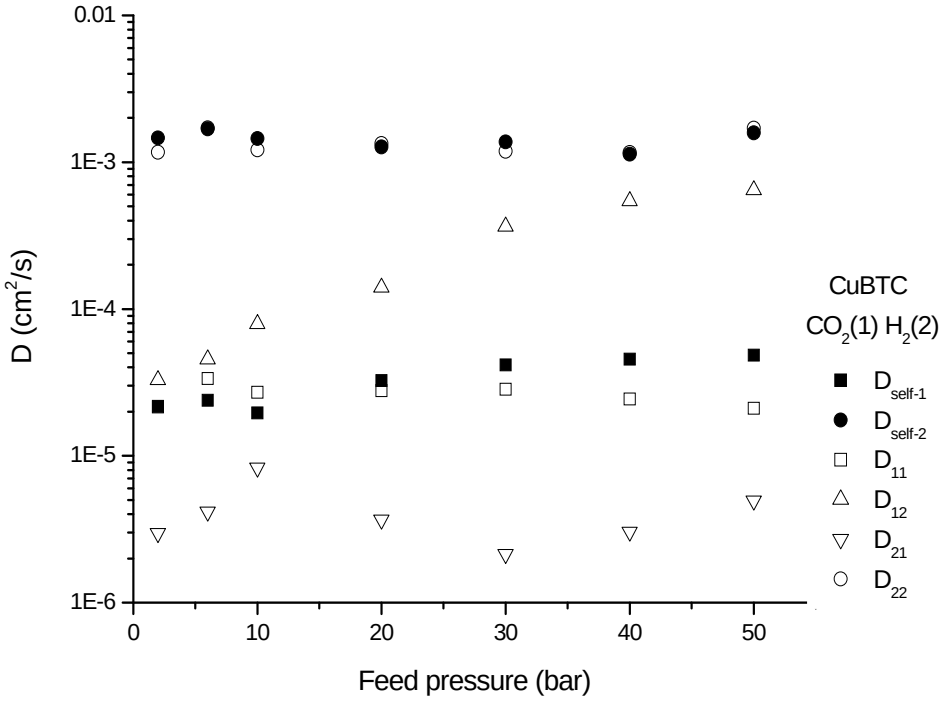

Figure 7.4 A comparison of the Fickian diffusivity matrix elements and mixture self diffusivities computed using MD as a function of feed pressure for CO_2/H_2 mixture with a bulk composition of 10/90 in CuBTC.

Under the conditions we have considered, the H_2 concentration gradient (∇c_2) is small compared to the CO_2 concentration gradient (∇c_1) across the membrane, so the effect of D_{12} being larger than D_{11} is unimportant. That is, for this example, the contributions of the off-diagonal diffusivities to the net flux are insignificant compared to the contributions of the diagonal diffusivities. Since the self diffusivities approximate the diagonal Fickian diffusivities well, our approximate method is accurate in this example.

We now turn to the selectivity of CO_2 from H_2 using COF-102. Since we did not apply the detailed calculation approach for this material we only compare the predictions of our approximate method with the direct MD calculations in Figure 7.5.

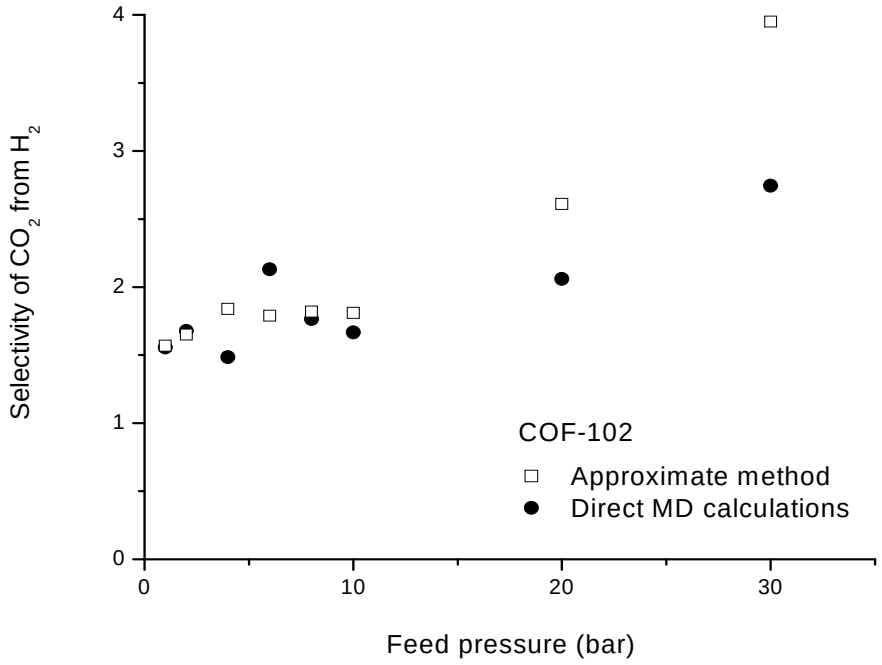

Figure 7.5 Predicted membrane selectivity of COF-102 for separation of CO_2/H_2 mixture. The feed gas composition is CO_2/H_2:10/90.

Similar to CuBTC, our approximate method does a reasonable job in predicting selectivities for COF-102. Figure 7.5 shows that the agreement between the approximate method and direct MD simulations is better at low pressures, as might be expected. The mixture self diffusivities and transport diffusivities calculated by MD simulations for CO_2/H_2 in COF-102 are shown in Figure 7.6. The mixture self diffusivities of each species are very similar to the diagonal transport diffusivities. In contrast to CuBTC, both of the off-diagonal Fickian diffusion coefficients are smaller in magnitude than the diagonal ones at low pressures and approximate to the values of diagonal diffusivity coefficients at high pressures.

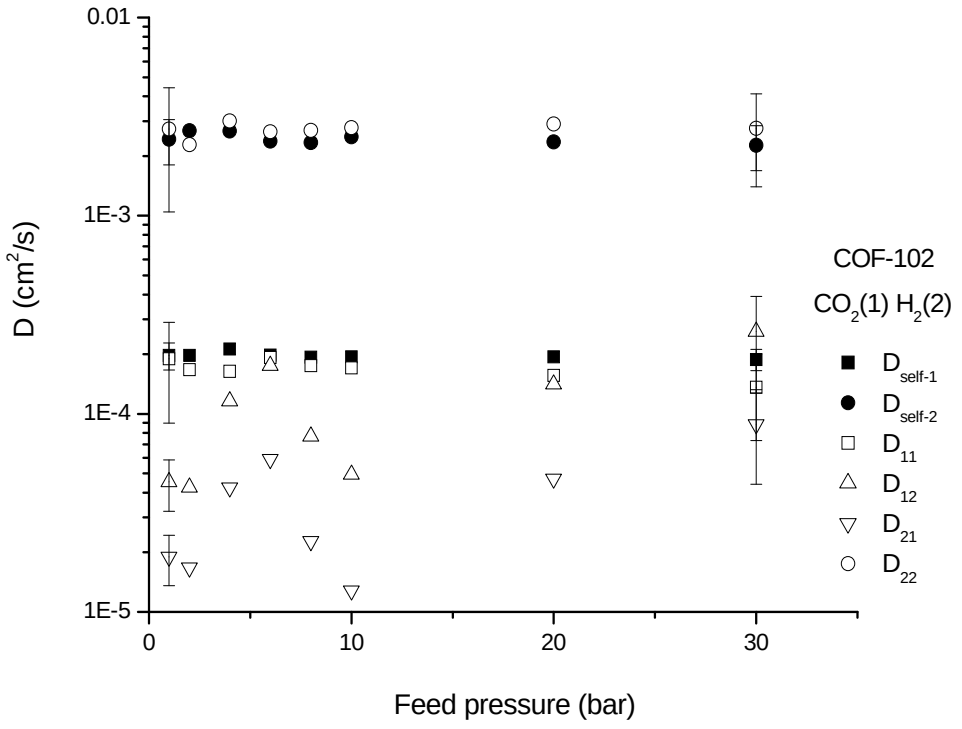

Figure 7.6 A comparison of the Fickian diffusivity matrix elements and mixture self diffusivities computed using MD as a function of feed pressure for CO_2/H_2 mixture with a bulk composition of 10/90 in COF-102.

One important question raised by the results in Figure 7.4 and Figure 7.6 is why the mixture self diffusivities are so similar to the diagonal Fickian diffusion coefficients. The diagonal Fickian diffusion coefficients are derived from Onsager coefficients and thermodynamic correction factors as shown in Equation 2.12. At low pressures, the diagonal (off-diagonal) thermodynamic correction factors approach unity (zero) (see Equation 2.10 and Figure 6.2). The diagonal Onsager coefficients by definition are equal to the mixture self diffusivity coefficients plus a term that arises due to correlated motions in pairs of adsorbates (see Equations 2.17 and 2.18)[3]. These correlation effects are insignificant at the dilute loadings corresponding to low pressures. Therefore, the value of the diagonal Onsager coefficients is very similar to the value of mixture self diffusion coefficients in this limit. Based on this reasoning, we can generically expect the diagonal Fickian coefficients to be close to the mixture self diffusivities at conditions corresponding to dilute loadings. The fractional loading of CO_2 and H_2 at the highest pressure of Figure 7.4 (Figure 7.6) is ~0.35 (0.1) and less than 0.1 (0.02), respectively, indicating that our calculations correspond to dilute loadings. It is therefore not surprising that the mixture self diffusivities are similar to the diagonal Fickian diffusion coefficients in Figures 7.4 and 7.6. This agreement of mixture self diffusivities and diagonal Fickian diffusivities is not exact, however, for non-dilute loadings.

Due to the nature of MD simulations, accumulating accurate statistics for the off-diagonal Onsager coefficients that is used to calculate the Fickian diffusivities is intrinsically more difficult than that of diagonal ones.[8] For clarity, we did not show the uncertainties on the Fickian diffusivities in the figures discussed above. For the CO_2/H_2 mixture in COF-102 at 30 bar, for example, the value of D_{11} (D_{22}) is calculated to be

$(1.36 \pm 0.63) \times 10^{-5}$ cm^2/s ($(2.75 \pm 1.03) \times 10^{-3}$ cm^2/s) whereas the value of D_{12} (D_{21}) is $(2.6 \pm 1.31) \times 10^{-4}$ cm^2/s ($(8.83 \pm 4.46) \times 10^{-3}$ cm^2/s). Under the same conditions, the mixture self diffusivity of CO_2 (H_2) is $(1.88 \pm 0.23) \times 10^{-4}$ cm^2/s ($(2.27 \pm 0.58) \times 10^{-3}$ cm^2/s). These results show that the uncertainties associated with computing self diffusion coefficients with MD are far smaller than the uncertainties associated with MD-calculated Onsager coefficients. We return to this discussion in the next section.

In order to assess the importance of the off-diagonal diffusivities on the final membrane selectivity, we repeated some membrane calculations while setting the off-diagonal coefficients (D_{12} and D_{21}) to zero for adsorbed CO_2/H_2 mixture in COF-102 at 30 bar. In this case, the membrane's selectivity for CO_2 dropped from 2.74 to 2.36. This means only ~15% of the membrane selectivity in this example is due purely to the off-diagonal Fickian coefficients. At higher pressures the effect of the off-diagonal Fickian coefficients may become significant due to multi-component effects.

The third example introduced at the beginning of this chapter was the permeation of CO_2/H_2 mixtures through IRMOF-9. Since we did not use SSK-based calculations for this material we only compare the predictions of our approximate method with the direct MD calculations in Figure 7.7. Our approximate method predicts the CO_2 selectivities for an IRMOF-9 membrane with reasonable accuracy. Although the agreement between the direct MD simulations and our approximate method is not as good as for CuBTC and COF-102, the predictions of the approximate method can be viewed as good enough to make a qualitative decision about the performance of the IRMOF-9 membrane. Specifically, the membrane selectivity predicted by both methods is too low to make IRMOF-9 a promising membrane material.

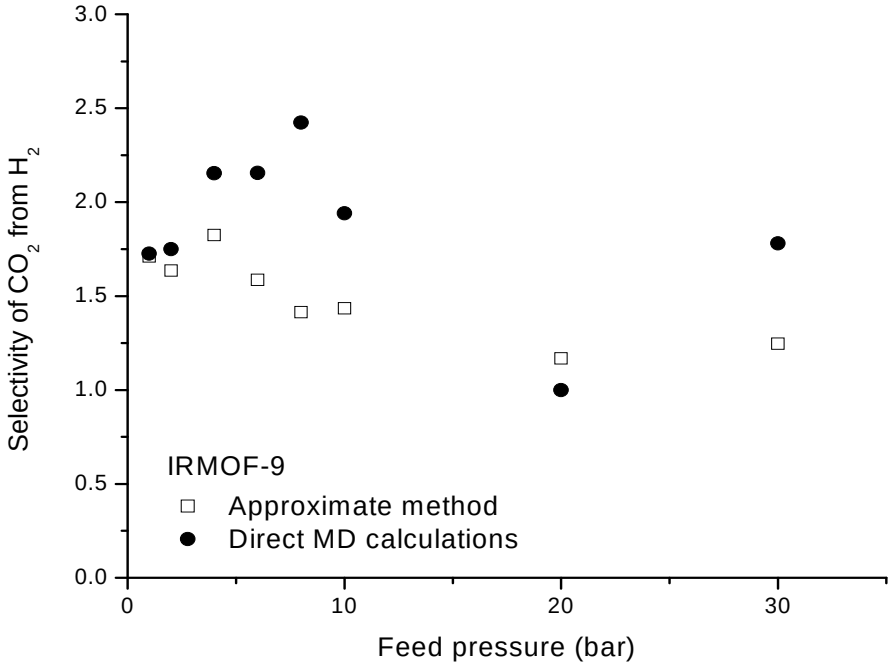

Figure 7.7 Predicted membrane selectivity of IRMOF-9 for separation of CO_2/H_2 mixture. The feed gas composition is CO_2/H_2:10/90.

Figure 7.8 shows the mixture self diffusivities and the Fickian diffusivities for CO_2/H_2 mixture in IRMOF-9. The mixture self diffusivities do not match with the diagonal Fickian diffusivities in IRMOF-9 as well as they did for CuBTC and COF-102. In IRMOF-9, the mixture self diffusivities systematically underestimate the diagonal Fickian diffusivities. However, given the relatively large uncertainties of Fickian diffusion coefficients compared to mixture self diffusivity coefficients within the calculations, the ratio of mixture self diffusivities represents the ratio of diagonal Fickian diffusivities with reasonable accuracy.

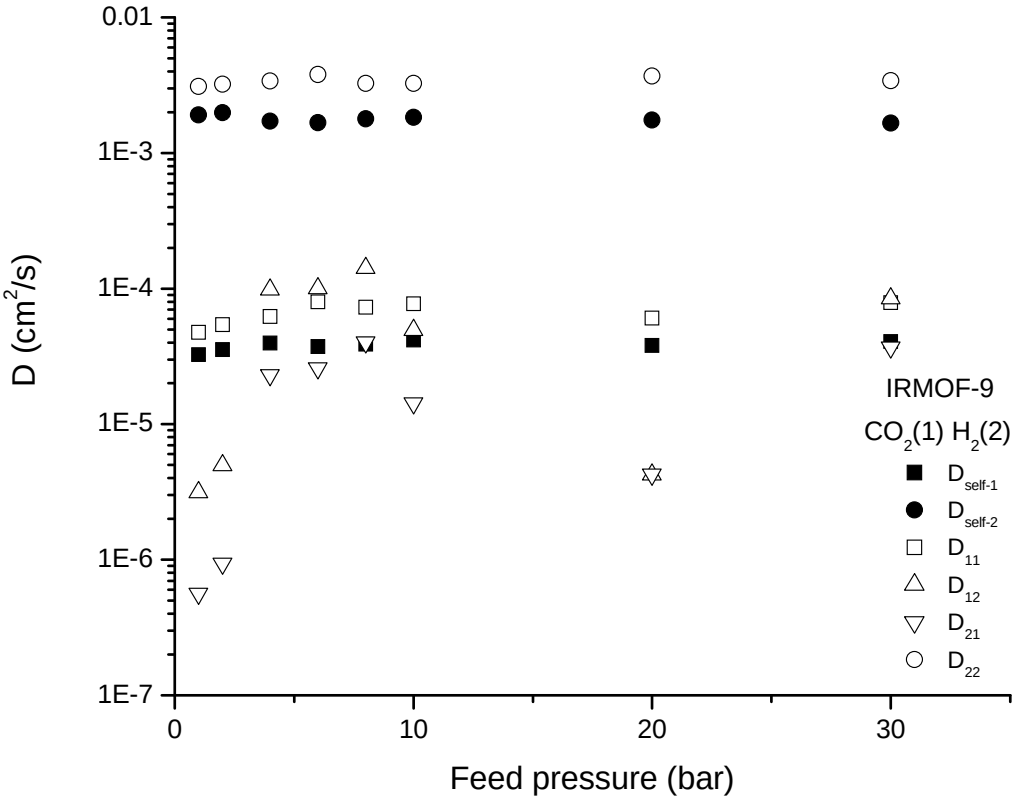

Figure 7.8 A comparison of the Fickian diffusivity matrix elements and mixture self diffusivities computed using MD as a function of feed pressure for CO_2/H_2 mixture with a bulk composition of 10/90 in IRMOF-9.

The adsorbed CO_2/H_2 mixture in IRMOF-9 is an important example for the robust screening strategy which we discuss in the next section: The mixture self diffusivities of CO_2/H_2 in IRMOF-9 did not represent the diagonal Fickian diffusivities with high precision, indicating that multi-component mixture effects may be important for this example. We used our approximate method to predict the selectivity of IRMOF-9 membrane even though the approximate method was validated to work only for examples where mixture effects are insignificant (see Chapter 6). If the predicted membrane

selectivity from our approximate method was promising (i.e. high), then more detailed calculations would be carried out to obtain a more accurate answer for membrane selectivity. We discuss this idea more fully in section 7.3.

We also used direct MD simulations to predict the selectivity of CH_4 from CH_4/H_2 mixtures in CuBTC, COF-102 and IRMOF-9. These were the cases where IAST did a good job in estimating the mixture adsorption isotherms and our approximate method was validated for predicting the membrane selectivity in Chapter 6. Figure 7.9(a) compares calculations based on SSK, our approximate self diffusion based method and direct MD calculations for the selectivity of CH_4 from H_2 in a CuBTC membrane. The predictions of these three methods agree well with each other. The good agreement between the SSK-based calculations and the direct MD simulations is not surprising since we previously showed that the SSK theory estimates the macroscopic diffusion coefficients well for this gas mixture in CuBTC (see Chapter 5). The agreement between the approximate method and the direct MD calculations are also good for the predicted membrane selectivity of COF-102 and IRMOF-9 for separation of CH_4/H_2 mixture, as shown in Figure 7.9(b) and (c).

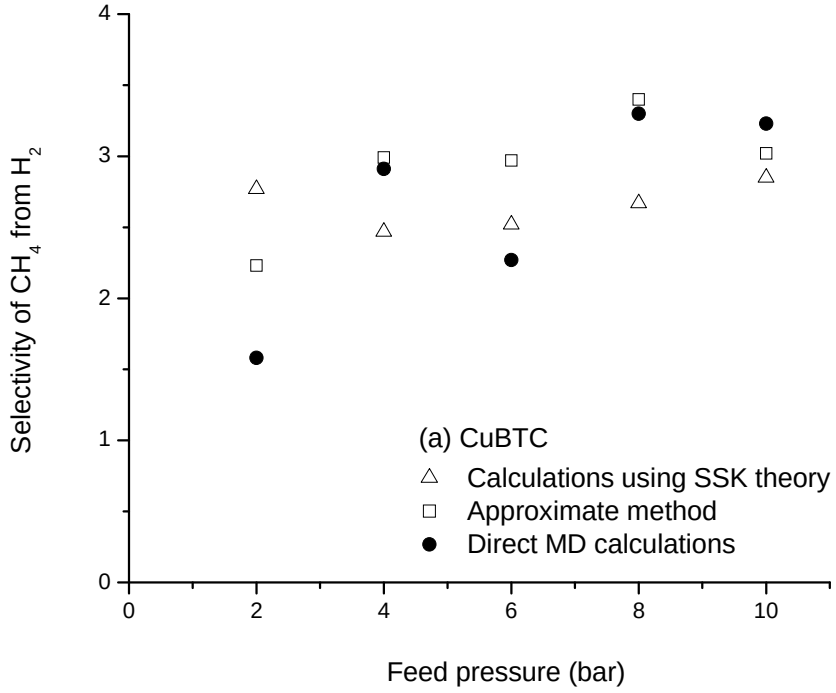

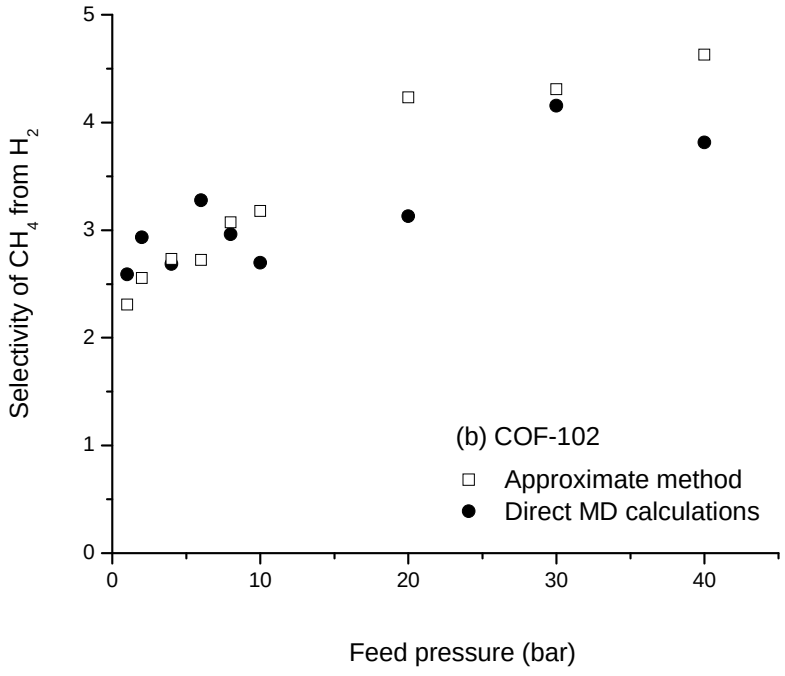

Figure 7.9 Predicted membrane selectivity of (a) CuBTC (b) COF-102 and (c) IRMOF-9 for separation of CH_4/H_2 mixture. The feed gas composition is CH_4/H_2:50/50.

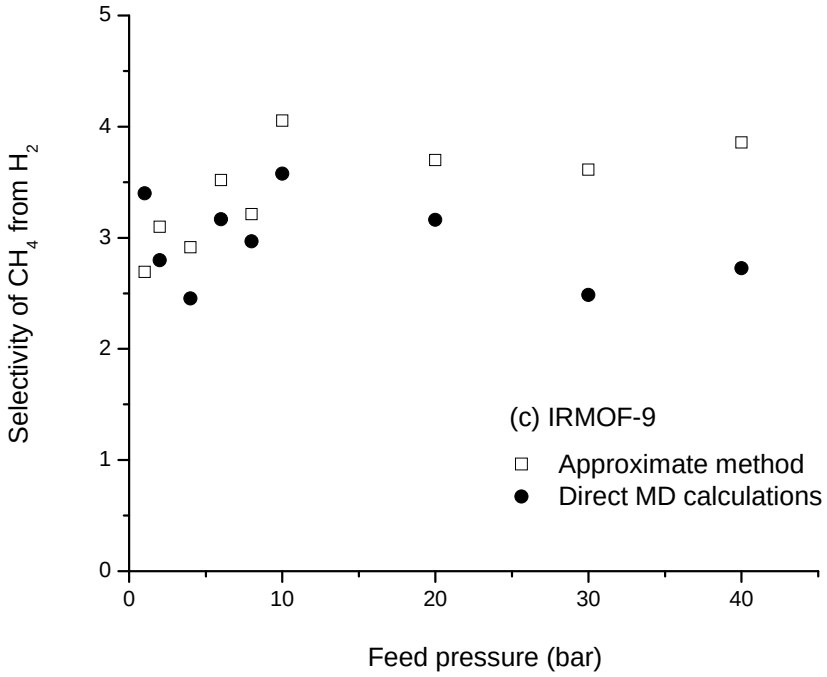

Figure 7.9 Continued

7.3 A Robust Screening Strategy for MOF Membranes

In this thesis, we have developed and tested several different models to predict the performance of MOFs as membranes. In this section, we draw these methods together and propose a robust screening strategy that should be used for future efforts in this area. The available methods for predicting the performance of a MOF membrane are briefly summarized in Table 7.1, and we comment on each method further below.

Table 7.1 Strengths and limitations of modeling approaches for MOF membranes.

Method	Comments/Limitations
Sanborn/Snurr method	. Accurate results for all operating conditions. . Statistical uncertainties are difficult to quantify. . Data for mixture adsorption and Onsager coefficients at a large collection of loadings must be collected to apply this method.
SSK theory based calculations	. Accurate predictions for all operating conditions if IAST is accurate. . Statistical uncertainties are difficult to quantify. . Data for mixture adsorption, single component self and corrected diffusivities at a large collection of loadings must be collected to apply this method.
Direct MD calculations	. Accurate results. . Statistical uncertainties are typically large. . Only applicable for vacuum permeate conditions. . Only data for mixture adsorption and Onsager coefficients at the loadings of interest must be collected to apply this method.
Mixture self diffusivity based approximate method	. Accurate predictions if the mixture effects are not significant. . Statistical uncertainties are typically small. . Only applicable for vacuum permeate conditions. . Only predicts membrane selectivity, not permeability. . Only data for mixture adsorption and mixture self diffusivity coefficients at the loadings of interest must be collected to apply this method.

The most comprehensive method to model crystalline nanoporous membranes was suggested by Sanborn and Snurr.[4,9] This method requires computing the matrix of Onsager coefficients at a large collection of loadings in the membrane material using EMD, which makes the approach very computationally demanding. Once this data and similar data for the mixture adsorption are collected and fitted to continuous functions, the Sanborn/Snurr method can be applied with confidence under all possible operating conditions. Although this approach is computationally demanding, it can be contemplated for materials that are expected to have very interesting properties. This approach has been used in the literature to predict the diffusivities of gas mixtures in zeolites and carbon nanotubes.[4,9,10] We did not use Sanborn/Snurr method for any example in this thesis.

The calculation approach which uses the SSK theory in a central way to predict mixture transport diffusion coefficients requires computing single component self and corrected diffusivities of each species and fitting them to continuous functions (see Chapter 3, 4 and 5). Once this is done, this approach can be applied to any feed pressure and pressure drop of the membrane. One of the important results in Chapter 5 was that this approach can be used with confidence for simple gas mixture/MOF combinations where IAST accurately predicts the mixture isotherm.

Earlier in this chapter we introduced a direct MD approach based on calculating the mixture transport diffusivities from EMD measurements of Onsager coefficients at specific loadings in a membrane. In this method, the permeate side of the membrane is assumed to be vacuum, a step that greatly simplifies the problem relative to the more general situation considered by the Sanborn/Snurr or SSK-based method. This direct MD

method invokes no assumption about the behaviors of the mixture diffusivities, and it gives accurate results when the permeate side is a vacuum.

The fourth modeling approach that is available is the approximate method that we described in the previous chapter. Applying this method requires calculation of the mixture self diffusivities at specific well-defined loadings in the membrane. These loadings are defined in a simple way only if the permeate side is assumed to be vacuum. Our results indicate that this approach is accurate for cases where mixture effects are not important, regardless of the success of IAST.

The discussion above has focused on the physical accuracy of the various modeling methods. In this sense, an accurate method gives results in agreement with the 'true' result, while a less accurate invokes mathematical approximations that are not necessarily valid, leading to possible disagreement with the true results. Two other factors must also play an important role in assessing the various modeling methods, namely, statistical uncertainties and computational efficiency. Below we examine these two issues separately.

The statistical uncertainties associated with the direct MD method and the approximate method based on mixture self diffusivities were discussed in the previous section. The basic observation that underlies this discussion is that the uncertainties associated with computing self diffusion coefficients with MD are far smaller than the uncertainties associated with MD-calculated Onsager coefficients or single component corrected diffusivities. As a result, the intrinsic uncertainties in results from the direct MD method are much larger than those for the approximate self diffusion coefficient-based method. This implies that if the two methods give results that are consistent, the

approximate method should be preferred for exploring a range of operating conditions. We return to this point in discussing a screening strategy below. The uncertainties in the Sanborn/Snurr and SSK-based methods are more difficult to quantify because the uncertainties in the MD-derived quantities are somewhat masked by the continuous functions fitted to these quantities. It is clear, however, that the net uncertainties in these methods are considerably larger than in the approximate self diffusion-based method.

We now turn to the computational efficiency of the four methods listed above. As in most computational models, there is a trade-off between physical accuracy (and the range of conditions that are described) and computational effort. The physical accuracy (computational effort) of the methods described here increases (decreases) going from the approximate method to Sanborn/Snurr approach. In Table 7.2 we approximate the computational requirement of each approach to examine one operating condition of the membrane. In determining the computational requirement of each method, we assumed that calculating mixture adsorption isotherm using GCMC at one loading is 'free' relative to calculating any diffusion term using MD since GCMC requires negligible computational effort compared to MD. Performing single component corrected diffusivity calculations or mixture Onsager coefficients is assumed to require at least 20 MD simulations at one loading. Mixture self diffusivity calculations require no extra effort if the mixture Onsager coefficients are calculated, otherwise these calculations are assumed to require 10 EMD simulations.

Table 7.2 Computational requirements of modeling approaches.

Method	**Computational requirement to examine one operating condition**	**Additional effort for each additional operating condition**	**Effort to examine 10 operating conditions**
Sanborn/Snurr method	Onsager coefficients at 100 loadings = 2000 EMD	None	=2000 EMD
SSK-based calculations	Corrected diffusivities at 20 loadings = 400 EMD	None	=400 EMD
Direct MD calculations	Onsager coefficients at 1 loading = 20 EMD	Same as initial operating condition.	=200 EMD
Mixture self diffusivity based approximate method	Mixture self diffusivities at 1 loading =10 EMD	Same as initial operating condition.	=100 EMD

The Sanborn/Snurr method requires computing the matrix of Onsager coefficients using EMD at ~100 loadings and fitting them to continuous functions to use them in a continuum model of a membrane for examining one operating condition. Computing Onsager coefficients at 100 different loadings requires 100×20 EMD simulations. Once this EMD data is fitted to an appropriate set of continuous functions, this method can be

used under all possible operating conditions without performing further molecular simulations. Sanborn/Snurr method, therefore, requires ~2000 EMD simulations to examine one or more operating conditions of the membrane.

Using SSK-based calculations requires computing the single component self and corrected diffusivity coefficients using EMD at ~20 loadings and fitting them to continuous functions to examine one operating condition of the membrane. Computing the corrected diffusivity coefficients at 20 different loadings requires 20×20 EMD simulations. These calculations also give the self diffusivities without any additional simulations. Similar to the Sanborn/Snurr method, once EMD data is collected and fitted, this method can be used under all possible operating conditions without further molecular simulations. The SSK-based calculations, therefore, requires ~400 EMD simulations to examine one or more operating conditions.

The direct MD method (mixture self diffusivity based approximate method) requires computing the matrix of Onsager coefficients (mixture self diffusivities) using EMD at just one specific loading in the membrane to examine one operating condition. Computing Onsager coefficients (mixture self diffusivities) at a single loading requires 20 (10) EMD simulations. Unlike the two methods discussed above, however, the effort required to examine another operating condition is the same as the initial operating condition. The direct MD method (mixture self diffusivity based approximate method), therefore, requires 20 (10) EMD simulations for one operating condition and 20 (10) more EMD simulations for each additional one.

Based on the accuracy and computational efficiency of the given methods, we suggest a robust screening strategy not only for MOF membranes but for all crystal

nanoporous membranes. The aim of this screening strategy is to predict the membrane selectivity of a nanoporous material for a specific binary gas mixture separation in an efficient way. The inputs of this approach are the crystal structure of the material (which is generally available from the experimental studies) and the interatomic potentials for all relevant degrees of freedom. In this thesis, for example, we treated MOFs as rigid structures, yet if desired any flexibility in nanoporous structure can be included in the input of the potential parameters. Once this input is ready, the calculation flowsheet given in Figure 7.10 can be applied to have an initial estimate of the membrane selectivity at the desired feed pressures and feed gas compositions. Figure 7.10 represents a robust screening approach to predict a nanoporous membrane's selectivity when permeate side is vacuum assuming that the membrane selectivity for a vacuum permeate is good proxy for all operating conditions. If the membrane selectivity is found to be low for a vacuum permeate condition at the end of these calculations, the candidate material for the membrane application is rejected and a new one is chosen. If the membrane selectivity is found to be high and more general operating conditions of the membrane are of interest, than more detailed approaches can be applied as shown in Figure 7.11.

For example, in Chapter 6 of this thesis, we applied the robust screening approach given in Figure 7.10 to IRMOF-8, -9, -10, -14, COF-102 and $Zn(bdc)(ted)_{0.5}$ to predict the performance of these materials as membranes for separation of CH_4/H_2, CO_2/CH_4 and CO_2/H_2 mixtures. In all cases, the predicted membrane selectivities of these materials were low compared to those of well known polymer and zeolite membranes. For this reason, we did not move to the calculation scheme given in Figure 7.11. Therefore, we can consider the robust screening strategy shown in Figure 7.10 as an efficient negative

screening effort to eliminate the materials which are not good candidates for making highly selective membranes. This step is significant to find materials with high performance before investigating a large amount of time and resources into fabricating a membrane.

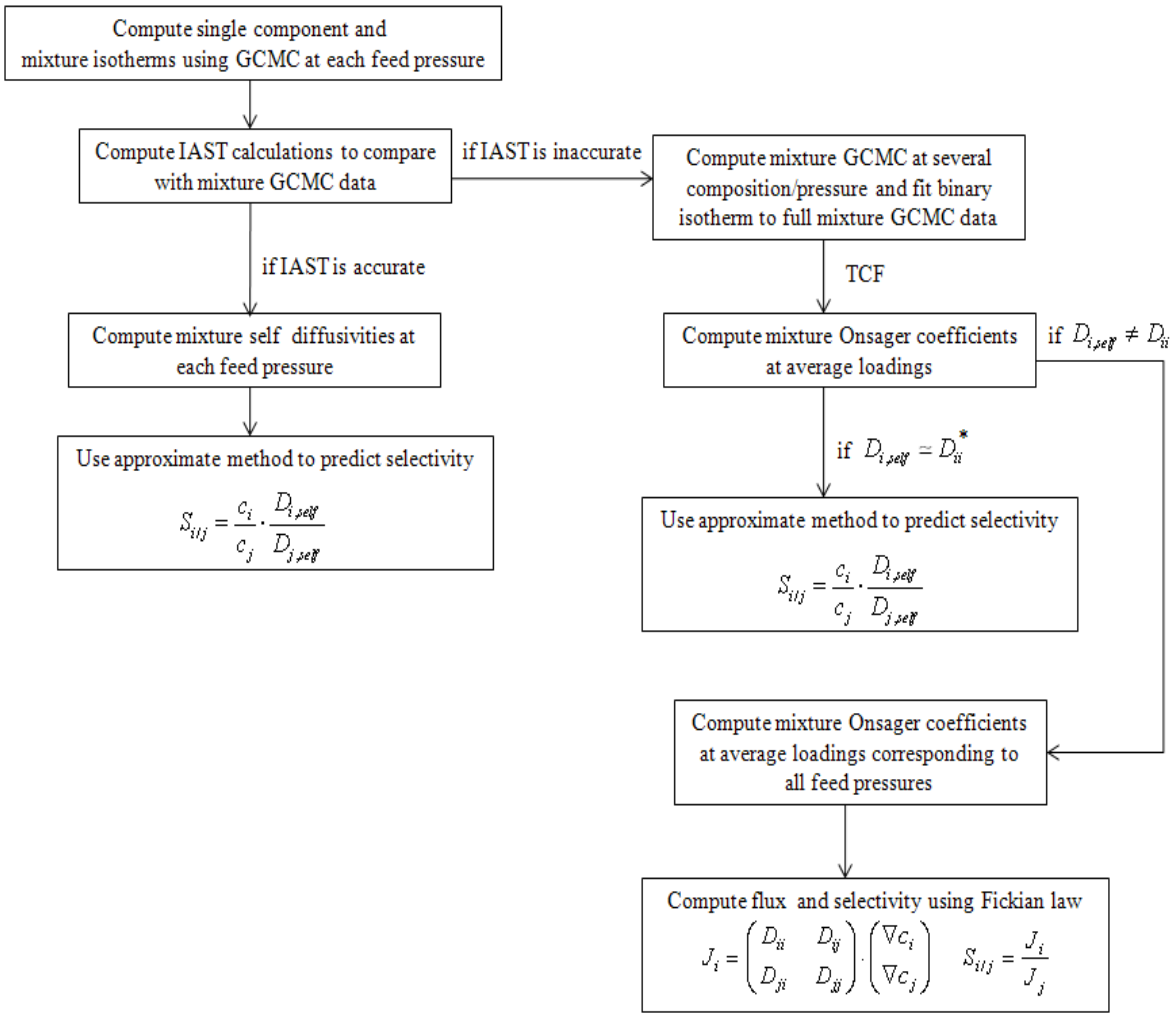

Figure 7.10 A robust screening approach to predict a nanoporous membrane's selectivity when permeate side is vacuum. *If mixture effects are not important. (TCF: Thermodynamic Correction Factors, IAST: Ideal Adsorbed Solution Theory, GCMC: Grand Canonical Monte Carlo)

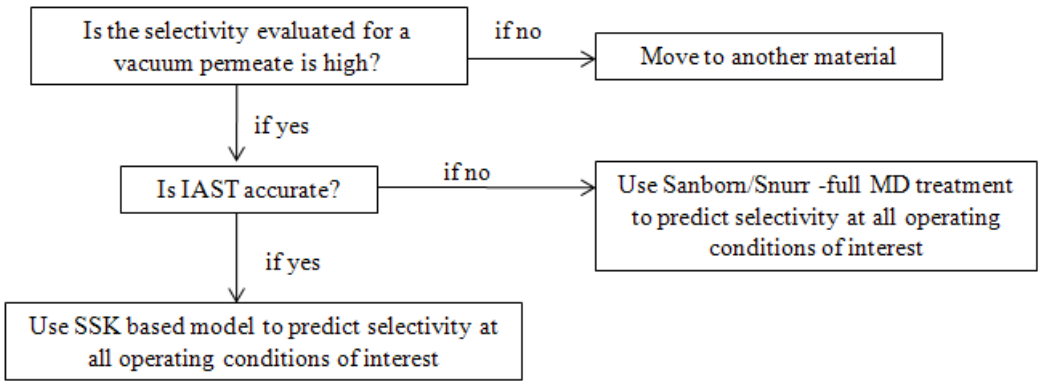

Figure 7.11 A robust screening approach to predict a nanoporous membrane's selectivity at all operating conditions.

7.4 References

(1) Keskin, S.; Sholl, D. S. *J. Phys. Chem. C* **2007**, *111*, 14055.

(2) Keskin, S.; Sholl, D. S. *Langmuir* **2009**, in press.

(3) Krishna, R.; van Baten, J. M. *Chem. Eng. Sci.* **2008**, *63*, 2130.

(4) Sanborn, M. J.; Snurr, R. Q. *Sep. Purif. Technol.* **2000**, *20*, 1.

(5) Theodorou, D. N.; Snurr, R. Q.; Bell, A. T. *Molecular Dynamics and Diffusion in Microporous Materials. In Comprehensive Supramolecular Chemistry*; Pergamon Press: New York, 1996; Vol. 7.

(6) Onsager, L. *Phys. Rev.* **1931**, *37*, 405.

(7) Onsager, L. *Phys. Rev.* **1931**, *38*, 2265.

(8) Kärger, J.; Ruthven, D. *Diffusion in Zeolites and Other Microporous Materials*; John Wiley & Sons: New York, 1992.

(9) Sanborn, M. J.; Snurr, R. Q. *AIChE J.* **2001**, *47*, 2032.

(10) Chen, H.; Sholl, D. S. *J. Membr. Sci.* **2006**, *269*, 152.

CHAPTER 8

CONCLUSIONS

Metal organic frameworks (MOFs) are one of the most exciting recent developments in nanoporous materials with potential applications for adsorption and other chemical separations. Because of the large number of known MOFs, efforts to predict the performance of MOFs as adsorbents, catalysts and/or membranes using molecular modeling can potentially play a significant role in selecting materials for specific applications. Molecular simulations of MOFs provide a detailed picture on the molecular scale that is not easily accessible from experiments. Molecular simulations are also helpful to develop design principles for MOFs by studying the effect of molecular level properties such as pore size, pore shape or surface area. In this chapter, we first summarize the results of our molecular simulation studies to assess the performance of MOF membranes for separation of gas mixtures and then review the challenges and opportunities for molecular simulation of MOFs for future studies.

8.1 Outlook

Since fabrication of membranes from new crystalline materials is challenging, very little is currently known about what advantages MOFs may have over more conventional materials for membrane-based separations. In this thesis, we presented the first results examining the ability of MOFs to act as gas separation membranes using atomically detailed simulations. A combination of atomistic modeling and continuum modeling was used to predict permeance of binary mixtures of CO_2/CH_4, CO_2/N_2, CO_2/H_2, CH_4/H_2, CH_4/N_2 and N_2/H_2 through IRMOF-1 membranes.[1,2] We compared the

predictions of our theoretical work for single component gas permeance of CO_2, H_2, CH_4 and N_2 through IRMOF-1 membranes with the only available experimental data[3] and showed that our predictions are in a good agreement with these experimental measurements. Our calculations showed that mixture effects can play a crucial role in determining the performance of MOF membranes, indicating that modeling or experimental studies that examine only single component gases will be insufficient to understand the properties of MOF based membranes in practical applications. We also showed that although the selectivity of IRMOF-1 membranes is low for CO_2/CH_4 separations relative to many polymeric membranes, IRMOF-1 membranes can exceed the upper bound established for polymeric membranes by exhibiting very large fluxes relative to polymeric membranes.[4]

The permeance of CO_2/CH_4, CO_2/H_2 and CH_4/H_2 mixtures through CuBTC membranes was also examined to understand the effect of MOF structure on the performance of the membrane.[5] The predicted selectivity of CuBTC membranes was found to be higher than that of IRMOF-1 membranes. Most of this increase in membrane's selectivity was associated with the higher adsorption selectivity of CuBTC. Changes in the characteristics of molecular diffusion between the two materials also contributed to the variation in membrane performance, but it appeared that focusing attention on adsorption selectivity will be a useful path forward for selecting MOFs suitable as membranes. This is a useful observation because the design or selection of materials with enhanced adsorption selectivity is a conceptually easier problem than the analogous task for diffusion-based selectivity. These results were the first specific

example of the idea that varying the structure of a MOF can lead to large changes in the performance of a MOF-based membrane.

We presented the first test of well known mixing theories for adsorption and diffusion of adsorbed gas mixtures in MOFs.[6] The accuracy of methods for predicting macroscopic mixture diffusion coefficients, mixture self diffusivity coefficients and mixture isotherms from single component data was examined for adsorbed mixtures of CH_4/H_2 in CuBTC. This study showed that it is possible to predict mixture properties from single component data with a high degree of accuracy. This conclusion had important implications for predicting the possible utility of MOFs in chemical separations, especially in applications that rely on mass transport of adsorbed species. By using these correlations, it is possible to rapidly examine a large range of potential operating conditions for chemical mixtures as soon as information on each species in the MOF of interest is known.

Finding the most promising membrane material among several MOF candidates was time consuming with the detailed calculation approach that we used to study IRMOF-1 and CuBTC. Therefore, we introduced an efficient approximate method which only uses limited information from molecular simulations to estimate the performance of MOF membranes.[7] The validity of this approach was examined by comparison with our earlier detailed calculations. A connection between two computationally efficient correlations predicting mixture adsorption and mixture self diffusion properties and the validity of our approximate method was proposed. This new approximate method was applied to several MOFs including IRMOF-1, -8, -9, -10 and -14, CuBTC, COF-102 and

$Zn(bdc)(ted)_{0.5}$ to study the effect of chemical diversity and interpenetration on the performance of MOF membranes for light gas separations.

Our results based on the approximate method provided some insights to the structural characteristics of MOFs which exhibit high membrane selectivity for specific gas separations. For example, small pore MOFs provide strong confinement for adsorbed CO_2 molecules in CO_2/H_2 mixtures, which lead to a high CO_2 selectivity over H_2. MOFs with open metal sites, on the other hand, enhanced the adsorption selectivity of CO_2 over H_2 due to strong electrostatic interactions. Therefore, MOFs with relatively small pores such as COF-102, IRMOF-9 and the ones with unsaturated metal corners such as CuBTC were suggested as promising candidates for separation of CO_2/H_2 mixtures. On the other hand, separation of CO_2 from CH_4 using large pore MOF membranes was found to be not very favorable compared to polymer and zeolites membranes that are already well developed. However, we recently focused on MOFs in which large cages are connected with narrow windows and showed that these MOFs have unprecedentedly high selectivity for membrane-based separation of CO_2/CH_4 mixtures.[8]

In this thesis, we introduced three different modeling approaches based on detailed molecular simulations to efficiently and accurately search through numerous MOFs for identifying the promising membrane candidates. We started with the description of a detailed calculation approach that is able to predict mixture permeation properties based on single component information taken from molecular simulations. We then described an approximate method requiring very limited amount of molecular simulations which is very efficient for initial screening aims. The cases where these two approaches work accurately were identified and an alternative approach, which is

computationally much more demanding, was described to provide the 'correct' answer for the cases where the previous two methods fail. Finally, based on the computational limitations and needs of these approaches, a robust screening strategy was outlined to study MOF materials.

8.2 Challenges and Opportunities for Molecular Simulation of MOFs

Molecular modeling calculations using empirical classical potentials have been widely used to study pure and mixed fluid adsorption in MOFs and diffusive transport of adsorbed fluids in MOFs.[9] As is evident from the volume of literature cited in this thesis, the application of molecular simulations to MOFs is growing rapidly. To conclude, we list what we feel are the main challenges and opportunities for using simulations to contribute to the development of practical applications of MOFs. We also include the quantum mechanical (QM) calculations used to study MOFs in this discussion. We begin with the challenges:

1. *Predicting structural properties*: QM methods can give accurate structural information about MOFs such as lattice constants. Most work[10-13] to date has focused on comparing quantum mechanical structural information with data that is already readily available from experiments. The opportunities that exist to use this capability to consider new structures have not yet been widely explored.

2. *Physisorption calculations*: The use of QM calculations to either directly characterize physisorption of molecules in MOFs is faced with several challenges. Multiple papers[14-20] have used Density Functional Theory calculations to examine the weak interactions of H_2 with MOFs, but this QM approach is well-known to not describe

van der Waals interactions accurately, so it is currently unclear that these calculations give anything other than qualitative information.

3. *Assigning point charges*: QM calculations have been useful in defining point charges, but it is important to note that no unique way to accomplish this task exists, and different charge decomposition methods can give rather different results. The effect of various charge decomposition methods on adsorption and diffusion calculations of gas species in MOFs has not completely been explored.[21]

4. *Defining interatomic potentials*: The development of accurate classical interatomic potentials for describing adsorption in MOFs remains challenging. Strong variations among different experimental measurements of adsorption in what is nominally the same material have been reported due to complications arising from residual solvent from the synthesis of a MOF being present in the materials' pores.[22,23] Careful judgment should be used by modelers before investing significant efforts in adapting intermolecular potentials to any one adsorption experiment. From the modeling perspective, it is important to use adsorption data from a broad range of conditions to parameterize potentials whenever this is practical.

5. *Considering flexibility of MOFs*: Most simulations of molecular adsorption and diffusion in MOFs approximate the MOF as a rigid structure. This assumption creates tremendous savings in computational effort. A limited amount of work[24-26] has considered the flexibility of the MOF structures in molecular simulations to date. Nevertheless, careful studies that establish when this approach is viable would be useful.

6. *Predicting stability of MOFs*: Atomistic simulations typically make no predictions about the long-term stability of MOFs. The stability of these materials is a

serious issue in practical applications. Some recent efforts have begun to use atomistic modeling to understand the mechanism of water-induced decomposition of IRMOF-1.[27] Using the methods developed in this work to consider the stability of other MOFs may be useful, although it is likely that this issue is more straightforward to address experimentally.[28] To aid the development of MOFs for real applications it would be very helpful if experimental reports of new synthesis explicitly included information on stability with respect to simple parameters such as temperature and humidity.

The most significant opportunities that exist for atomistic modeling of MOFs lie in areas where experiments for some property of interest are challenging, not in reiterating properties that have already been addressed experimentally. Several examples of this idea include:

1. *Design of new materials*: Atomistic simulations can be used to test hypothetical structures for particular applications if the metric describing the performance of a material for the application can be directly calculated. A good example of initial success in this area is the work of Snurr and co-workers on designing materials with large adsorption capacities for methane.[29]

2. *Predicting mixture adsorption*: Charactering the adsorption of chemical mixtures in MOFs (or other porous materials) is tedious experimentally. Relatively routine applications of Grand Canonical Monte Carlo (GCMC) simulations, however, allow mixture adsorption to be assessed efficiently once a forcefield for the adsorbing components is defined. We do not, however, advocate extensive GCMC simulations of mixture adsorption as a path forward in this topic. As we discussed in previous chapters, most examples of mixture adsorption in MOFs to date can be accurately predicted using

Ideal Adsorbed Solution Theory (IAST) based on single component adsorption data. We suggest that in any consideration of mixture adsorption using simulations, the accuracy of IAST first be considered by comparing its predictions with a small number of GCMC mixture simulations. If IAST is found to be accurate, then no further mixture simulations are required.

3. *Predicting mixture transport*: The development of quantitative information about molecular diffusion in MOFs is only just beginning.[30-35] Detailed characterization of diffusion in MOFs will be helpful for considering possible applications of MOFs such as membrane-based separations where molecular transport rates are crucial.[1] One important avenue in advancing the ability to simulate diffusion in MOFs will be to make careful comparisons with experimental measurements in materials that are known to give unambiguous results when characterized by adsorption. A second direction where simulation is likely to play a crucial role is in understanding mixture diffusion in MOFs. The small amount of data that is available on this topic suggests that mixing theories that use single-component information to predict mixture properties can yield accurate results for at least simple chemical mixtures in MOFs.[6]

4. *Developing new mixing theories*: An interesting direction in this area will be to consider the applicability of mixing theories to mixtures that are more chemically complex than the relatively simple mixtures that have been examined to date. Our calculations showed that modification of existing theories or development of new ones are necessary to predict mixture behavior of some combinations of gas mixture/MOF systems, specifically when highly polar species are adsorbed in very narrow pores of MOFs.

5. *Understanding mechanical characteristics*: Molecular simulation studies recently started to focus on thermal and mechanical properties of MOF materials.[36-39] Measuring thermal conductivity and electrical conductivity of MOFs and monitoring responses of MOFs to external forces such as applied pressure or temperature are significant topics to study since several MOFs have been proposed to be efficient chemical sensors, catalysts and bio-devices.[40]

6. *Predicting mixed matrix membrane properties*: Although making membranes directly from thin films of MOFs may ultimately have important advantages in terms of device performance, shorter term application of MOFs in membranes is likely to be in mixed matrix membranes where MOF crystals are embedded within a permeable polymer matrix. Two mixed matrix membranes that combine Cu-based MOF crystals within a polymeric membrane and IRMOF-1 crystals within a polymeric membrane have been already reported.[41,42] Considering the very high gas permeance through MOFs, it will be interesting to study different combinations of MOFs and polymers. To select MOF/polymer pairs that yield useful properties for gas separations in thse composite films, knowledge of adsorption and transport properties of the permeating species in MOF crystals is vital. Molecular simulations predicting the characteristics of the gas permeance in individual MOF crystals will be very helpful to describe the mixed matrix membranes including MOF crystals.

8.3 References

(1) Keskin, S.; Sholl, D. S. *J. Phys. Chem. C* **2007**, *111*, 14055.

(2) Keskin, S.; Sholl, D. S. *Ind. Eng. Chem. Res.* **2009**, *48*, 914.

(3) Liu, Y.; Ng, Z.; Khan, E. A.; Jeong, H.-K.; Ching, C.-B.; Lai, Z. *Micropor. Mesopor. Mater.* **2009**, *118*, 296.

(4) Robeson, L. M. *J. Membr. Sci.* **1991**, *62*, 165.

(5) Keskin, S.; Liu, J.; Johnson, J. K.; Sholl, D. S. *Micropor. Mesopor. Mater.* **2009**, *125*, 101.

(6) Keskin, S.; Liu, J.; Johnson, J. K.; Sholl, D. S. *Langmuir* **2008**, *24*, 8254.

(7) Keskin, S.; Sholl, D. S. *Langmuir* **2009**, in press.

(8) Watanabe, T.; Keskin, S.; Nair, S.; Sholl, D. S. *Phys. Chem. Chem. Phys.* **2009**, in press.

(9) Keskin, S.; Liu, J.; Rankin, R. B.; Johnson, J. K.; Sholl, D. S. *Ind. Eng. Chem. Res.* **2009**, *48*, 2355.

(10) Bahr, D. F.; Reid, J. A.; Mook, W. M.; Bauer, C. A.; Stumpf, R.; Skulan, A. J.; Moody, N. R.; Simmons, B. A.; Shindel, M. M.; Allendorf, M. D. *Phys. Rev. B* **2007**, *76*, 184106.

(11) Civalleri, B.; Napoli, F.; Noel, Y.; Roetti, C.; Dovesi, R. *Cryst. Eng. Comm.* **2006**, *8*, 364.

(12) Fuentes-Cabrera, M.; Nicholson, D. M.; Sumpter, B. G.; Widom, M. *J. Chem. Phys.* **2005**, *123*, 124713.

(13) Mattesini, M.; Soler, J. M.; Induráin, F. *Phys. Rev. B* **2006**, *73*, 094111.

(14) Gao, Y.; Zeng, X. C. *J. Phys. Condens. Matter.* **2007**, *19*, 386220.

(15) Mueller, T.; Ceder, G. *J. Phys. Chem. B* **2005**, *109*, 17974.

(16) Mulder, F. M.; Dingemans, T. J.; Wagemaker, M.; Kearley, G. J. *Chem. Phys.* **2005**, *317*, 113.

(17) Sagara, T.; Klassen, J.; Ortony, J.; Ganz, E. *J. Chem. Phys.* **2005**, *123*, 014701.

(18) Samanta, A.; Furuta, T.; Li, J. *J. Chem. Phys.* **2006**, *125*, 084714.

(19) Zhou, W.; Yildirim, T. *Phys. Rev. B* **2006**, *74*, 180301.

(20) Nagaoka, M.; Ohta, Y.; Hitomi, H. *Coord. Chem. Rev.* **2007**, *251*, 2522.

(21) Ramsahye, N.; Maurin, G.; Bourrelly, S. *Phys. Chem. Chem. Phys.* **2007**, *9*, 1059.

(22) Wong-Foy, A. G.; Matzger, A. J.; Yaghi, O. M. *J. Am. Chem. Soc.* **2006**, *128*, 3494.

(23) Liu, J.; Culp, J. T.; Natesakhawat, S.; Bockrath, B. C.; Zande, B.; Sankar, S. G.; Garberoglio, G.; Johnson, J. K. *J. Phys. Chem. C* **2007**, *111*, 9305.

(24) Tafipolsky, M.; Amirjalayer, S.; Schmid, R. *J. Comput. Chem.* **2007**, *28*, 1169.

(25) Greathouse, J. A.; Allendorf, M. D. *J. Phys. Chem. C* **2008**, *112*, 5795.

(26) Amirjalayer, S.; Tafipolsky, M.; Schmid, R. *Angew. Chem. Int. Ed.* **2007**, *46*, 463.

(27) Greathouse, J. A.; Allendorf, M. D. *J. Am. Chem. Soc.* **2006**, *128*, 10678.

(28) Yazaydin, A. O.; Benin, A. I.; Faheem, S. A.; Jakubcza, P.; Low, J. J.; Willis, R. R.; Snurr, R. Q. *Chem. Mater.* **2009**, *21*, 1425.

(29) Düren, T.; Sarkisov, L.; Yaghi, O. M.; Snurr, R. Q. *Langmuir* **2004**, *20*, 2683.

(30) Skoulidas, A. I. *J. Am. Chem. Soc.* **2004**, *126*, 1356.

(31) Skoulidas, A. I.; Sholl, D. S. *J. Phys. Chem. B* **2005**, *109*, 15760.

(32) Yang, Q.; Zhong, C. *J. Phys. Chem. B* **2005**, *109*, 11862.

(33) Stallmach, F.; Groger, S.; Kunzel, V.; Kärger, J.; Yaghi, O. M.; Hesse, M.; Muller, U. *Angew. Chem. Int. Ed.* **2006**, *45*, 2123.

(34) Jhon, Y. H.; Cho, M.; Jeon, H. R.; Park, I.; Chang, R.; Rowsell, J. L. C.; Kim, J. *J. Phys. Chem. C* **2007**, *111*, 16618.

(35) Babarao, R.; Jiang, J. *Langmuir* **2008**, *24*, 5474.

(36) Huang, B. L.; McGaughey, A. J. H.; Kaviany, M. *Int. J. Heat Mass Transfer* **2007**, *50*, 393.

(37) Huang, B. L.; Ni, Z.; Millward, A.; McGaughey, A. J. H.; Uher, C.; Kaviany, M.; Yaghi, O. *Int. J. Heat Mass Transfer* **2007**, *50*, 405.

(38) Han, S. S.; Goddard, W. A. I. *J. Phys. Chem. C* **2007**, *111*, 15185.

(39) Dubbeldam, D.; Walton, K. S.; Ellis, D. E.; Snurr, R. Q. *Angew. Chem. Inter. Ed.* **2007**, *46*, 4496.

(40) Mueller, U.; Schubert, M.; Teich, F.; Puetter, H.; Schierle-Arndt, K.; Pastré, J. *J. Mater. Chem.* **2006**, *16*, 626.

(41) Perez, E. V.; Balkus, K. J.; Ferraris, J. P.; Musselman, I. H. *J. Membr. Sci.* **2009**, *328*, 165.

(42) Zhang, Y.; Musselman, I. H.; Ferraris, J. P.; Balkus, K. J. *J. Membr. Sci.* **2008**, *313*, 170.